Effect of light supply in photobioreactors on the biomass productivity and energy efficiency of *Scenedesmus sp.*

Aliya Habibti Gani

A thesis submitted in partial fulfilment of the requirements for the degree of

Masters of Science in Engineering

in the Centre for Bioprocess Engineering Research

Department of Chemical Engineering

UNIVERSITY OF CAPE TOWN

September 2013

Plagiarism declaration

I know the meaning of plagiarism and declare that all the work in the document, save for that which is properly acknowledged, is my own.

Signed.....

Acknowledgements

First and foremost, I would like to thank my supervisor Prof Sue Harrison for her valuable guidance, encouragement and support throughout this project.

I would also like to extend my gratitude to the following people:

- Emmanuel Ngoma, Sharon Rademeyer and Frances Pocock -for your help and support in the labs.
- Melinda Griffiths - for teaching me how to grow algae and for all of your invaluable advice and suggestions.
- Peter Dobias and Joachim Macke - for helping me with different workshop projects.

I would also like to thank the CeBER algae group for the great advice, support, assistance and informative discussions. A special thanks to my friends in the department (Nozonke, Rukaya, Sarah, Latifa, Marc, Naadia and Caroline) for always being supportive and helpful and for making this time enjoyable.

I am grateful to the National Research Foundation (NRF) and to CeBER for funding this project.

Lastly, I would like to express my deepest gratitude to my family for their unconditional love and support.

Synopsis

Production of biofuel from microalgae is an attractive and sustainable option for meeting rising global energy demands and mitigating global warming. However, for commercial production of microalgae to be economically feasible, high biomass productivities and low auxiliary energy inputs must be achieved in large photobioreactors. According to literature, one of the main factors limiting growth is the inefficiency of light utilization (Posten, 2009; Janssen *et al.*, 2003; Carvalho *et al.*, 2006). In a photobioreactor, as biomass concentration and depth of culture increase, the amount of light that is able to penetrate the culture decreases exponentially. This occurs because of mutual shading of algal cells via adsorption of pigments or via scattering of cells.

The purpose of this study was to optimize biomass productivity and biomass concentration by developing a thorough understanding of the microalgal response to light. In particular, the effects of light source, light intensity, configuration (internal and external), reactor design and the related variation in light/dark cycling were investigated. The key objectives of this study were:

- To determine how *Chlorella vulgaris* and *Scenedesmus sp*., respond to similar changes in lighting conditions
- To design and evaluate the performance of an internally lit LED airlift reactor
- To determine the effect of different light sources (fluorescent and LEDs) on biomass productivity
- To assess the effect of light/dark cycling on *Scenedesmus sp*.
- To analyse the effect of reactor configuration (flat plate, airlift and tubular) on algal cultivation in terms of biomass productivity and energy utilization.

To meet the 1st objective, *Chlorella vulgaris* and *Scenedesmus sp.* were grown in 3.2 L vertical airlift reactors at 24±1°C. *Scenedesmus sp.* achieved both higher biomass concentrations and linear growth rates (3.62 $g.L^{-1}$ and 0.0118 $g.L^{-1}.h^{-1}$) than *Chlorella vulgaris* (1.88 $g.L^{-1}$ and 0.0097 $g.L^{-1}.h^{-1}$) when the light intensity was increased from 300 to 600 $\mu mol.m^{-2}.s^{-1}$ after 2 days. Further, *Scenedesmus sp.* could withstand higher light intensities at lower biomass concentrations without becoming photoinhibited. Based on these findings, *Scenedesmus sp.* was selected for the remainder of the experimental work.

To meet the 2nd and 3rd objectives, the effect of light intensity (160, 300, 460, 600 μmol.m^{-2}.s^{-1}) and configuration (external fluorescent and internal LED) on the growth of *Scenedesmus sp.* in the airlift reactors at 26±1°C was investigated. Across the range of light intensities investigated, the linear productivity of *Scenedesmus sp.* was light limited. At a depth of 2 cm, less than 100 μmol.m^{-2}.s^{-1} was available at biomass concentrations of 0.5 g.L^{-1} or greater.

At 300 μmol.m^{-2}.s^{-1}, the internally lit LED reactor achieved slightly lower maximum specific and linear growth rates (0.0248 h^{-1} and 0.0064 g.L^{-1}.h^{-1}) than the standard externally lit fluorescent airlift reactor (0.0275 ± 0.0012 h^{-1} and 0.0070 ± 0.0016 g.L^{-1}.h^{-1}). The poorer performance of the LEDs was attributed to the ‗point-specific' light distribution of LEDs i.e. the light intensity is high at the site of an LED but drops off between successive LEDs (1059 to 35 μmol.m^{-2}.s^{-1}).

The combination reactors (internal LED with external fluorescent light) at 460 and 600 μmol.m^{-2}.s^{-1} achieved maximum specific growth rates and linear productivities that were approximately 21-36% and 53-56% greater than those achieved in the externally lit fluorescent photobioreactor at 300 μmol.m^{-2}.s^{-1} respectively. Further, the combination reactor at 600 μmol.m^{-2}.s^{-1}, achieved a maximum specific growth rate that was 18% greater than that of the externally illuminated airlift photobioreactor at 600 μmol.m^{-2}.s^{-1}. The better performance of the combination reactors is attributed to the reduced light path length and the increase in light intensity, which improved light exposure in the reactor.

The effect of temperature (24-30°C) investigated in the externally illuminated airlift reactors showed that the maximum specific growth rate is modified by temperature according to the Arrhenius equation. As expected, similar activation energies of 39.7 and 38.7 kJ.mol^{-1} were required at 300 and 600 μmol.m^{-2}.s^{-1} respectively. However, a poor correlation existed between temperature and the linear growth rate such that activation energies could not be reliably estimated in terms of linear growth rate. Further studies should be performed before a conclusion can be reached.

The effects of light/dark cycling were investigated in 209 mL and 330 mL glass tubular reactors with a light path length of 7 mm to enable its effective control (objective 4). Cycle times of 21 and 33 s were investigated, each at light intensities of 300 and 600 μmol.m^{-2}.s^{-1} and light fractions of 0.4, 0.75 and 1.00. Both an increase in light intensity and light fraction resulted in an increase in the specific growth rate. Further, at 21 s, algal cells spent a shorter fraction of time (0.54) exposed to high light intensities

compared to the duration at 33 s (0.60) and hence had a greater fraction of time to recover in the light-limited riser from the effects of photoinhibition. The highest specific growth rate of 0.1035 h^{-1} was obtained at full light exposure of 600 μmol.m^{-2}.s^{-1} and 21s.

In the 1.6 L perspex flat plate reactor, it was found that increasing the aeration rate from 2.5 to 5 L.min^{-1}, which improved mixing and decreased the mean circulation time, had a minimal effect on the linear growth rate up to 125 hours at a constant light intensity of 300 μmol.m^{-2}.s^{-1}. However, increasing the light intensity to 600 μmol.m^{-2}.s^{-1} resulted in a 22-42% increase in the linear growth rate. After 125 hours, a change in the linear slope occurred, and it was observed that increasing the aeration rate allowed the linear growth rate to be maintained for longer so that the maximum biomass concentration could be obtained more quickly. These results highlight the importance of mass transfer at higher biomass concentrations (1.26-2.43 g.L^{-1}). Additionally, lower specific (14-18%) and linear growth rates (12-21%) were obtained when an LED light bank was used as compared to a fluorescent light bank to provide illumination at 300 μmol.m^{-2}.s^{-1}. This result was attributed to the ‗point-specific' light distribution of LEDs.

From the comparative evaluation, it was found that the tubular reactors achieved the highest specific growth rates (0.0725-0.1035 h^{-1}), followed by the flat plate (0.0459-0.0642 h^{-1}) and airlift reactors (0.0248-0.0443 h^{-1}).These results were attributed to the highest degree of light exposure per unit culture volume experienced in the tubular reactor (65-143 mmol.m^{-3}.s^{-1}), followed by the flat plate (14.2-28.4 mmol.m^{-3}.s^{-1}) and airlift reactors (8.9-17.7 mmol.m^{-3}.s^{-1}) respectively. In terms of energy efficiency (including light and mixing energy inputs), it was found that the flat plate reactor achieved 0.088-0.140 g.W^{-1}.day^{-1}, followed by the tubular and airlift reactors that achieved 0.041-0.095 g.W^{-1}.day^{-1} and 0.060-0.064 g.W^{-1}.day^{-1} respectively. In terms of net energy ratios (including light and mixing energy inputs), all the reactors achieved values well below 1, indicating their infeasibility for cultivating energy products at present. If 100% of the light energy requirement was supplied from solar energy (assuming halved productivity based on diurnal cycling), the tubular, flat plate and airlift photobioreactors could achieve NERs of between 254 to 390, 7.3 to 13.4 and 0.64 to 1.35 under the mixing and mass transfer regimes used respectively. Thus, it is evident that in order to improve the efficiency of algal reactors, the amount of solar energy captured and the efficiency of light supply systems to reactors needs to be improved.

Table of Contents

List of Figures

List of Tables

Nomenclature

A	cross-sectional area of the reactor	m
A_b	surface area of a bubble	m^2
$A_{i,\ total}$	total gas-liquid interfacial area	m^2
A_i	incident area	m^2
A_c	Arrhenius constant	h^{-1}
A_r	cross-sectional area of the riser	m^2
A_d	cross-sectional area of the downcomer	m^2
C^*	saturation concentration of CO_2 in the media	$g.L^{-1}$
$C_{exp\ –\ linear\ downcomer}$	biomass concentration at which growth transitions from the exponential to the linear phase in the downcomer	$g.L^{-1}$
C_L	liquid concentration of CO_2 in the media	$g.L^{-1}$
C_x	biomass concentration at time *t* (h)	$g.L^{-1}$
C_{xo}	biomass concentration at t = 0 h	$g.L^{-1}$
D	tube diameter	m
D_{CO2}	diffusivity of CO_2 in water	$m^2.s^{-1}$
D_{O2}	diffusivity of O_2 in water	$m^2.s^{-1}$
d_b	mean bubble diameter	m
E_a	growth activation energy	$kJ.mol^{-1}$
E_L	energy input per unit culture volume	$W.m^{-3}$

$E_{M,A}$	energy input per unit culture volume for airlift bioreactors	$W.m^{-3}$
$E_{M,B}$	energy input per unit culture volume for bubble columns	$W.m^{-3}$
f	gas flow rate	$L.min^{-1}$
f	light fraction	
Gr	Grashof number	
g	acceleration due to gravity	$m.s^{-2}$
H_g	enthalpy of dry biomass	$kJ.g^{-1}$ DW
h	culture depth	m
h_D	sparged liquid height	m
h_L	unsparged liquid height	m
ID	internal diameter	m
$I_{exp - linear\ downcomer}$	light intensity when growth transitions from exponential to the linear phase	$\mu mol.m^{-2}.s^{-1}$
I_o	average light intensity	$\mu mol.m^{-2}.s^{-1}$
IPAR	PAR ($kJ.m^{-2}.day^{-1}$) x illumination surface (m^2)	$kJ.day^{-1}$
k_La	overall mass transfer coefficient	s^{-1}
L	light path length	m
N_b	number of bubbles	
od	outer diameter	m
PAR	photosynthetically active radiation	$kJ.m^{-2}.day^{-1}$
P	volumetric biomass productivity	$g.L^{-1}.day^{-1}$

PE	photosynthetic efficiency	%
P/E	biomass productivity per unit power input	$g.W^{-1}.day^{-1}$
P/E_M	biomass productivity per unit mechanical power input	$g.W^{-1}.day^{-1}$
Q	linear productivity	$g.L^{-1}.h^{-1}$
q	volumetric gas flow rate	$m^3.s^{-1}$
R	universal gas constant	$J.mol^{-1}.K^{-1}$
Re	Reynolds number	
r_g	maximum daily growth rate	$g\ DW.day^{-1}$
SA/V	illumination surface area to volume ratio	m^{-1}
Sc	Schmidt number	
T	temperature	°C
t_c	cycle time	s
t_{exp}	time of exponential growth	s
t_m	mixing time	s
U_g	superficial gas velocity	$m.s^{-1}$
U_L	superficial liquid velocity	$m.s^{-1}$
V	culture volume	m^3
V_G	volume of gas in the reactor	m^3
V_L	volume of liquid in the reactor	m^3
v	velocity in the tube	$m.s^{-1}$
vvm	gas sparged per unit culture volume per min	$m^3min^{-1}.m^{-3}$
x	length of the circulation path	m

X_{max}	maximum biomass concentration	$g.L^{-1}$
γ	specific weight of the broth	$N.m^{-3}$
η	fluid viscosity	$kg.s^{-1}.m^{-1}$
ρ	fluid density	$kg.m^{-3}$
$\Delta\rho$	difference between water and air density	$kg.m^{-3}$
μ_{H2O}	viscosity of water	$kg.m^{-1}.s^{-1}$
μ_{max}	maximum specific growth rate	h^{-1}
ε	overall gas holdup	

Abbreviations

ALR	Airlift photobioreactor
CIALR	Combination of illuminated airlift photobioreactor with external fluorescent lighting
F	Fluorescent light
FP	Flat plate photobioreactor illuminated with fluorescent light
FPL	Flat plate photobioreactor illuminated with LEDs
IALR	Internally illuminated airlift photobioreactor
LED	Light-emitting diode
NER	Net energy ratio
PBR	Photobioreactor
PMMA	Polymethyl methacrylate (perspex)
TBR1	209 mL tubular photobioreactor
TBR2	330 mL tubular photobioreactor

1. Introduction

1.1 Context and scope of this study

One of the main challenges facing mankind today is the development of environmentally sustainable and economically viable renewable sources of energy that can be used to reduce and ultimately replace fossil fuels and hence mitigate climate change (Mata *et al.*, 2010; Kunjapur and Eldridge, 2010). In recent years, renewed interest in algal biotechnology has been shown as microalgal production offers an attractive solution to the development of renewable bioenergy sources as well as a means to reduce carbon dioxide emissions. Microalgae can be used to produce biodiesel, biohydrogen and biogas (Chisti, 2008;Tamburic *et al.*, 2011;Schamphelaire and Verstraete, 2009). Algal biomass can also be combusted to generate heat and electricity or fermented to liquid fuels such as ethanol (Amin, 2009; Bruhn *et al.*, 2011). Apart from bioenergy products, microalgae can also be used to produce a wide variety of high value products such as nutritional supplements, pharmaceuticals, pigments, fine chemicals and secondary metabolites (Eriksen, 2008; Molina *et al.*, 2001; Ugwu *et al.*, 2008; Borowitzka, 1999).

However, industrial production of microalgae has been limited due to the lack of efficient photobioreactors. In order to improve biomass productivity, a thorough understanding of growth aspects such as light distribution and the hydrodynamic characteristics associated with different photobioreactor designs is required (Ugwu *et al.*, 2008; Lehr and Posten, 2009; Kunjapur and Eldridge, 2010). According to literature, one of the main factors currently limiting algal growth in photobioreactors is the inefficiency of light delivery and its distribution amongst the photosynthetic algal cells (Carvalho *et al.*, 2006; Eriksen 2008; Janssen *et al.*, 2003; Lee and Palsson, 1994). As the size of a photobioreactor increases and the overall surface area that is exposed to light decreases, the amount of light that is able to penetrate the culture decreases rapidly. Thus, a fraction of the photobioreactor remains dark and limits the overall biomass productivity that can be achieved. In order to improve light availability in photobioreactors, design parameters such as the illumination surface area to volume ratio and the light path length need to be optimized (Richmond, 2004; Degen *et al.*, 2001). Provision of adequate mixing is also essential to ensure that sufficient mass transfer of CO_2 and O_2 occurs. An increase in mixing rate also promotes higher light/dark cycling frequencies.

Furthermore, in order to make the production of microalgae economically viable, the high capital and downstream processing costs as well as the auxiliary energy costs need to be reduced, whilst maintaining a high biomass productivity. In this project, the light and mixing energy requirements associated with different photobioreactor designs (column, tubular and flat plate) are considered. Analysis of the capital and downstream processing costs associated with different photobioreactor designs are beyond the scope of this project.

The aim of this thesis is to acquire a rigorous understanding of the response of microalgae to light to optimize both the overall biomass productivity and biomass concentration achieved. For this study the performance of the three most common types of closed photobioreactors used in industry, namely: a vertical column airlift photobioreactor, a flat plate photobioreactor and a tubular photobioreactor, are evaluated in terms of biomass productivity and energy efficiency as a function of light provision. In particular, the effects of light intensity, light path length and the illumination surface area to volume ratio in each of the photobioreactors are considered. In the airlift photobioreactors, light is provided either externally or internally or as a combination of both, in order to determine whether or not the provision of internal illumination results in improved biomass productivity. The effect of using fluorescent and light-emitting diode (LED) light sources on the biomass productivity obtained in the airlift and flat plate photobioreactors is also assessed. Furthermore, the effect of varying light intensity, light fraction and cycle time on the maximum specific growth rate and biomass productivities obtained in the tubular photobioreactors is investigated. In each of the photobioreactors, adequate mixing and excess CO_2 are provided to ensure that growth is not limited by mass transfer.

1.2 Thesis structure

In Chapter 2, a literature review is presented to review algal growth parameters. A comparison of the most commonly used photobioreactors (column, tubular, flat plate) is presented. The energy efficiency and the current challenges associated with different designs are also outlined. The materials, methods, reactor systems and data analysis used in this study are described in Chapters 3 and 4. While Chapter 3 describes the reactor systems available for the project, in Chapter 4 the design and construction of the flat plate and tubular reactor systems is described.

In Chapter 5, the effects of light intensity on the growth of *Scenedesmus sp.* and *Chlorella vulgaris* are presented. Based on these results, the species which could utilize the additional light intensity more effectively for growth is selected for the remainder of experimental work. Subsequently, the results obtained for investigating the effect of light intensity and configuration (external fluorescence and internal LED light sources) on the growth of *Scenedesmus sp.* are presented. The effect of an increase in temperature, which is caused both by the presence of internal illumination and an increase in light intensity, on growth is also investigated.

In Chapter 6, the effects of varying light intensity, light fraction and cycle time on the maximum specific growth rate of *Scenedesmus sp.* in the two tubular photobioreactors are presented. The results obtained for investigating the effects of light intensity on the growth of *Scenedesmus sp.* in the flat plate photobioreactor are also presented. Lastly, the performance of the vertical airlift, tubular and flat plate photobioreactors are assessed comparatively in terms of biomass productivity, light utilization and energy efficiency for the cultivation of *Scenedesmus sp*. cultures. The conclusions of this study are presented in Chapter 7 and their significance and limitations are discussed.

2. Literature Review

2.1 Introduction

2.1.1 Microalgae

Algae are photosynthetic organisms, representing a huge diversity of species that vary in colour, shape and size, and occur in a large variety of environments (Barsanti and Gualtieri, 2006). Microalgae are typically small (less than 2 mm in diameter) aquatic unicellular organisms whereas macroalgae are larger, multicellular organisms that can be seen without the aid of a microscope (Griffiths, 2011). Microalgae can be used to produce a wide variety of high value products such as nutritional supplements, pharmaceuticals, pigments, fine chemicals and secondary metabolites as well as different forms of bioenergy (Ugwu *et al.,* 2008; Molina *et al.,* 2001). The desire to exploit algae for CO_2 sequestration and bioenergy production requires good productivity at low energy input. Figure 2.1 illustrates some of the potential sources of energy that can be obtained from microalgae. According to Sheehan *et al.* (1998), some of the most commonly used species of microalgae for biodiesel production are green algae in the chlorophyta phylum. This literature review will consider phototrophic green algae only. In particular, focus will be placed on *Chlorella vulgaris* and *Scenedesmus sp.* because of the high specific growth rates as well as the high lipid contents that can be obtained from these species (Griffiths and Harrison, 2009).

2.1.2. Requirements for commercial production

Commercial production of microalgae has been limited because of the high capital and downstream processing costs as well as the high auxiliary energy demands associated with current cultivation systems (Posten, 2009; Eriksen, 2008; Borowitzka, 1999; Pulz and Scheibenbogen, 1998). Despite the high cost, renewed interest has been shown in the industrial cultivation of microalgae for bioenergy products because of the current problems of diminishing fossil fuels and global warming (Kunjapur and Eldridge, 2010; Ryu *et al.*, 2009; Usui and Ikenouchi, 1997). Producing a renewable source of energy from microalgae is advantageous for numerous reasons. As microalgae are photosynthetic organisms, carbon dioxide is utilized as a substrate during cultivation, thereby mitigating the effects of carbon dioxide emissions. In addition, algal biofuel is the preferable alternative to biofuel produced from food crops, in that higher areal yields are achieved

and competition with food crops is eliminated. Microalgae also have higher growth rates than terrestrial plants (Chisti *et al.,* 2007; Pulz, 2001).

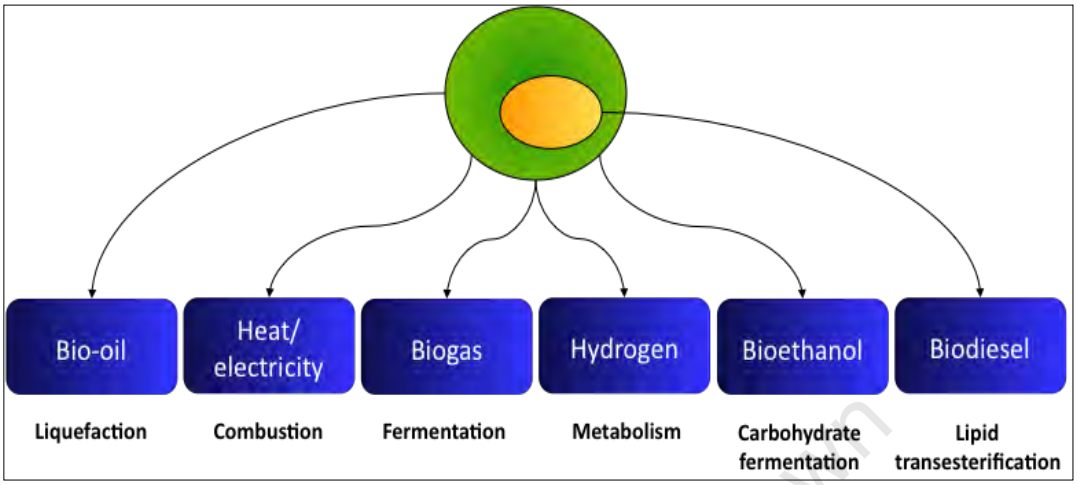

Figure 2. 1: Potential sources of energy that can be obtained from microalgae (Griffiths, 2011)

In order to make the commercial production of microalgae viable, a number of key factors need to be addressed. Firstly, microalgae species that exhibit high biomass productivities and can be cultivated in low cost photobioreactors and harvested cheaply should be sourced (Benemann, 2010). Secondly, a simple, low cost photobioreactor, of easy construction needs to be designed. Since microalgae are photosynthetic organisms, the current inefficiency of light utilization, a key factor limiting algal growth, needs to be optimized (Posten, 2009; Ogbonna and Tanaka, 2000; Janssen *et al.*, 2003). In a typical photobioreactor, as biomass concentration and the depth of culture increase, the amount of light that is able to penetrate the culture decreases exponentially. Thus, a fraction of the total photobioreactor volume remains dark and limits the overall biomass productivity that can be achieved (Richmond, 2004; Degen *et al.*, 2001). In order to improve light utilization, design parameters such as the incident surface area to culture volume ratio and the light path length need to be optimized (Carvalho *et al.*, 2006). The scope of this thesis is to optimise the supply and distribution of light to a photobioreactor in order to obtain maximum biomass productivities based on a rigorous understanding of the algal response to light. In particular, the effect of photobioreactor type (column, tubular and flat plate), light source as well as the related variation in light/dark cycling and intensity on algal growth and biomass productivity are investigated.

2.2 Algal growth requirements

Most microalgae utilize the process of photosynthesis to synthesize organic compounds directly from carbon dioxide, water, and light. The overall general reaction for photosynthesis is given by Equation 2.1.

$$nCO_2 + nH_2O + \text{light} \rightarrow (CH_2O)_n + nO_2 \quad (2.1)$$

Two main reactions occur during photosynthesis: the light and the dark reactions. The light reaction occurs in the thylakoid membrane. During the light reaction, photons are absorbed by photosynthetic pigments, primarily *chlorophylls* and *carotenoids*. The absorbed energy is used for the formation of adenosine triphosphate (ATP) and for the electron transfer from water (H_2O) to nicotinamide adenine dinucleotide phosphate (NADP). This reaction is illustrated by Equation 2.2 (Williams *et al.,* 2002):

$$8 \text{ photons} + 2H_2O + 2NADP^+ + 3ADP + 3Pi \rightarrow O_2 + 2H^+ + 2NADPH + 3ATP \quad (2.2)$$

The dark reaction does not necessarily occur in the dark, but does not require light energy. During this reaction, inorganic carbon is fixed and reduced via the Calvin Benson Bassham Cycle. The enzyme Ribulose – 1, 5 – bisphosphate carboxylase oxygenase (RuBisCo) plays a crucial role in catalysing this cycle. The net reaction is given by Equation 2.3 (Williams *et al.,* 2002):

$$6CO_2 + 18ATP + 12NADPH + 12H_2O \rightarrow C_6H_{12}O_6 + 18ADP^+ \; 18P_i + 12NADP^+ + 6H^+ \quad (2.3)$$

The light and dark reactions occur simultaneously as illustrated in Figure 2.2.

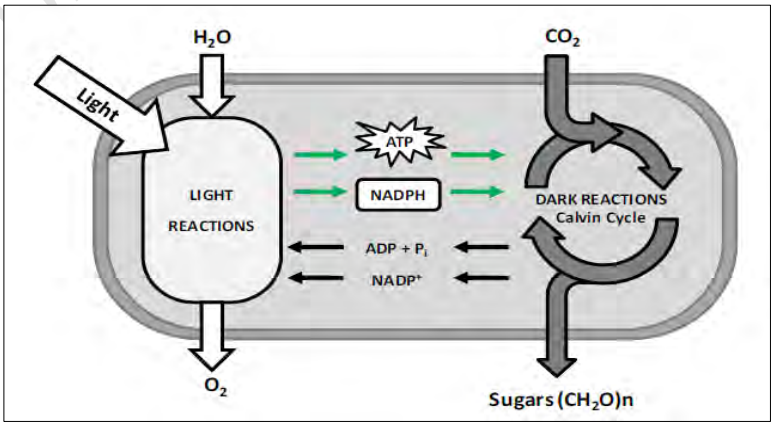

Figure 2. 2: Schematic of interaction between light and dark reactions during photosynthesis (Fraser, 2011)

In order to obtain optimal biomass productivity in a photobioreactor, the reactor design parameters in conjunction with the biological needs of the selected algal strain need to be considered. These key requirements for algal growth are illustrated in Figure 2.3 and are discussed in the ensuing sections.

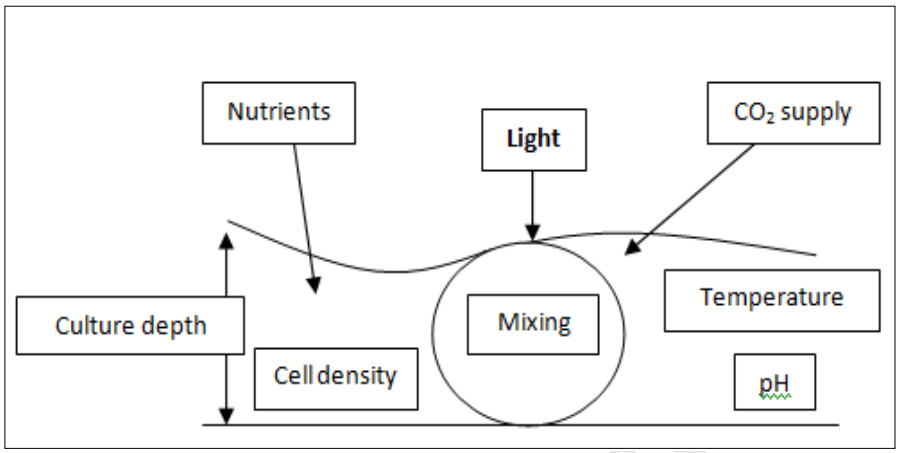

Figure 2. 3: Key variables associated with algal growth in a photobioreactor (Adapted from Grobbelaar, 2000)

2.2.1 Nutrient supply

The key nutrients required for microalgal growth are nitrogen and phosphorous, with diatoms, silicoflagellates and chrysophytes also requiring silicon (Anderson, 2005). Other nutrients required include carbon, oxygen, hydrogen, calcium, sodium, sulphur, potassium, chlorine and magnesium. Certain micro-elements required in trace amounts are iron (essential), boron, manganese, copper, molybdenum, vanadium, cobalt, nickel, silicon and selenium. The exact nutrient requirements is species specific (Chisti, 2007). Through limitation of nitrogen or phosphorus in the presence of an adequate carbon supply, the microalgae culture can be stressed into producing algal cells with higher lipid content. However, inducing stress impedes the growth rate. Hence there is a trade off between lipid content, lipid productivity and the overall biomass productivity (Kunjapur and Eldridge, 2010). The exact composition and the quantities of the nutrients used to cultivated *Chlorella vulgaris* and *Scenedesmus sp.* are provided in Section 3.1.2.

2.2.2 Temperature control

For most species of microalgae, optimal growth temperatures generally range from 16 to 35°C (Harrison *et al.,* 2010). In outdoor cultivation systems, low temperatures in the evenings and in winter can cause a significant reduction in growth rates. However, when

the temperature exceeds the optimal by only a few degrees, culture death occurs (Mata *et al.,* 2010). For example, Sanchez *et al.,* (2008) found that *Scenedesmus almeriensis* had an optimal growth temperature of 35°C and could withstand temperatures up to 45°C, beyond which cell death occurred. Typical temperature ranges and the optimal temperatures at which different algal species grow are presented in Table 2.1.

Table 2. 1: Typical temperature ranges and the optimal temperatures for growth of different algal species and strains

Species	T_{range} (°C)	$T_{optimal}$ (°C)	Reference
Scenedesmus sp. LX1	10-30	25	Xin *et al.* (2011)
Scenedesmus almeriensis	10-45	35	Sanchez *et al.* (2008)
Scenedesmus sp.	27-42	30	Westerhoff *et al.* (2010)
Chlorella 7-11-05	22-43	39	Sorokin (1960)
Chlorella pyrenoidosa	18-29	26	Sorokin (1960)
Chlorella vulgaris CCAP 211	25-38	30	Converti *et al.* (2009)

2.2.3 pH control

Most algae grow optimally within a pH range of 7 and 9 (Harrison *et al.,* 2010). According to Anderson (2005), pH control is important for two reasons. Firstly, the pH provides a measure of the acidity of a microalgae culture, which is known to have significant physiological effects on algal cells. Secondly, by controlling the pH, the equilibrium between aqueous CO_2 and HCO_3^- can be controlled (Figure 2.4). Hence, the amount of inorganic carbon available for photosynthesis can be controlled (Langley *et al.*, 2012).

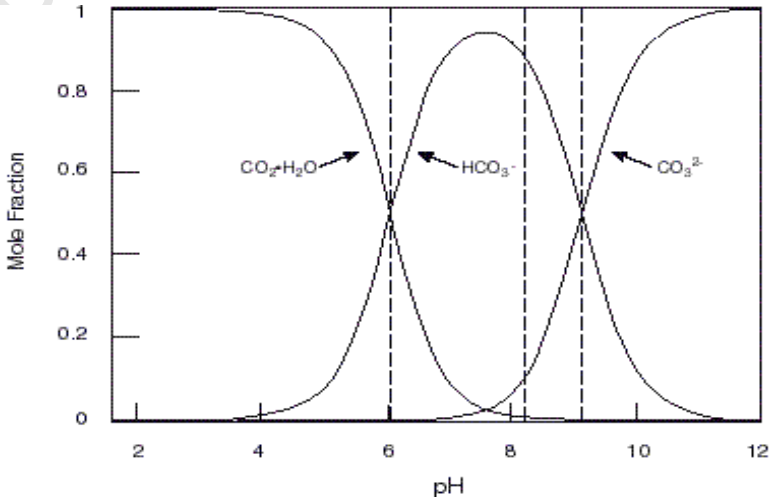

Figure 2. 4: Equilibrium between aqueous CO_2 and HCO_3^- as a function of pH (acmg.seas.harvard.edu)

2.2.4 CO_2 gas-liquid mass transfer

Adequate mass transfer of CO_2 from the gas phase into the liquid algal culture is essential to prevent any limitations on algal growth from CO_2 provision. The minimum carbon dioxide mass transfer rate required can be calculated on a stoichiometric basis if the carbon content of the biomass is known. For most microalgae, the stoichiometric CO_2 requirement is approximately 1.85 g CO_2/g biomass or higher (Posten, 2009). According to mass transfer theory, the rate of mass transfer of CO_2 is dependent on the overall mass transfer coefficient and the concentration driving force between the saturation concentration of CO_2 and the instantaneous concentration of CO_2 in the liquid phase. The rate of mass transfer of CO_2 can be calculated using Equation 2.4 (Chisti, 2002). Thus, it is evident that the overall mass transfer coefficient can be used to provide an indication of the CO_2 mass transfer capability of a specific cultivation system. The overall mass transfer coefficient is a function of the reactor design parameters and operating conditions. In particular, it is highly dependent on bubble size, the agitation rate, temperature, superficial gas velocity and media composition (Chisti, 2002; Posten, 2009). Typically, most photobioreactors operate with k_La values between 0.002 and 0.02 s^{-1} (Ugwu *et al.*, 2008). However, for practical reasons $k_La(O_2)$ is easier to measure accurately than $k_La(CO_2)$. There is general consensus (Chisti, 2002; Hulatt and Thomas, 2011; Molina *et al*., 1999) that $k_La(O_2)$ can be converted to $k_La(CO_2)$ representatively using Equation 2.5.

$$\frac{dC_L}{dt} = k_L a(C^* - C_L) \tag{2.4}$$

where:

- k_La is the overall mass transfer coefficient (s^{-1})
- C* is the saturation concentration of CO_2 in the media ($g.L^{-1}$)
- C_L is the actual liquid concentration of CO_2 in the media ($g.L^{-1}$)

$$k_L a(CO_2) = k_L a(O_2)\left[\frac{D_{CO_2}}{D_{O_2}}\right]^{0.5} \tag{2.5}$$

where:

- D_{CO2} is the diffusivity of CO_2 in water ($m^2.s^{-1}$)
- D_{O2} is the diffusivity of O_2 in water ($m^2.s^{-1}$)

2.2.5 Light

2.2.5.1 Qualitative light requirements for algal growth

Light requirement

In most green algae, the pigments *chlorophyll a* and *chlorophyll b* are most commonly used to absorb light for photosynthesis. The absorption spectra for these photosynthetic pigments indicate strong absorbance in blue light (410 to 500 nm) and red light (620 to 700 nm). This is illustrated in Figure 2.5. It can also be seen that low absorbance of light occurs in green light (500-600 nm). Another common pigment found in many algal species is *β-carotene* which absorbs blue light (400 to 500 nm). However, *β-carotene* does not play a significant role in photosynthesis (Kirk, 1994).

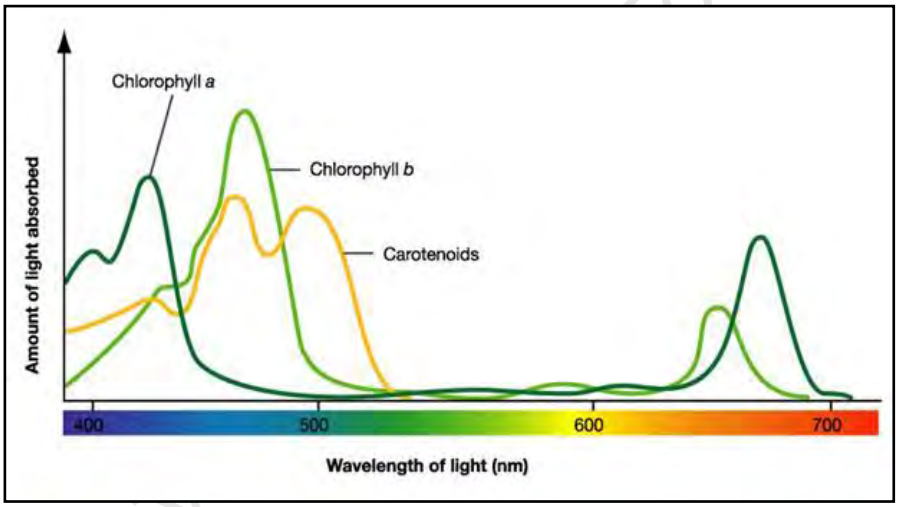

Figure 2. 5: Absorption spectra for photosynthetic pigments for most green algae species (UIC, 2010)

In order to optimize light utilization, it is important to select a light source which delivers light so that photon loss is minimized and hence the heat generated from unused wavelengths is minimized.

Light supply

In outdoor cultivation systems, the daily fluctuations in solar light intensity is the main factor that affects algal growth (Franco, 2011). The changes in solar cycles affects temperature which also has a significant effect on growth. South Africa has great potential for the exploitation of solar energy to cultivate microalgae commercially.

Figure 2.6 illustrates the average annual irradiation received in the different provinces of South Africa in 2008. It can be observed that parts of the Northern Cape received the greatest amounts of irradiation, that were between 7500-8000 W $h.m^{-2}.day^{-1}$. On average, most of the country received between 5895-7000 W $h.m^{-2}.day^{-1}$. Based on the conversion factor of 18.7 kJ $s.d^{-1}.\mu mol^{-1}$ for converting between $kJ.m^{-2}.day^{-1}$ and $\mu mol.m^{-2}.s^{-1}$ (Hall *et al.*, 1993; Converti *et al.*, 2006), it was calculated that the ranges of maximum and average irradiation received per day could be expressed as 1438-1534 $\mu mol.m^{-2}.s^{-1}$ and 1130-1341 $\mu mol.m^{-2}.s^{-1}$ respectively.

In laboratory cultivation systems, artificial lighting is used to investigate algal growth under controlled conditions. Currently, the most common sources of artificial light are halide lamps, incandescent lamps, halogen and fluorescent lights (Harrison *et al.,* 2010). According to Geider and Osbourne (1996), most types of light bulbs emit light within a specific region of the visible spectrum. For example, metal halide bulbs emit a low amount of red light whereas incandescent and halogen bulbs emit low amounts of blue light (Langley, 2010). At present, fluorescent light bulbs are most commonly used because they emit a more evenly distributed spectrum of light, which is very similar to sunlight (Geider and Osbourne, 1996). However, one of the major problems associated with these types of light sources is heat generation which means an increase in temperature.

In previous years, light-emitting diodes (LEDs) were not used primarily because they were unable to provide sufficiently high light intensities. However, with recent technological developments, LEDs have become a viable option. The main advantages associated with LEDs are that they are cheap, energy efficient, durable and compact. In addition, LEDs can operate within a narrow spectral output for photosynthesis, meaning that heat generation from the emission of light at unusable frequencies can be avoided (Lee and Palsson, 1994; Posten, 2009).

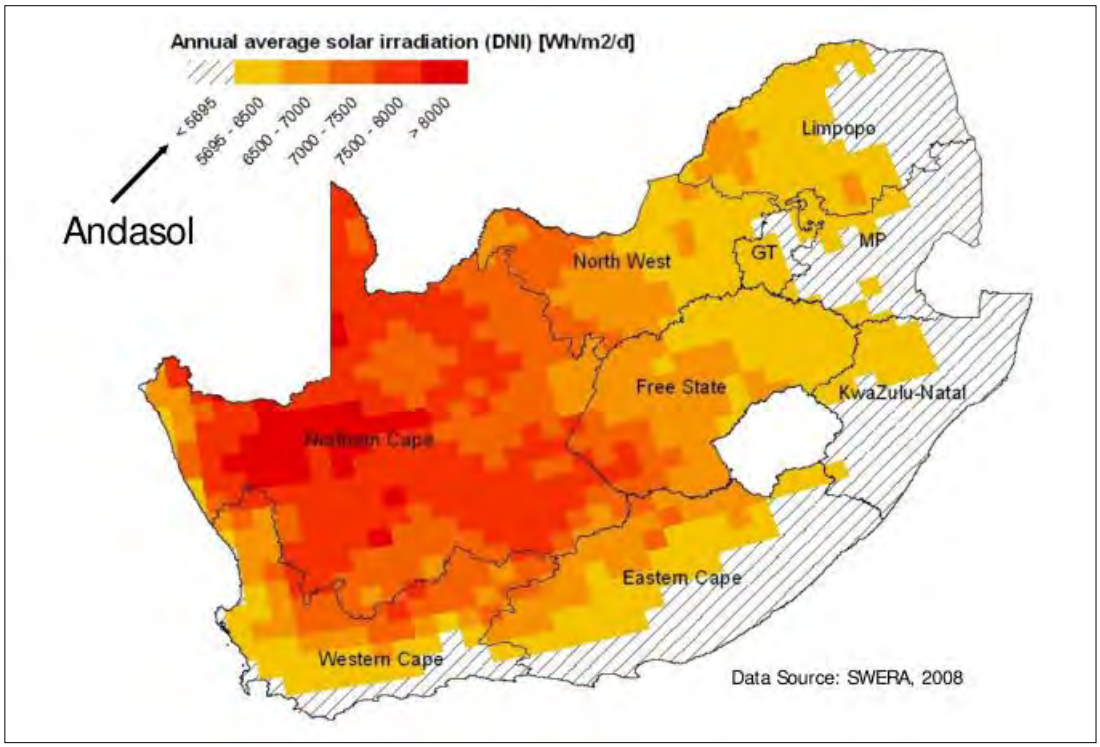

Figure 2. 6: Annual average solar irradiation map for South Africa (SWERA, 2008)

2.2.5.2 Quantitative light requirements for algal growth

Light delivery and distribution

In a typical photobioreactor, as the depth of the cell culture increases, the penetration of light into the photobioreactor decreases. Furthermore, the penetration of light into the photobioreactor further decreases as the cell density increases (Langley *et al.*, 2012; Janssen *et al.*, 2000). This occurs because of mutual shading by the algal cells via adsorption by the pigments or via scattering of the cells (Posten, 2009). Hence there is always a fraction of the total photobioreactor volume that is dark.

Thus, there are four lighting zones that exist simultaneously in a photobioreactor: complete dark, light limitation, light saturation and light inhibition zones (Ogbonna and Tanaka, 2000). This is illustrated in Figure 2.7. In the light limited region, insufficient light is available to sustain the maximum rate of the light dependent reactions and thus, the photosynthetic rate is limited. In the light saturation region, maximum biomass productivity is achieved. However, any further increase in light intensity results in photoinhibition, leading to a decrease in the photosynthetic rate. During photoinhibition, over absorption of photons occurs, resulting in a decrease in the photochemical efficiency of functional reaction centres (Barsanti and Gualtieri (2006), Wu and Merchuk (2001)

postulated that excessive light exposure causes temporary damage to the chromophores D1 proteins. Algal cells are able to reverse and recover from the effects of photoinhibition with time, however excessive exposure over time can lead to cellular death. It is important to note that above a certain light intensity, growth is inhibited. The light intensity at which this occurs is species specific. Ideally, maximal biomass productivity would be obtained if light at the saturation intensity were homogeneously distributed within the entire photobioreactor; however, this is not readily attainable for a scalable photobioreactor.

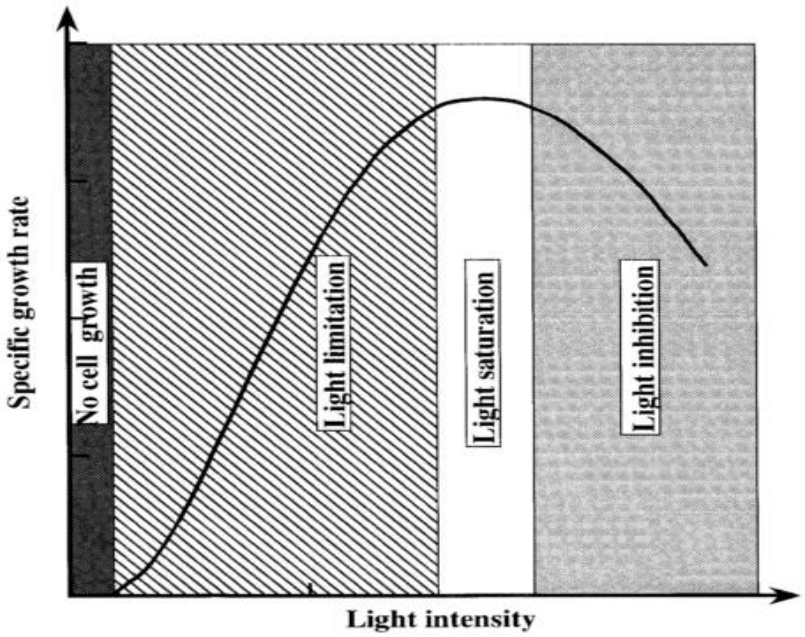

Figure 2. 7: Effect of light intensity on photoautotrophic growth of photosynthetic cells (Ogbonna and Tanaka, 2000)

Photosynthetic efficiency

The photosynthetic efficiency of a photobioreactor is defined as the fraction of light energy converted to chemical energy, where light is supplied in the photosynthetic activation range (400-700 nm) and can be calculated using Equation 2.6 (Franco, 2011; Converti *et al.*, 2006; Watanabe and Saiki, 1997). Theoretically, the maximum photosynthetic efficiency that can be achieved in the photosynthetic activation range is 18.1% (Pulz and Scheibenbogen, 1998; Pulz, 2001). However, according to literature, most photobioreactors have been reported to achieve a photosynthetic efficiency of between 5–9% because of poor light utilization in photobioreactors (Eriksen 2008; Carvalho *et al.*, 2006; Tamburic *et al.*, 2011).

$$PE = \frac{r_g H_g \times 100}{IPAR} \quad (2.6)$$

where:

- PE is the photosynthetic efficiency (%)
- r_g is the maximum daily growth rate (g DW.day^{-1})
- H_g is the enthalpy of dry biomass (kJ.g^{-1} DW)
- IPAR = PAR (kJ.m^{-2}.day^{-1}) x illumination surface (m^2)

2.2.5.3 Effect of altering light conditions on algal growth

Diurnal Cycling

In outdoor algal cultivation systems, growth is mainly dependent on the daily solar cycles. The fluctuations of light intensity, both on a daily basis as well as on a seasonal basis, have a significant effect on the growth rate of algae. In addition, the light intensity has a direct effect on the temperature of the system which also has a significant effect on the growth rate (Sanchez *et al.,* 2008). Temperature regulation is important, especially achieving this in a cost effective manner for large scale cultivation. In comparison to closed photobioreactors with constant illumination, the aerial biomass productivities achieved in open systems with natural light are typically much lower (Ugwu *et al.,* 2008). However, it should be noted that in all cultivation systems as microalgae cultures grow and become denser, the efficiency of light utilization decreases (Richmond, 2004). In addition, other factors that can account for the lower productivities in outdoor cultivation systems could include inefficient mass transfer, evaporative losses and contamination by predatory species (Ugwu *et al.,* 2008). Direct comparison of indoor and outdoor cultivation is rare. Typically, these comparisons are made across very different reactor systems, hence these additional factors.

Light/dark cycling

Shown in Figure 2.7, the four lighting zones that exist simultaneously in a photobioreactor are: complete dark, light limitation, light saturation and light inhibition zones. By applying different mixing regimes in a photobioreactor, light utilization can be improved through minimizing the effects of mutual shading and photoinhibition by cycling the algal cells through the light and dark zones illustrated in Figure 2.7

(Janvanmardian and Palsson, 1991). An increase in mixing can promote higher light/dark cycling frequencies. According to Posten (2009), significantly higher biomass productivities can be obtained when using light/dark cycles between 1 Hz and 1 kHz. However, the frequency should be selected giving cognisance to the algal species response to mixing intensities i.e. above a certain degree of mixing the algal cells can be damaged through shear stress (Wu and Merchuk, 2004). It is important to note that the frequency of light/dark cycling in a photobioreactor also depends on the culture density and the photobioreactor design (Richmond, 2004). In addition, by increasing the mixing intensity, the energy requirement for the process increases substantially thus leading to an increase in cost (Richardson, 2011; Pegallapati and Nimalakhandan, 2011).

2.2.6 Mixing and hydrodynamics

The most common methods of providing adequate mixing in photobioreactors are through using the air-lift principle, sparging, static mixers, impellers, paddles and baffles (Ugwu *et al.,* 2008; Posten, 2009). Mixing is essential for keeping the algal cells in suspension, eliminating thermal and light stratification and promoting adequate mass transfer (Lee and Palsson, 1994; Richmond, 2004; Grobbelaar, 2000). Sufficient mixing is also essential for preventing a build up of dissolved oxygen in the microalgae culture, which can inhibit photosynthesis (Richmond, 2004). As discussed in Section 2.2.5.3, high mixing rates can improve light utilization by cycling algal cells through the light and dark zones of a photobioreactor at high frequencies.

However, when considering mixing, it is important to take into account shear stress. According to Wu and Merchuk (2004), the critical shear stress for a cultivation system can be defined as the amount of shear stress required to cause cell disruption. Alternatively, this could be defined in terms of impaired metabolic activity. The critical shear stress is species specific. It is important to note, that while higher mixing rates provide enhanced supply of light and CO_2 to cells, they require a substantial increase in energy input to the cultivation system, thereby increasing the cost (Richardson, 2011).

2.3 Energetic evaluation of photobioreactors

Commercial production of microalgae, particularly for bioenergy, has been limited because of the high capital cost as well as the high auxiliary energy demands associated with current cultivation systems. Thus, it is important to consider the biomass

productivity per unit power input as well as the net energy ratios achieved when evaluating the performance of a photobioreactor.

2.3.1 Calculation of energy input of photobioreactors

The energy input to a photobioreactor includes the light energy required for illumination and the mechanical energy required for aeration and mixing. Where natural sunlight is used, only the mechanical energy for mixing and mass transfer need be considered.

The energy input for illumination can be quantified as the light supply coefficient which is defined as the amount of light energy supplied to a photobioreactor per unit culture volume and can be calculated using Equation 2.7 (Pegallapati and Nirmalakhandan, 2011). It should be noted that the conversion factor of 1 $\mu mol.m^{-2}.s^{-1}$ = 0.2176 J (Ogbonna *et al.*, 1995) was used to convert the light energy input from $\mu mol.m^{-3}.s^{-1}$ to $W.m^{-3}$.

$$E_L = \frac{0.22 I_O A}{V} \tag{2.7}$$

where:

- E_L is the energy input per unit culture volume ($W.m^{-3}$)
- I_O is the light intensity per unit incident area ($\mu mol.m^{-2}.s^{-1}$)
- A is the incident area (m^2)
- V is the culture volume (m^3)

According to Chisti (1998), in airlift photobioreactors, mixing energy includes both the energy required for the isothermal expansion of gas as it moves up the reactor and the kinetic energy of the gas supplied at the injection point of the reactor. The kinetic energy contribution can be neglected as it typically contributes less than 1.5% of the energy provided by the isothermal expansion of gas. The mixing energy inputs per unit culture volume for airlift and bubble column photobioreactors can be calculated from Equations 2.8 and 2.9 respectively. The key differences between airlift and bubble column photobioreactors are discussed in detail in Section 3.4.2.2.

For airlift photobioreactors:

$$E_{M,A} = \left\lfloor \frac{\gamma U_g}{1 + \frac{A_d}{A_r}} \right\rfloor \tag{2.8}$$

For bubble column photobioreactors:

$$E_{M,B} = \frac{Q\gamma h}{V} \tag{2.9}$$

where:

- $E_{M,A}$ is the energy input per unit culture volume for airlift bioreactors ($W.m^{-3}$)
- γ is the specific weight of the broth ($N.m^{-3}$)
- U_g is the superficial gas velocity ($m.s^{-1}$)
- A_r is the cross-sectional area of the riser (m^2)
- A_d is the cross-sectional area of the downcomer (m^2)
- $E_{M,B}$ is the energy input per unit culture volume for bubble columns ($W.m^{-3}$)
- Q is the volumetric gas flow rate ($m^3.s^{-1}$)
- h is the culture depth (m)

2.3.2 Calculation of biomass productivity per unit power input

The biomass productivity per unit power input is defined as the biomass productivity achieved per unit power input. Typically, the total power input to a photobioreactor includes both the light and mixing energy inputs and Equation 2.10 can be used to calculate the biomass productivity per unit power input. For the case where the light energy requirement would be provided from solar irradiation, Equation 2.11 can be used to calculate the biomass productivity per unit mechanical power input (Pegallapati and Nirmalakhandan, 2011).

$$P / E = \frac{P}{E_L + E_M} \tag{2.10}$$

$$P / E_M = \frac{P}{E_M} \tag{2.11}$$

where:

- P/E is the biomass productivity per unit power input ($g.W^{-1}.day^{-1}$)
- P/E_M is the biomass productivity per unit mechanical power input ($g.W^{-1}.day^{-1}$)
- P is the volumetric biomass productivity ($g.L^{-1}.day^{-1}$)

2.3.3 Calculation of net energy ratio

The net energy ratio (NER) of a cultivation system is defined as the ratio of the amount of energy accumulated in the biomass produced and the process energy requirement and can be calculated using Equation 2.12 (Burgess and Fernandez-Velasco, 2007; Richardson, 2011).

$$\text{NER} = \frac{\text{Energy out}}{\text{Energy in}} = \frac{\text{Energy accumulated in biomass}}{\text{Energy input}} \tag{2.12}$$

2.4 Photobioreactor design

2.4.1 Open and closed cultivation systems

Microalgae can either be cultivated in open or closed systems. Open systems consist primarily of natural systems such as ponds, lakes and lagoons or of artificial systems such as containers. The most commonly used type of open system in industry is the raceway pond (Figure 2.8). The shallow algal culture (< 30 cm) is continuously circulated through the raceway pond by a paddle wheel and CO_2 is sparged at multiple points throughout the photobioreactor (Fraser, 2011; Ugwu *et al.,* 2008; Kunjapur and Eldridge, 2010). Although open ponds can be used effectively for the mass production of certain algal species that grow at extreme conditions, their main shortcoming is their low biomass productivity. According to Chisti (2007) and Pulz (2001), biomass productivities of between 0.05 and 0.1 $g.L^{-1}.day^{-1}$ can be achieved in outdoor pond systems. These low productivities may be attributed to poor light utilization, inefficient mass transfer, evaporative losses and contamination by predatory species (Ugwu *et al.,* 2008).

For the production of high-value commodities from algae, the use of closed photobioreactors (transparent plastic bags, vessels and tubes) is preferred primarily because of the greater degree of control that is available over the process parameters (Ugwu *et al.,* 2008; Pulz, 2001). Thus, many of the limitations of using open ponds can be overcome. The biomass productivities obtained in closed photobioreactors are comparatively much greater than the productivities that can be attained in open systems. For closed systems, biomass productivities of between 0.8 and 1.3 $g.L^{-1}.day^{-1}$ can be achieved (Pulz, 2001). However, closed photobioreactors are more costly to build and operate as the energy demands for aeration and illumination are far greater than open systems. The advantages and disadvantages associated with open and closed cultivation systems are illustrated in Table 2.2.

Figure 2. 8: Seambiotic Ltd. Commercial Scale raceway ponds (http://www.seambiotic.com)

Table 2. 2: Comparison of open and closed algal cultivation systems (Adapted from Pulz, 2001)

Parameter	Open cultivation system	Closed cultivation system
Process Control	Low	High
Contamination risk	High	Low
Amount of space required	High	Low
Biomass productivity	Low	High
Energy input required	Low	High
Reproducibility of production	Low	High
Overall cost	Low	High

2.4.2 Closed photobioreactors

As mentioned in Section 2.2.5, the most prominent factor limiting algal growth is the inefficient utilization of light (Carvalho *et al.*, 2006). Thus, a crucial parameter to consider when designing a photobioreactor is the surface area for light provision. A high surface area to volume ratio can provide algal cells in a photobioreactor with more frequent exposure to the external light source, thus increasing the biomass productivity and improving the photosynthetic efficiency (Tamburic *et al.*, 2011). According to Posten (2009), most photobioreactors typically have a surface area to volume ratio within the range of 80-100 $m^2.m^{-3}$. The mixing regime of a photobioreactor is also a key parameter to consider, as the mixing rate has a direct impact on the mass transfer properties of the systems as well as on the frequency of light/dark cycling. Currently, the three most common types of photobioreactors used in industry to meet these requirements are column, tubular and flat-plate photobioreactors (Carvalho *et al.*, 2006).

2.4.2.1 Flat plate photobioreactors

Flat plate photobioreactors typically consist of two sheets that are glued together to form a photobioreactor (Posten, 2009). The light path length (width) is generally in the range of 1.3-10 cm (Carvalho *et al.,* 2006). Mixing and aeration is provided by sparging with CO_2 enriched air (Tamburic *et al*., 2011). The main advantage of using a flat plate photobioreactor is the high surface area to volume ratio that can be attained, which leads to improved light utilization. Reducing the light path length can also result in an increase in light utilization and hence the biomass productivity. According to literature, flat plate photobioreactors with very short light path lengths ($\leq$ 1 cm) have been reported to support

high density algal cultures which can exceed 80 g. L^{-1} in extreme cases (Eriksen, 2008; Hu *et al.*, 1998). However, the key disadvantages associated with flat plate photobioreactors are temperature control and issues with mixing such as hydrodynamic stress for certain algal species (Ugwu *et al.*, 2008; Kunjapur and Eldridge, 2010). Figure 2.9 illustrates an example of pilot-scale flat plate photobioreactor units at the University of Almeria in Spain. Molina Grima reported that in 2008, the 5.0 m^3 cultivation units achieved a biomass productivity of 0.6 $g.L^{-1}.day^{-1}$ (Lehr and Posten, 2009; Zemke *et al*., 2007).

Figure 2. 9: Photograph of "green wall panel" photobioreactors (GWP) at the University of Almeria in Spain (Lehr and Posten, 2009)

2.4.2.2 Vertical column photobioreactors

Vertical column photobioreactors can be categorized as bubble columns or airlift reactors. A bubble column photobioreactor consists of a single cylinder in which microalgae is cultivated. Typically, aeration of the culture is provided at the base of the photobioreactor and the air traverses once through the reactor with little axial mixing. An airlift photobioreactor is similar to a bubble column, but contains a central draft tube to superimpose a defined flow pattern and promote more effective axial mixing. The presence of the draft tube enables one to separate the photobioreactor into three regions: the riser which is the section inside the draft tube for an internal circulation airlift, the downcomer and the gas separator (Wu and Merchuk, 2004; Fraser, 2011). The key

differences between the two types of photobioreactors are illustrated in Figure 2.10. Furthermore, variation in the arrangement of the riser and downcomer (external loop, split cylinder or inclined configurations) have been reported (Chisti, 1989). It is evident that one of the main advantages of airlift photobioreactors are the well defined liquid circulation patterns, whereas in bubble columns, liquid circulation is random (Chisti, 1989). Hence, both the photosynthetic efficiency of an airlift photobioreactor and its mass transfer rate can be improved by altering the gas flow rate, which will directly affect the light/dark cycle frequency. However, it is difficult to assess from literature, whether airlift or bubble column photobioreactors are better for algal cultivation. Certain studies reported that airlift photobioreactors achieved higher biomass productivities than bubble column photobioreactors, operated under similar experimental conditions (Merchuk *et al.*, 2000; Kaewpintong *et al.*,2007; Degen *et al.*, 2001) However, other studies found that airlift and column photobioreactors performed similarly and achieved similar biomass productivities (Chiu *et al.*, 2009; Janssen *et al.,* 2003; Miron *et al.,* 2002).

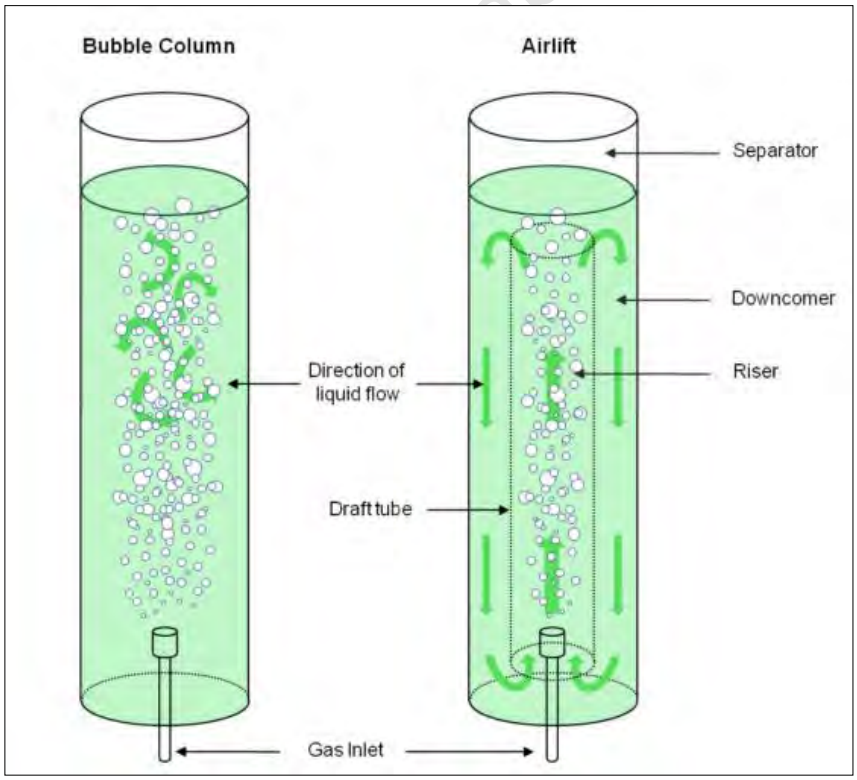

Figure 2. 10: Diagrams of bubble column and airlift photobioreactors (Fraser, 2011)

However, one of the main disadvantages associated with scaling up vertical airlift and bubble column photobioreactors is that the surface area to volume ratio available for light

exposure decreases significantly as the column diameter increases. As a result less light is able to penetrate the algal culture, leading to a decrease in biomass productivity and the photosynthetic efficiency (Ugwu *et al.*, 2008; Carvalho *et al.*, 2006).

2.4.2.3 Tubular photobioreactors

Tubular photobioreactors are generally considered to be the best option for algal cultivation because of the high surface area to volume ratio (>100 m^{-1}) that is available for light exposure (Ugwu *et al.*, 2008). Aeration and mixing is typically provided using an airlift pump (Carvalho *et al.*, 2006). Figure 2.11 illustrates an example of the commercial scale Bisantech plant in Germany. The cultivation system is made up of 20 units of 35 m^3 tubular photobioreactors. Each unit consists of 4 cm ID glass tubes with a total length of 25 000 m. It was reported that the annual production volume was approximately 100 $t.a^{-1}$ (Posten, 2009; Eriksen, 2008). Although it is evident that tubular photobioreactors can achieve higher biomass productivities than open systems, there are numerous limitations that become more evident with scale-up. For example, mass transfer becomes limited which subsequently leads to a build up of dissolved oxygen in the tubes, as the overall length is increased. Furthermore, increasing the diameter of the tubes leads to a decrease in the surface area to volume ratio, which leads to less light penetration, and as a result a decrease in biomass productivity. It is also difficult to control the culture temperature, which can become expensive to regulate (Ugwu *et al.*, 2008).

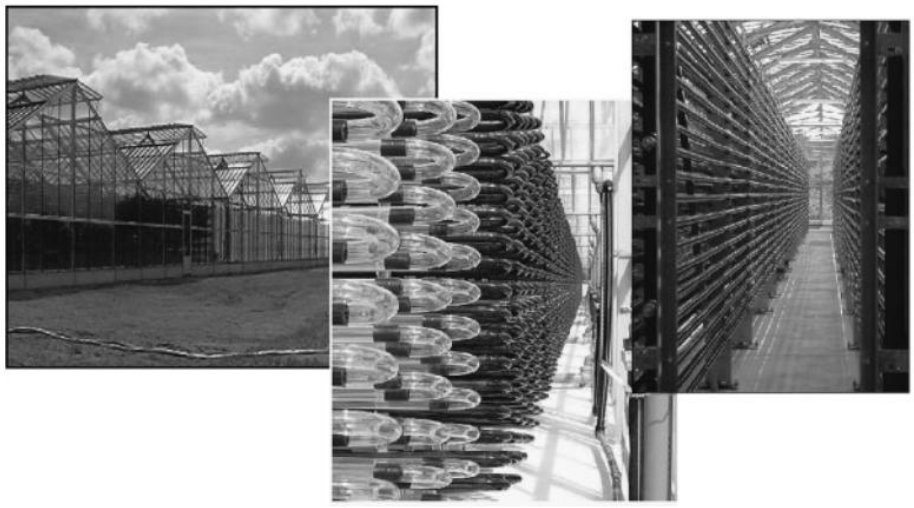

Figure 2. 11: Photographs of Bisantech tubular photobioreactor in Germany, with kind permission of Bioprodukte Prof. Steinberg GmbH (Posten, 2009)

2.4.2.4 Internally illuminated photobioreactors

In order to improve light delivery and distribution, a number of internally illuminated photobioreactors with built-in transparent compartments and different light supply systems have been designed and developed (Pulz and Scheibenbogen, 1998; Posten, 2009). In some studies, light was provided directly from artificial light sources such as fluorescent light bulbs and light emitting diodes (LEDs) (Lee and Palsson, 1994; Nirmalakhandan and Pegallapati, 2011), whereas in other studies, light from solar, artificial or a combination of the two light sources, was first captured by a solar collector and then transmitted via optic fibres to internal light distribution plates inside the photobioreactor (Janssen *et al.*, 2003; Javanmardian and Palsson, 1991; Usui and Ikenouchi, 1997; Ogbonna *et al.*, 1999).

In a study performed by Lee and Palsson (1994), the effect of using 680 nm monochromatic red LEDs on the growth of *Chlorella vulgaris* in a vertical flat plate photobioreactor was investigated. Two LED units were mounted on 5.08 cm x 10.16 cm printed circuit boards that were placed on either side of the photobioreactor and provided an overall average light intensity of 1058 $\mu mol.m^{-2}.s^{-1}$. Adequate mass transfer was provided by internally sparging 100 $mL.min^{-1}$ of air enriched with 5% CO_2, via four 3 mm ID nozzles that were placed half an inch apart from the base of the photobioreactor. The main findings of this study illustrated that cell concentration greater than 2 x 10^9 $cells.mL^{-1}$ were attained when a shorter light path of 1.00 cm as opposed to 1.55 cm was used. However, Lee and Palsson (1991) did not provide biomass productivity in terms of dry weight. It should be noted that the dimensions of the photobioreactor were not provided. Thus, the energy efficiency of the reactor could not be evaluated.

Pegallapati and Nirmalakhandan (2011) investigated the effect of providing internal fluorescent lighting on the growth of *Scenedesmus sp.* in an 18 L column photobioreactor. A schematic of the photobioreactor design is illustrated in Figure 2.12. Two 30 W fluorescent light bulbs were installed within the inner tube and provided an average light intensity of 91.4 $\mu mol.m^{-2}.s^{-1}$. The algal culture was sparged with air enriched with carbon dioxide (4% CO_2) at a gas flow rate of 800 $mL.min^{-1}$, through four porous silica diffusers located at the base of the photobioreactor (Figure 2.12). The authors found that

the annular internally illuminated photobioreactor achieved a biomass productivity of 0.40 $g.L^{-1}.day^{-1}$.

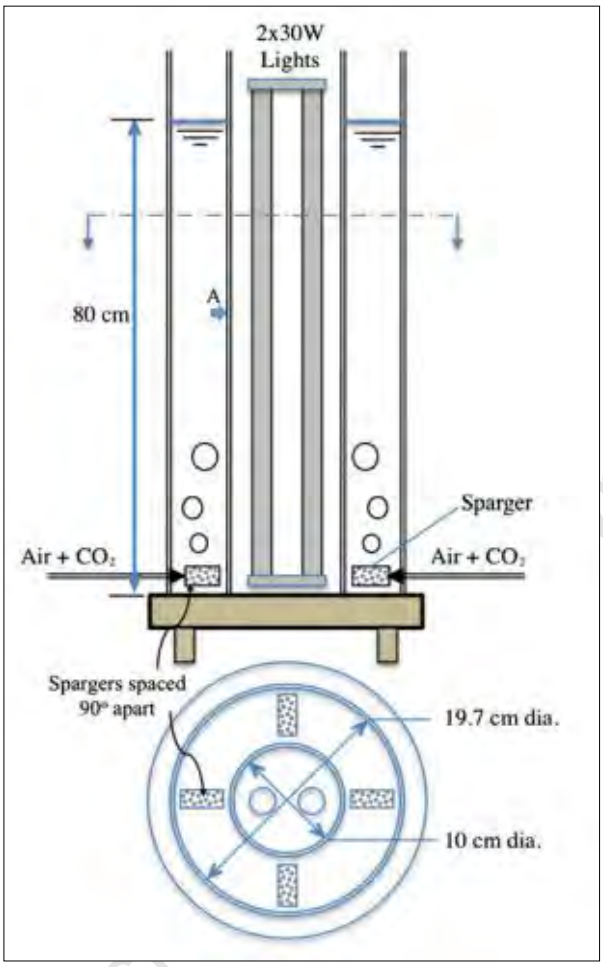

Figure 2. 12: Schematic of annular internally illuminated photobioreactor (Pegallapati and Nirmalakhandan, 2011)

Janssen *et al.* (2003) proposed the design of a 132.5 m^3 photobioreactor that would effectively utilize sunlight for biomass production from *Chlorella vulgaris*. Figure 2.13 shows the basic design of the vertical airlift flat plate photobioreactor with 80 internally illuminated plates, which were 0.03 m thick and placed 0.03 m apart. Aeration would be provided via nozzles placed between the plates and the area between the two central plates would act as a downcomer. The authors estimated that if the photobioreactor was supplied with light intensities of between 1200-2000 $\mu mol.m^{-2}.s^{-1}$ at the surface of the redistribution plates, a theoretical biomass productivity of 2.1 $g.L^{-1}.day$ could be achieved. However, this estimation is subject to a large number of assumptions and missing data. For example, the authors did not provide any information about the composition and flow rate of the gas feed. They estimated that a 20% loss of light would occur during transmission of light through the optic fibres to the photobioreactor.

However, no reason, or basis for selecting this percentage was provided. A similar lab-scale cultivation system was developed by Javanmardian and Palsson (1991). These authors found that a 600 mL internally illuminated cylindrical photobioreactor, using a Xenon lamp at 78 $\mu mol.m^{-2}.s^{-1}$ and supplied with a gas flow rate of 300 $mL.min^{-1}$, achieved a biomass productivity of 0.06 $g.L^{-1}.day^{-1}$ for *Chlorella vulgaris.* In another study performed by Ogbonna *et al.* (1999), a 3.5 L internally illuminated stirred tank photobioreactor was supplied with solar illumination via optic fibres which transported light to illumination plates that were spaced 4.6 cm apart within the photobioreactor. When the light intensity dropped below 50 $\mu mol.m^{-2}.s^{-1}$, a light intensity sensor triggered an automated response that switched on a metal halide lamp. The stirred tank photobioreactor was sparged with air enriched with 5% CO_2 at 0.3 vvm and was operated at an agitation speed and cultivation temperature of 120 rpm and 36°C respectively. At these conditions, the authors found that the biomass productivity of *Chlorella sorokiniana* varied from 0.11 to 0.30 $g.L^{-1}.day^{-1}$, depending on the daily fluctuations in the average solar light intensity.

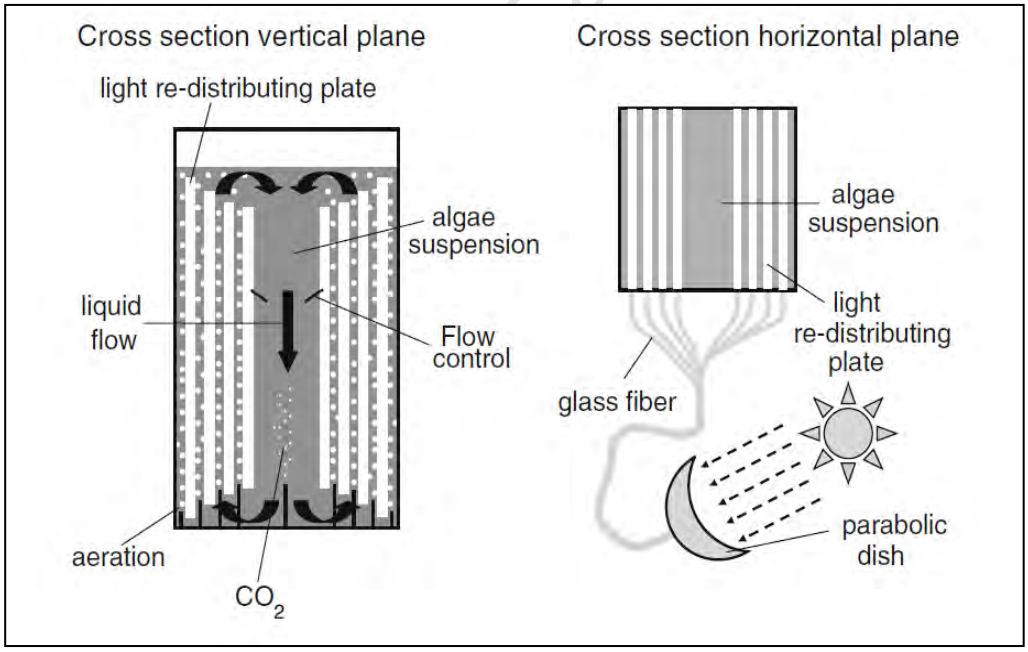

Figure 2. 13: Design of rectangular airlift photobioreactor with optic fibres and light redistributing plates (Janssen *et al.*, 2003)

It should be noted that there are key disadvantages associated with internally illuminated photobioreactors. Providing internal illumination in photobioreactors causes an increase in culture temperature, which can become expensive to regulate. There are also a number of disadvantages associated with the use of fibre optics. Firstly, loss of light occurs at the

coupling points between different light guide fibres and during transport of the light through the fibres (Gordon, 2002; Ogbonna *et al.*, 1999). Secondly, light supplied from the fibres is not evenly distributed throughout the internal compartments within the photobioreactor. Another key disadvantage is the cost and complexity associated with scaling up a fibre optic based system.

2.4.3.4 Evaluation of photobioreactors compiled from literature

In order to evaluate the energy efficiency of different types of photobioreactors, performance data from literature for various photobioreactor systems was collected into Table 2.3. For this analysis, Equations 2.7 and 2.8 or 2.9 were used to calculate the light energy and the mixing energy inputs per unit culture volume respectively. Subsequently, the biomass productivity achieved per unit total power input and the biomass productivity achieved per unit mechanical power input were calculated using Equations 2.10 and 2.11 respectively. It should be noted that, in most studies, data for operational parameters such as the overall mass transfer coefficient (k_La) and liquid circulation time (t_c) were not reported. Thus, it is difficult to evaluate the efficiency of the different types of photobioreactors based on their hydrodynamic and mass transfer characteristics.

As can be seen from Table 2.3, the general trend observed across the different types of photobioreactors was that increasing both the incident surface area to culture volume ratio and the light intensity resulted in an increase in biomass productivity. This is indicative that light is a major factor limiting microalgal growth. For example, it can be seen that in the flat plate photobioreactor designed by Ratchford *et al.* (1992) when the light intensity was increased from 100 to 200 $\mu mol.m^{-2}.s^{-1}$, the biomass productivity increased by 14.7% and 11.6% for *Chlorella vulgaris* and *Scenedesmus sp.* respectively. However, it should be observed that with the increase in light intensity, the light energy input doubled and as a result the energy efficiency of the reactor in terms of the biomass productivity achieved per unit power input decreased by approximately 30% for both microalgae species. Furthermore, Degen *et al.* (2001) found that by reducing the light path length of a flat plate airlift photobioreactor from 30 mm to 20 mm, the incident surface area to volume ratio doubled. Thus, theoretically twice as many algal cells would be exposed to light at any given point in time. This is supported by the fact that Degen *et al.* (2001) found that reducing the light path resulted in an increase in biomass productivity from 0.045 $g.L^{-1}.day^{-1}$ to 0.11 $g.L^{-1}.day^{-1}$. However, it should be noted that the actual

dimensions of the photobioreactor were not provided. Thus, the energy efficiency of the reactor could not be evaluated. Table 2.3 also shows that the tubular photobioreactor designed by Converti *et al.* (2006) had the highest incident surface area to volume ratio and the shortest light path length of 0.01 m. It can be argued that due to the high degree of light exposure, the 5.50 L tubular photobioreactor could obtain a maximum biomass concentration of 10.6 $g.L^{-1}$ and a biomass productivity of 0.42 $g.L^{-1}.day^{-1}$ for a culture of *Spirulina platensis*. Although insufficient information was available to calculate the mixing energy input, it was reported that the tubular photobioreactor achieved an energy efficiency of 0.22 $g.W^{-1}.day^{-1}$. The low energy efficiency of the tubular photobioreactor may be attributed to the high light energy input as well as the high mixing energy input that may have been required to sustain adequate mass transfer and prevent wall growth (Ugwu *et al.*, 2008; Carvalho *et al.*, 2006; Lehr and Posten, 2009).

Degen *et al.* (2001) also investigated the difference in performance between an airlift flat plate photobioreactor and a bubble column photobioreactor. The dimensions and shapes of the two reactors were identical, with the exception being that the airlift reactor contained internal baffles. These authors found that the biomass productivity of the airlift photobioreactor was 1.6 times greater as compared to the bubble column. The higher biomass productivity in the airlift photobioreactor can be attributed to the well defined liquid circulation patterns in the airlift reactor compared to the bubble column (Chisti, 1989). Furthermore, the presence of baffles promoted better mixing which could have improved the mass transfer rate. However, this is in conflict with the findings of Chui *et al.* (2009) who also investigated the difference in performance between a vertical column internal loop airlift photobioreactor and a bubble column photobioreactor (Figure 2.9). From Table 2.3, it can be seen that both reactor configurations achieved similar biomass productivities (0.59-0.63 $g.L^{-1}.day^{-1}$). The only significant difference between the reactors was the fact that the mixing energy required in the airlift photobioreactor was approximately four times greater as compared to the bubble column. Since both reactors were sparged with the same volume of gas per unit culture volume per min, the difference in the mixing energy requirement may be attributed to the different reactor configurations. In the airlift photobioreactor, the ratio of the areas of the downcomer and riser was 4.94. From inspection of Equation 2.8 it is evident that the ratio of the areas of the downcomer and riser had a significant impact on the mixing energy input.

Table 2. 3: Comparison of the performance and energy efficiency of different photobioreactors

Type of PBR[a]	Species[b]	Light source[c]	I_o ($\mu mol.m^{-2}.s^{-1}$)	L (m)[d]	V (L)	SA/V ($m^2.m^{-3}$)[e]	Aeration ($m3.min^{-1}.m^{-3}$)[f]	X_{max} ($g.L^{-1}$)	P ($g.L^{-1}.d^{-1}$)[g]	E_L ($W.m^{-3}$)[h]	E_M ($W.m^{-3}$)[i]	P/E ($g.W^{-1}.d^{-1}$)[j]	P/E_M ($g.W^{-1}.d^{-1}$)[k]	Reference
FPALR	*Sp*	N	80	0.15	50.0	7.30	0.30	1.81	0.12	134.4	12.2	0.82	9.84	Reyna-Velarde *et al.* (2010)
FPALR	*Cv*	H	980	0.03	3.00	28.0	0.45	4.10	0.045	6037	*	*	*	Degen *et al.* (2001)
FPALR	*Cv*	H	980	0.02	1.50	56.0	0.45	4.80	0.11	12074	*	*	*	Degen *et al.* (2001)
FPBC	*Cv*	H	980	0.03	3.00	28.0	0.45	3.50	0.028	6037	*	*	*	Degen *et al.* (2001)
FPALR	*Cv*	HPS	100	0.02	10.0	50.0	0.20	1.48	0.29	1100	534	0.18	0.54	Ratchford *et al.* (1992)
FPALR	*Cv*	HPS	200	0.02	10.0	50.0	0.20	1.71	0.34	2200	534	0.12	0.64	Ratchford *et al.* (1992)
FPALR	*Sc*	HPS	100	0.02	10.0	50.0	0.20	2.27	0.38	1100	534	0.23	0.71	Ratchford *et al.* (1992)
FPALR	*Sc*	HPS	200	0.02	10.0	50.0	0.20	2.60	0.43	2200	534	0.16	0.81	Ratchford *et al.* (1992)
BC	*Cv*	F	350	0.04	1.40	72.0	0.0029	3.79	0.47	5528	7.47	0.08	62.90	Hulatt and Thomas (2011)
BC	*Ch*	F	100	0.05	0.40	87.0	2.10	2.02	0.34	946	15.0	0.35	22.60	Ryu *et al.* (2009)
BC	*Ch*	F	300	0.10	4.00	20.0	0.25	2.36	0.59	1685	4.09	0.35	144.30	Chiu *et al.* (2009)
ALR	*Ch*	F	300	0.10	4.00	20.0	0.25	2.53	0.63	1685	17.3	0.37	36.40	Chiu *et al.* (2009)
ALR	*Ch*	F	350	0.30	100	13.0	0.0011	*	0.21	1029	11.2	0.20	18.70	Zhang *et al.* (2002)
Tubular	*Sp*	F	120	0.01	5.50	135.0	0.82	10.6	0.42	1920	*	0.22	*	Converti *et al.* (2006)
Tubular	*Sp*	S	1152	0.03	145	54.0	*	6.3	1.50		*	*	*	Torzillo *et al.* (1993); Janssen *et al.* (2003)
AIIP	*Sc*	F	91.4	0.11	18.0	32.0	0.044	*	0.40	277	5.90	1.42	67.80	Pegallapati and Nirmalakhandan (2011)
IFPALR	*Cv*	S	1200-2000	0.03	132 000	60.4	*	*	2.10		334	0.01	6.29	Janssen *et al.* (2003)
IFPALR	*Cv*	LEDs	1058	0.02	0.10	125.0	1.00	*	*	29095	3.17	*	*	Lee and Palsson (1994)
AIIP	*Cv*	X	78	*	0.60	320.0	0.50	1.5	0.06	5333	*	0.01	*	Javanmardian and Palsson (1991)

[a] FPALR flat plate airlift ; FPBC flat plate bubble column; BC bubble column; ALR airlift column; AIIP Annular internally illuminated column ; IFPALR internally illuminated flat plate airlift photobioreactor; [b]*Sp, Spirulina platensis*; *Cv, Chlorella vulgaris*; *Sc, Scenedesmus sp.; Ch, Chlorella sp.;* [c] N neon lamp; H HQI-vapour lamp; HPS high pressure sodium lamp; F fluorescent lights; S sunlight; LEDs light emitting diodes; X xenon lamp; [d] L light path length; [e] SA/V incident surface area to culture volume ratio; [f] vvm gas sparged per unit volume per minute; [g] Overall biomass productivity; [h] E_L light energy input; [i] E_M mixing energy input; [J] Biomass productivity per unit power input (includes light and mixing energy inputs); [k] Biomass productivity per unit power input (excluding light energy input);* Insufficient information provided.

In terms of energy efficiency, it can be observed from Table 2.3, that the light energy input varied between 134.4-29095 $W.m^{-3}$, 946-5528 $W.m^{-3}$ and 277-1685 $W.m^{-3}$ in the flat plate airlift, bubble column and airlift photobioreactors respectively. From inspection of Equation 2.7, it is evident that the light energy input is highly dependent on the light intensity of the external light source as well as the incident surface area to culture volume ratio. For example, the highest light energy input of 29095 $W.m^{-3}$ was required for the flat plate airlift photobioreactor designed by Lee and Palsson (1994) because of the high light intensity and large incident area to volume ratio (1058 $\mu mol.m^{-2}.s^{-1}$ and 125 $m^2.m^{-3}$). Table 2.3 also shows that the mixing energy inputs varied between 3.17-534 $W.m^{-3}$, 4.10-15.0 $W.m^{-3}$ and 5.9-17.3 $W.m^{-3}$ in the flat plate airlift, bubble column and airlift photobioreactors respectively. The higher mixing energy inputs in the airlift photobioreactors may be attributed to the fact that the mixing energy requirement is highly dependent on the gas flow rate and the ratio of the areas of the downcomer and riser (Equation 2.8), whereas in the bubble column photobioreactors, it is only dependent on the gas flow rate and depth of culture (Equation 2.9).

Table 2.3 illustrates that the most efficient design in terms of biomass productivity per unit power input, where light energy is included, is the internally illuminated photobioreactor designed by Pegallapati and Nirmalakhandan (2011) which achieved 1.42 $g.W^{-1}.day^{-1}$. It can be observed that the annular internally illuminated photobioreactor and the flat plate photobioreactor designed by Ratchford *et al.* (1992) achieved similar biomass productivities for cultures of *Scenedesmus* (0.38-0.40 $g.L^{-1}.day^{-1}$) at similar light intensities. However, there are a key number of differences between the two cultivation systems. For instance, the annular internally illuminated photobioreactor had a larger volume and light path length. Also, the volume of gas sparged per unit culture volume per min in the flat plate photobioreactor was approximately 4.5 times greater compared to the annular internally illuminated photobioreactor. The different photobioreactor dimensions and the different aeration rates would have affected the amount of light utilization as well as the hydrodynamics and mass transfer rates in each of the photobioreactors. Consequently, the total energy input was far lower in the internally illuminated photobioreactor as compared to the flat plate photobioreactor in terms of both the mixing energy input (~1%) and light energy input (10-20%). In terms of the performance of the other internally illuminated photobioreactors shown in Table 2.3, it can be seen that the photobioreactors designed by

Janssen *et al.* (2003) and Javanmardian *et al.* (1991) achieved biomass productivities per unit power input as low as 0.01 $g.W^{-1}.day^{-1}$. The inefficiency of these systems could be due to the fact that fibre optic systems were used to provide light to these photobioreactors. As mentioned earlier, there are currently numerous disadvantages associated with fibre optics and the efficiency of light transmission (Section 2.3.2.4). Overall, it was found that the flat plate airlift, bubble column and airlift photobioreactors achieved energy efficiencies of 0.23-0.82 $g.W^{-1}.day^{-1}$, 0.08- 0.35 $g.W^{-1}.day^{-1}$ and 0.20-0.37 $g.W^{-1}.day^{-1}$ respectively (Table 2.3). Different energy efficiencies were obtained in the different types of photobioreactors because of the different photobioreactor dimensions and hydrodynamic characteristics which affected both the amount of light utilization as well as the mass transfer rate. It should be noted that the energy efficiency was also highly dependent on the species of microalgae that was cultivated.

2.5 Challenges to improve energy efficiency of photobioreactors

In order to improve the performance of photobioreactors, the current inefficiency of light utilization, a major factor limiting algal growth (Posten 2009; Ogbonna and Tanaka 2000; Janssen *et al.* 2003), needs to be improved. The hydrodynamics affects light delivery and mass transfer characteristics as well as the mixing energy requirements associated with different types of photobioreactors (Reyna-Verlarde *et al.*, 2010). In order to optimize light utilization, the supply of light to the photobioreactor and its distribution to algal cells needs to be considered. Ideally, maximal biomass productivity would be obtained if light at the saturation intensity were homogenously distributed within a well mixed photobioreactor. From literature, it is evident that light utilization can be improved by reducing the light path length and increasing the incident surface area per unit culture volume of a photobioreactor (Degen *et al.*, 2001; Converti *et al.*, 2006). Additionally, if the photobioreactor has a well defined circulation pattern, the aeration rate can be manipulated to improve light utilization by increasing the frequency of light/dark cycling of algal cells. However, it should be noted that above a certain degree of mixing, algal cells can be damaged through shear stress, depending on the species that is cultivated (Janssen, 2002; Grobbelaar, 2000; Wu and Merchuk, 2004). Furthermore, increasing the aeration rate and altering the configuration of the riser and downcomer would both have a significant effect on the mixing energy requirement (Pegallapati and Nirmalakhandan, 2011; Langley, 2010). According to literature, internally illuminated photobioreactors

have also been reported to yield improved biomass productivity, as the surface illumination area to volume ratio can be greatly increased as compared with the external surface illumination area (Pulz and Scheibenbogen, 1998). However, from analysis of studies performed by various authors, it was found that the efficiency of light utilization was highly dependent on the method of light supply i.e. direct light supply from fluorescent light bulbs or LEDs, or via fibre optics and internal illumination plates (Section 2.4.2.4).

It is evident that, in order to improve the energy efficiency of a photobioreactor, a thorough understanding of how microalgal cultures respond to light in different photobioreactors (column, tubular and flat plate) needs to be acquired. In particular, the effect of different light sources, incident surface area to volume ratios, light path lengths and the frequency of light/dark cycling on algal growth should be investigated.

2.6 Objectives

Based on the review of the literature on light delivery in algal photobioreactors and its influence on productivity, the objectives of this study are as follows:

- To demonstrate that inefficient light supply is a major factor limiting algal growth
- To determine how different species, namely *Chlorella vulgaris* and *Scenedesmus sp*., respond to similar changes in lighting conditions
- To determine the effect of different light sources on biomass productivity i.e. the effect of fluorescent light vs. light-emitting diodes (LEDs) on biomass productivity
- To design and evaluate the performance of an internally lit airlift photobioreactor containing LEDs, in order to investigate the effect of variation of the incident surface area to culture volume ratio on biomass productivity
- To analyse the effect of reactor configuration (flat plate, airlift and tubular) on algal cultivation in terms of biomass productivity and energy utilization.
- To assess the effect of light/dark cycling on *Scenedesmus sp*.

2.7 Hypotheses and key questions

2.7.1 Hypotheses

- The internally illuminated airlift photobioreactors achieve a higher biomass productivity than a similarly externally illuminated airlift photobioreactor because of the higher degree of light provision that is provided by the larger incident surface area to volume ratio coupled with the reduced light path length.
- The flat plate photobioreactor achieves a higher biomass productivity than the airlift photobioreactors because of the higher degree of light provision that is provided by the larger incident surface area to volume ratio coupled with the reduced light path length.
- Higher biomass productivities are obtained when using LEDs as compared to fluorescent lighting, since LEDs are able to emit light at higher light intensities.
- Higher maximum specific growth rates and biomass productivities are obtained in the tubular photobioreactors at shorter light/dark cycling times coupled with higher incident surface area to volume ratios.

2.7.2 Key questions

- How does maximum biomass concentration attainable and productivity vary with increasing light intensity and cultivation time? How does increasing biomass concentration and depth of culture affect light attenuation?
- How will changes in light intensity affect the growth of *Chlorella vulgaris* and *Scenedesmus sp.* in the airlift photobioreactors? Which species is able to utilize higher light intensities for growth more efficiently?
- What effect do fluorescent and LED light sources have on the growth of *Scenedesmus sp.* in the airlift and flat plate photobioreactors?
- How does the presence of internal lighting affect biomass productivity as compared to providing light at the same intensity externally to a similar photobioreactor? Is it more energy efficient to utilize internal lighting at lower light intensities as compared to using a high light intensity external to the photobioreactor?
- What effect does internal lighting have on the culture temperature? How do changes in temperature affect the specific growth rate of *Scenedesmus sp*.?

- What effect does altering the aeration rate have on the circulation time and the overall mass transfer coefficient in the flat plate photobioreactor?
- Does the reduced light path length in the flat plate photobioreactor have a significant impact on light availability and consequently growth?
- What is the effect of light/dark cycling on the maximum specific growth rate of *Scenedesmus sp.* in the tubular photobioreactors? How does cycle time and the volume fraction of the tubular photobioreactor that is exposed to light affect the growth of *Scenedesmus sp.*?
- Can the efficiency of light/dark cycling in the vertical airlift and flat plate photobioreactors be evaluated?
- How do the vertical airlift, flat plate and tubular photobioreactors compare to one another in terms of biomass productivity achieved per unit power input? What is the maximum biomass productivity that can be achieved? How does this compare to literature?

For this project, the vertical column airlift and tubular photobioreactors previously designed, constructed and commissioned by Langley (2010) and Fraser (2011) in CeBER will be used to investigate the effects of external fluorescent light provision on algal growth. In order to determine whether or not the provision of internal illumination results in improved biomass productivity, a standard airlift photobioreactor will be modified to incorporate a strip of internal LED tape. Furthermore, a simple and robust 1.6 L perspex flat plate photobioreactor will also be designed and constructed.

The effect of an increase in temperature, which is caused by the presence of internal illumination and an increase in light intensity, on growth is investigated. The effect of different photobioreactor designs (column, tubular and flat plate) on biomass productivity and light utilization is also evaluated. In particular, the different incident surface area to volume ratios, light path lengths as well as the hydrodynamic and mixing regimes in each of the photobioreactors are considered. The effect of using fluorescent light and LEDs on the biomass productivity obtained in the airlift and flat plate photobioreactors is also assessed. Furthermore, the effect of varying light intensity, light fraction and cycle time on the maximum specific growth rate and biomass productivities obtained in the tubular photobioreactors is investigated. The materials, methods and reactor systems used for this study are presented in Chapters 3 and 4 and the results obtained are presented in Chapters 5 and 6.

3. Materials and methods

3.1 Materials

3.1.1 Algal cultures and stock culture maintenance

Chlorella vulgaris was obtained from the microalgal culture collection at the University of Texas (UTEX 395). *Scenedesmus sp.* was isolated in our laboratory by PhD student Melinda Griffiths from a sample collected from pilot ponds operated in Upington, South Africa for the development of an astaxanthin process.

Stock cultures of *Chlorella vulgaris* and *Scenedesmus sp.* were grown in modified 3N BBM media and maintained in 200 mL glass bottles that were sparged with air at ambient temperature. Constant illumination was provided from one side of the bottles from two 18 W cool white fluorescent light bulbs which provided an average light intensity of 120 $\mu mol.m^{-2}.s^{-1}$. Prior to carrying out experiments, stock cultures were scaled up to 500 mL glass bottles and maintained at stock culture conditions for 7 to 10 days. The starting concentration for all experiments was maintained within the range of 0.08-0.25 $g.L^{-1}$.

3.1.2 Media

A modified 3N BBM media was used for both stock culture maintenance and growth experiments for the freshwater algal species. The 3N BBM media consisted of: 0.75 $g.L^{-1}$ $NaNO_3$; 0.025 $g.L^{-1}$ $CaCl_2.3H_2O$; 0.075 $g.L^{-1}$ $MgSO_4.7H_2O$; 0.075 $g.L^{-1}$ K_2HPO_4; 0.175 $g.L^{-1}$ KH_2PO_4; 0.025 $g.L^{-1}$ NaCl; 1 $mL.L^{-1}$ thiamine; 1 $mL.L^{-1}$ of cyanocobalamin. In addition 6 $mL.L^{-1}$ of the following trace element solution was added: 0.75 $g.L^{-1}$ Na_2EDTA; 0.017 $g.L^{-1}$ $FeCl_3.6H_2O$; 0.041 $g.L^{-1}$ $MgCl_2.4H_2O$; 0.005 $g.L^{-1}$ $ZnCl_2$; 0.002 $g.L^{-1}$ $CoCl_2.6H_2O$; 0.004 $g.L^{-1}$ $Na_2MoO_4.2H_2O$.

3.1.3 Cultivation photobioreactors

3.1.3.1 Introduction

For this study the performance of the three most common types of photobioreactors used in industry, namely: a vertical column airlift photobioreactor, a flat plate photobioreactor and a tubular photobioreactor, were evaluated in terms of biomass productivity and energy efficiency as a function of light provision. In the airlift photobioreactor, light was provided either externally or internally or as a combination of both. In the flat plate and tubular

photobioreactors light was provided externally from fluorescent light or light-emitting diodes (LEDs).

In this dissertation, the vertical column airlift photobioreactor and the tubular photobioreactors that were designed, constructed and commissioned by Langley (2010) and Fraser (2011) respectively, were used to assess the effects of external light provision on algal growth. These photobioreactors are fully described in Sections 3.1.3.2 and 3.1.3.3. Based on the design proposed by Tamburic *et al.* (2011), a simple and robust 1.6 L perspex flat plate photobioreactor was designed and constructed. The key design criteria were to optimize the light path length of the flat plate photobioreactor for light penetration, while taking into account the working volume, and to design a cheap and efficient gas supply system in order to promote adequate mass transfer of CO_2 for algal growth. Furthermore, in order to assess whether or not internal illumination had a greater impact on the algal growth rate as compared to external illumination, a standard airlift photobioreactor was modified to include an internal glass compartment to house a strip of cool white LEDs. Full descriptions of these two new photobioreactor designs and their standard cultivation conditions are provided in Sections 4.2 and 4.3 respectively.

3.1.3.2 Airlift photobioreactor

Standard glass and stainless steel internal loop airlift photobioreactors with a working volume of 3.2 L (Figure 3.1), designed by Langley (2010), were used for algal cultivation. Under standard conditions, constant illumination was provided at 300 $\mu mol.m^{-2}.s^{-1}$ from a bank of three 18 W cool fluorescent light bulbs situated on one side of the photobioreactor at a distance of 3 cm from the column surface. A mixture of air containing 10 000 ppm CO_2 at a flow rate of 2 $L.min^{-1}$ was filtered through a 0.45 μm filter (Millipore, USA) prior to being sparged at the base of the draught tube through a 0.22 μm stainless steel HPLC inlet filter. The flow rate and air composition was regulated and maintained using a Brooks 5850S Thermal Mass Flow Controller.

The airlift photobioreactors, media and distilled water were sterilized in a laboratory autoclave at 121°C for 20 minutes (Everlight Vertical Type Autoclave, Laboratory Supplies, SA) prior to all experiments. At the beginning of a run, 20 μL of antifoam (Antifoam 204, Sigma Life Science) was added to each photobioreactor to reduce foaming.

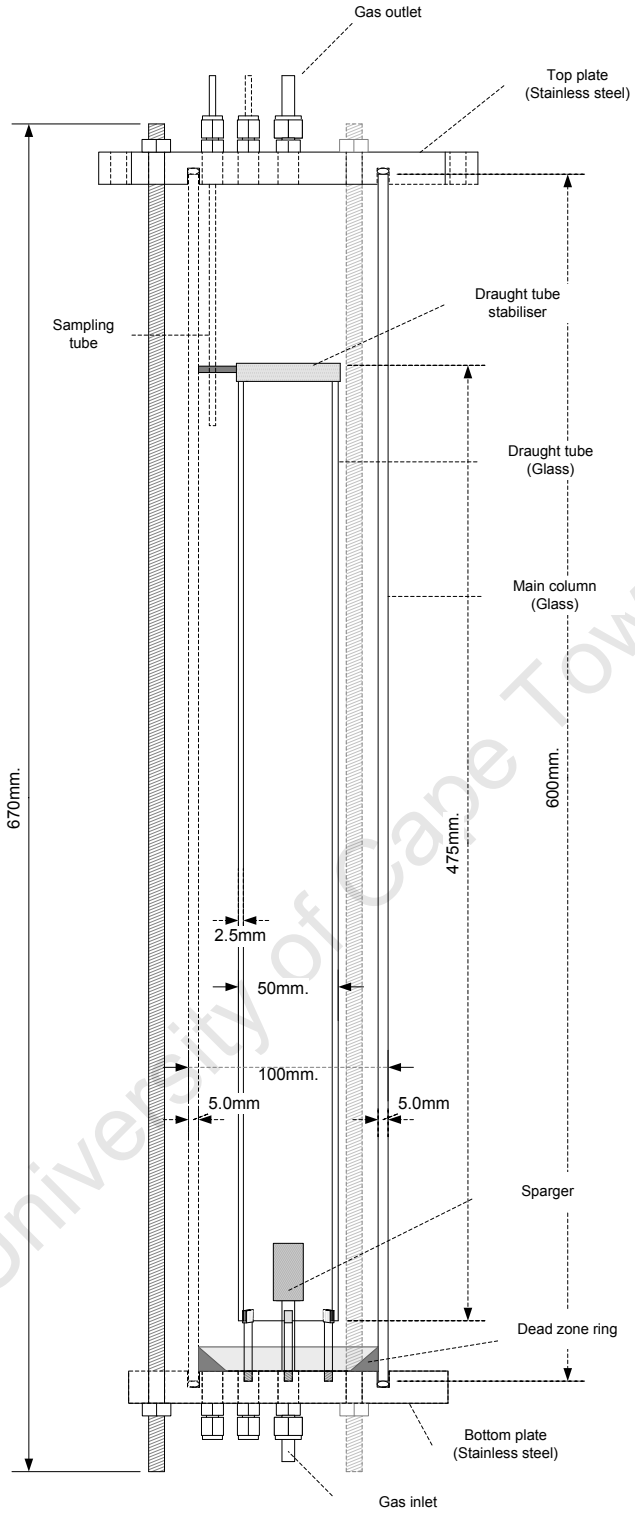

Figure 3. 1: Diagram of airlift photobioreactor illustrating key dimensions (Langley, 2010)

During runs, the culture temperature was measured on a daily basis using a digital thermometer and remained between 25 and 27°C. Approximately 120 mL of sterile distilled water was added to the reactors on a daily basis to replace water lost due to evaporation. For

conditions at higher light intensity, a second bank of fluorescent lights was placed on the opposite side of the photobioreactor. Under these conditions, a fan was used to maintain the temperature at 26±1°C.

3.1.3.3 Tubular photobioreactor

Two glass tubular photobioreactors with working volumes of 209 and 330 mL, designed by Fraser (2011), were used to cultivate algae under different light/dark cycling conditions. The reactors comprised of a downcomer, a riser and a top cup as illustrated in Figure 3.2. The downcomer was made up of a series of straight glass tubes with 7 mm ID connected at 5° angles with glass U-bends. The riser consisted of a glass tube with 18 mm ID attached to a glass top cup with a 4.5 cm ID and a height of 15 cm. Further details of the reactor systems are provided in Table 3.1. The reactor system was closed by using an airlift pump.

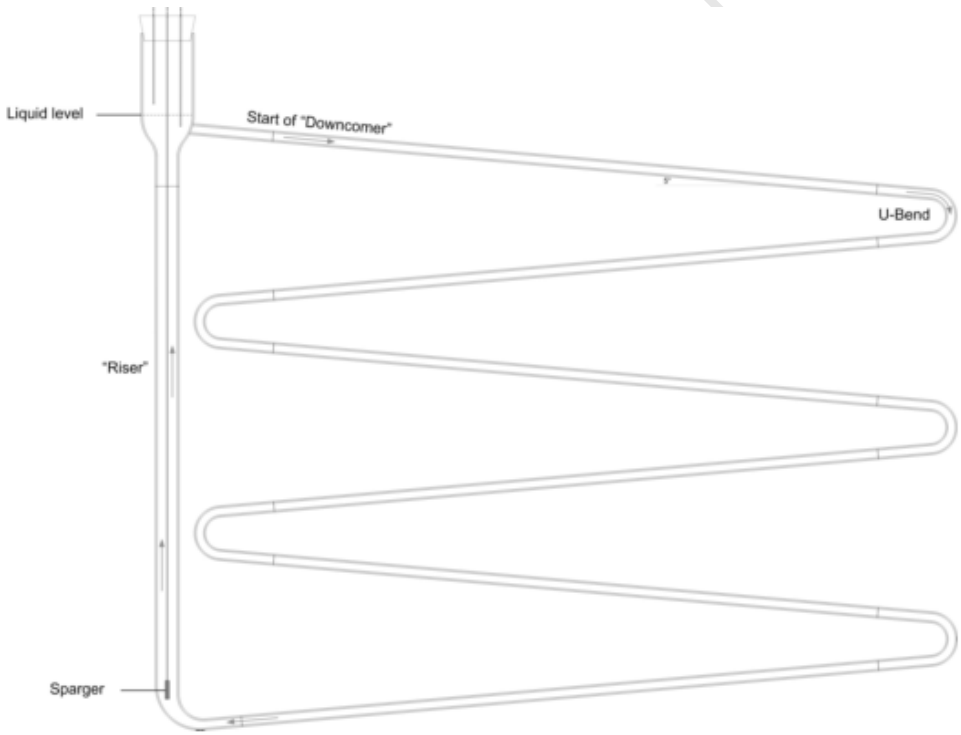

Figure 3. 2: Schematic of 330 mL tubular photobioreactor (Fraser, 2011)

Table 3. 1: Basic design details of tubular photobioreactors (Fraser, 2011)

Reactor	Volume (mL)	Riser Height (m)	Downcomer length (m)	Number of U-bends
6 tubes	330	0.50	4.24	5
4 tubes	209	0.28	2.86	3

Constant illumination was provided by banks of eight 18 W cool white fluorescent light bulbs which were placed a distance of 2 cm from the reactor. One or two fluorescent light banks were used such that experiments could be performed at average light intensities of 300 and 600 $\mu mol.m^{-2}.s^{-1}$ respectively. The culture was aerated with CO_2-enriched air containing 10 000 ppm CO_2 through a sparger made from a 6 mm OD stainless steel sintered metal tube (SIKA R-10, GKN Metals) The gas flow rates of the air and CO_2 were controlled using rotameters. For this study, cycle times of 21 s and 33 s were achieved by operating the 209 and the 330 mL reactors at total inlet air flow rates of 423 and 376 $mL.min^{-1}$. Different light/dark fractions were achieved by covering sections of the downcomer and riser in aluminium foil (Fraser, 2011). This is discussed in further detail in Section 3.3.3.

The culture temperature was measured on a daily basis and remained between 23 and 25°C. Approximately 10 mL of sterile distilled water was added to the reactor on a daily basis to replace water lost due to evaporation. When using two light banks, a fan was required to maintain the temperature at 26±1°C.

3.2 Analytical methods

3.2.1 General measurements

3.2.1.1 Temperature

The temperature of algal cultures in all photobioreactors was measured using a MT630 hand-held digital thermometer (MajorTech, SA).

3.2.1.2 pH

The pH was measured using a Cyberscan 2500 pH meter. The pH probe was submersed in an undiluted algal sample and recorded when the reading stabilized. The pH meter was calibrated on a daily basis using pH 4.0 and pH 7.0 buffers (Merck, SA).

3.2.1.3 Microscopy

Cells from *Chlorella vulgaris* and *Scenedesmus sp.* stock cultures were examined regularly, using a light microscope (Olympus BX40) to check that contamination with other algal species had not occurred.

3.2.1.4 Light intensity

Light intensity was measured using a LI-250 L-COR light meter, which was calibrated for use in air and measured light in the PAR range (400-700 nm) with a 2π solid angle (Heinz Walz GmbH, Germany). For each reactor configuration, the average light intensity was determined by using a grid technique which incorporated measuring the incident light intensity at equidistant points across the length and breadth of the light bank. These light intensities were measured at a distance of 3 cm from the light bank. The average light intensity was then calculated as the average of total number of incident light intensity readings. Figure 3.3 illustrates the grid points at which the incident light intensities were measured for the tubular reactor fluorescent light bank.

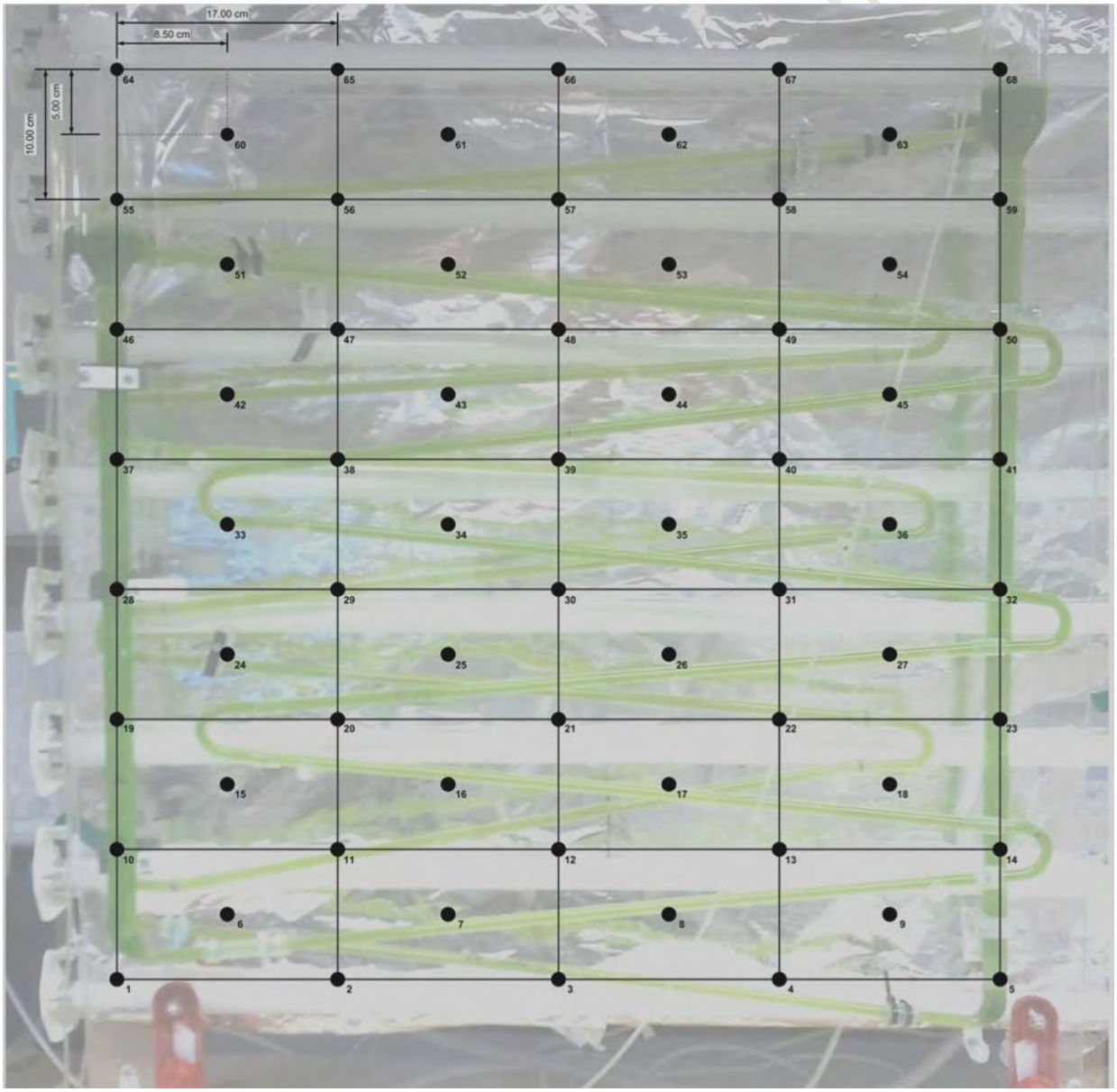

Figure 3. 3: Diagram of grid points used to measure the average light intensity (Fraser, 2011)

3.2.2 Biomass concentration from dry weight

Biomass was measured gravimetrically by filtering 10 mL algal samples through pre-dried and pre-weighed 0.45 μm cellulose nitrate filter paper. The filter paper with algal biomass was placed in an oven at 80°C for three days. These samples were then cooled to room temperature in a desiccator and weighed. Dry weight measurements were done in duplicate and it was found that over the course of a growth cycle, the average relative error between duplicate readings was 4.7%.

3.2.3 Biomass concentration from absorbance

The optical density of 4 mL algal samples was measured at 750 nm using a Helios spectrophotometer to obtain a rapid estimation of biomass concentration. The wavelength of 750 nm was selected to minimise the effect of changing chlorophyll concentrations on absorbance readings (Griffiths *et al.,* 2011a). Samples were measured in triplicate and diluted to ensure absorbance readings below 1.0 such that a linear relationship between concentration and absorbance was maintained in accordance with the Beer-Lambert law.

The optical density and dilution of samples could then be used to calculate the dry weight by using the standard calibration curve that was generated from plotting the optical density readings and the dry weight data over a growth cycle. The average relative error between triplicate optical density readings was 2.1%.

It should be noted that in this study, the biomass concentration was measured from both absorbance and dry weight independently to validate culture conditions. The standard calibration curves obtained in each of the photobioreactors can be found in Appendix C-4.

3.2.4 Estimation of circulation and mixing times

The circulation times (t_c) in a reactor were estimated visually by adding a phenolphthalein indicator to the reactor, containing 3N BBM media only. The phenolphthalein indicator remains colourless when the system pH is below pH 8.2. In the pH range 8.2-12, the indicator turns pink. To measure the circulation time at a particular flow rate, a slug of sodium hydroxide was added to the reactor and the time taken for the slug to circulate around the reactor recorded. Sulphuric acid was used to return the indicator to a colourless state between measurements (Langley, 2010). For this study, the mixing time (t_m) was estimated visually by recording the time it took for all of the liquid in the reactor to turn pink.

3.2.5 Determination of overall mass transfer coefficient (k_La)

The dynamic gassing-in method (Bailey and Ollis, 1986; Chisti, 2002) was used to determine the overall mass transfer coefficient of oxygen ($k_La(O_2)$). In this study, a Mettler Toledo 4100e dissolved oxygen probe was used to measure the dissolved oxygen concentration in the flat plate photobioreactor. The probe was placed in the sampling port that was closest to the centre of the flat plate photobioreactor. Initially, nitrogen gas was sparged into the photobioreactor containing modified 3N BBM media (Section 3.1.2), until the dissolved oxygen concentration reached zero (C_o), at which point the nitrogen gas supply was stopped. The photobioreactor was then sparged with air and the rate at which the dissolved oxygen concentration increased recorded until the dissolved oxygen concentrations reached a stable equilibrium (C^*). Subsequently, the overall mass transfer coefficient of oxygen ($k_La(O_2)$) was calculated using Equation 2.4. It was assumed that the gas phase had a constant composition and the liquid phase was well mixed (Contreras *et al.,* 1998). Thus, $k_La(CO_2)$ may be calculated using Equation 2.5.

All runs were performed in duplicate at each gas flow rate that was considered. The average relative error between duplicate oxygen concentration measurements was 3.1%. Furthermore, in order to assess the accuracy of the overall mass transfer coefficient data, the response time of the dissolved oxygen probe was measured. According to Tribe *et al*., (1995), the overall mass transfer data obtained becomes inaccurate when the response time constant of the probe (τ), which is the time taken for the probe to reach 63.2% of its final value when exposed to a change in concentration is less than $1/(k_La)$. For all of the runs performed, it was found that $\tau < 1/(k_La)$.

From previous experimental work carried out by Langley (2010), it was found that the vertical airlift photobioreactors achieved an overall mass transfer coefficient ($k_La\ (CO_2)$) of $0.0094 \pm 0.00026\ s^{-1}$ at a gas flow rate of 2 $L.min^{-1}$. This correlated well with the estimated $k_La\ (CO_2)$ of $0.0105\ s^{-1}$ which Langley (2010) estimated from design calculations for the airlift photobioreactor (Figure 3.4). It can be observed from Figure 3.4, that the ratios of the areas of the riser and downcomer (A_r/A_d) has a significant impact on $k_La\ (CO_2)$ and the circulation times. This occurs because altering the A_r/A_d had a direct impact on the overall gas hold up in the airlift photobioreactor, which has a significant effect on $k_La\ (CO_2)$ (Chisti, 2002).

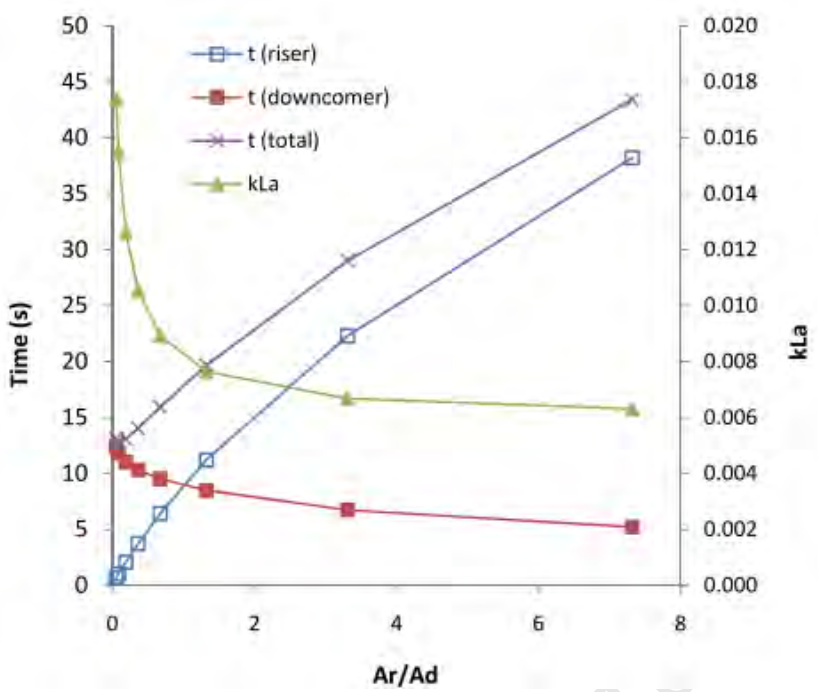

Figure 3. 4: Estimated overall mass transfer coefficient ($k_La(CO_2)$) and circulation times (t_c) in the airlift photobioreactor as a function of the ratio of the areas of the riser and downcomer (Langley, 2010)

3.3 Experimental approach

3.3.1 Introduction

The experimental plans for the vertical column airlift, tubular and flat plate photobioreactors are presented in Sections 3.2.2, 3.3.3 and 3.3.4 respectively. In order to compare the performance of these reactor systems to one another in terms of biomass productivity, light utilization and energy efficiency, a standardized mixture of air containing 10 000 ppm CO_2 was supplied to each of the reactors for all runs to ensure that algal growth was not limited by the provision of CO_2 (Daya, 2011). As mentioned earlier, *Scenedesmus sp*. and *Chlorella vulgaris* were selected for cultivation in these photobioreactors because of the high specific growth rates as well as the high lipid content that can be obtained from these species (Griffiths *et al*., 2011). Although the initial starting concentration for all experiments was maintained within the range of 0.08-0.25 $g.L^{-1}$, the starting concentration used for the majority of runs was approximately 0.18 $g.L^{-1}$. For all runs, triplicate samples were taken to measure absorbance at 750 nm thrice a day. Additionally, one sample was taken daily for duplicate dry weight measurements. The culture temperature was also recorded on a daily basis in each of the photobioreactors.

3.3.2 Vertical column airlift photobioreactor

The airlift photobioreactor described in Section 3.1.3.2 was used to perform the experimental runs presented in Tables 3.2, 3.3 and 3.4. For all of the runs, a flow rate of 2 $L.min^{-1}$ of a mixture of air and CO_2 was sparged at the base of the draught tube through a 0.22 µm stainless steel HPLC inlet filter. To determine the response of *Chlorella vulgaris* and *Scenedesmus sp.* to similar changes in lighting conditions, two sets of runs were performed using 18 W cool white external fluorescent light banks, at the conditions shown in Table 3.2. Subsequently, *Scenedesmus sp.* was cultivated in airlift photobioreactors at the light intensities illustrated in Table 3.3. To assess the effect of internal illumination, and thereby the reduced light path length, on light availability and biomass productivity, a standard airlift photobioreactor was modified to provide constant light intensities of 160 $\mu mol.m^{-2}.s^{-1}$ and 300 $\mu mol.m^{-2}.s^{-1}$ from cool white LED tape internally (Section 4.3.3). At light intensities above 300 $\mu mol.m^{-2}.s^{-1}$, a fan was used to maintain the temperature at 26 ± 1°C. To test the reproducibility of data, runs were repeated when external fluorescent light was used to provide light intensities of 300 and 600 $\mu mol.m^{-2}.s^{-1}$ for both *Chlorella vulgaris* and *Scenedesmus sp*.

Table 3. 2: Experimental runs to investigate the effect of similar changes in external fluorescent lighting intensity on *Chlorella vulgaris* and *Scenedesmus sp.* in airlift photobioreactors at 24 ± 1°C (Run number given)

	I_o ($\mu mol.m^{-2}.s^{-1}$)			
Species	300	600	300 to 600 after 2 days	300 to 600 after 7 days
Chlorella vulgaris	1, 2	1, 2	1	1
Scenedesmus sp.	2	2	2	

Table 3. 3: Experimental runs to investigate the effect of light intensity and configuration on the growth of *Scenedesmus sp.* in airlift photobioreactors at 26 ± 1°C (Run number given)

I_o ($\mu mol.m^{-2}.s^{-1}$)	Internal LEDs	External Fluorescent	Combination
160	3		
300	4	3, 4, 5	
460			5
600		3, 4	6

To investigate the effect of temperature on the specific growth rate of *Scenedesmus sp.* at light intensities of 300 μmol.m^{-2}.s^{-1} and 600 μmol.m^{-2}.s^{-1}, runs were performed using external fluorescent lighting at the conditions illustrated by Table 3.4. A standard airlift photobioreactor illuminated at 300 μmol.m^{-2}.s^{-1} was heated up to 30°C using a heat exchanger that provided a flow rate of heated water from a laboratory water bath, through a heating coil at the base of the draught tube (see Figure 3.1). Runs were repeated at conditions of 300 μmol.m^{-2}.s^{-1} at 26°C and 600 μmol.m^{-2}.s^{-1} at 30°C to assess the reproducibility of data.

Table 3. 4: Experimental runs to investigate the effect of temperature and external fluorescent light intensity on the specific growth rate of *Scenedesmus sp.* in airlift photobioreactors (Run number given)

	I_o (μmol.m^{-2}.s^{-1})	
T (°C)	300	600
24	2	2
26	3 ,4 , 5	3
30	7	8, 9

3.3.3 Tubular photobioreactor

As cell density and the depth of culture increase, light penetration into a photobioreactor decreases exponentially. This occurs because of mutual shading of the algal cells via adsorption by the pigments or via scattering of the cells (Posten, 2009). Hence there is always a fraction of the total photobioreactor volume that is dark. An increase in mixing can improve cycling of algal cells through the light and dark zones and hence promote more efficient light utilization.

In order to assess the impact of increasing the frequency of light/dark cycling on algal growth, the two tubular photobioreactors discussed in Section 3.1.3.3 were used to cultivate *Scenedesmus sp.* at the conditions illustrated in Table 3.5. Cycle times of 21 s and 33 s were achieved by operating the 209 mL and 330 mL reactors at aeration rates of 423 mL.min^{-1} and 376 mL.min^{-1} respectively. The light/dark fractions were achieved by covering sections of the downcomer and riser in aluminium foil. The exact lengths covered are provided in Table 3.6. Repeat runs 12, 17, 18 and 25 were performed to test the reproducibility of data.

Table 3. 5: Experimental run number used to evaluate the effect of light/dark cycling frequencies and different light intensities on the specific growth rate of *Scenedesmus sp.* in tubular photobioreactors

Light intensity (μmol.m^{-2}.s^{-1})	300		600	
Cycle time (s)	**21**	**33**	**21**	**33**
Light fraction				
0.4	10	14	19	22
0.75	11, 12	15	20	23
1.00	13	16, 17, 18	21	24, 25

Table 3. 6: Exact lengths of tubular reactor covered with aluminium foil to achieve different light/dark fractions (Fraser, 2011)

	6 tube		4 tube	
Riser length (cm)	50		28	
Downcomer length (cm)	424.3		286.4	
Light fraction	**RC[1] (cm)**	**DC[2] (cm)**	**RC (cm)**	**DC (cm)**
0.40	30.0	254.6	16.8	171.8
0.75	12.5	106.1	7.0	71.6
1.00	0	0	0	0

[1] RC is the length of the riser that is covered with foil; [2] DC is the length of the downcomer covered in foil.

Furthermore, the light/dark cycling data can be used to mimic the movement of the algal cell cycle through the light and dark zones in the vertical airlift photobioreactor. From these results, it would be possible to select the optimal aeration rate for improving light utilization in the airlift photobioreactors. To date, this is based on the assumption that the riser and the downcomer are exclusively dark and light zones respectively. The concomitant study of Brighton (Brighton *et al.,* 2013) seeks to quantify the relative light intensity as a function of path length and light path through this.

3.3.4 Flat plate photobioreactor

To further investigate the role of light supply as the major factor limiting algal growth, *Scenedesmus sp.* was cultivated in a flat plate photobioreactor at light intensities of 300 μmol.m^{-2}.s^{-1} and 600 μmol.m^{-2}.s^{-1} respectively. Constant illumination was provided from 18 W fluorescent light bulbs. In order to investigate the effect of mass transfer on biomass productivity, runs were carried out at the aeration rates specified in Table 3.7. For runs at 600 μmol.m^{-2}.s^{-1}, a fan was used to maintain the temperature at 26 ± 1°C. In order to

investigate the effect of different light sources on the biomass productivity of *Scenedesmus sp.*, runs were carried out in the flat plate photobioreactor at a constant light intensity of 300 μmol.m^{-2}.s^{-1} using LED and fluorescent light banks under the conditions specified in Table 3.8. Repeat runs 27 and 35 were carried out to test the reproducibility of data.

Table 3. 7: Experimental run number used to evaluate the effect of light intensity and mass transfer on the growth of *Scenedesmus sp.* in the flat plate photobioreactor

F (L.min^{-1})	300 μmol.m^{-2}.s^{-1}	600 μmol.m^{-2}.s^{-1}
2.5	26, 27	30
3.5	28	31
5.0	29	32

Table 3. 8: Experimental run number used to determine the effect of using fluorescent and LED light sources on the growth of *Scenedesmus sp.* in the flat plate photobioreactor

F (L.min^{-1})	LED light bank	Fluorescent light bank
2.5	33	26, 27
3.5	34, 35	28
5	36	29

3.4 Data analysis

3.4.1 Calculation of algal growth rates

Algal growth is typically characterized by the sequence of growth phases illustrated in Figure 3.5. During the initial lag phase, the algal culture adapts to conditions in the photobioreactor. This is followed by exponential growth which occurs in the absence of limitations. Once a limitation becomes apparent (i.e. light or CO_2 supplied at a constant rate), growth transitions to the linear phase. Eventually, the culture reaches a stationary phase and is able to maintain a constant cell concentration for a short period of time (growth rate = death rate) before the death phase becomes dominant. For this study, only the exponential and linear growth phases are considered. The exponential growth rate can be modelled by the linearized form of the Malthus equation (Fraser, 2011):

$$\ln(C_x) - \ln(C_{xo}) = \mu t \tag{3.1}$$

where:

- C_x is the biomass concentration ($g.L^{-1}$) at time *t* (h)
- C_{xo} is the biomass concentration ($g.L^{-1}$) at t = 0 h
- μ is the maximum specific growth rate (h^{-1})

The linear growth rate, which is equivalent to biomass productivity can be estimated directly from the plot of biomass concentration ($g.L^{-1}$) against time (h) during the linear phase of growth (Figure 3.5).

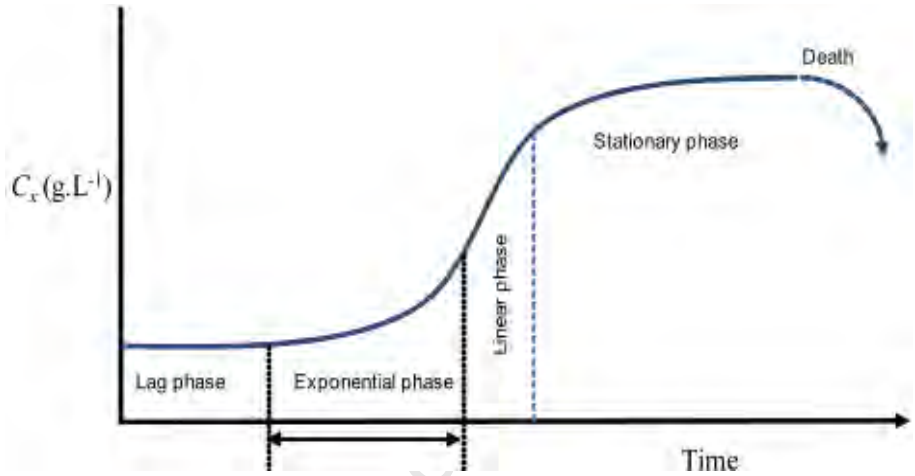

Figure 3. 5: Schematic of a typical algal growth curve illustrating the different growth phases (Adapted from Fraser, 2011)

3.4.2 Evaluation of the effect of temperature on growth

The Arrhenius equation was used to investigate the relationship between the maximum specific growth rate of *Scenedesmus sp.* and culture temperature (McNaught and Wilkinson, 1997):

$$\mu = A.\exp\left(-\frac{E_a}{RT}\right) \tag{3.2}$$

where:

- μ is the maximum specific growth rate (h^{-1})
- A is the Arrhenius constant (h^{-1})
- E_a is the growth activation energy ($kJ.mol^{-1}$)
- R is the universal gas constant ($J.mol^{-1}.K^{-1}$)

- T is the temperature (K)

Equation 3.2 can be linearized to:

$$\ln(\mu) = -\frac{E_a}{R}\frac{1}{T} + \ln(A) \tag{3.3}$$

A plot of ln(μ) against 1/T yields a straight line, where the gradient and intercept can be used to calculate E_a and A respectively, providing parameters to estimate μ as a function of T.

3.4.3 Comparison of different photobioreactors

In order to evaluate and compare the performances of the different types of photobioreactors, the maximum specific growth rate, the linear growth rate (biomass productivity) and the maximum biomass concentrations achieved in the vertical airlift, tubular and flat plate photobioreactors for *Scenedesmus sp.* were evaluated in terms of the amount of light utilization achieved (illumination surface area to volume ratio, light path length) as well as the hydrodynamic characteristics i.e. volume of gas sparged per unit culture volume per minute, overall mass transfer coefficient and cycle times associated with each of the photobioreactors. Subsequently, the light and mixing energy requirements for the different types of photobioreactors were calculated using Equations 2.7 and 2.8 respectively. Finally, energy efficiencies of the different photobioreactors were then assessed in terms of the biomass productivity achieved per unit power input (Equations 2.10 and 2.11) and net energy ratios. (Equation 2.12). Table 3.6 presents a summary of the conditions and the run numbers used (Sections 3.2.2, 3.3.3 and 3.3.4) to evaluate and compare the energy efficiencies of the different photobioreactors at 25±1°C.

Table 3. 9: Summary of run numbers used to evaluate and compare the performances of the vertical airlift, tubular and flat plate photobioreactors at 25±1°C

PBR	Light source	I_o ($\mu mol.m^{-2}.s^{-1}$)	Flow rate ($L.min^{-1}$)	Run numbers
ALR	F	300	2.00	3, 4, 5
ALR	F	600	2.00	3, 4
IALR	LED	160	2.00	3
IALR	LED	300	2.00	4
CIALR	LED +F	460	2.00	5
CIALR	LED + F	600	2.00	6
TBR 1	F	300	0.42	13
TBR 1	F	600	0.42	21
TBR 2	F	300	0.38	16, 17, 18
TBR 2	F	600	0.38	24, 25
FP	F	300	2.50	26, 27
FP	F	300	3.50	28
FP	F	300	5.00	29
FP	F	600	2.50	30
FP	F	600	3.50	31
FP	F	600	5.00	32
FP	LED	300	2.50	33
FP	LED	300	3.50	34, 35
FP	LED	300	5.00	36

3.5 Conclusions

The stock cultures, media, previously commissioned cultivation units (vertical airlift and tubular photobioreactors) and the analytical methods required for this study are presented. The experimental plans developed to investigate the effects of light intensity, light source and configuration (internal or external) as well as temperature and light/dark cycling on growth are also provided. The approach taken to compare and evaluate the performance of the vertical airlift, tubular and flat plate photobioreactors is also presented. The 1.6 L perspex flat plate photobioreactor and the modified internally illuminated vertical airlift photobioreactor that were designed and developed for this study are fully described in Chapter 4.

4 Photobioreactor design

4.1 Introduction

In this dissertation, the provision of light to the algal culture is compared across the airlift photobioreactors, illuminated both internally and externally, the tubular photobioreactor and the flat plate photobioreactor. While the airlift photobioreactor with external illumination and the tubular photobioreactor had been previously designed and commissioned in the CeBER laboratories by Langley (2010) and Fraser (2011), the remaining designs were developed in this study. A 1.6 L perspex flat plate photobioreactor was designed and constructed based on previous studies by Tamburic *et al.* (2011), Reyna-Velarde *et al.* (2010) and Sierra *et al.* (2008). Section 4.2.1 presents the design objectives for the flat plate photobioreactor. Section 4.2.2 presents the methodology for estimating the theoretical hydrodynamic regimes and overall mass transfer coefficients at different operating conditions. The final overall reactor design selected and constructed is provided in Section 4.2.3. In Section 4.2.4, tests were conducted to verify the theoretical estimations made in Section 4.2.2. The standard operating conditions for the reactor are provided in Section 4.2.5. Furthermore, the standard airlift photobioreactor design by Langley (2010) was modified to provide internal illumination via a strip of cool white LEDs. The design objectives and constraints for this reactor are provided in Section 4.3.1. The overall design and standard operating conditions are presented in Section 4.3.2.

4.2 Flat plate photobioreactor

4.2.1 Design objectives

The design objectives for the flat plate photobioreactor were as follow:

1. To ensure that an optimal geometric configuration is used in order to attain sufficient light exposure.
2. To optimize the light path length to allow for sufficient light penetration into an algal culture while taking into account the total reactor volume.
3. To design a cheap and efficient gas supply system to promote sufficient mass transfer of CO_2 for algal growth.
4. To eliminate or minimize the settling of algae in dead zones in the reactor.

4.2.2 Estimation of theoretical correlations

In order to match the flat plate photobioreactor to the airlift photobioreactor, an informed design was required to provide similar operating conditions. Thus, the flat plate photobioreactor was initially designed using Microsoft Excel™ to simulate the dimensions, volume, velocities, mean circulation time and overall mass transfer coefficient via a number of literature correlations. The calculations made to estimate the hydrodynamics and overall mass transfer coefficient are presented in Section 4.2.2.1 and Section 4.2.2.2 respectively.

4.2.2.1 Hydrodynamic calculations

1. Selection of reactor dimensions

Most large-scale flat plate photobioreactors are sparged from the base of the photobioreactor and operate similarly to bubble columns (Zhang *et al*., 2001; Feng *et al.*, 2011), characterized by random flow patterns (Figure 2.9). According to literature, more compact designs can be used to induce well-defined flow patterns, similar to airlift photobioreactors (Degen *et al.*, 2001; Ugwu and Aoyagi, 2012). For this study, a compact reactor body of 270 mm x 280 mm x 59 mm (length x height x width) was selected based on similar dimensions proposed by Tamburic *et al.* (2011). From these dimensions, the reactor volume could be calculated. In order to estimate a working volume, it was assumed that the algal culture would occupy 80% of the reactor.

2. Selection of sparger

The size of sparger holes is a key design parameter to achieve appropriate bubble size to provide the gas-liquid interfacial area that is available for mass transfer (Chisti, 1989). For this study, a 0.0064 m ID stainless steel sparger that was perforated with evenly spaced 1 mm circular holes was selected for supplying gas near the base of the reactor. These sparger dimensions were selected based on the specifications provided by Tamburic *et al.* (2011).

3. Overall gas holdup

The overall gas hold up is the volume fraction of the gas phase in a gas-liquid phase system and can be calculated using Equation 4.1 (Chisti, 1989). The overall gas holdup is an important design parameter to consider as it influences the residence time of a gas in a liquid, the interfacial area available for mass transfer and the total design volume.

$$\varepsilon = \frac{V_G}{V_G + V_L} \tag{4.1}$$

where:

- Ɛ is the overall gas holdup
- V_G is the volume of gas in the reactor (m^3)
- V_L is the volume of liquid in the reactor (m^3)

Although the compact shape of the flat plate photobioreactor would induce a well-defined circular liquid flow pattern, the design of the flat plate photobioreactor is still representative of a bubble column configuration because there are no partitions present to divide the photobioreactor into distinct riser and downcomer zones and hence axial fluid flow may be random. Thus, Equation 4.2 developed by Hills (1976) for bubble columns can be used to estimate the overall gas holdup in the reactor. It is evident that the overall gas hold up is highly dependent on both the superficial gas and liquid velocities.

$$\varepsilon = \frac{U_G}{0.24 + 1.35(U_G + U_L)^{0.93}} \tag{4.2}$$

where:

- U_G is the superficial gas velocity ($m.s^{-1}$)
- U_L is the superficial liquid velocity ($m.s^{-1}$)

4. Sparged liquid height

Once the overall gas holdup is known or estimated, the sparged liquid height could be calculated using Equation 4.3 (Reyna-Verlade *et al.*, 2010).

$$h_D = \frac{h_L}{(1-\varepsilon)} \tag{4.3}$$

where:

- h_D is the sparged liquid height (m)
- h_L is the unsparged liquid height (m)

5. Superficial gas velocity

The superficial gas velocity can be calculated using Equation 4.4 (Chisti, 1989).

$$U_G = \frac{V_G}{A} \tag{4.4}$$

where:

- U_G is the superficial gas velocity ($m.s^{-1}$)
- V_G is the volumetric flow rate ($m^3.s^{-1}$)
- A is the cross-sectional area of the reactor (m^2)

6. Superficial liquid velocity

According to numerous studies performed in literature (Molina *et al.*, 1997; Ugwu *et al.*, 2007; Posten, 2009; Reyna-Verlarde *et al.*, 2010), it has been reported that the fluid dynamics of a photobioreactor have a significant effect on microalgal growth. In particular, the aeration rate, flow patterns, sparger design and the degree of turbulence affect the overall gas hold up, liquid circulation time and frequency of exposure to light for algal cells between light and dark zones in the photobioreactor. However, few studies have reported the actual hydrodynamic parameters and empirical correlations associated with flat plate photobioreactors. For this study, an initial estimate of the superficial liquid velocity can be calculated from the empirical correlation developed by Changhai *et al.* (2005). These authors investigated the effect of aeration rate on the liquid circulation velocity in a glass flat plate photobioreactor (70 x 50 x 10 cm), aerated through a tube that extended through the base of the photobioreactor. It was found that the photobioreactor exhibited a circular flow pattern and that the relationship between aeration rate and the liquid circulation velocity could be expressed by Equation 4.5. The high R^2 value of 0.997 obtained indicates the goodness of fit for the experimental data.

$$U_L = -0.42vvm^4 + 1.49vvm^3 - 1.20vvm^2 + 0.90vvm + 0.14 \tag{4.5}$$

where:

- U_L is the superficial liquid velocity ($m.s^{-1}$)

In order to obtain a more accurate and proportional estimate of the superficial liquid velocities for the flat plate photobioreactor considered in this dissertation, Equation 4.5 can be divided by the ratio of the reactor volumes of the photobioreactor designed by Changhai *et al.* (2005) and the photobioreactor used in this study. The superficial liquid velocities in the 1.6 L flat plate photobioreactor can be estimated using Equation 4.6.

$$U_L = \frac{-0.42vvm^4 + 1.49vvm^3 - 1.20vvm^2 + 0.90vvm + 0.14}{8} \tag{4.6}$$

7. Mean circulation time

The mean circulation time in the reactor could be calculated using Equation 4.7. It is assumed that the liquid follows a circular path due to the physics of the system (Tamburic *et al.*, 2011).

$$t_c = \frac{x}{U_L} \tag{4.7}$$

where:

- t_c is the mean circulation time (s)
- x is the length of the circulation path (m)
- U_L is the superficial liquid velocity ($m.s^{-1}$)

Figure 4.1 illustrates the effect of the aeration rate on the superficial liquid velocity and the mean circulation time in the flat plate photobioreactor obtained using Equations 4.6 and 4.7 respectively. It can be seen that increasing the superficial gas velocity by increasing the aeration rate results in an increase in the superficial liquid velocity and consequently results in a decrease in the mean circulation time. Furthermore, it was found that over the range of aeration rates considered in Figure 4.1, the overall gas hold-up increased from 0.008 to 0.02. According to the summary of data compiled from literature by Chisti and Moo-Young (1988), provided in Figure 4.2, it can be observed that at a superficial gas velocity of 0.01 $m.s^{-1}$, the overall gas hold is estimated to be approximately 0.03. Thus, the values predicted for the gas hold up correlate relatively well to literature values. For a detailed set of the sample calculations made to estimate the hydrodynamics of the flat plate photobioreactor, see Appendix A-1.

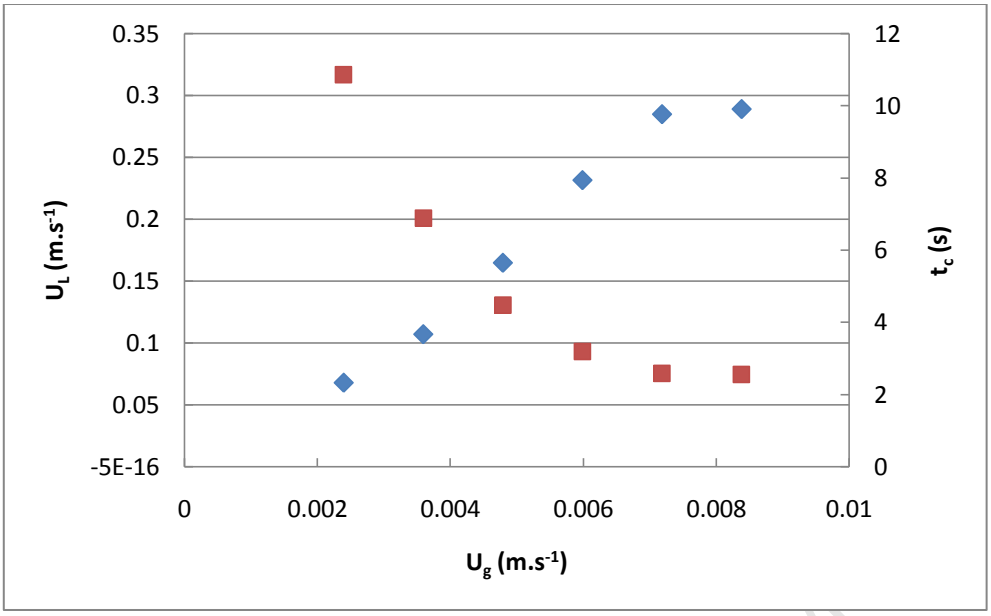

Figure 4. 1: The effect of the superficial gas velocity on the superficial liquid velocity (blue diamond) and the mean circulation time (red square) in the flat plate photobioreactor using Equations 4.6 and 4.7

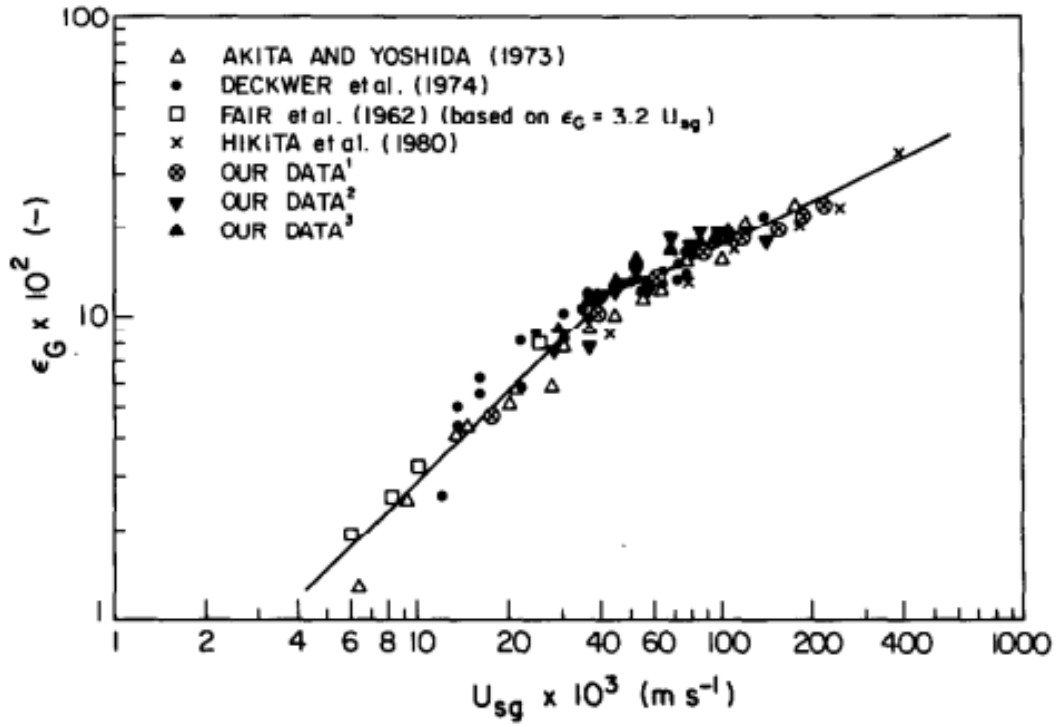

Figure 4. 2: The effect of superficial air velocity on the gas-hold up in bubble columns; the data shown cover column diameter and height ranges, of 0.10-1.067 m and 1.37-5.87 respectively; [1] rectangular bubble column, [2] circular bubble column with diameter and liquid height of 0.243 m and 3 m respectively, [3] circular bubble column with diameter and liquid height of 0.243 m and 1.50 m respectively (Chisti and Moo-Young, 1988).

4.2.2.2 Mass transfer calculations

As mentioned previously in Section 2.2.4, the overall mass transfer coefficient (k_La) is an important design parameter to consider as it determines the rate at which CO_2 is transferred from the gas phase to the liquid phase. The overall mass transfer coefficient is a function of the gas holdup, bubble size distribution, aeration rate and temperature profile and is thus highly system specific (Chisti, 2002). In order to support a high algal growth rate in a photobioreactor, the reactor needs to be designed such that a sufficiently high CO_2 mass transfer rate from the gas to liquid phase is achieved. Based on the literature review performed by Griffiths and Harrison (2009), a target CO_2 transfer rate of 20 $mg.L^{-1}.h^{-1}$ was selected. Assuming that the liquid concentration of CO_2 was zero and that the photobioreactor was sparged with air containing 400 ppm CO_2, it was calculated from Equation 2.4 that a k_La of 0.014 s^{-1} would be required to support this target CO_2 transfer rate (Langley, 2010). By feeding gas enriched with 10 000 ppm CO_2 to the photobioreactor, the k_La requirement could be reduced and values above 0.0006 s^{-1} were considered acceptable.

Outlined below are the steps taken to calculate the overall mass transfer coefficient for the flat plate photobioreactor.

1. Selection of sparger and predicted bubble size

As mentioned previously, the selection of a sparger and the resulting bubble size distribution has a significant impact on the gas-liquid interfacial area that is available for mass transfer (Chisti, 1989). A 0.0064 m ID stainless steel sparger was selected with 1 mm holes spaces 10 mm apart. Based on preliminary testing and photographic evidence, it was found that the sparger produced bubbles with a mean diameter (d_b) of 3 mm (Figure 4.9).

2. Calculation of gas-liquid interfacial area

The gas-liquid interfacial area that is available for mass transfer is dependent on the size and geometry of a cultivation unit, the operating conditions and the physical and chemical properties of the liquid media (Bouaifi *et al.*, 2001; Shah *et al.*, 1982). From the estimates made for the overall gas hold up (ε) and the working volume (V_L) in Section 4.2.2.1, the total gas volume (V_G) could be calculated from Equation 4.1. Assuming that the bubbles produced are spherical, the surface area of a bubble (A_b), the volume of a bubble (V_b) and the total

number of bubbles (N_b) produced could be estimated. Thus, the gas-liquid interfacial area that is available for mass transfer could be calculated using Equation 4.7 (Langley, 2010).

$$A_{itotal} = N_b A_b \tag{4.7}$$

where:

- $A_{i,\,total}$ is the total gas-liquid interfacial area (m^2)
- N_b is the number of bubbles
- A_b is the surface area of a bubble (m^2)

3. Estimation of the overall mass transfer coefficient

The correlation proposed by Calderbank and Moo-Young (1961) for the transfer of gaseous solutes such as CO_2 from a swarm of bubbles into a liquid phase in an aerated mixing vessel was used to estimate k_La in the flat plate photobioreactor:

$$\frac{k_L a d_b}{D_{CO_2.H_2O}} = 0.31 Gr^{\frac{1}{3}} Sc^{\frac{1}{3}} \frac{A_{i,total}}{V_L} \tag{4.8}$$

where:

- k_La is the overall mass transfer coefficient (s^{-1})
- d_b is the mean bubble diameter (m)
- $D_{CO2.H2O}$ is the diffusivity of CO_2 in H_2O ($m^2.s^{-1}$)
- Gr is the Grashof number
- Sc is the Schmidt number

The Grashof and Schmidt numbers can be calculated using Equations 4.9 and 4.10 respectively.

$$Gr = \frac{d_b{}^3 \rho_{H_2O} g \Delta\rho}{\mu_{H_2O}{}^2} \tag{4.9}$$

$$Sc = \frac{\mu_{H_2O}}{\rho_{H_20} D_{CO_2.H_2O}} \tag{4.10}$$

where:

- ρ_{H2O} is the density of water ($kg.m^{-3}$)

- g is acceleration due to gravity ($m.s^{-2}$)
- $\Delta\rho$ is the difference between water and air density ($kg.m^{-3}$)
- μ_{H2O} is the viscosity of water ($kg.m^{-1}.s^{-1}$)

Figure 4.3 illustrates the effect of the superficial gas velocity on the overall mass transfer coefficient in the flat plate photobioreactor. It can be seen that k_La values predicted are sufficiently high to achieve the target CO_2 transfer rate of 20 $mg.L^{-1}.h^{-1}$. It is also evident that k_La is highly dependent on the superficial gas velocity. This occurs because the superficial gas velocity affects the overall gas holdup (ε) which in turn affects the gas-liquid interfacial area ($A_{i,\ total}$) available for mass transfer. A full set of sample calculations for estimating k_La is provided in Appendix A-2.

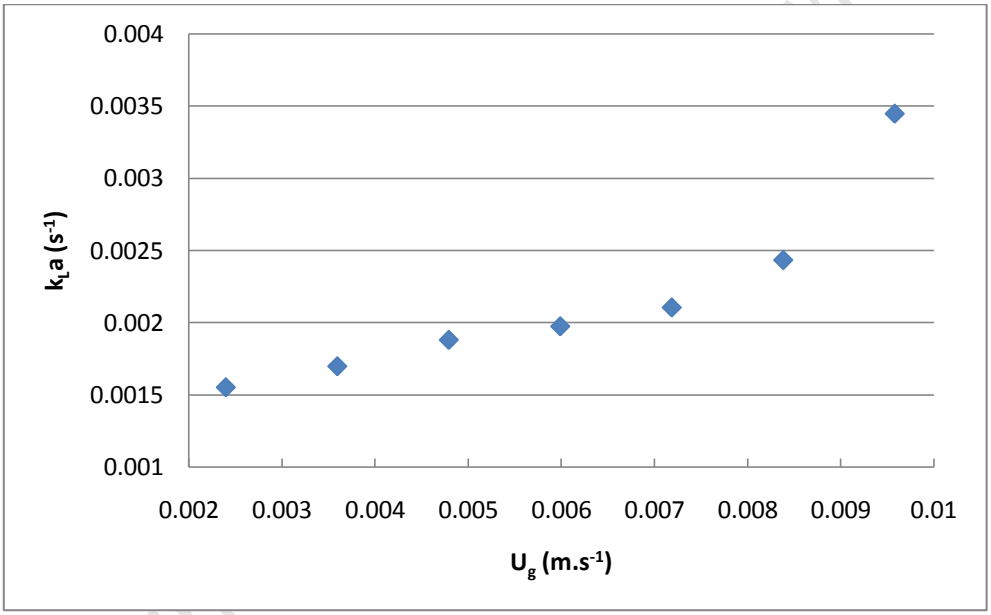

Figure 4. 3: The effect of the superficial gas velocity on the overall mass transfer coefficient in the flat plate photobioreactor, calculated from Equation 4.8

4.2.3 Flat plate photobioreactor design and construction

4.2.3.1 Reactor dimensions

A rectangular photobioreactor with a length, height and width of 270 mm x 280 mm x 59 mm was designed and constructed. The low aspect ratio was selected so that a circular flow pattern could be established in the flat plate photobioreactor to ensure a defined flow pattern and minimise settling of the algae (design objective 4). In addition, a trade off was made between the light path length and the overall reactor volume in order to satisfy design objective 2. A light path length of 59 mm was selected based on previous light attenuation

studies performed by Langley (2010), who investigated the effect of increasing depth and culture density on the amount of light penetration achieved for a culture of *Chlorella vulgaris* in a 1 L glass beaker. The light path length selected was also well within the range of light path lengths (1.3-10 cm) for flat plate photobioreactors suggested by Carvalho *et al.* (2006). Figure 4.4 illustrates a schematic of the vertical flat plate photobioreactor design.

4.2.3.2 Gas supply

The gas flow rate is an important design parameter owing to its effect on gas holdup and mass transfer in a reactor. In order to meet design objective 3, a 0.0064 m ID stainless steel sparger was designed to supply gas to the reactor. A 240 mm long sparger with 1 mm holes spaced 10 mm apart was constructed based on the sparger design used by Tamburic *et al.* (2011). The sparger was designed, such that gas could be supplied to one end or both ends of the sparger, as illustrated in Figure 4.4. The sparger was placed 5 mm from the base of reactor in order to promote the liquid circulation pattern and to minimize dead zones. In order to supply the reactor with a mixture of air containing 10 000 ppm CO_2, the gas flow rates of air and CO_2 were controlled by two rotameters. A third rotameter was used for mixing and to control the total flow rate of the gaseous mixture to the reactor. Prior to being sparged at the base of the reactor, the gaseous mixture was filtered through a 0.45 μm filter (Millipore, USA).

4.2.3.3 Sample ports, drainage and cleaning

Two 15 mm ID holes were drilled into the top section of the flat plate photobioreactor (Figure 4.4) to provide a port for sampling and a port for filling the reactor with media and distilled water. At the end of a run, the gas flow rate to the reactor was stopped and the rubber tubing on both sides of the sparger were clamped shut. The reactor was then tipped over and drained through the two top ports. The reactor was then taken apart and washed. The dried components were sprayed with 70% ethanol to ensure viable micro-organisms remained negligible, prior to reassembling the reactor.

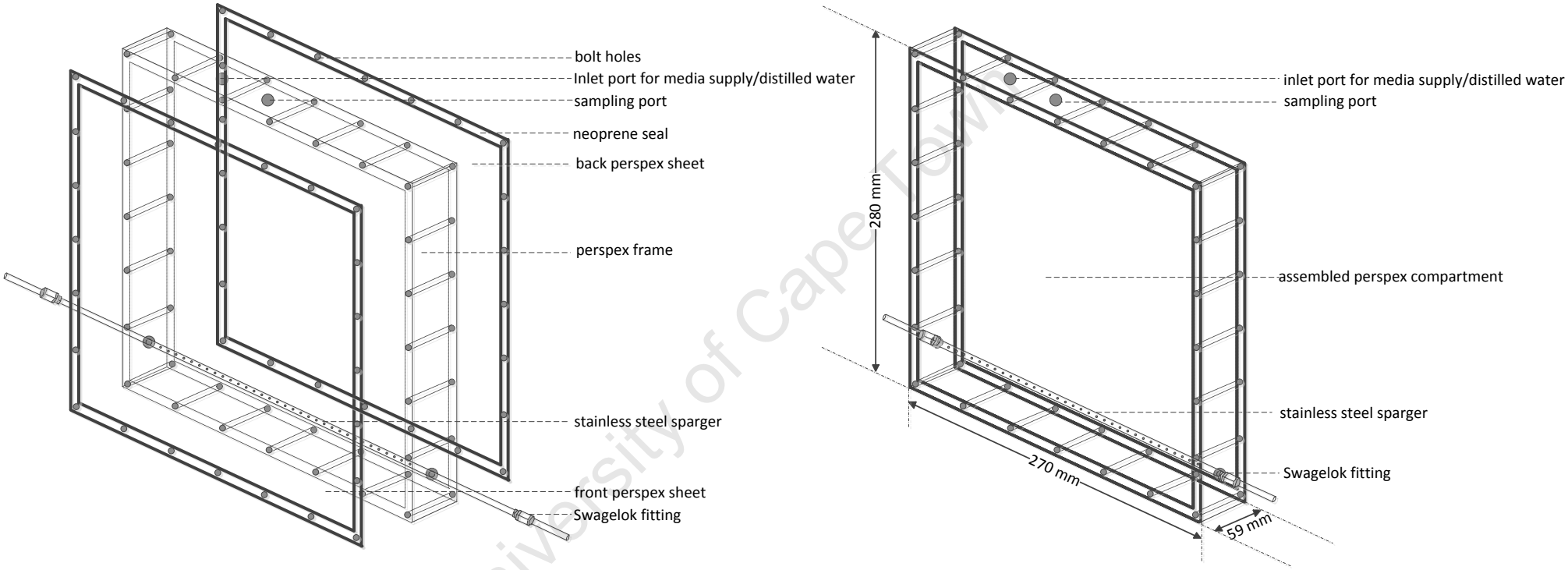

Figure 4. 4: Schematic of vertical flat plate photobioreactor (left: exploded view; right: assembled view)

4.2.3.4 Material selection

As mentioned previously, one of the most prominent factors limiting algal growth is the inefficient utilization of light energy. Thus, it is essential to select a material with good optical properties. In most laboratory scale photobioreactors, glass is commonly used because of its high refractive index, which affects both the propagation and transmission of light into the photobioreactor. However, polymethyl methacrylate (perspex) can be used as a cheaper, light weight and shatter resistant alternative to glass. As can be seen in Table 4.1, the optical properties of perspex are similar to that of glass, except that the refractive index of perspex is slightly lower than that of glass. In order to meet design objectives 1and 2 (Section 4.2.1), 15 mm thick perspex was used to construct the body of the flat plate photobioreactor which consisted of a rectangular frame and two sheets (Figure 4.4). A 15 mm thickness was selected to prevent the photobioreactor walls from warping due to an increase in pressure during operation. The perspex was polished after construction of the reactor in order to improve its optical transparency.

Table 4. 1: Comparison of the optical properties of glass and polymethyl methacrylate (perspex)

Material	Refractive index	Reflection of surface (%)	Transmission of light (%)	Reference
Glass	1.500	4	92	Bass *et al.* (2009)
PMMA	1.486	4	92	Kasarova *et al.* (2007)

The perspex sheets were sealed to the frame with 1 mm thick neoprene gaskets which were compressed using stainless steel bolts (grade 316). Neoprene was selected based on its maintenance of flexibility over a wide temperature range. Stainless steel (grade 316) was used to construct a 0.0064 m ID sparger due to its resistance to high temperatures and corrosion.

4.2.3.5 Light provision

Fluorescent and light-emitting diode (LED) light banks were used to provide constant illumination of the reactors used. The fluorescent light bank consisted of eight Osram 18 W cool white fluorescent bulbs (Figure 3.3). The reactor was placed 3 cm from the light bank to provide an average light intensity of 300 $\mu mol.m^{-2}.s^{-1}$. For a more detailed explanation of how the average light intensity was calculated, see Section 3.2.1.4. A second fluorescent light bank was placed on the opposite side of the photobioreactor, when an average light intensity of 600 $\mu mol.m^{-2}.s^{-1}$ was required. Figure 4.5 provides a schematic of the two fluorescent light

banks that were used to provide an average light intensity of 300 μmol.m^{-2}.s^{-1} on either side of the reactor.

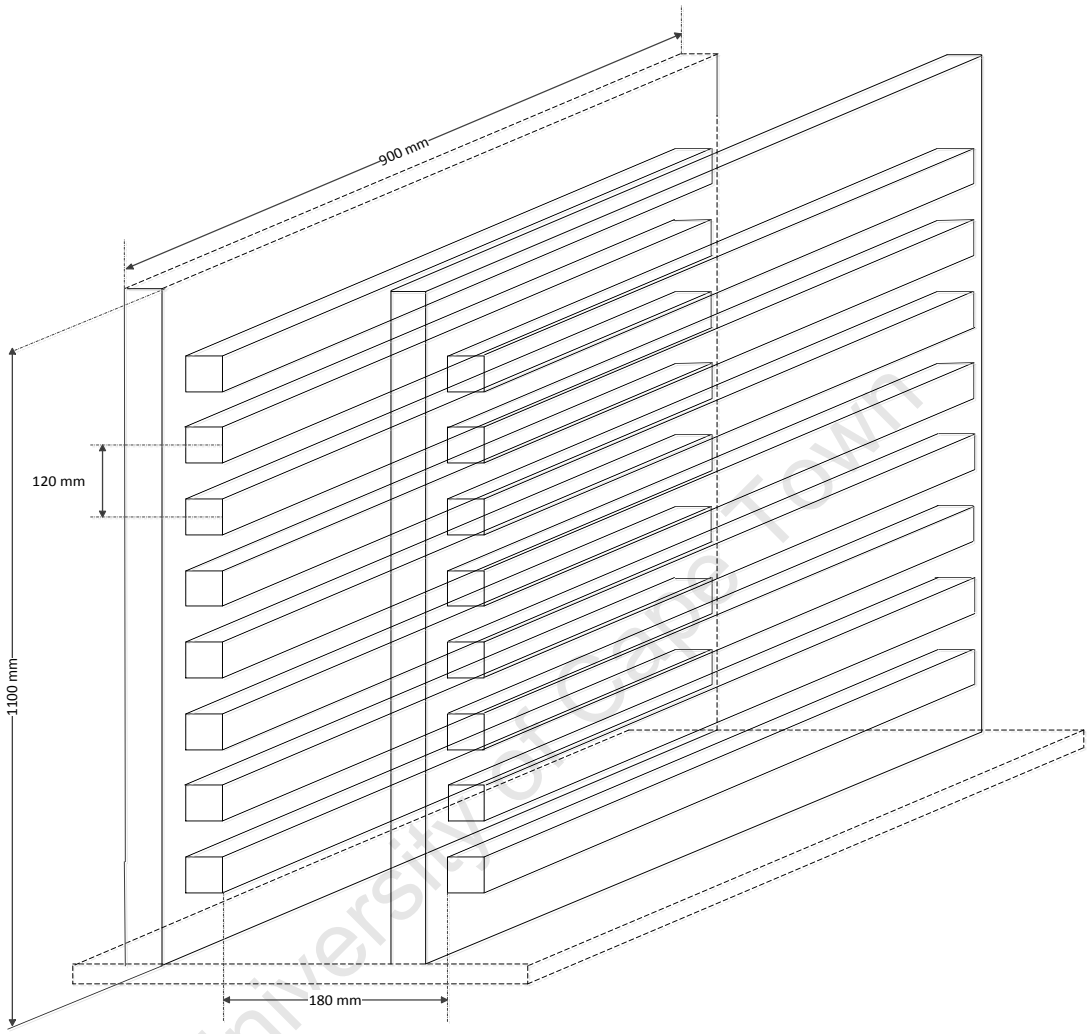

Figure 4. 5: Schematic of fluorescent light banks (not drawn to scale) (Adapted from Fraser, 2011)

The LED light bank consisted of thirteen 8 W Flash cool white T5 LED wall light bulbs, which each contained a strip of 40 LEDs (Figure 4.7) . The reactor was placed 1 cm from the light bank to provide an average light intensity of 300 μmol.m^{-2}.s^{-1}. Figure 4.6 provides a schematic of the LED light bank dimensions. For the raw data used to estimate the average light intensities of the fluorescent and LED light banks, see Appendix B-1. Figure 4.7 is a photograph of the operational flat plate photobioreactor (LED light bank was switched off).

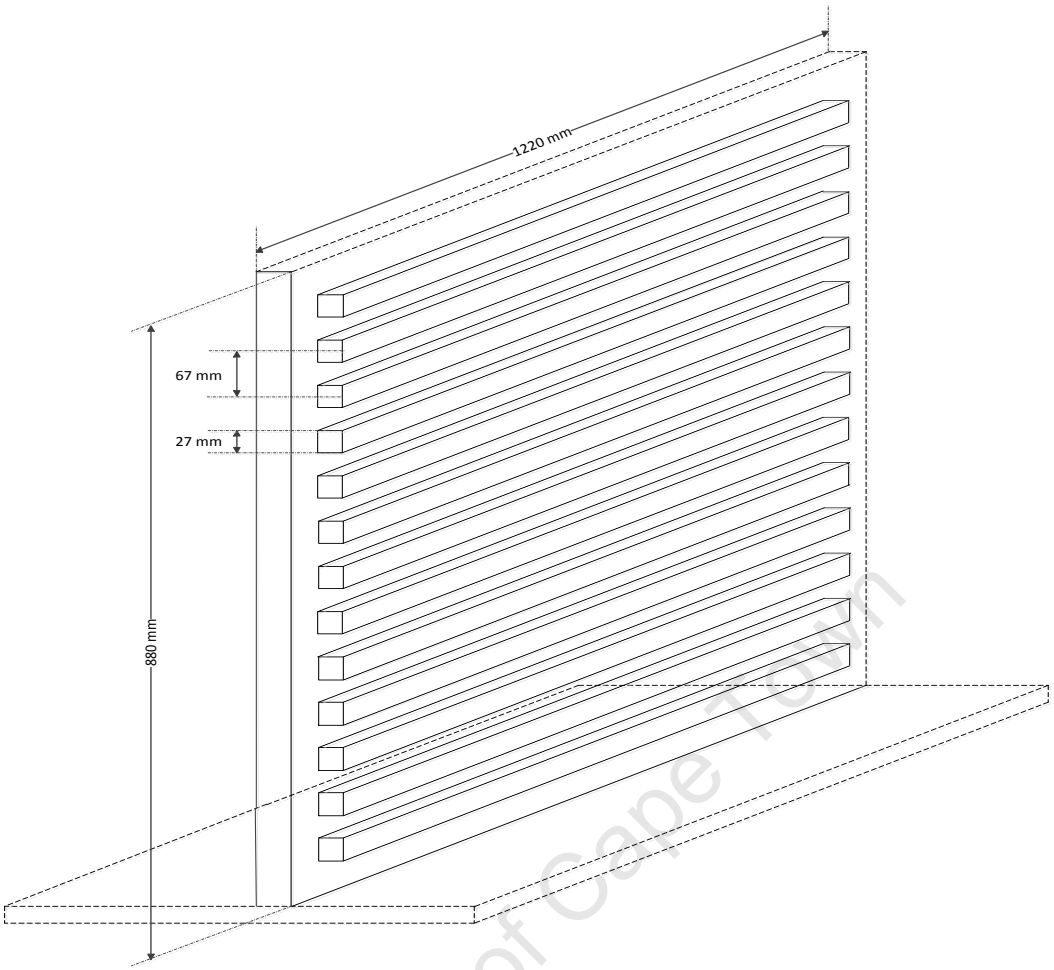

Figure 4. 6: Schematic of LED light bank (not drawn to scale)

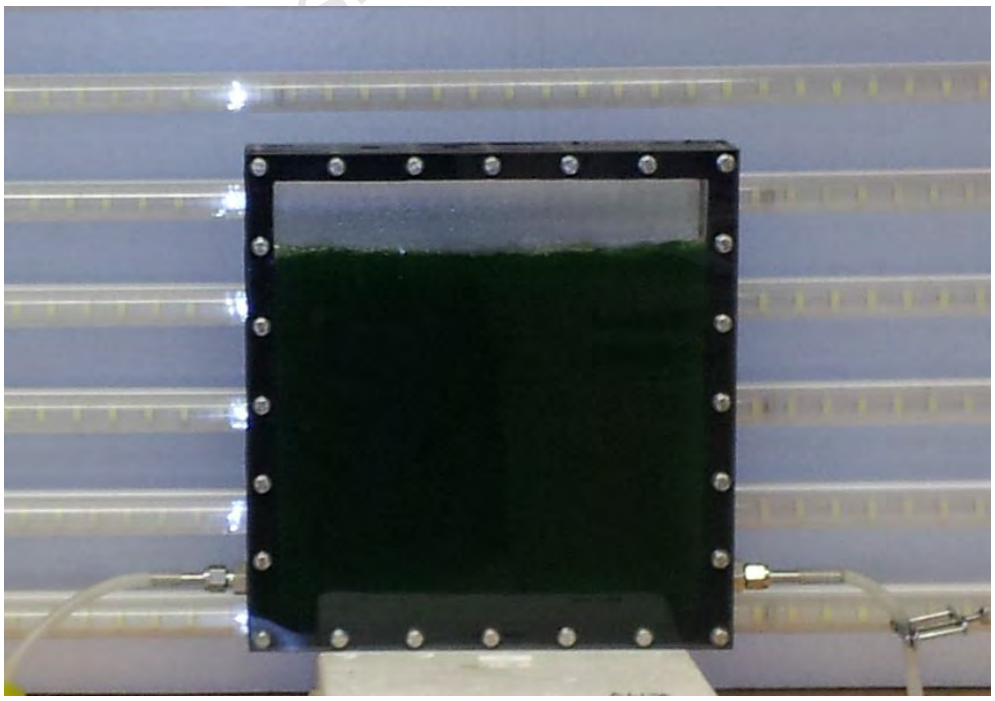

Figure 4. 7: Photograph of operational flat plate photobioreactor with LED light bank

4.2.4 Characterisation of flat plate photobioreactor

After construction, the circulation times and the overall mass transfer coefficients of the flat plate photobioreactor were measured, using the methods outlined in Sections 3.2.4 and 3.2.5 respectively. This allowed assessment of reactor performance against design characteristics.

4.2.4.1 Circulation time

The circulation times obtained in the flat plate photobioreactor as a function of gas flow rate are presented in Figure 4.8. Runs were performed in triplicate at each of the gas flow rates tested, in order to test the reproducibility of data.

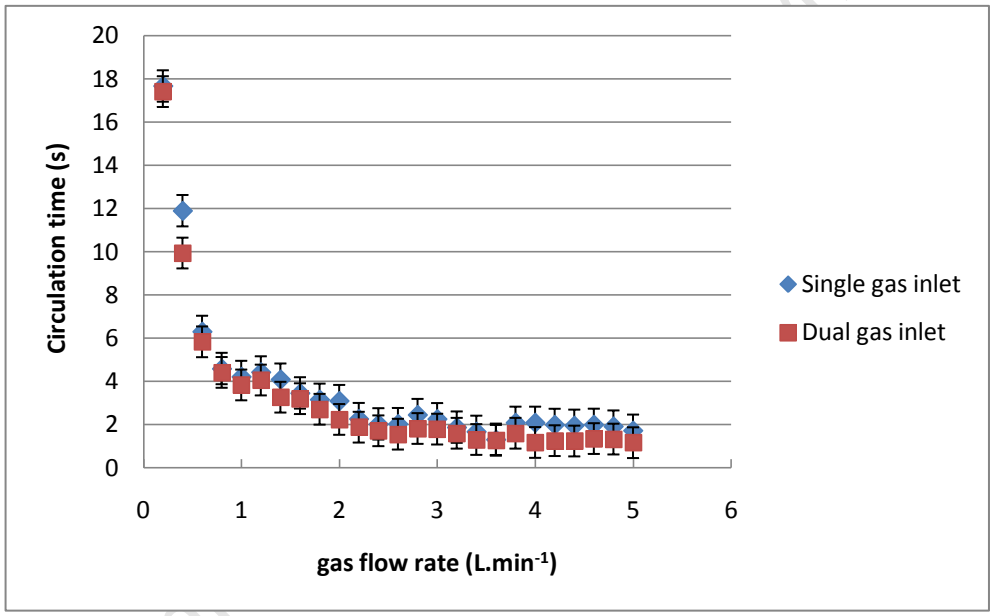

Figure 4. 8: Circulation times at different gas flow rates in the flat plate photobioreactor (An average experimental error of 5.2% was assumed based on repeat runs)

It can be seen that the mean circulation time decreased with increasing gas flow rate up to a gas flow rate of 2 $L.min^{-1}$. Increasing the gas flow rate further had a negligible effect on improving the mean circulation time below approximately 2.2 s. It can also be observed that there were no significant differences between the mean circulation times obtained when the single and dual gas inlet spargers were used, owing to the compact shape of the reactor which forced a circular liquid flow pattern. In Section 4.2.2.1, it was predicted that at a gas flow rate of 2 $L.min^{-1}$, the mean circulation time would be 4.48 s and that the photobioreactor would only achieve a mean circulation time of 2.50 s at a gas flow rate of 3 $L.min^{-1}$. The discrepancy between the predicted and experimental mean circulation

times may be due to the fact that the correlation between the superficial liquid velocity and the aeration rate provided by Equation 4.6 was system specific and thus could only provide a first estimate (Section 4.2.1). The average experimental error of 5.2% was calculated based on repeat runs. The experimental error could be the result of the human error associated with responding in time to record when the pink slug circulated around the reactor, especially when this occurred in less than 3 s.

When the experiments were performed to determine the mean circulation times obtained at different aeration rates in the flat plate photobioreactor, it was observed that the liquid followed a circular flow pattern. This is illustrated by the series of photographs in Figure 4.9, which show the progression of pink fluid in the flat plate photobioreactor at a gas flow rate of 2 L.min^{-1}.

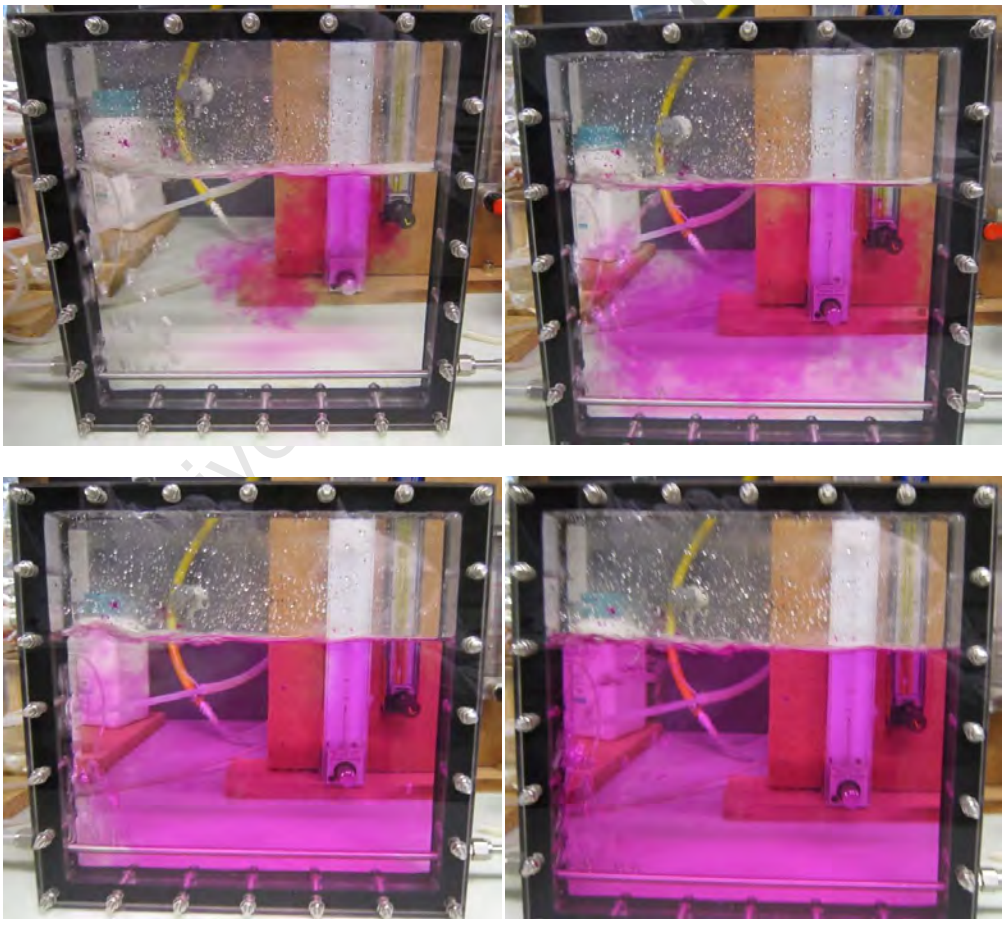

Figure 4. 9: Set of photographs indicating the progression of the liquid from colourless to pink (phenolphthalein indicator) in the flat plate photobioreactor at an aeration rate of 2 L.min^{-1}

In order to ascertain whether or not the axial fluid flow in the flat plate photobioreactor had a defined flow pattern, the movement of the pink slug in the axial direction was recorded using a video camera. The video was slowed down and the flow pattern was observed. The still images obtained at a flow rate 2.5 L.min^{-1} are illustrated in Figure 4.10. It can be observed that the axial fluid flow was random and that the transition from colourless to pink fluid occurred rapidly (less than 2 s).

a) pink slug initially added at t = 46 s

b) pink slug progression at t = 46.5 s

c) pink slug progression at t = 47 s

d) pink slug progression at t = 48 s

Figure 4. 10: Still images of the progression of the pink slug in the axial direction at a gas flow rate of 2.5 L.min^{-1} in the flat plate photobioreactor

4.2.4.2 Overall mass transfer coefficient

For practical reasons $k_La(O_2)$ was easier to measure than $k_La(CO_2)$ (Section 3.2.5). Duplicate runs were performed at each gas flow rate to assess the reproducibility of data. The effect of aeration rate on $k_La(O_2)$ and the conversion of $k_La(O_2)$ to $k_La(CO_2)$ using Equation 2.5 can be found in Appendix C-3-1. The $k_La(CO_2)$ obtained in the flat plate photobioreactor over a range of gas flow rates is presented in Figure 4.11. The general trend observed from Figure 4.11 showed an increase in aeration rate resulted in an increase in $k_La(CO_2)$. Furthermore, it can be seen that the $k_La(CO_2)$ values obtained using a dual sparger were slightly higher than those obtained using the single inlet sparger. It was also found that the addition of antifoam to the media had a negligible effect on $k_La(CO_2)$ (data not shown). For instance, at gas flow rates of 3.5 and 5 $L.min^{-1}$, $k_La(CO_2)$ values of 0.0080 s^{-1} and 0.0098 s^{-1} were obtained respectively. These values are approximately 3% and 1.5% greater than the $k_La(CO_2)$ values obtained at flow rates of 3.5 and 5 $L.min^{-1}$, without the addition of antifoam.

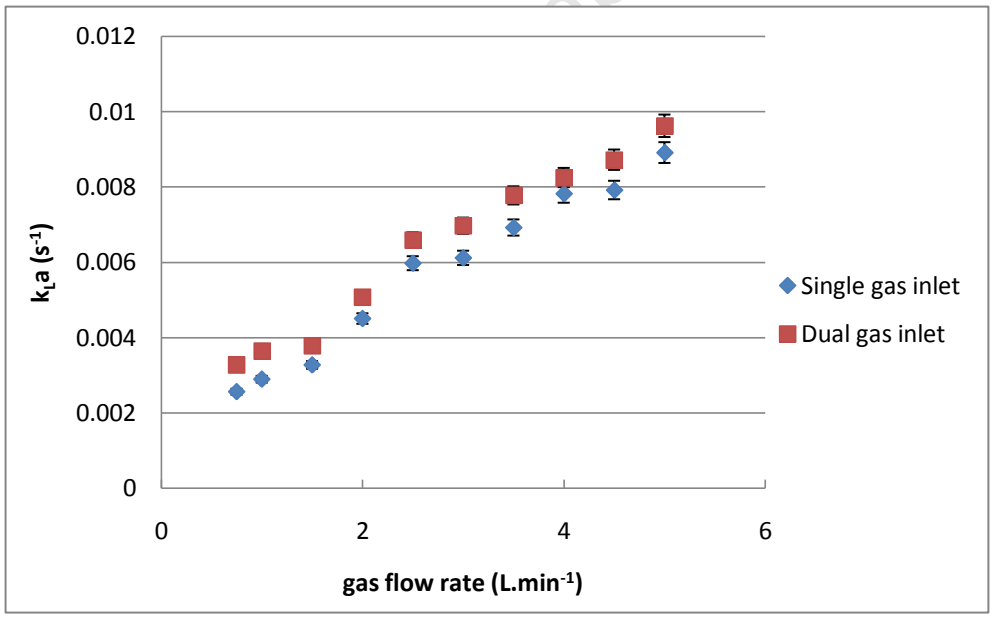

Figure 4. 11: Overall mass transfer coefficient of CO_2 at different gas flow rates in the flat plate photobioreactor filled with media (no antifoam) at 23±1°C (Error bars represent standard deviation for duplicate runs)

In Section 4.2.2.2, a similar increase in $k_La(CO_2)$ with increasing aeration rate was predicted. However, it can be observed that a significant difference existed between the experimental $k_La(CO_2)$ values and the theoretical values obtained from Equation 4.8 (Figure 4.3). For example, at a gas flow rate of 4 $L.min^{-1}$, the predicted and experimental

$k_La(CO_2)$ values were 0.0034 s^{-1} and 0.0082 s^{-1} respectively. The discrepancies between the predicted values from the theoretical correlation may be attributed to the inaccurate estimation of the overall gas holdup from Equations 4.2 and 4.6. The discrepancy between the predicted and experimental gas holdup may be due to the fact that the correlation between the superficial liquid velocity and the aeration rate provided by Equation 4.6 was system specific and thus could only provide a first estimate of the overall gas holdup (Section 4.2.2.1). In order to validate this theory, the change in liquid height as a function of gas flow rate was measured and Equation 4.3 was used to calculate the overall gas hold up (Appendix C-3-1). Figure 4.12 illustrates the difference between the theoretical gas holdup and the experimental gas hold up for the flat plate photobioreactor. Consequently, lower $k_La(CO_2)$ values were predicted as the gas holdup had a direct impact on the gas-liquid interfacial area that was available for mass transfer (Equation 4.8).

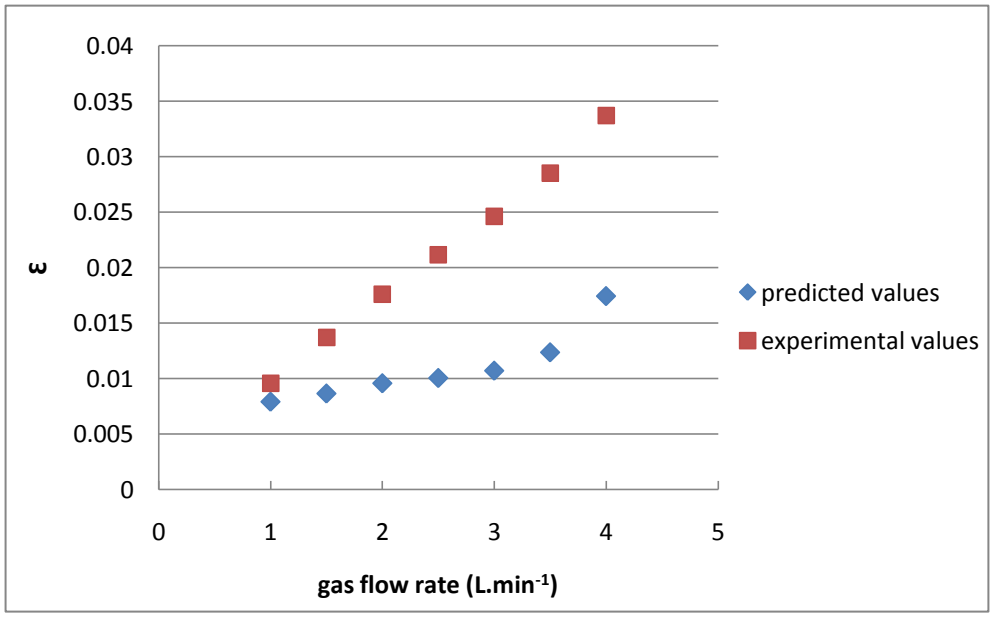

Figure 4. 12: Differences between the predicted gas holdup values obtained from Equations 4.2 and 4.6 and the experimental values calculated from Equation 4.3

4.2.5 Standard operating conditions for flat plate photobioreactor

In order to evaluate and compare the performance of the flat plate photobioreactor to that of the vertical airlift photobioreactor and tubular photobioreactor in terms of light utilization, under standard conditions, constant illumination at 300 $\mu mol.m^{-2}.s^{-1}$ was provided from a bank of eight Osram 18 W cool fluorescent light bulbs situated on one

side of the flat plate photobioreactor at a distance of 3 cm from the reactor surface. Furthermore, to ensure that the flat plate and vertical airlift photobioreactors operated at similar $k_La(CO_2)$ values, a mixture of air containing 10 000 ppm CO_2 at a flow rate of 5 $L.min^{-1}$ was filtered through a 0.45 μm filter (Millipore, USA) prior to being sparged at the base of the flat plate photobioreactor. At these conditions, the k_La (CO_2) and mean circulation time in the flat plate photobioreactor were 0.0101 ± 0.00029 s^{-1} and 1.72 ± 0.088 s respectively.

At the beginning of each run, 10 μL of antifoam (Antifoam 204, Sigma Life Science) was added to the reactor to reduce foaming. During runs, the temperature was monitored on a daily basis using a digital thermometer and remained at 26±1°C. Approximately 30 mL of distilled water was added to the reactor on a daily basis to replace water lost due to evaporation. For conditions of higher light intensity a second fluorescent light bank was placed on the opposite side of the photobioreactor. Under these conditions, a fan was used to maintain the temperature at 26±1°C.

4.3 Internally lit LED airlift photobioreactor

In order to assess the effect of providing internal illumination on the algal growth rate, a standard airlift photobioreactor, shown in Figure 3.1 was modified by constructing an internal compartment to house a strip of cool white light-emitting diode (LED) tape.

4.3.1 Design objectives

The design objectives for the internally illuminated photobioreactor were as follows:

1. To select a light source with a sufficiently high light intensity for algal growth which would generate minimal excess heat and could be positioned internally in the reactor.
2. To select an energy efficient, durable and compact light source.
3. To minimize the volume of the reactor occupied by internal lighting.
   To design a reactor that is easy to disassemble and clean.

4.3.2 Design of the internally lit airlift photobioreactor

4.3.2.1 Selection of a light source

In order to meet design objectives 1, 2 and 3, a compact light source with a sufficiently high light intensity, the 600 lumens per metre cool white TAPE LITE LED, was selected to provide constant internal illumination. A 5A 12V power supply was required to operate the LED tape. Figure 4.13 shows a section of the LED tape light. A USB 2000 Spectrometer (Ocean Optics Inc, SA) was used to analyze the emission spectra of common artificial light sources in the laboratory, in order to assess the feasibility of using LEDs to cultivate microalgae. Figure 4.14 illustrates the relative intensities of the different light sources, as a function of wavelength. The emission spectra for the cool white LEDs and the standard cool white fluorescent light bulbs are very similar, except for the LED peak between 400 and 500 nm.

Figure 4. 13: Section of cool white TAPE LITE LED

4.3.2.2 Material selection

In keeping with the design of a standard airlift photobioreactor (Langley, 2010), the compartment for the LED tape light was constructed using a glass cylinder with wall thickness of 2.5 mm that would fit around the draft tube of the airlift photobioreactor. Silicone (Smooth-Sil 950) was selected to mould seals for the internal glass compartment because of its resistance to corrosion (Langley, 2010) and because of the ease with which moulds could be constructed for purpose-made seals.

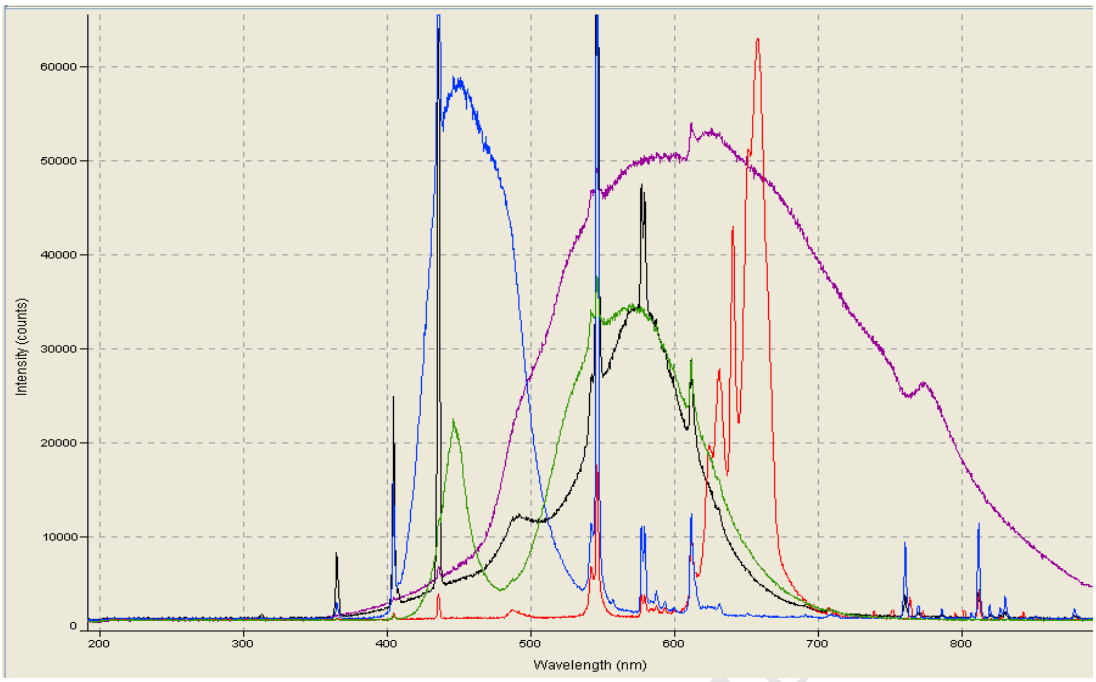

Figure 4. 14: Emission spectra of common artificial light sources (black-cool white fluorescent, red -red fluorescent, blue-blue fluorescent, green-cool white LEDs and purple-halogen lamp)

4.3.3 Design and construction of internally lit airlift photobioreactor

A simplified cross-sectional view of the photobioreactor is presented in Figure 4.15. The modified airlift photobioreactor was constructed in accordance with the dimensions provided in Figure 4.16. Silicon seals were placed at the top and the bottom of the two inner glass columns to create an air-tight compartment for the LEDs. These seals were compressed by tightening the nut on the top compression plate which created even pressure between the top and bottom steel plates. As an additional safety measure, the electrical lead at the base of the photobioreactor was insulated twice with insulation tape and Swagelok fittings were used to prevent any leaks from occurring. In order to provide internal light intensities of 160 and 300 $\mu mol.m^{-2}.s^{-1}$, 1 and 1.8 m strips of LED tape were coiled around the draught tube respectively. Details of how the average light intensities were calculated can be found in Appendix B-2. Figure 4.17 is a photograph of the modified reactor at a light intensity of 300 $\mu mol.m^{-2}.s^{-1}$.

Under standard conditions, the modified airlift reactor was operated at a constant internal illumination of 300 $\mu mol.m^{-2}.s^{-1}$. A mixture of air containing 10 000 ppm CO_2 at flow rate of 2 $L.min^{-1}$ was filtered through a 0.45 µm filter (Millipore, USA) prior to being sparged at the base of the draught tube through a 0.22 µm stainless steel HPLC inlet filter. The

flow rates of air and CO_2 were regulated and maintained using a Brooks 5850S Thermal Mass Flow Controller. An overall mass transfer coefficient for CO_2 of $0.0094 \pm 0.00026\ s^{-1}$ was achieved for the standard vertical airlift photobioreactors at a gas flow rate of 2 $L.min^{-1}$. This correlated well with the $k_La(CO_2)$ of $0.0105\ s^{-1}$ estimated by Langley (2010) from design calculations for the airlift photobioreactor (Figure 3.4). It can be seen, from Figure 3.4, that the increase in the ratio of the areas of the riser and downcomer from 0.3 to 0.5 on the provision of internal illumination had a minimal effect on the overall mass transfer coefficient achieved in the airlift photobioreactor. Thus, for this study, the effective $k_La(CO_2)$ was assumed to be $0.0094 \pm 0.00026\ s^{-1}$ in the modified internally illuminated photobioreactor.

Prior to all runs, the modified reactor was sterilized with distilled water and adding a sufficient amount of a 7500 ppm concentrate of chlorine dioxide to obtain a final concentration of 10-30 ppm. In order to ensure that the sterilization process was successful, the reactor was covered in tin foil to exclude light from the reactor, as it destroys chlorine dioxide. The reactor was then left to sterilize overnight. The reactor was then drained and filled with sterilized 3 N BBM media. At the beginning of each run, 20 µL of antifoam (Antifoam 204, Sigma Life Science) was added to the reactor to reduce foaming. The temperature of each experiment was monitored on a daily basis using a digital thermometer and was maintained at 26±1°C. When the modified photobioreactor was operated at 300 $\mu mol.m^{-2}.s^{-1}$, approximately 180 mL of distilled water was added to the reactor on a daily basis to replace water lost due to evaporation. At these conditions, a fan was used to maintain the temperature at 26±1°C. When the photobioreactor was operated at the lower light intensity of 160 $\mu mol.m^{-2}.s^{-1}$, approximately 140 mL distilled water was required on a daily basis to account for evaporation and no fan was required to maintain the temperature at 26±1°C.

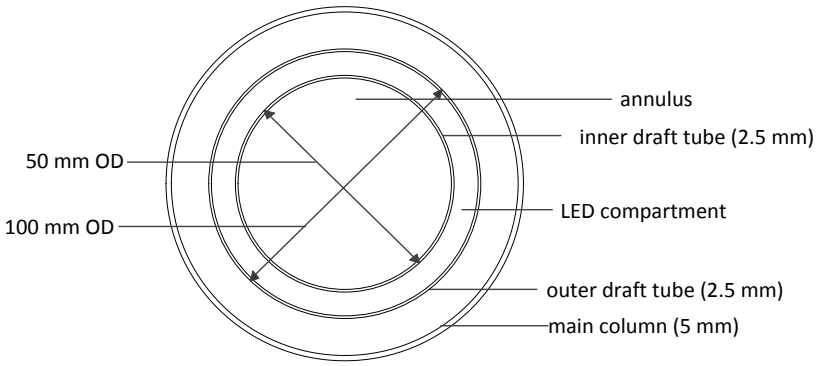

Figure 4. 15: Schematic of the cross-sectional view of the modified airlift photobioreactor

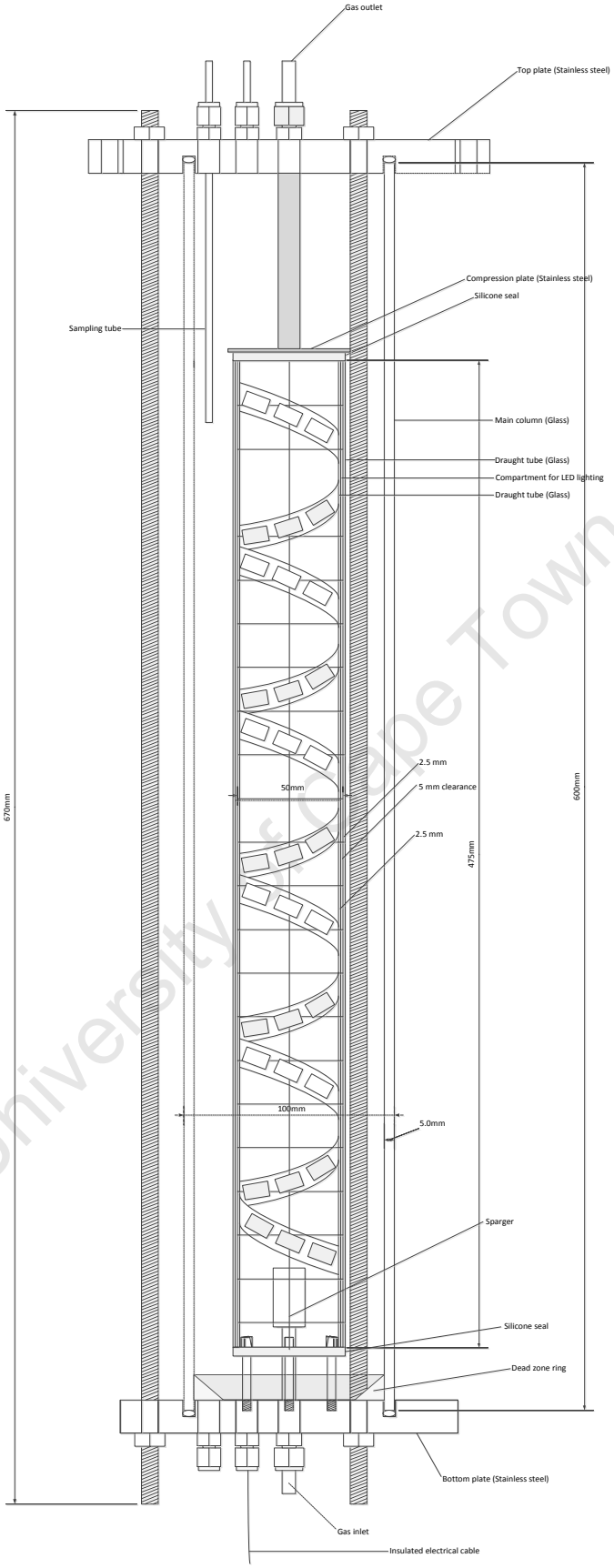

Figure 4. 16: Schematic of the modified airlift photobioreactor with the internal compartment (not drawn to scale)

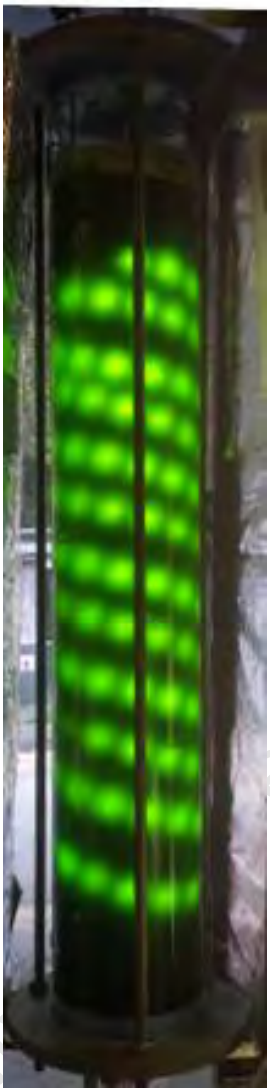

Figure 4. 17: Photograph of modified LED reactor with an average light intensity of 300 µmol.m^{-2}.s^{-1}

4.4 Conclusions

A 1.6 L perspex flat plate photobioreactor with a 0.0064 m ID stainless steel sparger was designed and constructed. Tests were performed to characterise the hydrodynamics and overall mass transfer coefficient of the system at different gas flow rates. Furthermore, a standard airlift photobioreactor was modified so that the effects of internal illumination on algal growth could be assessed. The modified airlift photobioreactor was characterised based on previous work performed by Langley (2010). These reactors, together with the standard airlift photobioreactor designed by Langley (2010) and the tubular reactors designed by Fraser (2011), provide a complete set of reactors across which to study the effect of light supply on algal growth and productivity, as reported in Chapters 5 and 6.

5. The effects of light intensity, light configuration and temperature on algal growth in airlift photobioreactors

5.1 Introduction

In this chapter, the results obtained for investigating the effects of light intensity on the growth of *Scenedesmus sp.* and *Chlorella vulgaris* are presented. From these results, the species which could utilize the additional light intensity more effectively for growth was selected for the remainder of experimental work. Subsequently, the effects of light intensity and configuration on growth were assessed using standard airlift photobioreactors with external cool white fluorescent light banks and a modified airlift photobioreactor with internal cool white LED light tape. Finally, the effect of temperature in the range 24 to 30°C on growth was evaluated, using external fluorescent light at light intensities of 300 and 600 $\mu mol.m^{-2}.s^{-1}$. Runs were performed in the airlift reactors according to the experimental plan provided in Section 3.3.2.

5.2.1 Investigation of the effect of light intensity on the growth of *Chlorella vulgaris* and *Scenedesmus sp.*

Initially, the effect of light intensity on the growth rate of *Chlorella vulgaris* was assessed. Runs were carried out in the airlift photobioreactors at 300 and 600 $\mu mol.m^{-2}.s^{-1}$ using external fluorescent lighting. As shown in Figures 5.1 and 5.2, *Chlorella vulgaris* became photo inhibited when the light intensity was increased to 600 $\mu mol.m^{-2}.s^{-1}$ at the beginning of a run. Thus, in order to assess the effect of a higher light intensity on growth, the light intensity of two airlift photobioreactors operated under standard conditions at 300 $\mu mol.m^{-2}.s^{-1}$ was increased to 600 $\mu mol.m^{-2}.s^{-1}$ after 2 and 7 days respectively. The additional 300 $\mu mol.m^{-2}.s^{-1}$ was provided after 2 and 7 days to allow sufficient time for the algal culture to become denser so that mutual shading between algal cells would minimize the effects of photoinhibition. Figures 5.1 and 5.2 illustrate the results obtained for investigating the effect of light intensity on the growth of *Chlorella vulgaris*.

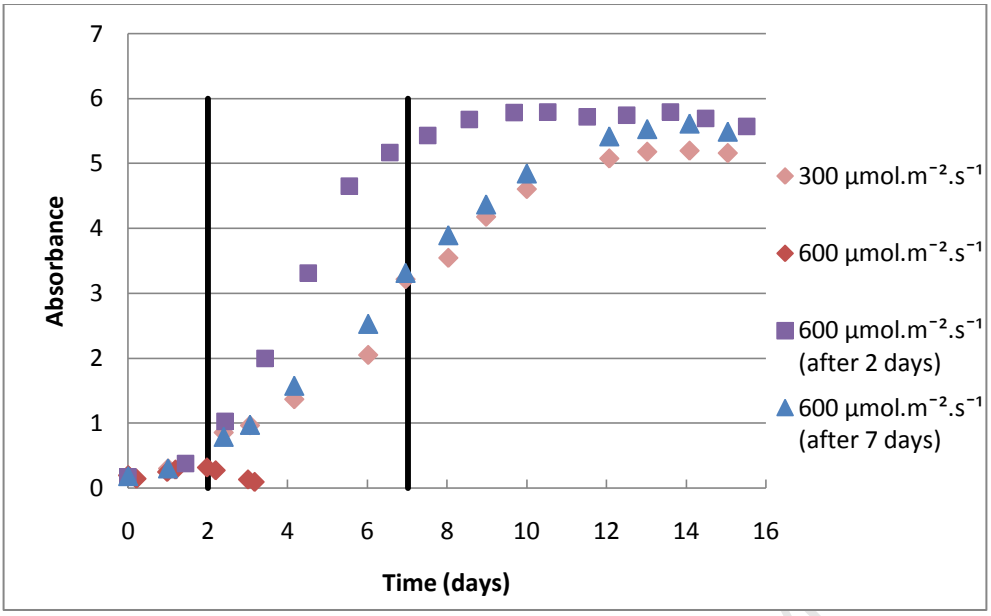

Figure 5. 1: The effect of light intensity on the growth of *Chlorella vulgaris* at 24±1°C (black lines indicate when the light intensity was increased from 300 to 600 µmol.m^{-2}.s^{-1} after 2 and 7 days respectively)

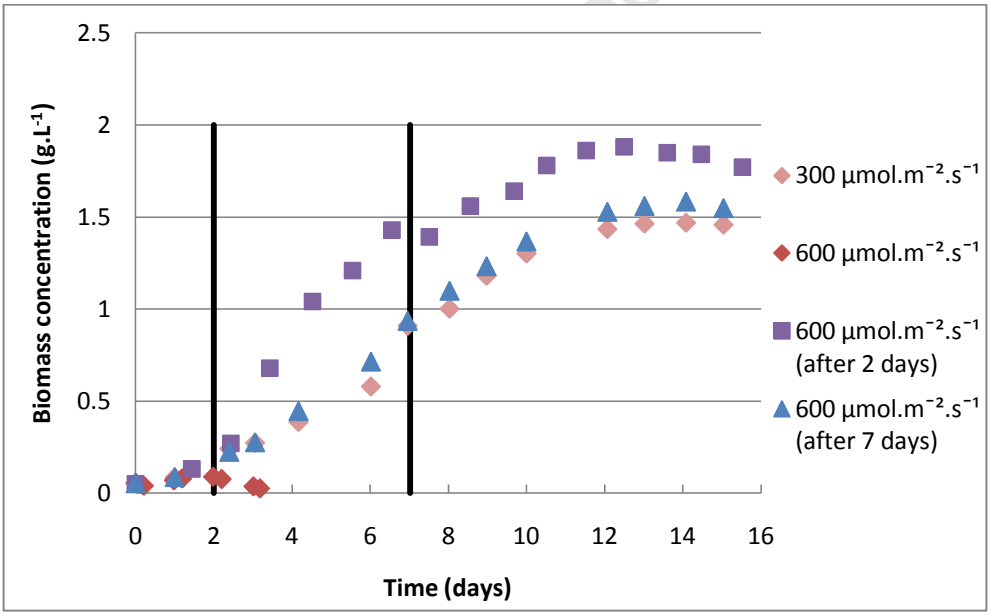

Figure 5. 2: The effect of of light intensity on the biomass concentration of *Chlorella vulgaris* at 24±1°C (black lines indicate when the light intensity was increased from 300 to 600 µmol.m^{-2}.s^{-1} after 2 and 7 days respectively)

From Figures 5.1 and 5.2, it can be seen that increasing the light intensity from 300 to 600 µmol.m^{-2}.s^{-1} after 2 days had a positive impact on the growth curve of *Chlorella vulgaris*. However, increasing the light intensity to 600 µmol.m^{-2}.s^{-1} after 7 days had a minimal effect on improving the growth rate and biomass concentration. It can be observed from Figure 5.2, that maximum biomass concentrations of 1.88 g.L^{-1} and

1.58 $g.L^{-1}$ were obtained after 12.5 and 14 days of cultivation, when the light intensity was increased to 600 $\mu mol.m^{-2}.s^{-1}$ after 2 and 7 days respectively. These can be compared to the maximum biomass concentration of 1.46 $g.L^{-1}$ at 300 $\mu mol.m^{-2}.s^{-1}$ obtained after 13 days. Table 5.1 provides the maximum specific growth rates and linear productivities obtained at the different lighting conditions. The R^2 values greater than 0.97 demonstrate the goodness of fit of the maximum specific growth rates and linear productivities respectively (Appendix C-1-1). The maximum specific growth rates achieved at 300 $\mu mol.m^{-2}.s^{-1}$ and when the light intensity was increased from 300 to 600 $\mu mol.m^{-2}.s^{-1}$ after 7 days were similar since both photobioreactors were exposed to 300 $\mu mol.m^{-2}.s^{-1}$ at the start of the run. However, increasing the light intensity to 600 $\mu mol.m^{-2}.s^{-1}$ after 7 days resulted in an increase in the linear productivity, which suggests that the linear growth rate was light-limited. Furthermore, it can be seen that increasing the light intensity to 600 $\mu mol.m^{-2}.s^{-1}$ after 2 days resulted in an increase in both the maximum specific growth rate and the linear productivity. A possible explanation for the increase in the maximum specific growth rate could be that increasing the light intensity increases the volume fraction of the photobioreactor that is exposed to light. This implies that the biomass concentration and light path length have a significant effect on the amount of light penetration that is achieved. From analysis of the raw data in Appendix C-1-1, it was found that exponential growth was maintained for approximately the first 58 hours and that the cultures transitioned from exponential to linear growth at biomass concentrations of between 0.23-0.53 $g.L^{-1}$ and 0.27-0.68 $g.L^{-1}$ at average light intensities of 300 and 600 $\mu mol.m^{-2}.s^{-1}$ after 2 days respectively.

Table 5. 1: The effect of light intensity on the maximum specific growth rate and linear productivity of *Chlorella vulgaris* at 24±1°C

	Maximum specific growth rate		Linear productivity	
I_o ($\mu mol.m^{-2}.s^{-1}$)	μ_{max} (h^{-1})	R^2 value	Q ($g.L^{-1}.h^{-1}$)	R^2 value
300	0.0262	0.9821	0.0056	0.9812
600 (after 2 days)	0.0287	0.9992	0.0097	0.9784
600 (after 7 days)	0.0252	0.9921	0.0067	0.9962

Figure 5.3 illustrates the results obtained for the comparison between the growth of *Scenedesmus sp.* and *Chlorella vulgaris* at different light intensities. The dry weight data for this experiment followed a similar trend to the data depicted in Figure 5.3 and can be seen in Figure C3 in Appendix C-1-1. It is clear from Figure 5.3, that an increase in light intensity had a positive impact on the growth rate and biomass concentration for both species. It is also evident that the increase in light intensity resulted in a significantly greater increase in the biomass concentration of *Scenedesmus sp.* compared to *Chlorella vulgaris.* For instance, increasing the light intensity from 300 to 600 $\mu mol.m^{-2}.s^{-1}$ after 2 days resulted in an increase in the biomass concentration of *Chlorella vulgaris* from 1.46 $g.L^{-1}$ to 1.88 $g.L^{-1}$ after 14 and 13 days of growth respectively. A similar increase in light intensity resulted in an increase in the biomass concentration of *Scenedesmus sp.* from 1.67 $g.L^{-1}$ to 3.62 $g.L^{-1}$ after 14 and 15 days of growth respectively. Further at 15 days, the *Scenedesmus sp.* biomass concentration had not reached a maximum.

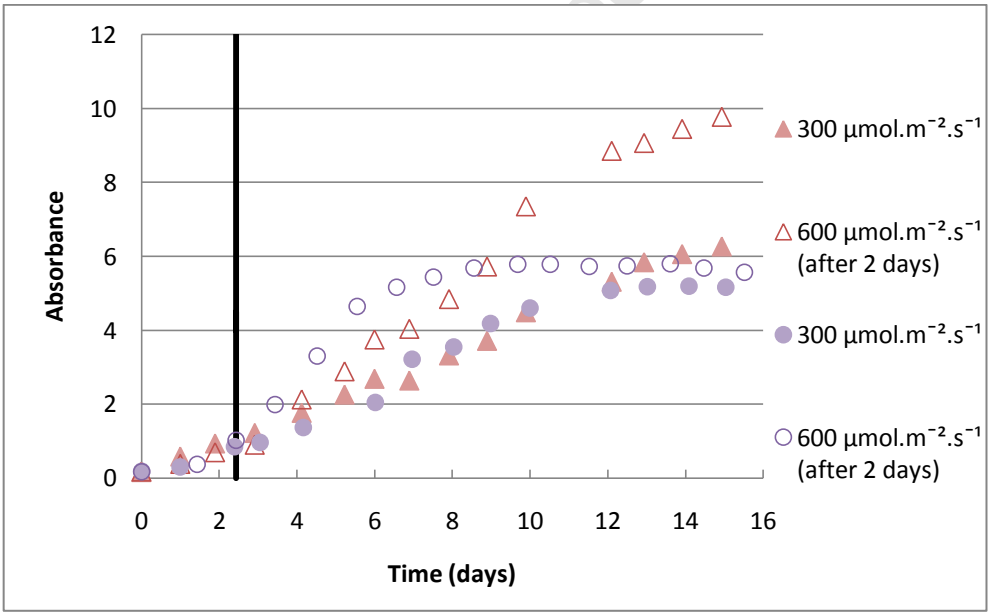

Figure 5. 3: Comparison between the growth curves of *Scenedesmus sp.* and *Chlorella vulgaris* at different light intensities and 24±1°C
(triangles and circles represent *Scenedesmus sp.* and *Chlorella vulgaris* respectively)

Table 5.2 illustrates the effect of light intensity on the maximum specific growth rates and linear productivities obtained for *Chlorella vulgaris* and *Scenedesmus sp.* respectively. The R^2 values greater than 0.97 indicate the goodness of fit for the maximum specific growth rates and linear productivities for both species (Appendix C-1-1). It can be seen from Table 5.2 that, at both light intensities, *Chlorella vulgaris* obtained a higher

maximum specific growth rate than *Scenedesmus sp.* From analysis of the experimental data in Appendix C-1-1, it was found that the exponential growth rate was maintained for approximately the first 58 and 48 hours of growth for *Chlorella vulgaris* and *Scenedesmus sp.* respectively. It was also observed that *Scenedesmus sp.* cultures transitioned from exponential to linear growth at biomass concentrations in the range of 0.28-0.44 $g.L^{-1}$ and 0.29-0.53 $g.L^{-1}$ at light intensities of 300 $\mu mol.m^{-2}.s^{-1}$ and 600 $\mu mol.m^{-2}.s^{-1}$ after 2 days respectively. As mentioned earlier, it was also observed that *Chlorella vulgaris* cultures transitioned from exponential to linear growth at biomass concentrations of between 0.23-0.53 $g.L^{-1}$ and 0.27-0.68 $g.L^{-1}$ at average light intensities of 300 $\mu mol.m^{-2}.s^{-1}$ and 600 $\mu mol.m^{-2}.s^{-1}$ after 2 days respectively. Thus, it is evident that *Scenedesmus sp.* and *Chlorella vulgaris* transitioned from exponential growth to linear growth within similar biomass concentration ranges.

Table 5. 2: Comparison of the effect of light intensity on the maximum specific growth rates and linear productivities of *Chlorella vulgaris* and *Scenedesmus sp.* at 24±1°C

		Maximum specific growth rate		Linear productivity	
Species	I_o ($\mu mol.m^{-2}.s^{-1}$)	μ_{max} (h^{-1})	R^2 value	Q ($g.L^{-1}.h^{-1}$)	R^2 value
Chlorella vulgaris	300	0.0262	0.9821	0.0056	0.9812
Chlorella vulgaris	600 (after 2 days)	0.0287	0.9992	0.0097	0.9784
Scenedesmus sp.	300	0.0242	0.9992	0.0053	0.9843
Scenedesmus sp.	600 (after 2 days)	0.0268	0.9826	0.0118	0.9933

In terms of the linear productivities, it can be seen that similar values were obtained for both species at 300 $\mu mol.m^{-2}.s^{-1}$. However, increasing the light intensity from 300 to 600 $\mu mol.m^{-2}.s^{-1}$ after 2 days resulted in a greater increase in the linear productivity of *Scenedesmus sp.* compared to *Chlorella vulgaris.* Furthermore, it can also be seen from Figure 5.3 that *Scenedesmus sp.* was able to sustain the linear growth rate for a longer period of time as compared to *Chlorella vulgaris.* A possible explanation for these results is that *Scenedesmus sp.* appears to be able to scavenge light more efficiently than *Chlorella vulgaris* at higher biomass concentrations. According to literature, an alternate explanation could be that at high cell densities, *Chlorella vulgaris* cells secrete a water-soluble substance that inhibits growth (Javanmardian and Palsson, 1991; Pratt, 1942). If this were the case, even at higher light intensities, the auto inhibitory substance would limit the maximum biomass concentration that could be attained. Based on these

results, it is evident that *Scenedesmus sp.* is a better candidate for attaining higher biomass concentrations at higher light intensities. In addition, *Scenedesmus sp.* is easier to cultivate as it does not become photo inhibited at 600 $\mu mol.m^{-2}.s^{-1}$ at low cell densities. Thus, *Scenedesmus sp.* was selected as algal species of choice for the remainder of the study.

5.2.2 The effect of light intensity and light configuration on the growth of *Scenedesmus sp.*

Figures 5.4 and 5.5 illustrate the results obtained for investigating the effects of light intensity (160, 300, 460 and 600 $\mu mol.m^{-2}.s^{-1}$) and light configuration (external fluorescence and internal LED light sources) on the growth of *Scenedesmus sp.* at 26±1°C. The general trend observed was that an increase in light intensity resulted in an increase in both the growth rate and the biomass concentration of *Scenedesmus sp*. It can be seen that the internally illuminated photobioreactor operated at 160 $\mu mol.m^{-2}.s^{-1}$ followed a linear growth curve from day one. Since the culture was not nutrient or CO_2 limited, the linear trend indicates that the growth of *Scenedesmus sp.* was light limited and that an average light intensity of 160 $\mu mol.m^{-2}.s^{-1}$ was insufficient for optimal growth in the airlift photobioreactor. The standard externally lit fluorescent airlift photobioreactor and the internally lit LED photobioreactor achieved similar growth curves at 300 $\mu mol.m^{-2}.s^{-1}$. A similar result was also observed when comparing the growth curves of the externally illuminated fluorescent airlift photobioreactor at 600 $\mu mol.m^{-2}.s^{-1}$ with the combination of the internally lit LED airlift photobioreactor at 300 $\mu mol.m^{-2}.s^{-1}$ with an external fluorescent light bank at 300 $\mu mol.m^{-2}.s^{-1}$.

Table 5.3 illustrates the maximum biomass concentrations and the times at which they were achieved for the different lighting conditions. It was found that the highest biomass concentration of 3.85 $g.L^{-1}$ was obtained after 15 days of growth when external fluorescent light bulbs at 600 $\mu mol.m^{-2}.s^{-1}$ were used to provide illumination. Figure 5.6 shows the maximum specific growth rates obtained for *Scenedesmus sp.*, determined at the start of the growth curve and Figure 5.7 illustrates the linear productivities achieved under limitation. The R^2 values for both the maximum specific growth rates and linear productivities were greater than 0.96, demonstrating the goodness of fit (Appendix C-1-2). It was also observed from the experimental data, that exponential growth lasted for approximately 46 to 54 hours over the range of light conditions investigated. It can be

seen that an increase in light intensity resulted in an increase in the maximum specific growth rate, productivity and biomass concentration. This occurred because as the light intensity increased, more light energy was available for photosynthesis to occur.

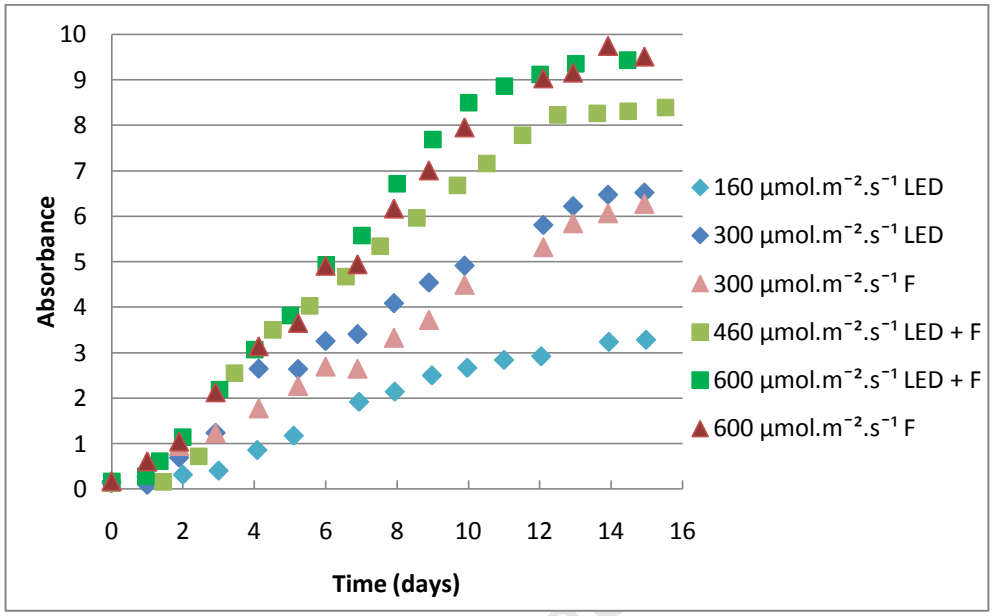

Figure 5. 4: The effect of light intensity and configuration on the growth rate of *Scenedesmus sp.* at 26±1°C measured as absorbance at 750 nm
(LED and F represent LED and fluorescent light sources respectively)

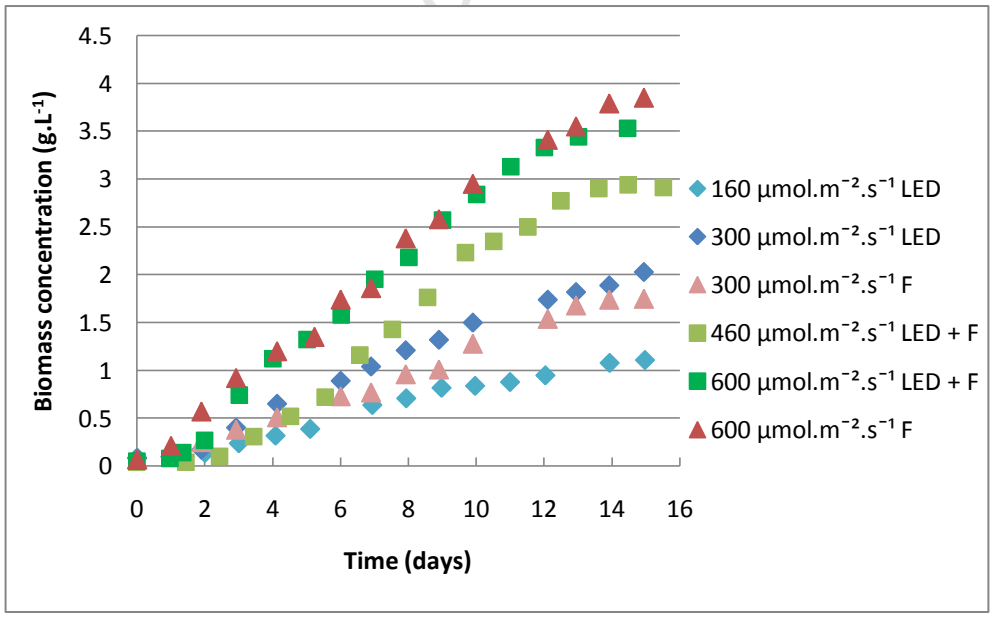

Figure 5. 5: The effect of light intensity and configuration on the biomass concentration of *Scenedesmus sp.* at 26±1°C
(LED and F represent LED and fluorescent light sources respectively)

Table 5. 3: The effect of light intensity on biomass concentration of *Scenedesmus sp.* at 26±1°C

Light source	I_o (µmol.m^{-2}.s^{-1})	X_{max} (g.L^{-1})	t_{max} (days)
LED	160	1.11	15
LED	300	2.03	15
Fluorescent	300	1.74	15
LED and fluorescent	460	2.94	14.5
LED and fluorescent	600	3.53	14.5
Fluorescent	600	3.85	15

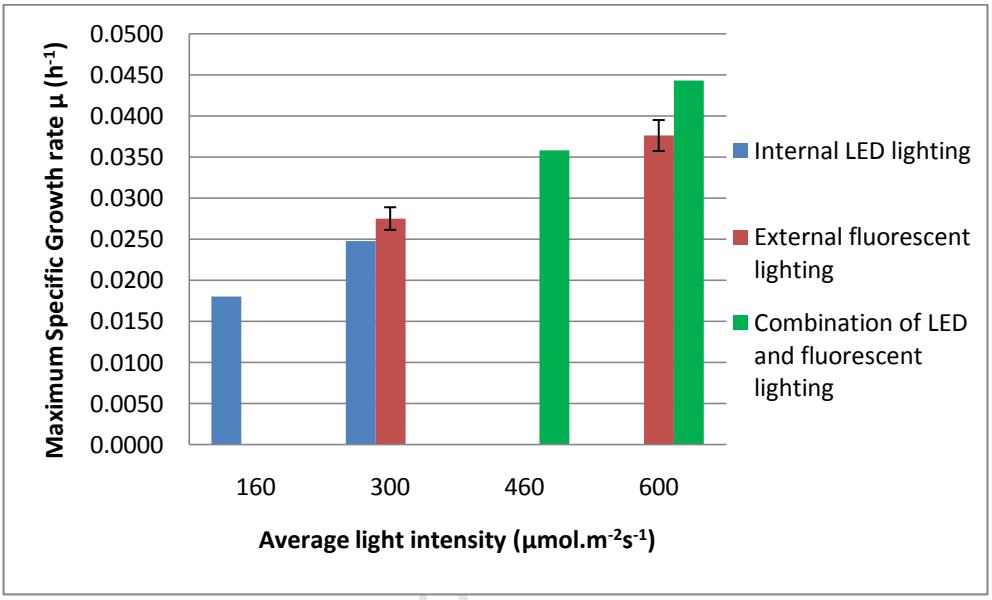

Figure 5. 6: The effect of light intensity and light configuration on μ_{max} of *Scenedesmus sp.* at 26±1°C (Error bars for external fluorescent light runs at 300 and 600 µmol.m^{-2}.s^{-1} represent standard deviations for duplicate runs)

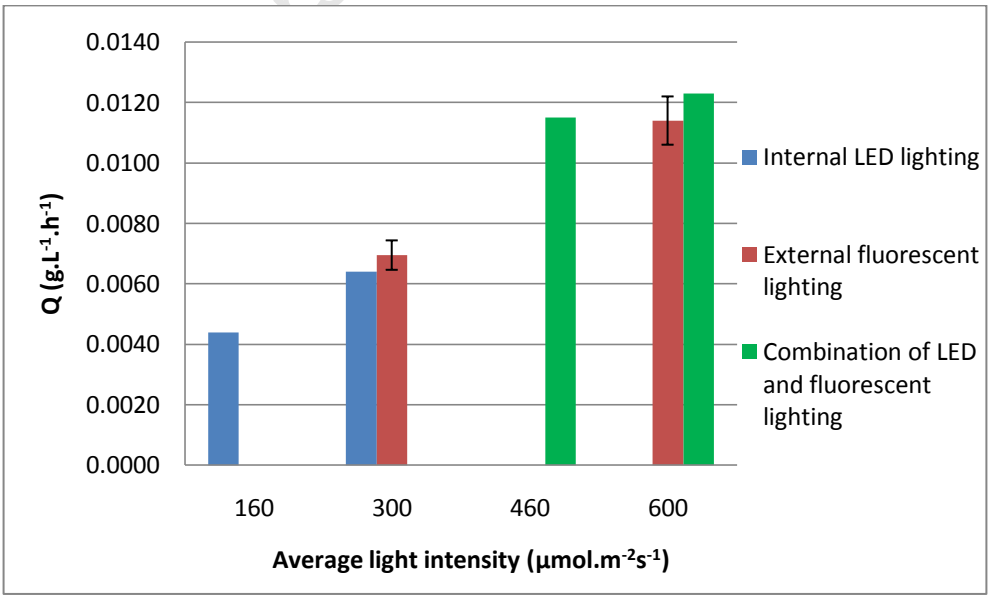

Figure 5. 7: The effect of light intensity and light configuration on the linear productivity of *Scenedesmus sp.* at 26±1°C
(Error bars for external fluorescent light runs at 300 and 600 µmol.m^{-2}.s^{-1} represent standard deviations for duplicate runs)

It can also be observed from Figure 5.6, that the externally illuminated fluorescent airlift photobioreactor had a slightly higher maximum specific growth rate compared to the internally lit LED photobioreactor at 300 μmol.m^{-2}.s^{-1}. This is contrary to expectation, since the presence of internal lighting reduced the light path length of the downcomer, leading to improved light penetration. A possible explanation for the lower maximum specific growth rate could be that LEDs provide light in a _point-specific manner', i.e. the light intensity at the site of the diode is high, but drops off between diodes. For instance, it can be seen in Table B-3 in Appendix B that the light intensity was approximately 1059 μmol.m^{-2}.s^{-1} and 35 μmol.m^{-2}.s^{-1} at the surface of the diode and at the spaces between diodes respectively. Thus, although the external fluorescent light bank and the internal LED light tape provided overall average light intensities of 300 μmol.m^{-2}.s^{-1}, more even distribution of light was obtained when fluorescent light banks were used as compared to the LED light tape.

Figure 5.6 also shows that the combination of the internally illuminated LED photobioreactor at 160 μmol.m^{-2}.s^{-1} with an external fluorescent light bank at 300 μmol.m^{-2}.s^{-1} achieved a maximum specific growth rate that was similar to that of the externally illuminated fluorescent photobioreactor at 600 μmol.m^{-2}.s^{-1}. Furthermore, the combination of the internally illuminated photobioreactor at 300 μmol.m^{-2}.s^{-1} with an external fluorescent light bank at 300 μmol.m^{-2}.s^{-1} achieved the highest maximum specific growth rate. The relatively high maximum specific growth rates obtained in the combination photobioreactors could be attributed to the reduced light path length and the increase in light intensity. Both of these factors would improve the exposure of algal cells in the photobioreactor to light, which would lead to an increase in the photosynthetic rate.

It can be seen that the linear productivities illustrated in Figure 5.7 followed a similar trend to the maximum specific growth rates shown in Figure 5.6. However, it should be noted that increasing the light intensity from 300 μmol.m^{-2}.s^{-1} to 600 μmol.m^{-2}.s^{-1} almost doubled the linear productivity. This result suggests that at biomass concentrations above 0.28 g.L^{-1}, the linear productivities of *Scenedesmus sp.* cultures became limited by light availability. Table 5.4 illustrates the range of biomass concentrations over which growth transitioned from the exponential to the linear phase at the different light conditions. It can be seen that the combination of internally illuminated airlift photobioreactors with external fluorescent light banks at average light intensities of 460 and 600 μmol.m^{-2}.s^{-1},

transitioned from exponential to linear growth at the highest range of biomass concentrations. The internally illuminated airlift photobioreactor at 300 μmol.m^{-2}.s^{-1} also transitioned from exponential to linear growth at a higher biomass concentration range than the standard externally illuminated fluorescent airlift photobioreactor at 300 μmol.m^{-2}.s^{-1}. These results show that an increase in light intensity and the reduction in light path length provided by internal light provision improved the amount of light penetration that was achieved. It should be noted that, the combination of internally illuminated airlift photobioreactors with external fluorescent light banks at average light intensities of 460 and 600 μmol.m^{-2}.s^{-1} achieved similar productivities. This result suggests that another factor such as mass transfer could become limiting.

Table 5. 4: The effect of light intensity and light configuration on the biomass concentration range at which growth transitions from the exponential to linear phase for *Scenedesmus sp.*

Light source	I_o (μmol.m^{-2}.s^{-1})	$X_{exp\text{-}linear}$ (g.L^{-1})
LED	160	0.11-0.44
LED	300	0.40-0.65
Fluorescent	300	0.28-0.44
LED and fluorescent	460	0.52-0.72
LED and fluorescent	600	0.74-1.12
Fluorescent	600	0.29-0.53

5.2.3 Investigation of the effect of temperature and light intensity on the growth of *Scenedesmus sp.*

Figures 5.8 and 5.9 illustrate the results obtained for investigating the effect of temperature at two different light intensities on the growth of *Scenedesmus sp.* Two general trends were observed from Figure 5.8. The first was that an increase in temperature at a constant light intensity resulted in an increase in the growth rate and productivity of *Scenedesmus sp.* The second was that an increase in light intensity at a constant temperature also resulted in an increase in growth rate and productivity. The dry weight data, presented in Figure 5.9, follow a similar trend. From Table 5.5, it can be seen that an increase in light intensity and temperature resulted in an increase in biomass concentration. Light intensity affects the overall biomass concentration more strongly. The highest biomass concentration of 3.96 g.L^{-1} was obtained at 600 μmol.m^{-2}.s^{-1} and 30°C after 11 days of growth. Figures 5.10 and 5.11 present the effects of temperature and light intensity on the maximum specific growth rate and the linear productivity of

Scenedesmus sp. The R^2 values for both the maximum specific growth rates and linear productivities were greater than 0.98, demonstrating the goodness of fit (Appendix C-1-3).

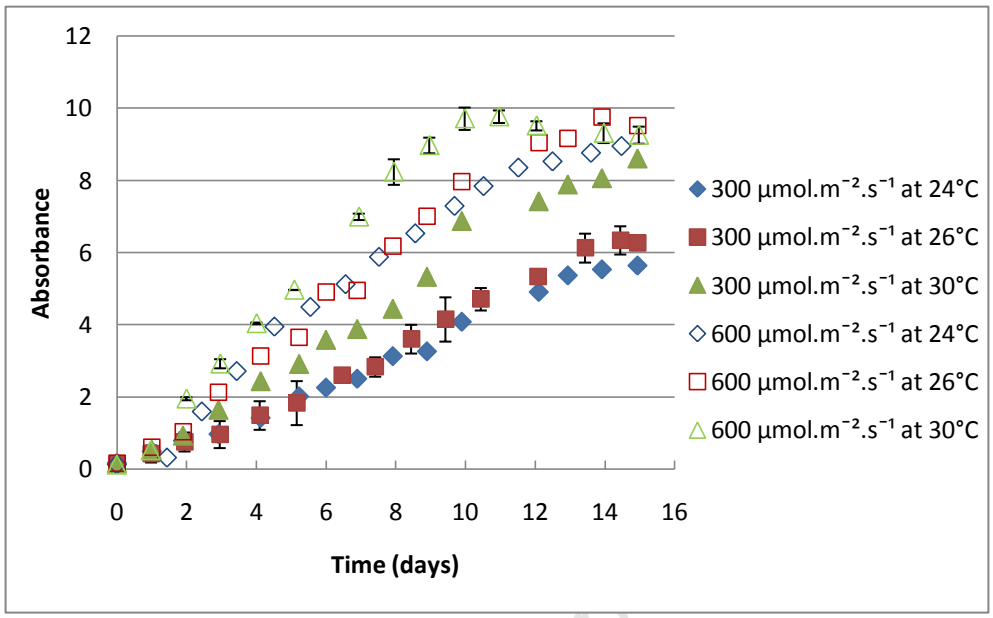

Figure 5. 8: The effect of temperature on the growth of *Scenedesmus sp.* at light intensities of 300 and 600 µmol.m^{-2}.s^{-1}
(closed and open symbols represent light intensities of 300 and 600 µmol.m^{-2}.s^{-1} respectively; error bars for runs at 300 µmol.m^{-2}.s^{-1} and 26°C, and 600 µmol.m^{-2}.s^{-1} and 30°C represent standard deviations for duplicate runs)

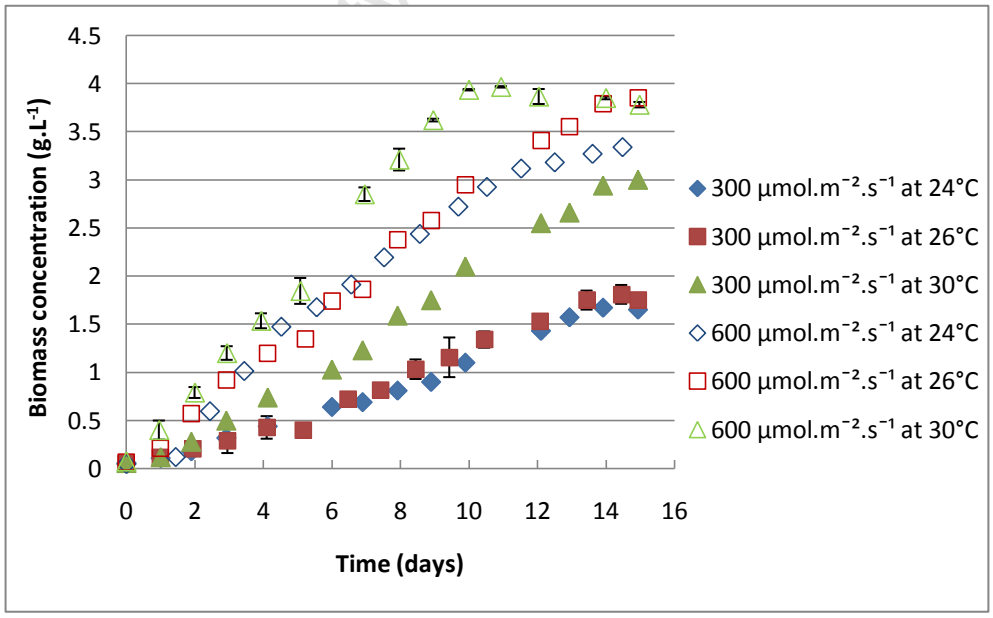

Figure 5. 9: The effect of temperature on the biomass concentration of *Scenedesmus sp.* at light intensities of 300 and 600 µmol.m^{-2}.s^{-1}
(closed and open symbols represent light intensities of 300 and 600 µmol.m^{-2}.s^{-1} respectively; error bars for runs at 300 µmol.m^{-2}.s^{-1} and 26°C, and 600 µmol.m^{-2}.s^{-1} and 30°C represent standard deviations for duplicate runs)

Table 5. 5: The effect of light intensity and temperature on the maximum biomass concentration of *Scenedesmus sp.*

	I_o = 300 µmol.m^{-2}.s^{-1}		I_o = 600 µmol.m^{-2}.s^{-1}	
Temperature (°C)	X_{max} (g.L^{-1})	t_{max} (days)	X_{max} (g.L^{-1})	t_{max} (days)
24	1.67	14	3.36	15.5
26	1.75	15	3.85	15
30	3.00	15	3.96	11

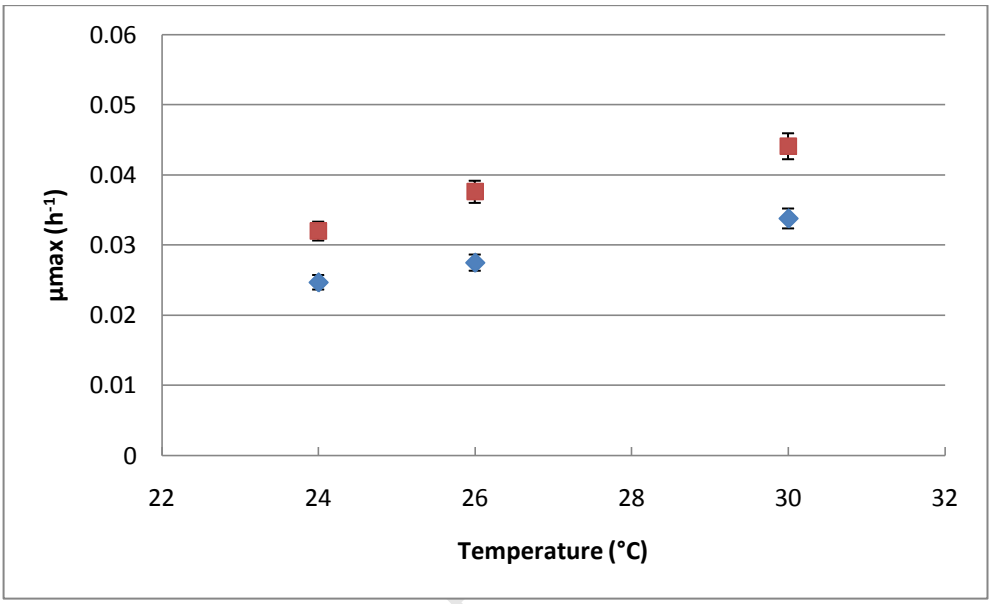

Figure 5. 10: The effect of temperature on the maximum specific growth rate of *Scenedesmus sp.* at light intensities of 300 µmol.m^{-2}.s^{-1} and 600 µmol.m^{-2}.s^{-1} (diamond and square symbols represent light intensities of 300 and 600 µmol.m^{-2}.s^{-1} respectively; error bars represent experimental error of 4.2 %, assumed from repeated runs)

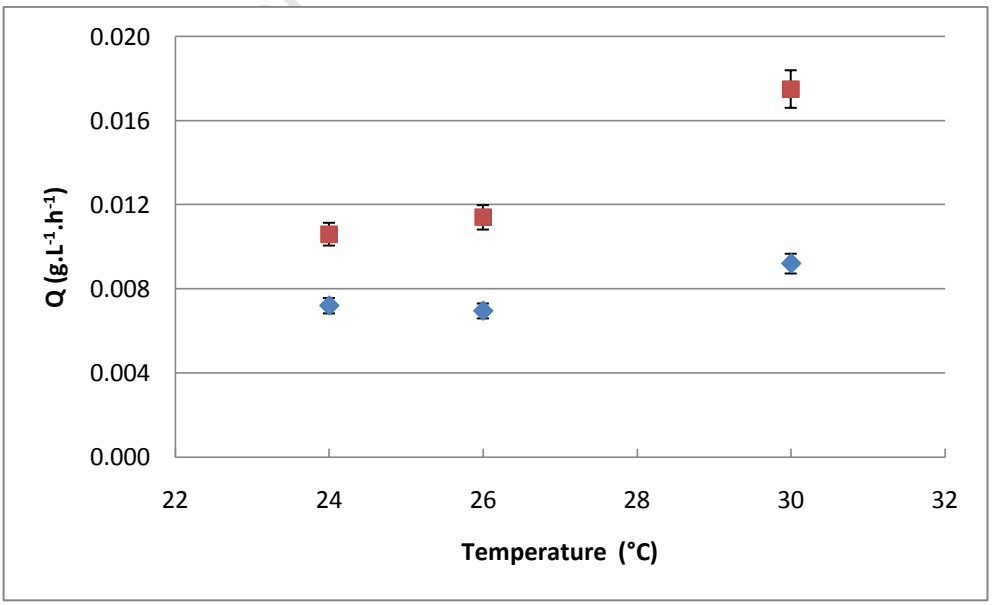

Figure 5. 11: The effect of temperature on the linear productivity of *Scenedesmus sp.* at light intensities of 300 µmol.m^{-2}.s^{-1} and 600 µmol.m^{-2}.s^{-1} (diamond and square symbols represent light intensities of 300 and 600 µmol.m^{-2}.s^{-1} respectively; error bars represent experimental error of 5.1 %, assumed from repeated runs)

From Figure 5.10, it can be seen that an increase in temperature resulted in a similar increase in the maximum specific growth rate at light intensities of 300 and 600 μmol.m^{-2}.s^{-1} respectively. Furthermore, it can also be seen that increasing the light intensity resulted in an increase in the maximum specific growth rate. Theoretically, during exponential growth there are no limitations present. This would mean that at both light intensities, the maximum specific growth rates obtained should be similar. From analysis of experimental data in Appendix C-1-3, it was found that exponential growth was maintained for approximately the first 48 hours and that the *Scenedesmus sp.* cultures transitioned from exponential to linear growth at biomass concentrations of between 0.28-0.44 g.L^{-1} and 0.29-0.53 g.L^{-1} at light intensities of 300 and 600 μmol.m^{-2}.s^{-1} respectively. A possible explanation for the increase in maximum specific growth rate observed in Figure 5.10 could be that increasing the light intensity improved the total fraction of the photobioreactor that was exposed to light from the start of the run.

It can be observed from Figure 5.11, that increasing the light intensity resulted in a significant increase in the linear productivity of *Scenedesmus sp.* at a constant temperature. These results suggest that at higher biomass concentrations, the linear growth rate was light-limited. The effect of increasing biomass concentration and depth of culture on light availability in a *Scenedesmus sp.* culture is discussed in more detail in Section 5.2.4. Furthermore, it can be seen that increasing the temperature resulted in an increase in the linear productivity at both light intensities. However, it should be noted that between 24°C and 26°C, there was no significant increase in linear productivity at both light intensities. A possible explanation that could account for the increase in linear growth with increasing temperature may be that increasing the temperature altered the fluid dynamics of the airlift reactor. For instance, an increase from 24 to 30°C would decrease the kinematic viscosity of water from 0.923 x 10^{-6} to 0.801 x 10^{-6} m^2.s^{-1} (Perry and Green, 2007). This means that the velocities of individual water molecules would increase, resulting in a decrease in the intermolecular forces. This would have caused an increase in the fluidity of the culture which could have caused an increase in the frequency of light/dark cycling in the airlift reactor. This in turn, would have lead to an improvement in light utilization and hence an increase in the biomass concentration and productivity.

The exponential growth rates provided in Figure 5.10 were fitted to the Arrhenius equation at light intensities of 300 and 600 $\mu mol.m^{-2}.s^{-1}$ (Appendix C-1-3). It was found that the dependence of the maximum specific growth rate of *Scenedesmus sp.* on temperature could be modelled by the Arrhenius equation. The calculated Arrhenius parameters for the maximum specific growth rate data at the two light intensities are presented in Table 5.6. The R^2 values greater than 0.96 demonstrate the goodness of fit. The activation energies are approximately the same at both light intensities. The difference between the activation energies at the two light intensities could be attributed to the different R^2 values obtained. The values of the activation energies in Table 5.5 agree well with values in literature for other strains of *Scenedesmus.* For example, Sanchez *et al.* (2008) investigated the effect of temperature in the range of 10-45°C on the exponential growth rate of *Scenedesmus almeriensis* which was cultivated in 2.0 L bubble columns at an aeration rate of 0.5 $v.v^{-1}.min^{-1}$. Illumination was provided from Phillips PL-32 W white-light lamps which simulated a solar cycle and varied light intensity from 625-1625 $\mu mol.m^{-2}.s^{-1}$. It was reported that at these conditions, the activation energy and the exponent of the Arrhenius constant were 37.5 $kJ.mol^{-1}$ and 12.7 h^{-1} respectively. Sanchez *et al.* (2008) also found that the optimal temperature for growth was 35°C and that *Scenedesmus almeriensis* could withstand temperatures up to 48°C at which culture death occurred.

In another study performed by Xin *et al.* (2011) on *Scenedesmus sp.* LX 1, the effect of temperature in the range of 10- 30°C on growth was investigated. The microalgae were cultivated in 200 mL Erlenmeyer flasks at a light intensity of 55-60 $\mu mol.m^{-2}.s^{-1}$ on a light/dark cycling period of 14/10 h. At these cultivation conditions, Xin *et al.* (2011) found that the activation energy and the exponent of the Arrhenius constant were 49.3 $kJ.mol^{-1}$ and 19.7 h^{-1} respectively. It should be noted that Xin *et al.* (2011) did not provide sufficient information on the cultivation conditions in the flasks. Thus, it is difficult to establish whether or not other limitations were present which may have dampened the increase in the growth rate with increasing temperature. Thus, it is apparent from literature that the optimal temperature and the minimum activation energy required is species specific.

Table 5. 6: Arrhenius parameters calculated from the maximum specific growth data of *Scenedesmus sp.* at 24-30°C

I_o (μmol.m^{-2}.s^{-1})	E_a (kJ.mol^{-1})	exp(A) (h^{-1})	R^2 value
300	39.70	12.36	0.9948
600	38.65	12.23	0.9649

In order to establish whether the linear growth rate of *Scenedesmus sp.* was also modified by the culture temperature according the Arrhenius equation, the linear growth rates provided in Figure 5.11 were fitted to the Arrhenius equation at light intensities of 300 and 600 μmol.m^{-2}.s^{-1} respectively (Appendix C-1-3). Table 5.7 presents the calculated Arrhenius parameters for the linear growth rates at the two light intensities. The significant increase from 28.43 kJ.mol^{-1} to 65 kJ.mol^{-1} with an increase in light intensity from 300 μmol.m^{-2}.s^{-1} to 600 μmol.m^{-2}.s^{-1} is unexpected. It is evident that the data does not follow expected trends. It can be observed from Table 5.7 and Figure 5.11 that the R^2 values were lower for the linear growth rates compared to the R^2 values of the maximum specific growth data (Table 5.6), indicating the poor fit of the linear growth rate data. Further studies should be carried out on the combined effects of light intensity and temperature on algal growth, before a conclusion can be reached.

Table 5. 7: Arrhenius parameters calculated from the linear growth data of *Scenedesmus sp.* at 24-30°C

I_o (μmol.m^{-2}.s^{-1})	E_a (kJ.mol^{-1})	exp(A) (h^{-1})	R^2 value
300	28.43	6.61	0.8576
600	65.10	21.76	0.9591

In order to understand the interaction between light intensity and temperature on the microalgal growth rate, it is necessary to understand how each parameter affects algal growth. An increase in culture temperature can affect growth in two ways. Firstly, an increase in temperature results in an increase in metabolic activity in cells by increasing enzyme activity in the ‗dark reaction' which would enhance the rate of carbon dioxide reduction. Secondly, increasing the culture temperature could affect the solubility of media components and CO_2 (Kruger and Eloff, 1978). It should be noted that for this set of experiments, the changes in solubility across the temperature range of 24-30°C are small. In terms of light, the amount of light energy captured and absorbed by algal cells is determined by the total pigment content of the algal cells as well as the amount of light exposure algal cells receive in a photobioreactor system. This determines the rate at

which the light reaction of photosynthesis occurs. Light utilization is typically improved through photobioreactor design, by increasing the overall light intensity, decreasing the light path length or by increasing the light/dark cycling rate. Thus, it is clear that both light intensity and temperature play important roles in photosynthetic growth. Although an increase in culture temperature can result in an increase in enzyme activity, if a culture is light limited algal growth will be limited as the light reaction of photosynthesis will not be able to occur.

5.2.4 The effect of light intensity and biomass concentration on light penetration in the airlift photobioreactors

Exponential growth was maintained for approximately the first 48 hours of growth in the airlift reactors whereafter *Scenedesmus sp.* cultures transitioned from exponential to linear growth at biomass concentrations of between 0.28-0.44 $g.L^{-1}$ and 0.29-0.53 $g.L^{-1}$ at light intensities of 300 and 600 $\mu mol.m^{-2}.s^{-1}$ respectively (Appendix C-1-2). It was shown in Section 5.2.3, that at higher cell densities, the availability of light became the major factor limiting the linear growth rate. In order to demonstrate the effect of culture density on light provision, an experiment was carried out in a glass beaker with similar dimensions to the airlift column to assess the penetration of light into the algal culture with increasing biomass concentration and depth. Figure 5.12 illustrates the results obtained for light penetration into a culture of *Scenedesmus sp.* at different biomass concentrations and culture depths. It can be seen that the average light intensity decreased exponentially with increasing biomass concentration and depth of solution. At a depth of 1 cm, more than 50 $\mu mol.m^{-2}.s^{-1}$ only penetrated cultures with a biomass concentration of 1 $g.L^{-1}$ or less. Since neither CO_2 mass transfer nor nutrient supply were limited, it can be assumed that light limitation caused the shift from exponential to linear growth in the airlift photobioreactors.

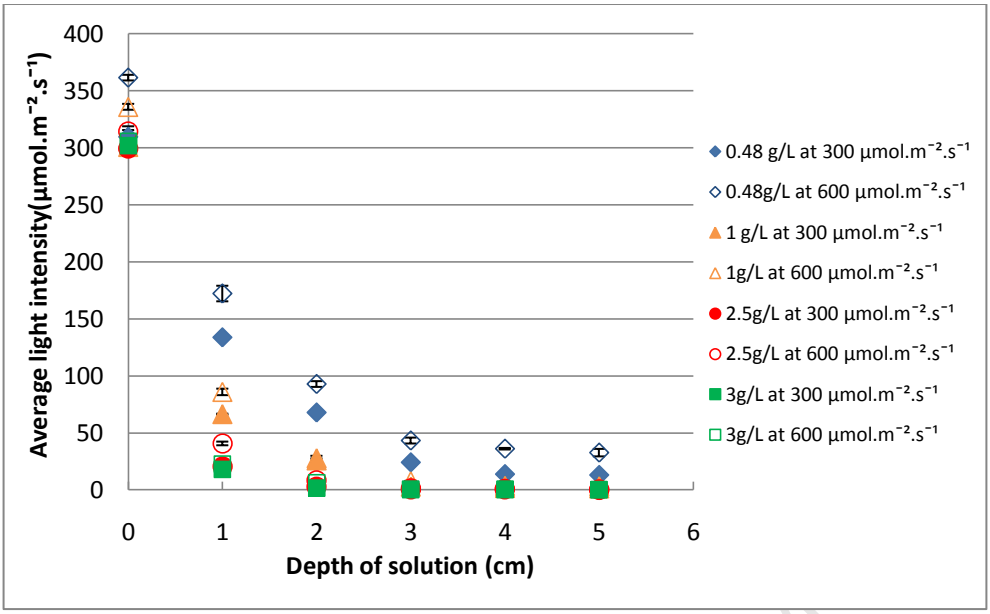

Figure 5. 12: Penetration of fluorescent light through *Scenedesmus sp.* with increasing biomass concentration and depth
(Error bars represent standard deviations for triplicate runs for all data sets)

5.3 Conclusions

From the results obtained for investigating the effects of light intensity on the growth of *Chlorella vulgaris* and *Scenedesmus sp.* at 24±1°C, it was found that when the light intensity was increased from 300 to 600 µmol.m^{-2}.s^{-1} after 2 days, *Scenedesmus sp.* was able to achieve and sustain a higher linear growth rate of 0.0118 g.L^{-1}.h^{-1} than *Chlorella vulgaris,* which achieved 0.0097 g.L^{-1}.h^{-1}. Maximum biomass concentrations of 1.88 g.L^{-1} and 3.62 g.L^{-1} were obtained for *Chlorella vulgaris* and *Scenedesmus sp.* after 13 and 15 days of growth respectively. Furthermore, it was found that *Scenedesmus sp.* could withstand high light intensities at low cell densities without becoming photo inhibited. Based on these findings, it was evident that *Scenedesmus sp.* would be a more promising candidate for cultivation in large scale photobioreactors. Thus, *Scenedesmus sp.* was selected as algal species of choice for the remainder of the study.

In terms of investigating the effects of light intensity and configuration on the growth of *Scenedesmus sp.*, it was found that the combination of the internally lit LED photobioreactor with an external fluorescent bank at overall average light intensities of 460 and 600 µmol.m^{-2}.s^{-1} allowed maximum specific growth rates and linear productivities to be achieved that were approximately 21-36% and 53-56% greater than

the maximum and linear growth rates achieved in the standard externally lit fluorescent photobioreactor at 300 μmol.m^{-2}.s^{-1} respectively. The increase in the maximum specific and linear growth rates may be attributed to the reduced light path length provided by internal illumination coupled with an increase in light intensity. Both of these factors contributed to increasing the volume fraction of the photobioreactor that was exposed to light as well as the amount of light penetration that was achieved in the downcomer region. Further comparison of the growth of *Scenedesmus sp.* across the range of light intensities of 160-600 μmol.m^{-2}.s^{-1} clearly indicated that the linear productivity is light limited.

The dependence of the maximum specific growth rate of *Scenedesmus sp.* on temperature could be modelled by the Arrhenius equation and it was found that similar activation energies of 39.7 and 38.7 kJ.mol^{-1} were required when external fluorescent illumination was provided at 300 and 600 μmol.m^{-2}.s^{-1} respectively. However, a poor correlation existed between the linear growth rate and temperature, which was evident from the low R^2 values at 300 μmol.m^{-2}.s^{-1}. It was observed that an increase in activation energy from 28.43 to 65 kJ.mol^{-1} occurred with an increase in light intensity from 300 to 600 μmol.m^{-2}.s^{-1}. This data does not follow expected trends. Further studies should be carried out on the combined effects of light intensity and temperature on algal growth, before a conclusion can be reached.

In conclusion, it was found that both the amount of light availability and the culture temperature had significant effects on the maximum specific and linear growth rates of *Scenedesmus sp.* respectively. Internal lighting reduced the light path length and hence improved the light distribution that could be achieved in the downcomer region of the airlift photobioreactor. Furthermore, increasing the light intensity from the start of a run resulted in an increase in the maximum specific growth rate of *Scenedesmus sp.* This result was attributed to the fact that increasing the overall illumination improved the total volume fraction of the photobioreactor that was exposed to light. The effects of light fraction and light intensity on the maximum specific growth rate of *Scenedesmus sp.* are analysed in more detail in Section 6.2.1.

The amount of light that is able to penetrate the photobioreactor was shown to decrease exponentially with increasing biomass concentration and depth. The transition from exponential to linear growth is attributed to the decreased light availability at 1 cm depth

and less than 100 μmol.m^{-2}.s^{-1} at depth of 2 cm and all concentrations of 0.5 g.L^{-1} or greater. Thus, at high biomass concentrations, the riser was essentially _dark'. In order to improve growth and light utilization, the effects of light/dark cycling must also be considered. This is also discussed in detail in Sections 6.2.1 and 6.2.2 as is the selection of reactor configuration to provide improved light delivery.

6. Effect of photobioreactor design on biomass productivity and energy efficiency in *Scenedesmus sp.* cultures

6.1 Introduction

One of the most prominent factors limiting algal growth is the inefficient utilization of light energy in closed photobioreactors (Carvalho *et al*., 2006; Posten, 2009; Eriksen, 2008; Grima *et al.*, 1998). This is clearly demonstrated for *Scenedesmus sp.* in Chapter 5. In order to improve light utilization, design parameters such as the illumination surface area to volume ratio and light path length need to be optimized. It is also essential to provide adequate mixing, as the mixing rate has a direct impact on both the mass transfer rate of CO_2 into an algal culture and on the rate at which cells cycle through the light and dark zones of a photobioreactor (Degen *et al*., 2001; Janssen, 2002; Richmond, 2004). Before carrying out the experimental comparison of different reactors, typical operating conditions and performance data reported for *Scenedesmus sp.*, *Chlorella vulgaris*, *Chlorella sp.* and *Spirulina platensis* cultures in literature was analysed. Figure 6.1 presents a brief assessment of the design characteristics and overall performance of the three most common types of photobioreactors used to cultivate microalgae, compiled from literature. Typical values for the ranges of illumination surface area to volume ratios, light path lengths, biomass productivities and biomass productivities per unit energy input were taken from Table 2.3. It should be noted that the biomass productivity per unit power input was calculated using Equations 2.10 which defined the total energy input as the sum of the light and mixing energy inputs. For the case where the light energy requirement would be provided from solar irradiation, Equation 2.11 was used to calculate the biomass productivity per unit mechanical power input.

Figure 6.1 shows that the highest light utilization and consequently the highest biomass productivities were achieved in the tubular photobioreactors, followed by the flat plate and column photobioreactors respectively. The better light utilization achieved in the tubular and flat plate photobioreactors could be attributed to the reduced light path lengths and large illumination surface area to volume ratios.

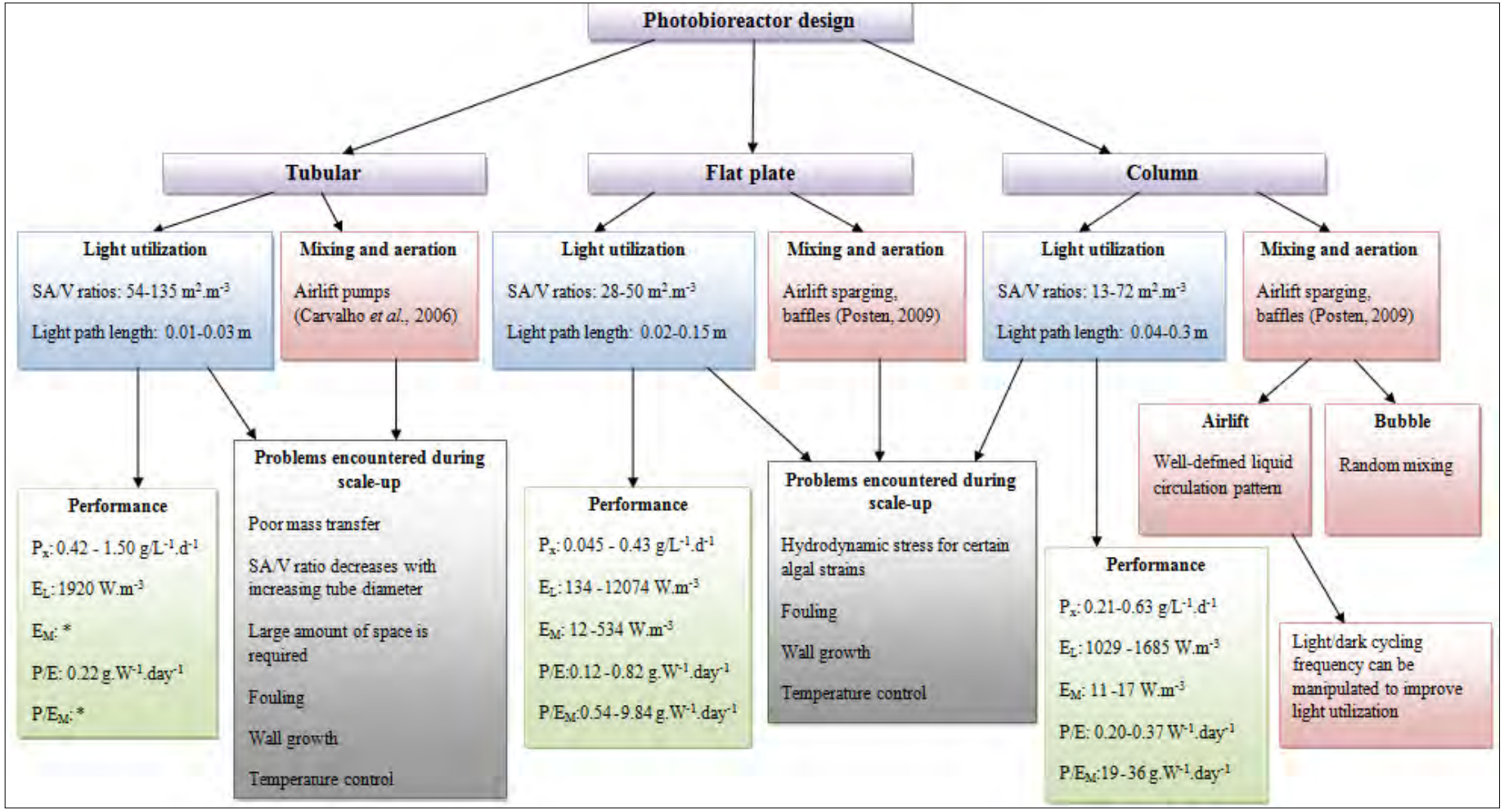

Figure 6. 1:Schematic of design characteristics and performance of tubular, flat plate and column photobioreactors compiled from literature

SA/V incident surface area to culture volume ratio; P_x Overall biomass productivity; E_L light energy input; E_M mixing energy input; P/E Biomass productivity per unit power input (includes light and mixing energy inputs); P/E_M Biomass productivity per unit mechanical power input (excluding light energy input);* Insufficient information provided; Algal species: *Spirulina, Chlorella vulgaris, Chlorella sp* and *Scenedesmus* (Converti *et al.*, 2006; Torzillo *et al*., 1993; Janssen *et al*., 2003;Reyna-Verlarde *et al*., 2010; Degen *et al*., 2001; Ratchford *et al*., 1992; Chui *et al*., 2009; Zhang *et al*., 2002)

In terms of energy efficiency, it can be seen that the flat plate photobioreactors achieved the highest biomass productivity per unit power input (including light and mixing energy inputs), followed by the column and tubular photobioreactors respectively. It can be seen that utilizing tubular photobioreactors on a commercial scale would not be feasible unless very high biomass productivities were achieved, due to the high energy input required and the numerous problems encountered during scale-up. Figure 6.1 also shows that the column photobioreactors achieved higher biomass productivities per unit mechanical power input than the flat plate photobioreactor. Thus, it is evident that the column and flat plate photobioreactors could be feasible alternatives for the cultivation of *Scenedesmus sp.* on a commercial scale, if light utilization could be improved through design modifications that would improve light exposure. From this dissertation, a number of key contributions to literature will be made. Firstly, data for *Scenedesmus sp.* in different reactor systems will be collected. Secondly, a direct comparison of different reactor systems using the same culture conditions, light sources and light intensities will be obtained. Further, the full collection of data allows for energy calculations on a consistent basis. Lastly, the efficiency of light/dark cycling and the performance data can be super-imposed and evaluated in different photobioreactor designs.

In this chapter, the effects of varying light intensity, light fraction and cycle time on the maximum specific growth rate of *Scenedesmus sp.* in the two tubular photobioreactors, described in Section 3.1.3.3, are presented. Based on these results, the efficiency of the vertical airlift photobioreactor was evaluated in terms of light/dark cycling. It was assumed that the downcomer and the riser of the vertical airlift photobioreactor (Figure 3.1) were the light and dark zones respectively. The results obtained for investigating the effects of light intensity on the growth of *Scenedesmus sp.* in the flat plate photobioreactor described in Section 4.2.3 at different aeration rates are also presented. In addition, the effect of using external fluorescent and LED light sources on the growth of *Scenedesmus sp.* was also assessed. However, the efficiency of the flat plate photobioreactor could not be evaluated in terms of light/dark cycling since the axial fluid flow between the plates was random (Section 4.2.4.1). Runs were performed in the tubular and flat plate photobioreactors according to the experimental plans provided in Sections 3.3.3 and 3.3.4 respectively. When required, a fan was used to maintain the culture temperature at 25±1°C.

Finally, the performance of the vertical airlift, tubular and flat plate photobioreactors were evaluated comparatively in terms of biomass productivity, light utilization and energy efficiency for the cultivation of *Scenedesmus sp*. cultures. For this analysis, it was assumed that the total energy input consisted of the light energy and mixing energy inputs which could be calculated from Equations 2.7 and 2.8 respectively. The energy efficiency of the different photobioreactors was then calculated in terms of biomass productivity per unit power input and net energy ratios using Equations 2.10 and 2.12 respectively. Finally, scenarios were considered where either all or a percentage of the light energy requirement would be provided from solar irradiation. In these cases, the feasibility of the photobioreactors in terms of energy efficiency were reassessed.

6.2 Light intensity, light fraction and cycle time and their effect on the growth of *Scenedesmus sp.* in the tubular photobioreactor

6.2.1 The effect of light intensity, light fraction and cycle time

The tubular photobioreactors described in Section 3.1.3.3 were used to investigate the effects of light intensity, light fraction and cycle time on the growth of *Scenedesmus sp.* at the conditions illustrated in Table 3.5. Cycle times of 21 s and 33 s were achieved by operating the 209 mL and 330 mL tubular photobioreactors at aeration rates of 432 mL.min^{-1} and 376 mL.min^{-1} respectively and light fractions of 0.4, 0.75 and 1 were simulated by covering sections of the downcomer and riser with aluminium foil according to the specifications provided in Table 3.6. Runs were performed in the tubular photobioreactors according to the experimental plan provided in Section 3.3.3. For the following set of results, only the maximum specific growth rate was considered as the tubular photobioreactors were designed to be used as a research tool to investigate growth under maximal light exposure and would not be considered for scale-up. As such, growth performance was considered prior to the onset of light limitation at which time the transition to linear growth occurs. It should be noted that at higher light intensities, great care was taken to keep cells from being photoinhibited. At these conditions, the second light bank was turned on after approximately 3 hours to allow the *Scenedesmus sp.* culture to adapt to the reactor and reach an OD of approximately 0.4.

Figures 6.2 and 6.3 present the results obtained for investigating the effect of light intensity and light fraction on the growth of *Scenedesmus sp.* in the 209 mL and 330 mL

tubular photobioreactors at cycle times of 21 s and 33 s respectively. It can be seen that increasing the light fraction (volume fraction of photobioreactor exposed to light) at light intensities of 300 and 600 $\mu mol.m^{-2}.s^{-1}$, resulted in an increase in the growth rate and biomass concentration at both cycle times. Increasing the light fraction from 0.4 to 1, on illumination at 300 $\mu mol.m^{-2}.s^{-1}$, improved the illumination surface area to volume ratios from 95.6 to 239 m^{-1}, and 86.4 to 216 m^{-1} in the 330 mL and 209 mL reactors respectively. Furthermore, increasing the light intensity at a fixed light fraction improved the growth rate and biomass concentration by improving the amount of light exposure and penetration that was achieved in both photobioreactors. The highest biomass concentrations of 2.75 $g.L^{-1}$ and 3.81 $g.L^{-1}$ were achieved in the 330 mL and 209 mL photobioreactors after 54 hours and 49 hours of growth respectively, at a light fraction of 1 and an average light intensity of 600 $\mu mol.m^{-2}.s^{-1}$.

Decreasing the cycle time from 33 s to 21 s also had a positive impact on the growth rate and biomass concentration. Although both of the tubular photobioreactors were designed with downcomers that consisted of 7 mm ID glass tubes for maximal light exposure, the risers consisted of 18 mm ID glass tubes. Due to this internal diameter, the risers experienced fluctuating light conditions which became more pronounced at higher biomass concentrations. In both the tubular reactors, the riser and downcomer had equal volume fractions. However, at the shorter cycle time of 21 s, algal cells were exposed to light in the downcomer for a shorter fraction of time (0.54) compared to a cycle time of 33 s (0.60), before being allowed to recover from photoinhibition in the riser. It is possible, that at a cycle time of 33 s, the longer length of light exposure in the downcomer reduced the efficiency of cellular recovery from photoinhibition in the riser and hence resulted in a decrease in growth rate and maximum biomass concentration. It should be noted that the different riser lengths (Table 3.6) may have affected the amount of mixing and mass transfer that occurred in each of the photobioreactors, also impacting the growth of *Scenedesmus sp.*

Figure 6.4 summarises the effect of light fraction and light intensity on the maximum specific growth rate of *Scenedesmus sp.* at cycle times of 21 s and 33 s. R^2 values greater than 0.97, found in Appendix C-2, on determining the specific growth rate demonstrate the goodness of fit of the experimental data. The maximum specific growth rate increased with increasing light fraction and light intensity at both cycle times. The highest values

were obtained at full light conditions (f = 1). *Chlamydomonas reinhardtii, Chlorella sorokiniana* and *D. tertiolecta* (Janssen, 2002) and *Porphyridium* (Merchuk *et al.*, 1998a) also exhibited a similar increase in the specific growth rate with increasing light fraction.

(a)

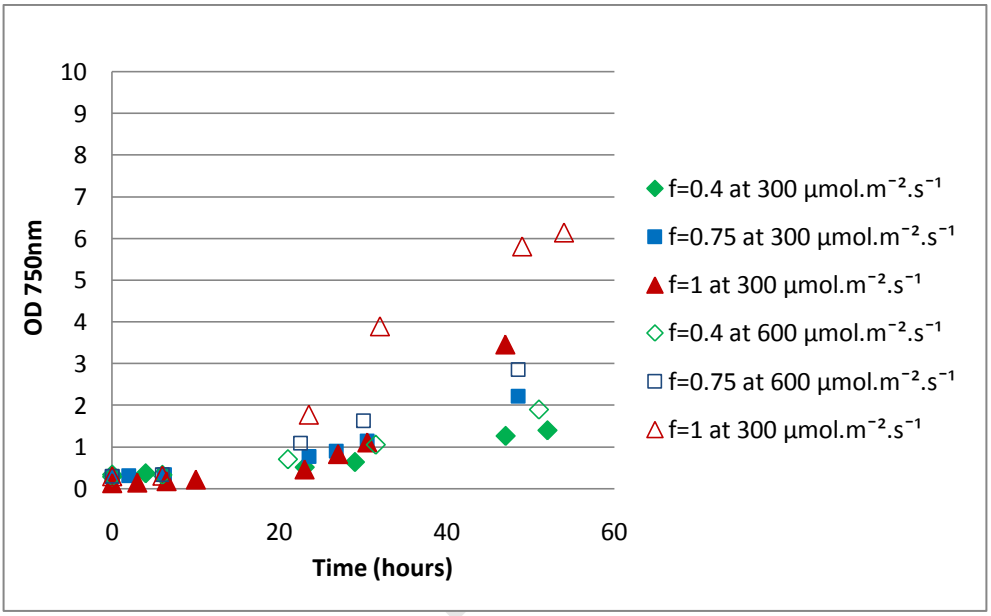

(b)

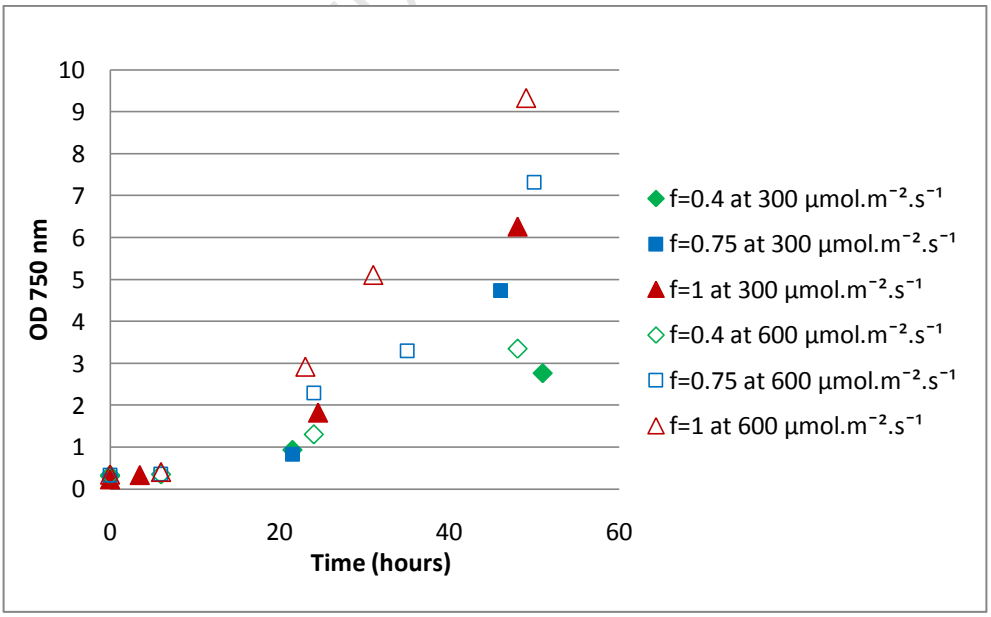

Figure 6. 2: The effect of light intensity and light fraction ($f = t_l/t_c$) on the growth of *Scenedesmus sp.* in the tubular photobioreactors at 25±1°C at (a) cycle time of 33 s and (b) cycle time of 21 s (diamond, square and triangle symbols represent light fractions of 0.4, 0.75 and 1 respectively)

(a)

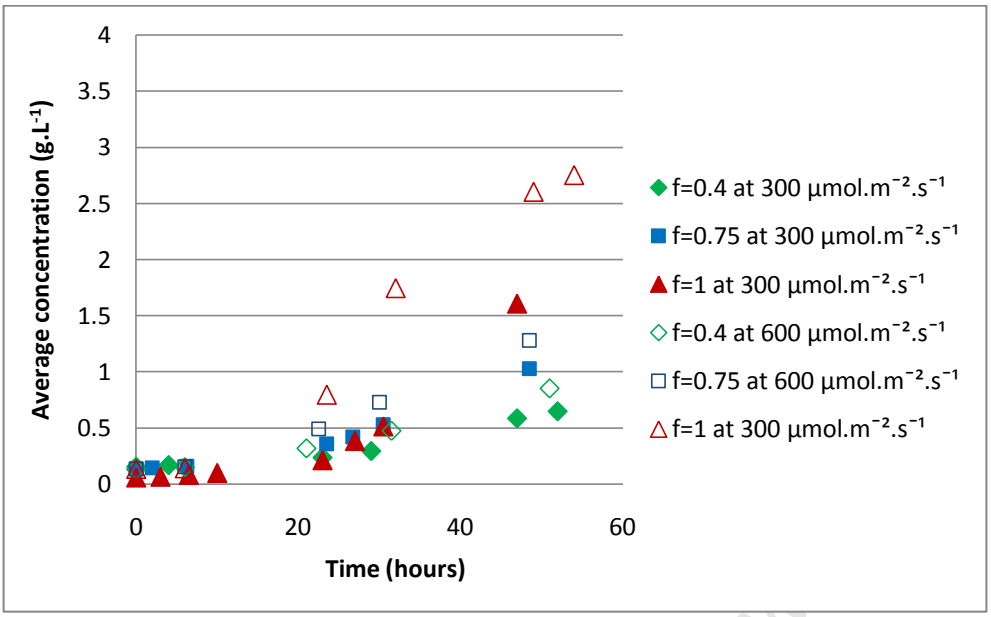

(b)

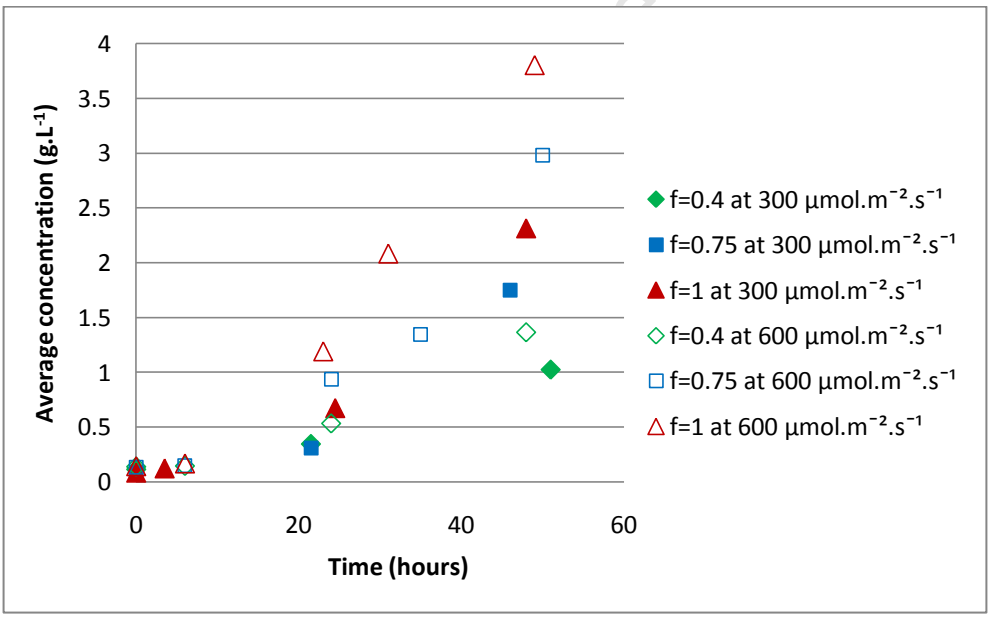

Figure 6. 3: The effect of light intensity and light fraction ($f = t_l/t_c$) on the biomass concentration of *Scenedesmus sp.* in the tubular photobioreactors at 25±1°C at (a) a cycle time of 33 s and (b) a cycle time of 21 s
(diamond, square and triangle symbols represent light fractions of 0.4, 0.75 and 1 respectively)

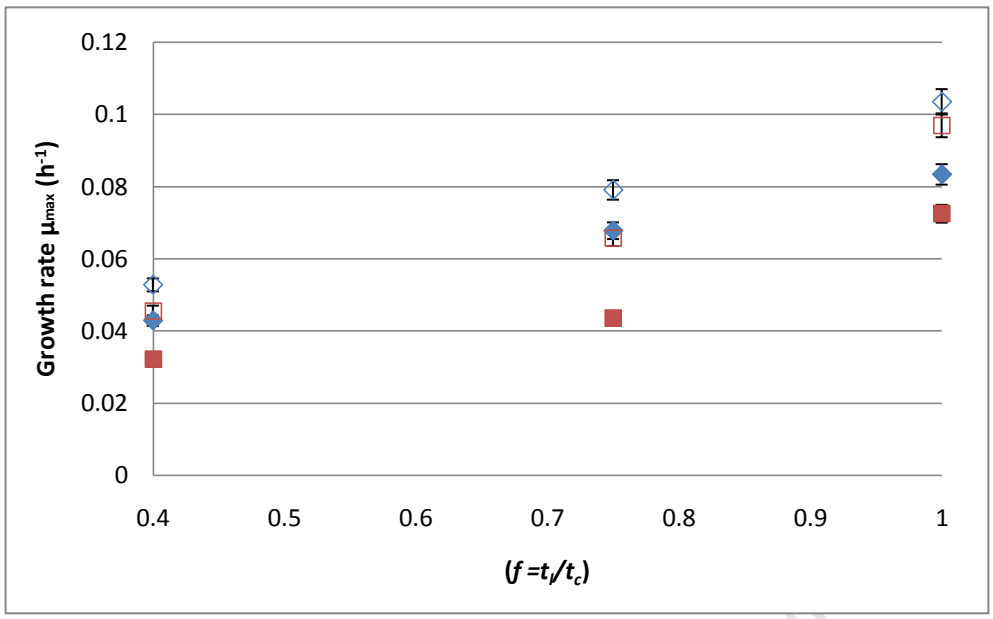

Figure 6. 4: The effect of light fraction ($f = t_l/t_c$), light intensity and cycle time on the maximum specific growth rate of *Scenedesmus sp.* in the 209 mL and 330 mL tubular photobioreactors at aeration rates of 423 mL.min^{-1} and 376 mL.min^{-1} respectively
(Error bars represent experimental error of 3.4%, assumed from repeated runs; Diamond and square symbols represent cycle times of 21 s and 33 s respectively; closed and open symbols represent light intensities of 300 and 600 μmol.m^{-2}.s^{-1} respectively)

It can be observed from Figure 6.4 that at 600 μmol.m^{-2}.s^{-1}, higher maximum specific growth rates were achieved at a cycle time of 21 s as compared to 33 s. As mentioned earlier, at the shorter cycle time of 21 s, higher maximum specific growth rates were achieved since the algal cells were able to utilize the additional light intensity more effectively, as they spent a shorter period of time in the downcomer under high light exposure in the downcomer before moving to the shaded riser where they could recover from photoinhibition. Furthermore, it can be seen that at 600 μmol.m^{-2}.s^{-1} and continuous light conditions (f = 1), similar maximum specific growth rates were obtained at both cycle times. A possible explanation for this result is that the provision of illumination from either side of the tubular photobioreactors minimised the effects of light limitation on the growth of *Scenedesmus sp.* in both of the tubular photobioreactors.

6.2.2 Evaluation of light/dark cycling in the airlift photobioreactors

In Section 6.2.1, two tubular photobioreactors were used as research tools to investigate the effects of light intensity and light/dark cycling on the maximum specific growth rate of *Scenedesmus sp.* that could be obtained under maximal light exposure. Based on the data collected for the tubular photobioreactors, the performance of the vertical airlift

photobioreactors, investigated in Sections 5.2.1, 5.2.2 and 5.2.3, were assessed in terms of light/dark cycling. In order to perform this analysis, it was assumed that the downcomer and the riser, illustrated in Figure 6.5, were the light and dark zones respectively. From the illumination data presented in Figure 5.12, it can be seen that even at the low biomass concentration of 0.48 $g.L^{-1}$, the light intensity that was available at a culture depth of 3 cm, was less than 50 $\mu mol.m^{-2}.s^{-1}$. Thus, it is reasonable to assume that all light for growth was provided in the lit downcomer region. Assuming exposure of algae to light throughout the riser (best case scenario valid at low biomass concentrations), the fraction of the airlift photobioreactor that was exposed to light could be calculated from the experimental circulation data provided by Langley (2010), and presented in Table 6.1. Hence the airlift photobioreactor could be compared to the tubular reactor data at a light fraction of approximately 0.75. Further refinement of this will be possible on completion of the analysis of Brighton (current PhD student at UCT) on the light availability in the riser. Here the analysis is limited to low cell concentrations under which simplifying assumptions hold.

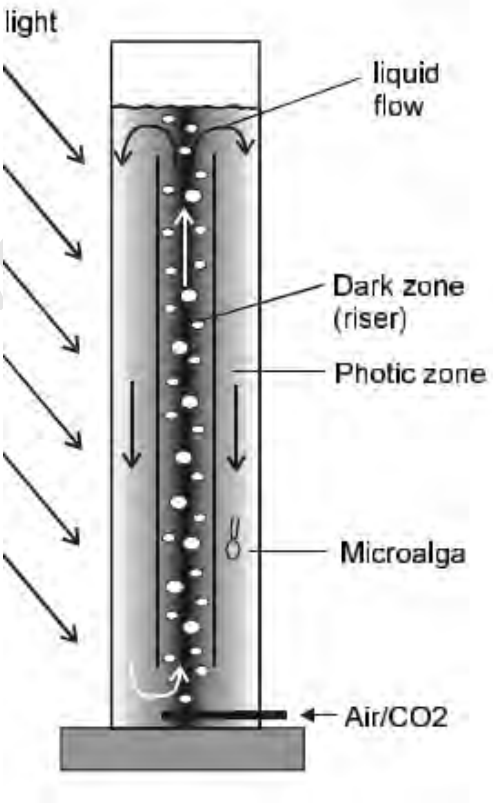

Figure 6. 5: Schematic of vertical airlift photobioreactor depicting the light and dark zones present (Janssen, 2002)

Table 6. 1: Circulation time data used to estimate the light fraction in the airlift photobioreactor (Langley, 2010)

	t_c (s)	Fraction of time spent in zone	
Total	7		
Riser	1.5	Dark	0.21
Downcomer	5.5	Light	0.79

Table 6.2 presents the maximum specific growth rates obtained in the airlift photobioreactors and the tubular photobioreactors at a light fraction of 0.75. Experimental errors of 4.2% and 3.4% were based on repeated runs for the vertical airlift photobioreactors and the tubular photobioreactors respectively (Appendices C-1-3 and C-2). Table 6.2 shows that the tubular photobioreactors attained significantly higher maximum specific growth rates than the airlift photobioreactors. It is also evident that increasing the light intensity from 300 to 600 $\mu mol.m^{-2}.s^{-1}$ resulted in an increase in the maximum specific growth rate for both photobioreactor types. The difference in the specific growth rates achieved for *Scenedesmus sp.* in the tubular and airlift photobioreactors may be attributed to the different growth conditions present in each of the photobioreactors.

Table 6. 2: Comparison of maximum specific growth rates at different cycle times in the airlift and tubular photobioreactors at a light fraction of approximately 0.75 at 25±1°C
(Standard errors of 4.2% and 3.4% based on repeated runs were assumed for the airlift and tubular photobioreactors respectively; IALR internally illuminated airlift reactor; ALR-airlift reactor; TBR1 209 mL tubular reactor; TBR2 330 mL tubular reactor)

		μ_{max} (h^{-1})	
Photobioreactor	t_c (s)	I_o = 300 $\mu mol.m^{-2}.s^{-1}$	I_o = 600 $\mu mol.m^{-2}.s^{-1}$
IALR	7	0.0248 ± 0.0010	0.0443 ± 0.0019
ALR	7	0.0275 ± 0.0012	0.0376 ± 0.0016
TBR1	21	0.0678 ± 0.0023	0.0791 ± 0.0027
TBR2	33	0.0436 ± 0.0015	0.0658 ± 0.0022

In terms of hydrodynamics, the different aeration rates of 0.38-0.42 $L.min^{-1}$ and 2.0 $L.min^{-1}$ in the tubular and airlift photobioreactors respectively, had a significant impact on the amount of mixing as well as the circulation time achieved in each of the photobioreactors (Table 6.2). In order to evaluate the degree of mixing that occurred, the Reynolds number was calculated using Equation 6.1. According to Coulson and Richardson (1999), fluid flow in a tube is considered laminar if Re < 2300 and turbulent if Re > 4000. In the region between 2300 and 4000, transitional flow occurs, where the

flow can be either laminar or turbulent, depending on the uniformity of flow and on pipe roughness.

$$\mathrm{Re} = \frac{\rho D v}{\eta} \tag{6.1}$$

- Re is the Reynolds number
- ρ is the fluid density ($kg.m^{-3}$)
- D is the tube diameter (m)
- v is the velocity in the tube ($m.s^{-1}$)
- η is the fluid viscosity ($kg.s^{-1}.m^{-1}$)

The downcomers of the 209 mL and 330 mL tubular photobioreactors had Reynolds numbers of 1519 and 1560 respectively, indicating laminar flow. The risers of the 209 mL and 330 mL photobioreactors had Reynolds numbers of 4010 and 3946 respectively, indicating turbulent flow (Fraser, 2011). In the airlift photobioreactor, the Reynolds numbers in the riser and the downcomer were 6660 and 2412 respectively. This indicates that in both photobioreactors, turbulent flow occurred in the riser which transformed to laminar flow in the downcomer. Although the Reynolds number for the downcomer of the airlift photobioreactor indicated that the flow was transitional, it was observed during experimental runs that the algal culture bubbled rapidly through the riser and then flowed smoothly and uniformly as the culture moved through the downcomer region. The greater degree of turbulent flow in the riser of the airlift photobioreactor improved mixing and the rate of transfer of carbon dioxide, nutrients and metabolites between algal cells and the media (Grobbelaar, 1994). From experimental data provided by Langley (2010), it was found that the overall mass transfer coefficient ($k_La(CO_2)$) in the airlift photobioreactor was 0.0094 ± 0.00026 s^{-1} at an aeration rate of 2 $L.min^{-1}$. However, there were no experimental data available for the overall mass transfer coefficient in the tubular photobioreactors. Fraser (2011) used a simplistic model to assess whether or not mass transfer limitation was expected in the tubular photobioreactors and estimated that CO_2 limitation would only become apparent when the photobioreactors were aerated with a mixture of air containing 0.2% CO_2. Thus, it is reasonable to assume that when the tubular photobioreactors were supplied with 1% CO_2, CO_2 mass transfer limitation was avoided.

Another key factor that affected the maximum specific growth of *Scenedesmus sp.* was the light availability or the lack thereof in the different photobioreactors. Parameters such as light intensity, the incident surface area to volume ratio and the light path length are important to consider as they affect the amount of light exposure as well as the degree of light penetration achieved in a photobioreactor (Degen *et al*. 2001; Ogbonna and Tanaka, 2000). From Table 6.3, it can be seen that the tubular photobioreactors had the highest incident surface area to volume ratios as well as the shortest light path lengths and hence experienced far better light exposure compared to the vertical airlift photobioreactors, resulting in the highest specific growth rate. Further, an increase in light intensity from 300 to 600 $\mu mol.m^{-2}.s^{-1}$ resulted in an increase in the maximum specific growth rate in all the photobioreactors. The highest maximum specific growth rate of $0.0791 \pm 0.0027\ h^{-1}$ was obtained in the 209 mL tubular photobioreactor which was operated at a cycle time of 21 s and 600 $\mu mol.m^{-2}.s^{-1}$.

Table 6. 3: The effect light intensity and availability on the maximum specific growth rate of *Scenedesmus sp.* and on the transition from exponential to linear growth (Standard errors of 4.2% and 3.4% based on repeated runs were assumed for the airlift photobioreactors and the tubular photobioreactors respectively; IALR internally illuminated airlift reactor; CIALR-combination of internally lit LED airlift reactor with external fluorescent light; ALR-airlift reactor; TBR1 209 mL tubular reactor; TBR2 330 mL tubular reactor)

PBR	I_o ($\mu mol.m^{-2}.s^{-1}$)	SA/V (m^{-1})	L (m) $_{downcomer}$	μ_{max} (h^{-1})	t_{exp} (h^{-1})	$C_{exp\text{-}linear}$ ($g.L^{-1}$)	$I_{exp\text{-}linear\ downcomer}$ ($\mu mol.m^{-2}.s^{-1}$)
IALR	300	30.3	0.0175	0.0248 ± 0.0010	53.5	0.40-0.65	60-75
CIALR	600	59.8	0.0175	0.0443 ± 0.0019	49.3	0.74-1.12	40-70
ALR	300	29.5	0.025	0.0275 ± 0.0012	48.0	0.28-0.44	45-60
ALR	600	58.9	0.025	0.0376 ± 0.0016	45.5	0.29-0.53	30-60
TBR1	300	239	0.007	0.0678 ± 0.0023	46.0	2.10-4.35	50-60
TBR1	600	478	0.007	0.0791 ± 0.0027	35.0	1.47-3.25	45 -80
TBR2	300	216	0.007	0.0436 ± 0.0015	30.5	0.53-1.03	80-150
TBR2	600	432	0.007	0.0658 ± 0.0022	30.0	0.72-1.66	90-160

Table 6.3 also shows that the combination of the internally illuminated vertical airlift photobioreactor with an external fluorescent light bank at 600 $\mu mol.m^{-2}.s^{-1}$ achieved approximately a 15% higher maximum specific growth rate than the standard airlift photobioreactor provided with external fluorescent illumination at 600 $\mu mol.m^{-2}.s^{-1}$. The increase in the maximum specific growth rate could be attributed to the reduced light path length from 0.025 m to 0.0175 m on internal light provision, and thus improved light penetration in the downcomer region. However, no substantial increase in the specific

growth rate was observed in the internally illuminated photobioreactor that was operated at 300 μmol.m^{-2}.s^{-1}, despite the reduced light path length. As mentioned previously in Section 5.2.2, a possible explanation could be that LEDs provide light in a _point-specific manner' and thus do not achieve the same degree of even light distribution as fluorescent light bulbs.

Table 6.3 also illustrates the duration of the exponential growth rate and the range of biomass concentrations over which growth transitioned from the exponential to the linear phase, when a limitation became apparent in each of the photobioreactors. Figure 5.12 was used to estimate the range of light intensities that were present when the cultures transitioned from exponential to linear growth in the downcomer regions of the vertical airlift and tubular photobioreactors respectively. It can be seen from Table 6.3, that exponential growth lasted for approximately 48 hours and that both the airlift and tubular photobioreactors transitioned to linear growth when the light intensity that was available in the respective downcomers decreased to approximately 30-75 μmol.m^{-2}.s^{-1}, with the exception of the 330 ml tubular photobioreactors, where the light intensities were between 80-160 μmol.m^{-2}.s^{-1}. It is evident that in order to optimize the performance of the photobioreactor, the light path length needs to be minimised in order to improve light exposure. It is for this reason that a flat plate photobioreactor was considered as a viable option for cultivating *Scenedesmus sp.*

6.3 Light intensity, light source and aeration rate and their effect on the growth of *Scenedesmus sp.* in the flat plate photobioreactor

6.3.1 Introduction

The short light path length and simplicity of design make the flat plate photobioreactor an attractive option for scale-up. An evaluation of the performance of the flat plate photobioreactor described in Section 4.2.3 and illustrated in Figure 6.1 is provided in Section 6.3.2. In order to investigate the effects of light intensity and mass transfer on the growth of *Scenedesmus sp.* in the flat plate photobioreactor, runs were performed at aeration rates of 2.5, 3.5 and 5 L.min^{-1}, corresponding to $k_La(CO_2)$ values of 0.0063 ± 0.00020 s^{-1}, 0.0073 ± 0.00023 s^{-1} and 0.0101 ± 0.00029 s^{-1} respectively. The flat plate and vertical airlift photobioreactors achieved similar $k_La(CO_2)$ values (0.0101 ± 0.00029 s^{-1} and 0.0094 ± 0.00026 s^{-1}) at aeration rates of 5 and 2 L.min^{-1} respectively.

Constant illumination was provided at average light intensities of 300 and 600 μmol.m^{-2}.s^{-1} from external fluorescent light banks. In addition, the effects of using fluorescent and LED light sources on the growth rate of *Scenedesmus sp.* in the flat plate photobioreactor was also evaluated at an average light intensity of 300 μmol.m^{-2}.s^{-1} using the light banks illustrated in Figures 4.5 and 4.6 respectively. These results are presented in Section 6.3.3. Runs were performed in the flat plate photobioreactor according to the experimental plan provided in Section 3.3.4. When required, a fan was used to maintain the culture temperature at 25±1°C.

6.3.2 Effect of light intensity and aeration on the growth of *Scenedesmus sp.* in the flat plate photobioreactor

Figures 6.6 and 6.7 illustrate the effect of light intensity and aeration rate on the growth of *Scenedesmus sp.* in the flat plate photobioreactor, in terms of absorbance and biomass concentration respectively. It can be observed that at a constant light intensity of 300 μmol.m^{-2}.s^{-1}, increasing the aeration rate had little effect on the growth rate up to approximately 125 hours. Since the flat plate photobioreactor was neither nutrient or CO_2 limited, the linear slopes up to 125 hours indicate that growth was light limited. However, after 125 hours of growth, the change in linear slope at each of the aeration rates indicate that another factor had become limiting. It can be seen that increasing the aeration rate from 2.5 L.min^{-1} to 3.5 and 5 L.min^{-1} after 125 hours allowed the linear slope to be maintained for longer such that the maximum biomass concentration was reached sooner. These results seem to suggest that at higher biomass concentrations (2.68 to 3.12 g.L^{-1}), the overall mass transfer coefficient had an important impact on the growth rate. This is consistent with the dependence of the CO_2 uptake rate required on the biomass concentration as well as the growth rate and specific CO_2 uptake rate.

It can also be observed that increasing the light intensity to 600 μmol.m^{-2}.s^{-1} resulted in an increase in growth rate at each of the aeration rates. This could be attributed to the fact that both increasing the light intensity and providing illumination on both sides of the flat plate photobioreactor increased the amount of light exposure and penetration that was achieved. It can be seen that by approximately 50 hours, the aeration rate had a significant effect on the growth rate. At 2.5 L.min^{-1} and 600 μmol.m^{-2}.s^{-1}, the system appeared mass-transfer limited, whereas at 3.5 L.min^{-1} and 5 L.min^{-1}, it appeared light limited. At biomass concentrations of between 1.26 and 2.43 g.L^{-1}, increasing the aeration rate also

allowed the linear slope to be maintained for longer so that the maximum biomass concentration was obtained more rapidly. These results further highlight the importance of mass transfer, which becomes more important to consider with increasing biomass concentration. It can be seen from Table 6.4 that the highest biomass concentration of 4.62 $g.L^{-1}$ was obtained after 5.3 days of growth, at 5 $L.min^{-1}$ and 600 $\mu mol.m^{-2}.s^{-1}$.

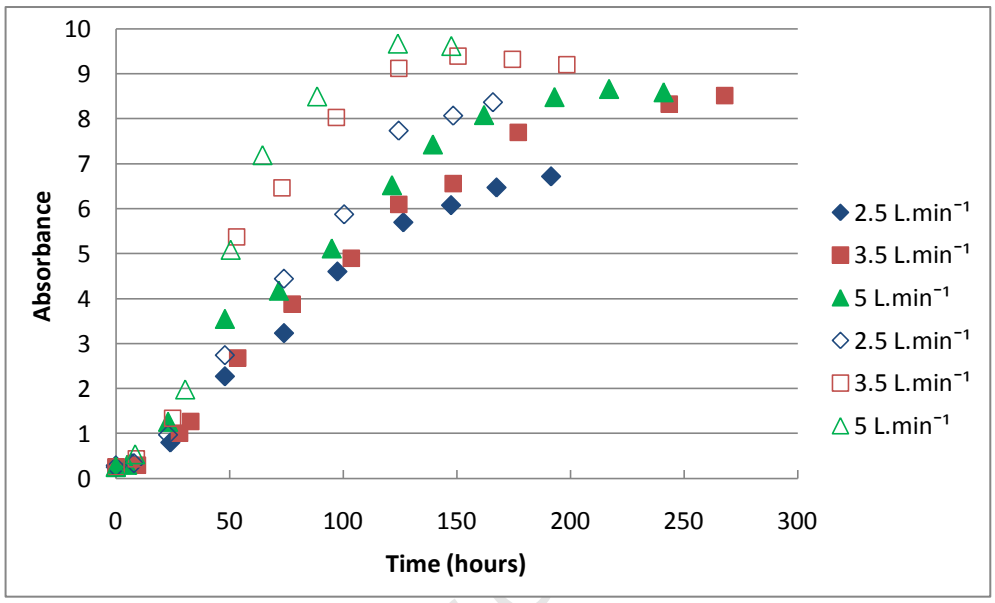

Figure 6. 6: The effect of light intensity and aeration rate on the growth rate of *Scenedesmus sp.* in the flat plate photobioreactor at 25±1°C in terms of absorbance, using external fluorescent lighting (closed and open symbols represent average light intensities of 300 and 600 $\mu mol.m^{-2}.s^{-1}$ respectively)

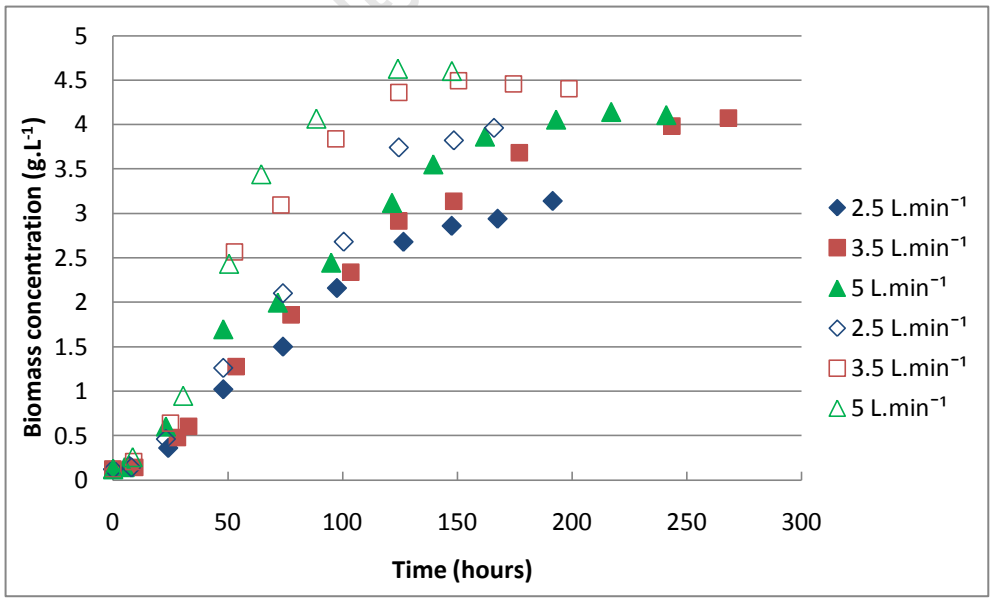

Figure 6. 7: The effect of light intensity and aeration rate on the biomass concentration of *Scenedesmus sp.* in the flat plate photobioreactor at 25±1°C, using external fluorescent lighting (closed and open symbols represent light intensities of 300 and 600 $\mu mol.m^{-2}.s^{-1}$ respectively)

Table 6. 4: The effect of light intensity and aeration rate on the maximum biomass concentration of *Scenedesmus sp.* in the flat plate photobioreactor using external fluorescent light at 25±1°C

Aeration rate ($L.min^{-1}$)	I_o ($\mu mol.m^{-2}.s^{-1}$)	X_{max} ($g.L^{-1}$)	t_{max} (days)
2.5	300	3.20	8.00
3.5	300	4.07	11.2
5.0	300	4.14	9.00
2.5	600	4.00	6.90
3.5	600	4.49	6.30
5.0	600	4.62	5.30

The maximum specific and linear growth rates obtained as a function of aeration rate and light intensity are presented in Table 6.5. The R^2 values of greater than 0.95 for both the maximum specific and linear growth rates, found in Appendix C-3-2, demonstrated the goodness of fit. It can be seen that an increase in aeration rate resulted in an increase in the maximum specific growth rate of *Scenedesmus sp.* at both light intensities. Relative to the maximum specific growth rate at 2.5 $L.min^{-1}$, this increased by 12-15% and 24-25% at 3.5 and 5 $L.min^{-1}$ respectively at either light intensity. A possible explanation for these results could be that increasing the aeration rate resulted in an increase in the amount of mixing that occurred, which subsequently led to an increase in the mass transfer rate of CO_2 gas into the algal culture (Richmond, 2004; Grobbelaar, 2000). At these biomass concentrations, light intensity was not expected to be limiting over a large fraction of the reactor. At the highest aeration rate of 5 $L.min^{-1}$, the highest overall gas-liquid mass transfer coefficient of 0.0101 ± 0.00029 s^{-1} and consequently the highest maximum specific growth rates were obtained at both light intensities in the flat plate photobioreactor. For a more detailed presentation of the overall mass transfer coefficient data as a function of aeration rate, see Figure 4.11 and Section 4.2.4.2.

Another key factor which also affected the growth rate was light availability. It can be seen from Table 6.5, that an increase in light intensity from 300 to 600 $\mu mol.m^{-2}.s^{-1}$ resulted in approximately a 9-12% and a 22-42% increase in the maximum specific and linear growth rates respectively, over the range of aeration rates investigated. The small increase in the maximum specific growth rate, with increasing light intensity could be attributed to the fact that at low biomass concentrations (<0.5 $g.L^{-1}$), light attenuation had a minimal effect on the part of the growth curve used to calculate the exponential growth rate. The greater fractional increase in the linear growth rates with increasing light intensity, results from the determination of linear growth rates at biomass concentrations where growth was light-limited, with the exception at 2.5 $L.min^{-1}$ (42%), where growth

was both light and CO_2 limited. From analysis of the experimental data provided in Appendix C-3-2, it was found that *Scenedesmus sp.* experienced exponential growth for approximately the first 48 hours before the cultures transitioned from exponential to linear growth at biomass concentrations of 0.38-0.60 $g.L^{-1}$ and 0.46-0.94 $g.L^{-1}$ at average light intensities of 300 and 600 $\mu mol.m^{-2}.s^{-1}$ respectively. It was found that at these conditions, growth became light limited, when the light intensity available decreased to 25-50 $\mu mol.m^{-2}.s^{-1}$.

Table 6. 5: The effects of light intensity and aeration rate on the maximum specific growth rate, linear growth rate of *Scenedesmus sp.*, overall mass transfer coefficient and cycle times achieved in the flat plate photobioreactor at 25±1°C
(Experimental errors of 3.1% and 5.2% were assumed based on repeated runs for the overall mass transfer coefficient and mean circulation time data respectively)

	I_0 = 300 $\mu mol.m^{-2}.s^{-1}$		I_0 = 600 $\mu mol.m^{-2}.s^{-1}$		Hydrodynamic parameters	
F ($L.min^{-1}$)	μ_{max} (h^{-1})	Q ($g.L^{-1}.h^{-1}$)	μ_{max} (h^{-1})	Q ($g.L^{-1}.h^{-1}$)	k_La (CO_2) (s^{-1})	t_c (s)
2.5	0.0459	0.0174	0.0512	0.0247	0.0063 ± 0.00020	2.02 ± 0.103
3.5	0.0527	0.0209	0.0577	0.0256	0.0073 ± 0.00023	1.72 ± 0.088
5.0	0.0571	0.0216	0.0642	0.0276	0.0101 ± 0.00029	1.48 ± 0.076

Thus, it can be concluded that both the amount of light available and the overall gas-liquid mass transfer coefficient had important effects on the growth rate, productivity and maximum biomass concentration of *Scenedesmus sp.* It was found that during the first part of the growth cycle (100-125 hours), increasing the aeration rate and consequently the overall mass transfer coefficient did not have a significant effect on the growth rate. During this period, growth became light limited with increasing biomass concentration. However, a shift in the linear slope of the growth curve after 100-125 hours, at both light intensities of 300 and 600 $\mu mol.m^{-2}.s^{-1}$ indicated that another factor had become limiting. At these conditions, it was observed that the aeration rate had a significant impact on the linear growth rate. It was found that the highest linear growth rates and maximum biomass concentrations were obtained at 5 $L.min^{-1}$ ($k_La(CO_2)$ 0.0101 ± 0.00029 s^{-1}). These results suggest that at higher biomass concentrations, both the provision of sufficient light and mass transfer become crucial to consider. At higher biomass concentrations, light availability decreases and consequently results in a decrease in the specific growth rate. However, if the light intensity and hence the light availability is increased and the specific growth rate is maintained for a longer period of time, the CO_2 uptake rate required increases and is eventually not met by the overall mass transfer coefficient of the reactor.

6.3.3 Effect of different light sources on the growth of *Scenedesmus sp.* in the flat plate photobioreactor

In order to assess the effects of fluorescent and LED light sources on the growth rate of *Scenedesmus sp.* in the flat plate photobioreactor, runs were performed according to the experimental plan provided in Table 3.8. The fluorescent and LED light banks illustrated in Figures 4.5 and 4.6 were used to provide an average light intensity of 300 µmol.m^{-2}.s^{-1}. Figures 6.8 and 6.9 illustrate the growth of *Scenedesmus sp.* as a function of aeration rate at an average light intensity of 300 µmol.m^{-2}.s^{-1} and 25±1°C, using external LED and fluorescent light sources respectively. At each aeration rate, the growth rates and maximum biomass concentrations achieved using the LED light bank were slightly lower than those with the fluorescent light bank. Table 6.6 shows the effect of using the different light sources on the maximum specific and linear growth rates as well as the maximum biomass concentrations obtained. The R^2 values greater than 0.97 demonstrate the goodness of fit (Appendix C-3-3). At aeration rates of between 2.5-5.0 L.min^{-1}, the maximum specific and linear growth rates were approximately 14-18% and 12-21% lower when the LED light bank was used to provide constant illumination, as compared to the fluorescent light bank. Furthermore, the maximum biomass concentrations achieved were roughly 7-14% less when the LED light bank was used.

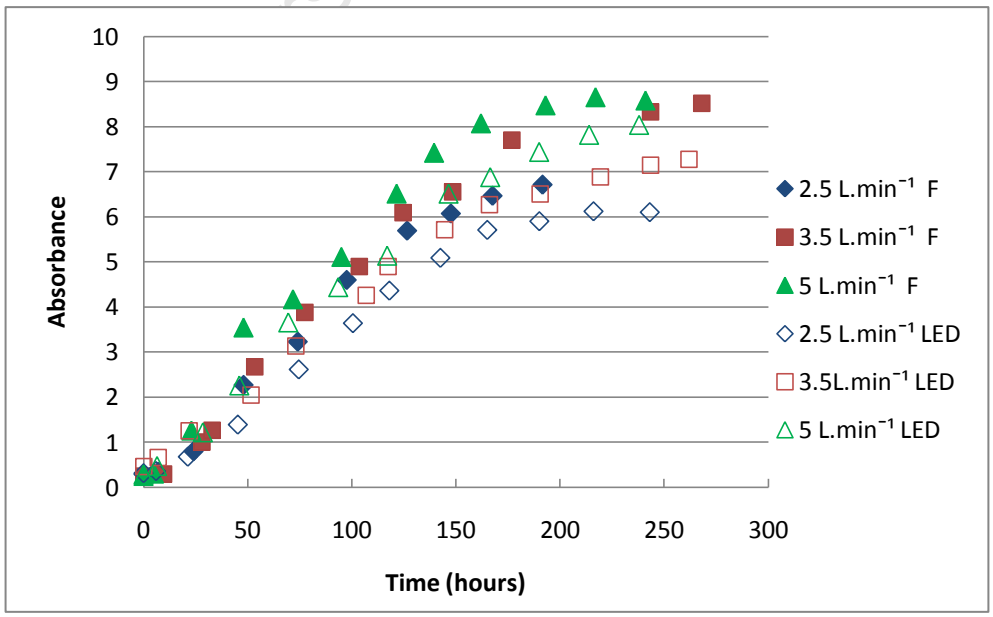

Figure 6. 8: Comparison of fluorescent (F) and LED light sources on the growth of *Scenedesmus sp.* at different aeration rates in the flat plate photobioreactor at 300 µmol.m^{-2}.s^{-1} and 25±1°C

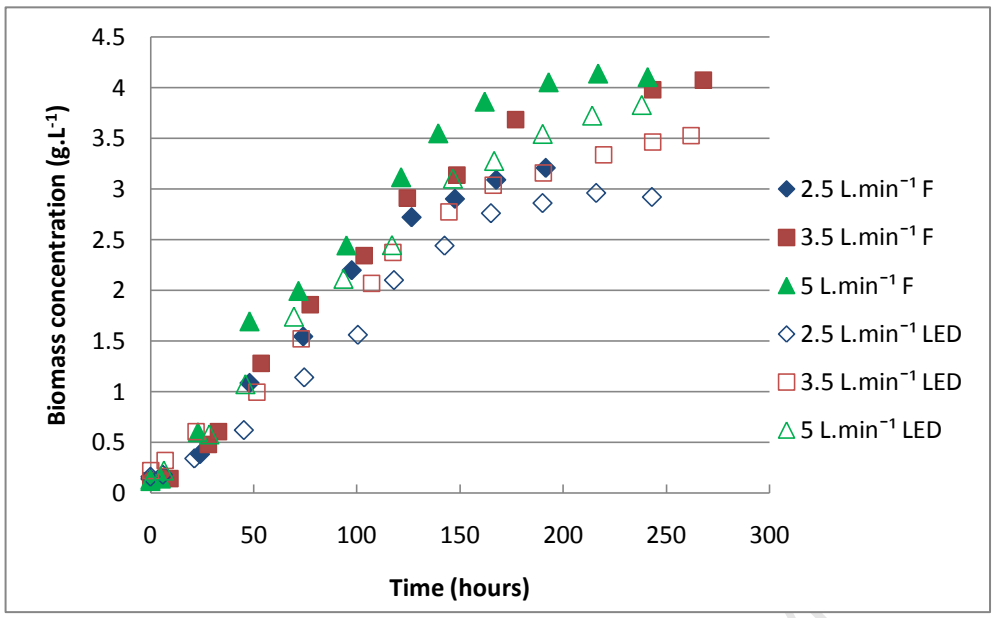

Figure 6. 9: Comparison of fluorescent (F) and LED light sources on the biomass concentration of *Scenedesmus sp.* at different aeration rates in the flat plate photobioreactor at 300 µmol.m^{-2}.s^{-1} and 25±1°C

Table 6. 6: The effects of using fluorescent and LED light sources on the maximum specific and linear growth rates of *Scenedesmus sp.* at 300 µmol.m^{-2}.s^{-1} 25±1°C, as a function of aeration rate

	Fluorescent light				LED light			
F (L.min^{-1})	μ_{max} (h^{-1})	Q (g.L^{-1}.h^{-1})	X_{max} (g.L^{-1})	t_{max} (days)	μ_{max} (h^{-1})	Q (g.L^{-1}.h^{-1})	X_{max} (g.L^{-1})	t_{max} (days)
2.5	0.0459	0.0174	3.20	8.00	0.0376	0.0154	2.97	9.00
3.5	0.0527	0.0209	4.07	11.1	0.0453	0.0166	3.52	11.0
5.0	0.0571	0.0216	4.14	9.04	0.0491	0.0180	3.83	9.92

Two possible explanations could account for the poorer performance of the LEDs: light penetration or the distribution of light (described in Section 5.2.2). To investigate light penetration, the amount of light penetration into a culture of *Scenedesmus sp.* measured in a glass beaker under fluorescent and LED illumination is reported in Figure 6.10. This builds on the investigation reported in Section 5.2.3. Figure 6.10 shows that better light penetration was achieved with both increasing biomass concentration and depth of culture for LED light compared to fluorescent light. Thus, the higher penetration of LED light does not provide explanation of the growth trends shown. An alternative explanation for these results could be the _point-specific' nature of LED illumination i.e. the light intensity is high at the LED but drops off between successive LEDs. To validate this theory, the light penetration in a culture of *Scenedesmus sp.* measured in line with the site of a LED and in the space between two LEDs is presented in Figure 6.11. Light intensity between LEDs is significantly lower than the light intensity emitted at the surface of a

LED. For example, at a biomass concentration of 0.48 $g.L^{-1}$, the surface light intensity decreased from approximately 370 to 170 $\mu mol.m^{-2}.s^{-1}$ as the algal culture moved past the surface of a diode to the space between two diodes respectively. Hence, in the spaces between diodes the algal cells at the surface of the reactor are exposed to a far lower light intensity. In Section 4.2.4.1, it was reported that the flat plate photobioreactor displayed a circular flow pattern with a cycle time of approximately 1.48 ± 0.076 s^{-1} at an aeration rate of 5 $L.min^{-1}$ (Table 6.5). Assuming that the algal cells passed approximately 10 diodes per cycle (Figure 4.7), it was estimated that the culture passed approximately 6 diodes per second and thus were exposed to light intensities of approximately 370 $\mu mol.m^{-2}.s^{-1}$ at least six times per second. The high cycle frequency of algal cells between diodes enabled the *Scenedesmus sp.* cultures to obtain reasonable growth rates in comparison to the results obtained using fluorescent lighting (Table 6.6). From the light intensity data collected for the fluorescent light bank, it was evident that the fluorescent light bulbs diffused light more evenly at an average light intensity of between 280-300 $\mu mol.m^{-2}.s^{-1}$ (see Appendix B-1). Thus, it can be concluded that the growth of *Scenedesmus sp.* was more limited by light availability when the LED light bank was used to provide constant illumination, compared to the fluorescent light bank.

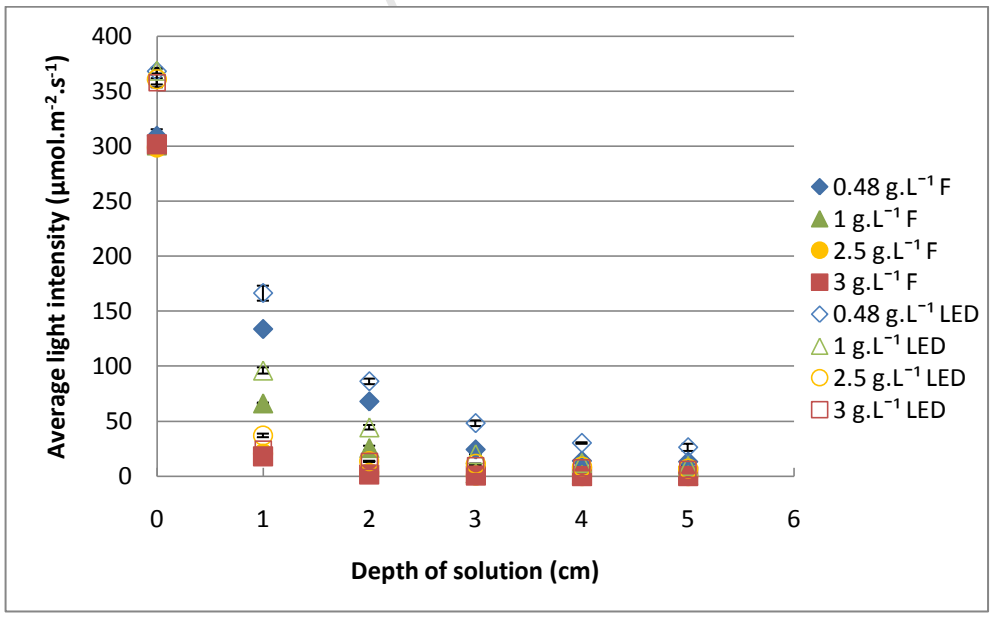

Figure 6. 10: Comparison of penetration of fluorescent (closed symbols) and LED (open symbols) light sources through *Scenedesmus sp.* culture of increasing biomass concentration and culture depth (Error bars represent standard deviations for triplicate runs for all data sets)

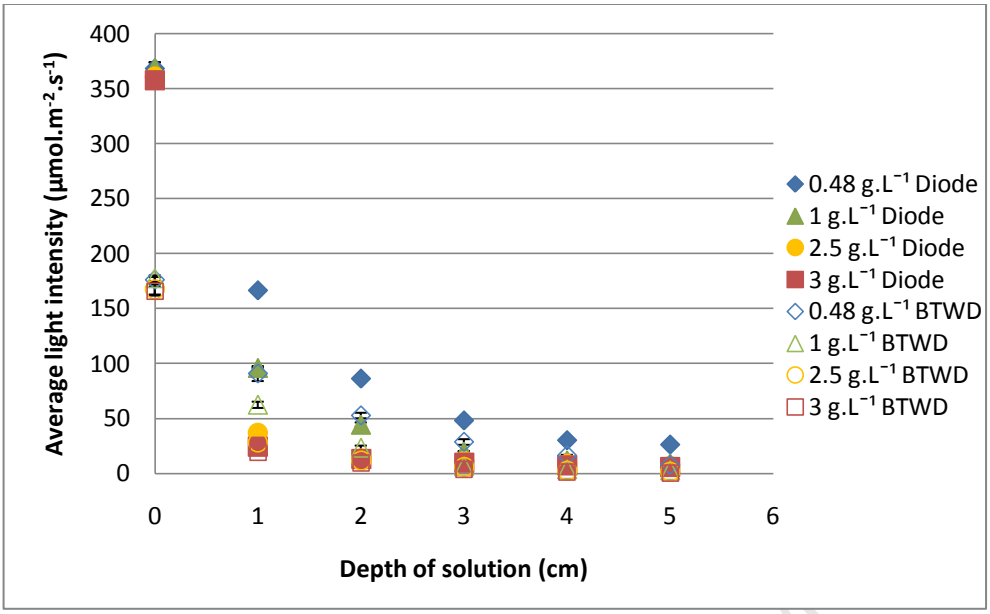

Figure 6. 11: Comparison between the light penetration obtained in a culture of *Scenedesmus sp.* at the point aligned with the site of a diode (DIODE) or the space between two diodes (BTWD) (Error bars represent standard deviations for triplicate runs for all data sets)

6.4 Performance evaluation of the different photobioreactors

6.4.1 Introduction

It is well recognised that photobioreactor design is important in terms of the volumetric and areal algal productivities attainable, as well as the productivity per unit energy used. In Section 6.4.2, the performance of the vertical airlift, tubular and flat plate photobioreactors are compared in terms of the maximum specific growth rates, the linear productivities and the maximum biomass concentrations that were attained for *Scenedesmus sp*. at the different operating conditions provided in Sections 3.3.2, 3.3.3 and 3.3.4, presented in Sections 5.2.2, 6.2.1, 6.3.2 and 6.3.3 respectively. Subsequently, an evaluation of the energetic performance of these photobioreactors is presented in Section 6.4.3. For this analysis, only the light and mixing energy requirements were considered and were calculated using Equations 2.7 and 2.8 respectively (Ogbonna *et al.*, 1995). The energetic performance of each of the photobioreactors was then assessed by calculating the biomass productivity obtained per unit power input using Equation 2.10. In addition, the net energy ratios were calculated using Equation 2.12, in order to assess the feasibility of cultivating *Scenedesmus sp.* as an energy product. Finally, different scenarios were considered where either all or a percentage of the light energy requirement

would be provided from solar irradiation. The energy efficiencies of the different photobioreactors were then reassessed at these conditions.

6.4.2. Evaluation of the growth of *Scenedesmus sp.* in the vertical airlift, tubular and flat plate photobioreactors

Light conditions and mixing regimes achieved affected the growth rates and biomass concentrations obtained for *Scenedesmus sp.* in the vertical airlift, tubular and flat plate photobioreactors significantly (Sections 5.2.2, 6.2.1, 6.3.2 and 6.3.3). The maximum specific and linear growth rates as well as the maximum biomass concentrations obtained at each light and mixing condition in each photobioreactor are presented in Table 6.7. Further, the reactor properties of illumination surface area to volume ratio, gas to liquid ratio, overall mass transfer coefficient and mean circulation times are given for each condition.

The general trend observed was that an increase in light intensity resulted in an increase in the maximum specific and linear growth rates at fixed aeration rates in each of the photobioreactors. The tubular photobioreactors achieved the highest maximum specific growth rates and biomass concentrations after 2.0 to 3.2 days of cultivation. These results may be attributed to the highest degree of light exposure per unit culture volume for the tubular photobioreactors (65-143 $mmol.m^{-3}.s^{-1}$). From Table 6.7, it can be seen that the tubular photobioreactors had the shortest light path length and the highest incident surface area to culture volume ratios, approximately five to eight times greater than the ratios obtained in the airlift and flat plate photobioreactors respectively. The highest maximum specific growth rate of 0.1035 h^{-1} was obtained in the 209 mL photobioreactor at 600 $\mu mol.m^{-2}.s^{-1}$ and at the shorter cycle time of 21 s. The maximum specific growth rates presented in Table 6.7 were obtained when the tubular photobioreactors were exposed to full light conditions (f =1) (Section 6.2.1). Furthermore, Table 6.7 shows that the volumes of gas sparged per unit culture volume per min were approximately two to three times greater in the tubular photobioreactors than the airlift photobioreactors. Previously, in Section 6.2.2, it was determined that the tubular photobioreactors exhibited laminar flow in the downcomer (Re < 2300) and were not mass transfer limited. However, no experimental data for the overall mass transfer coefficient in the tubular photobioreactors was available, so the effects of mixing rates and mass transfer rates of CO_2 on the growth of *Scenedesmus sp.* across the different types of photobioreactors could not be compared.

Table 6.7 also shows that the flat plate photobioreactor achieved both higher maximum specific and linear growth rates as well as greater biomass concentrations than the vertical airlift photobioreactors. Both the shorter light path length and greater illumination surface area to volume ratio in the flat plate photobioreactor resulted in better light penetration. The incident light was supplied at 14.2 to 28.4 $mmol.m^{-3}.s^{-1}$. Furthermore, increasing the volume of gas sparged per unit culture volume per minute resulted in an increase in the overall mass transfer coefficient in the flat plate photobioreactor, which consequently resulted in an increase in the maximum specific and linear specific growth rates. Similar overall mass transfer coefficients of 0.094-0.0101 s^{-} were obtained in the flat plate and airlift photobioreactors when the volumes of gas sparged per unit culture volume per minute were 3.1 and 0.625 $m^3.min^{-1}.m^3$ respectively. The volume of gas sparged per unit culture volume per min was approximately five times greater in the flat plate photobioreactor as compared to the vertical airlift photobioreactor. The greater degree of mixing in the flat plate photobioreactor resulted in a shorter mean circulation time, which improved the frequency of light/dark cycling (Section 6.2.1) and had a positive impact on growth.

Although the flat plate photobioreactor achieved greater maximum specific and linear growth rates than the vertical airlift photobioreactors, it can be observed that at the lower gas-to-liquid ratio, increasing the external fluorescent light intensity from 300 to 600 $\mu mol.m^{-2}.s^{-1}$ resulted in an increase in both the maximum specific and linear growth rates as well as the maximum biomass concentration in the airlift reactors (Table 6.7). Reducing the light path length through the provision of internal LED illumination at 300 $\mu mol.m^{-2}.s^{-1}$ resulted in a slightly lower maximum specific growth rate than the externally illuminated fluorescent airlift photobioreactor at 300 $\mu mol.m^{-2}.s^{-1}$. However, this result can be attributed to the ‗point-specific' light distribution pattern of LEDs (Section 5.2.2). The combination of internal illumination with external fluorescent light at overall average light intensities of 460 and 600 $\mu mol.m^{-2}.s^{-1}$ improved light penetration in the downcomer and thus resulted in an increase in both the maximum specific and linear growth rates. Thus, it is evident that if the illumination surface area to volume ratio is improved sufficiently, the airlift photobioreactors can be a feasible option for achieving high maximum specific growth rates and biomass productivities for *Scenedesmus sp.* cultures at a low gas to liquid ratio.

Table 6. 7: Comparison of the growth rates and biomass concentrations obtained for *Scenedesmus sp.* in the vertical airlift, tubular and flat plate photobioreactors at their respective operating conditions (1% CO_2 and 25±1°C)

PBR	Light source	I_o ($\mu mol.m^{-2}.s^{-1}$)	L (m)	SA/V (m^{-1})	Gas to liquid ratio ($m^3.min^{-1}.m^{-3}$)	$k_La(CO_2)$ (s^{-1})	t_c (s)	μ_{max} (h^{-1})	Q ($g.L^{-1}.h^{-1}$)	X_{max} ($g.L^{-1}$)	t_{max} (days)
ALR	F	300	0.09	29.5	0.625	0.0094	7	0.0275	0.0070	1.75	13.9
ALR	F	600	0.09	58.9	0.625	0.0094	7	0.0376	0.0114	3.85	15
IALR	LED	160	0.075	30.3	0.625	0.0094	7	0.0180	0.0044	1.11	15
IALR	LED	300	0.075	30.3	0.625	0.0094	7	0.0248	0.0064	2.03	15
CIALR	LED +F	460	0.075	59.8	0.625	0.0094	7	0.0358	0.0115	2.94	14.5
CIALR	LED + F	600	0.075	59.8	0.625	0.0094	7	0.0443	0.0123	3.53	14.5
TBR 1	F	300	0.007	239	2.02	[a]	21	0.0834	[b]	4.08	3.2
TBR 1	F	600	0.007	478	2.02	[a]	21	0.1035	[b]	3.80	2.0
TBR 2	F	300	0.007	216	1.14	[a]	33	0.0725	[b]	1.61	2.0
TBR 2	F	600	0.007	432	1.14	[a]	33	0.0970	[b]	2.75	2.3
FP	F	300	0.029	47.3	1.56	0.0063	2.02	0.0459	0.0174	3.20	8.0
FP	F	300	0.029	47.3	2.19	0.0073	1.72	0.0527	0.0209	4.07	11.2
FP	F	300	0.029	47.3	3.13	0.0101	1.48	0.0571	0.0216	4.14	9.0
FP	F	600	0.029	94.5	1.56	0.0063	2.02	0.0512	0.0247	4.00	6.9
FP	F	600	0.029	94.5	2.19	0.0073	1.72	0.0577	0.0256	4.49	6.3
FP	F	600	0.029	94.5	3.13	0.0101	1.48	0.0642	0.0276	4.62	5.3
FP	LED	185	0.029	47.3	1.56	0.0063	2.02	0.0376	0.0154	2.97	9.0
FP	LED	185	0.029	47.3	2.19	0.0073	1.72	0.0453	0.0166	3.52	11
FP	LED	185	0.029	47.3	3.13	0.0101	1.48	0.0491	0.0180	3.83	9.9

[a] No previous experimental data was available for the tubular photobioreactors

[b] The linear growth rates were not recorded as the tubular photobioreactors were used as research tools to determine the maximum specific growth rate that could be obtained when the dependence of growth on light limitation was minimised and hence were not considered for scale-up

6.4.3 Evaluation of the energetic performance of the vertical airlift, tubular and flat plate photobioreactors for cultivating *Scenedesmus sp.*

In order to evaluate the energetic performance of a photobioreactor, it is important to assess the ratio of light and mixing energy inputs and the biomass productivity. For this analysis, Equations 2.7 and 2.8 were used to calculate the light and mixing energy inputs for the different photobioreactors respectively. Figures 6.12 and 6.13 illustrate the relationship between light or mixing energy respectively and biomass productivity of *Scenedesmus sp.* across the photobioreactor types.

Figure 6.12 shows that an increase in the light energy supplied per unit culture volume resulted in an increase in the biomass productivity across the different types of photobioreactors. The highest biomass productivities were obtained in the tubular photobioreactor, followed by the flat plate photobioreactor. The lowest biomass productivities were obtained in the airlift photobioreactors. Light limitation was apparent in all of the photobioreactors and became more pronounced as the light path lengths increased and the incident surface area to volume ratios of the photobioreactors decreased (Table 6.7). It should be noted that the flat plate photobioreactor supplied with light energy inputs of 3119 and 6237 $W.m^{-3}$ was operated at different $k_La(CO_2)$ values (Section 6.3.2) which also affected the biomass productivity of *Scenedesmus sp.* At similar $k_La(CO_2)$ values of 0.094-0.0101 s^{-1}, biomass productivities of 0.87 and 0.24 $g.L^{-1}.h^{-1}$ at light energy inputs of 6237 and 3944 $W.m^{-3}$ were obtained in the flat plate and airlift photobioreactors respectively.

The mixing energy requirement of a photobioreactor is dependent on the photobioreactor design (airlift or bubble column), the reactor volume, fluid properties (specific weight of broth) and the aeration rate. From inspection of Equations 2.8 and 2.9, it is evident that the mixing energy input in airlift photobioreactors is highly dependent on the superficial gas velocity and the ratio of the areas of the riser and downcomer, whereas the mixing energy in a bubble column photobioreactor is dependent on the volumetric gas flow rate and the culture depth. Figure 6.13 shows that the tubular photobioreactors achieved the highest biomass productivities at the lowest mixing energies. The low mixing energies could be attributed to the fact that the tubular photobioreactors had the lowest aeration rates and working volumes. The flat plate photobioreactor achieved higher biomass productivities at lower mixing energy inputs compared to the airlift photobioreactors. It

should be noted that although the flat plate photobioreactor had no draft tube to distinguish separate riser and downcomer zones, it exhibited a circular liquid circulation pattern (Section 4.2.4.1). Thus, when calculating the mixing energy inputs for the flat plate photobioreactor, a ratio of 1 was assumed for the areas of the riser and downcomer.

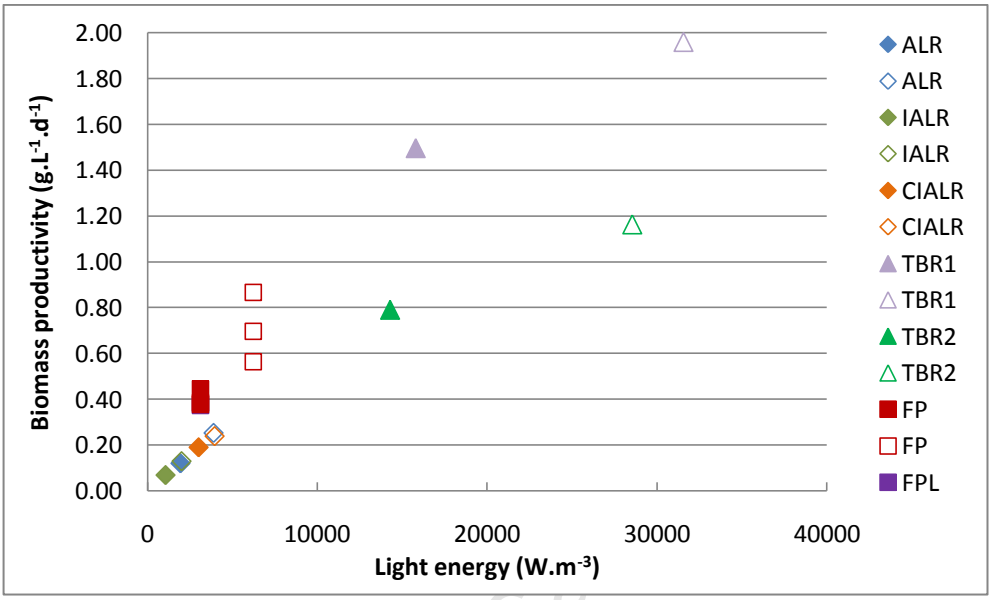

Figure 6. 12: Comparison of the effects of light energy supplied per unit culture volume on the biomass productivity of *Scenedesmus sp.* in the different photobioreactors (diamond, triangle and square symbols represent the vertical airlift, tubular and flat plate reactors respectively; TBR1 and TBR2 represent the 209 mL and 330 mL tubular reactors respectively; closed and open symbols represent light intensities of 300 and 600 µmol.m^{-2}.s^{-1} respectively)

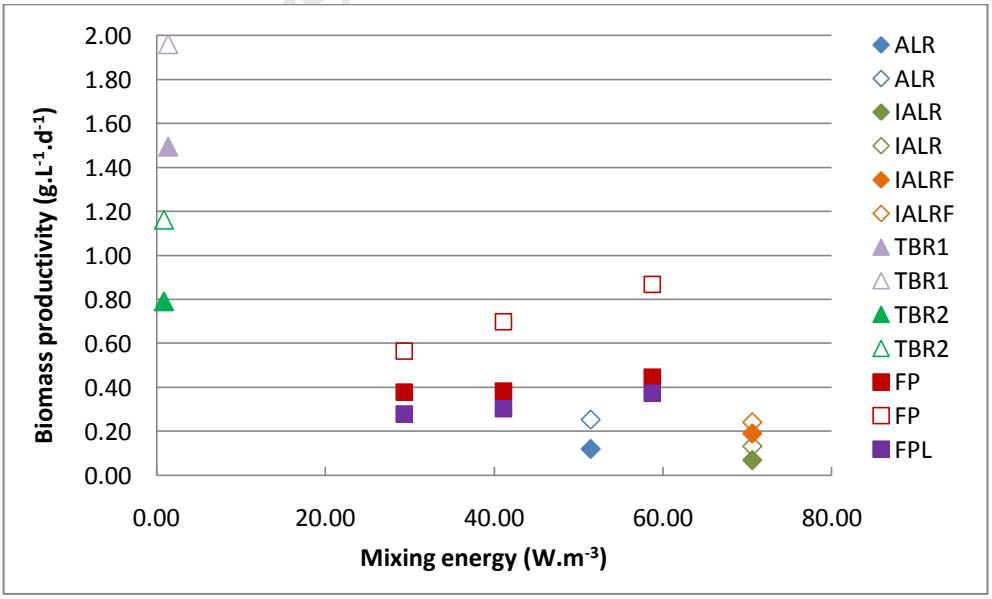

Figure 6. 13: Comparison of the effects of mixing energy per unit culture volume on the biomass productivity of *Scenedesmus sp.* in the different photobioreactors (diamond, triangle and square symbols represent the vertical airlift, tubular and flat plate reactors respectively; TBR1 and TBR2 represent the 209 mL and 330 mL tubular reactors respectively; closed and open symbols represent light intensities of 300 and 600 µmol.m^{-2}.s^{-1} respectively)

Furthermore, it can be observed from Figure 6.13, that the internally illuminated photobioreactor required a higher mixing energy input than the standard airlift photobioreactors. The increase in mixing energy in the internally illuminated photobioreactor may be attributed to the increased ratio of the areas of the riser and downcomer from 0.3 to 0.5. From inspection of Equation 2.8, it is evident that increasing the ratio of the areas of the riser and downcomer has a significant impact on the mixing energy requirement. However, the modification had a negligible effect on the biomass productivity achieved. Figure 6.13 also shows that an increase in mixing energy resulted in an increase in the biomass productivity achieved in the flat plate photobioreactor. This was more marked at the higher light intensity. Increasing the gas flow rate to a pneumatically agitated photobioreactor improves both mixing and circulation of algal cells in the photobioreactor. The increase in the light/dark cycling is expected to improve light utilization and the increase in mixing to result in an increase in the overall mass transfer coefficient (Posten, 2009; Pegallapati and Nirmalakhandan, 2011).

In Figure 6.14, it can be seen that an increase in the volume of gas sparged per unit culture volume per min in the flat plate photobioreactor resulted in an increase in the mixing energy and the overall mass transfer coefficient. Furthermore, the airlift photobioreactor attained a mass transfer coefficient of 0.094-0.0101s^{-1} at a lower gas to liquid ratio than the flat plate photobioreactor. The difference in the overall mass transfer coefficients achieved could be attributed to the different sparger designs. As mentioned previously, the overall mass transfer coefficient is highly dependent on design parameters such as the bubble size, agitation rate, gas hold up, temperature and superficial gas velocity (Chisti, 2002). In particular, the bubble size determines the specific interfacial area available for the mass transfer of CO_2 gas into the liquid algal culture. In the airlift photobioreactor, a 0.22 μm stainless steel HPLC sparger was used to produce bubbles with a mean diameter of 2 mm (Langley, 2010), whereas in the flat plate photobioreactor, a 0.0064 m stainless steel sparger with 1 mm holes spaced 10 mm apart was used to produce bubbles with a mean diameter of 3 mm. The bubble size in the flat plate photobioreactor was estimated by visual inspection of Figure 4.8. The difference in mixing energy requirements was caused by the different cross-sectional areas of the risers and the different ratios of the areas of the riser and downcomer, which were 0.3 and 1 in the airlift and flat plate photobioreactors respectively (Equation 2.8).

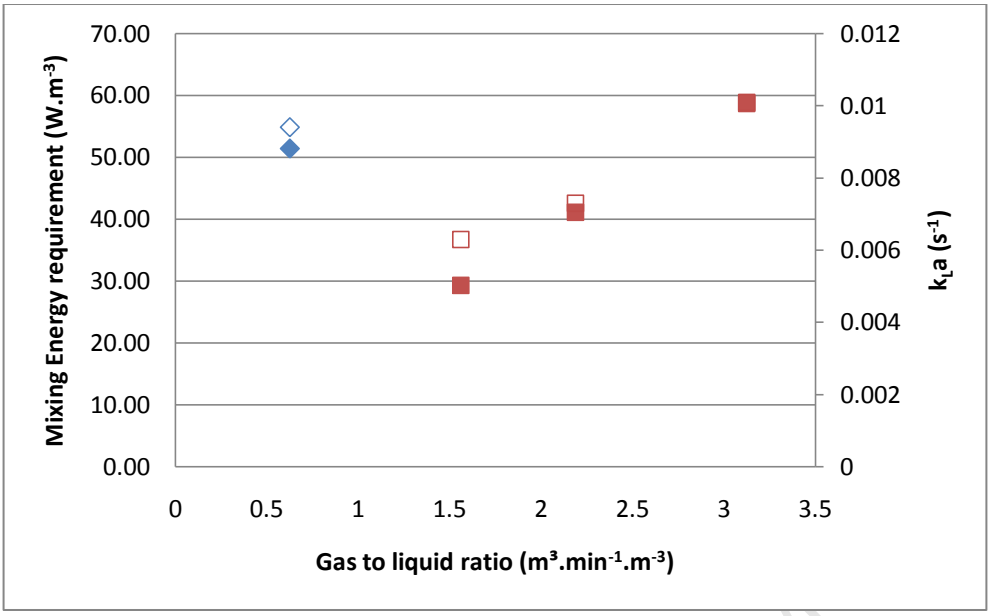

Figure 6. 14: The effect of the gas-liquid ratio on the overall mass transfer coefficient (open symbols) and the mixing energy requirement (closed symbols) in the flat plate (square) and airlift (diamond) photobioreactors

Table 6.8 presents a summary of the energy inputs and the biomass productivities achieved per unit power input, for each of the photobioreactors at their respective growth conditions. The flat plate photobioreactor achieved the highest biomass productivities per unit power input of 0.088 to 0.140 $g.W^{-1}.day^{-1}$ (accounting for both light and mixing energy), followed by the tubular and airlift photobioreactors that achieved 0.041 to 0.095 $g.W^{-1}.day^{-1}$ and 0.060 to 0.064 $g.W^{-1}.day^{-1}$ respectively. The different energy efficiencies obtained in the different photobioreactors may be attributed to the different light and mixing energy contributions in each of the photobioreactors. Table 6.8 shows that the tubular photobioreactors had the highest light energy inputs that were approximately five to eight times greater than the light energy inputs of the flat plate and airlift photobioreactors respectively. Consequently, the tubular photobioreactors achieved relatively low biomass productivities per unit power input, despite the high biomass productivities achieved (Figures 6.12 and 6.13). It can also be observed that the flat plate photobioreactor had higher light energy and lower mixing energy inputs than the vertical airlift photobioreactors, with the exception of the mixing energy input at the gas to liquid ratio of 3.13 $m^3min^{-1}.m^{-3}$. The better performance of the flat plate photobioreactor may be attributed to the better light utilization that was achieved through the improved incident surface area to volume ratio and the reduced light path length (Table 6.7).

Table 6. 8: Comparison of the energetic performance of the vertical airlift, tubular and flat plate photobioreactors

PBR	Light source	I_o ($\mu mol.m^{-2}.s^{-1}$)	Gas to liquid ratio ($m^3.min^{-1}.m^{-3}$)	Light energy ($W.m^{-3}$)	Mixing Energy ($W.m^{-3}$)	Total energy input ($W.m^{-3}$)	P/E [a] ($g.W^{-1}.d^{-1}$)	P/E [b] ($g.W^{-1}.d^{-1}$)	P/E [c] ($g.W^{-1}.d^{-1}$)
ALR	F	300	0.625	1944	51.40	1995	0.060	0.085	1.169
ALR	F	600	0.625	3888	51.40	3939	0.064	0.091	2.462
IALR	LED	160	0.625	1067	70.57	1138	0.060	0.083	0.482
IALR	LED	300	0.625	2001	70.57	2071	0.063	0.089	0.924
CIALR	LED +F	460	0.625	3011	70.57	3081	0.062	0.087	1.346
CIALR	LED + F	600	0.625	3944	70.57	4015	0.060	0.085	1.700
TBR 1	F	300	2.02	15779	1.384	15780	0.095	0.135	540.3
TBR 1	F	600	2.02	31558	1.384	31560	0.062	0.089	708.0
TBR 2	F	300	1.14	14272	0.861	14273	0.055	0.079	459.1
TBR 2	F	600	1.14	28545	0.861	28545	0.041	0.058	675.0
FP	F	300	1.56	3119	29.36	3148	0.120	0.171	6.445
FP	F	300	2.19	3119	41.11	3160	0.121	0.173	4.669
FP	F	300	3.13	3119	58.73	3177	0.140	0.198	3.786
FP	F	600	1.56	6237	29.36	6266	0.090	0.128	9.609
FP	F	600	2.19	6237	41.11	6278	0.111	0.158	8.477
FP	F	600	3.13	6237	58.73	6296	0.138	0.196	7.380
FP	LED	185	1.56	3119	29.36	3148	0.088	0.125	4.725
FP	LED	185	2.19	3119	41.11	3160	0.096	0.136	3.680
FP	LED	185	3.13	3119	58.73	3177	0.117	0.166	3.172

[a] Biomass productivity per unit power input was calculated when the light energy input was provided by artificial illumination.
[b] Biomass productivity per unit power input was calculated based on the assumption that 30% of the total light energy requirement was provided by solar irradiation (similar percentage was used by Janssen *et al*., 2003)
[c] Biomass productivity per unit power input was calculated when the light energy input was provided by solar irradiation

For all the photobioreactors, the light energy input accounted for over 93.4% of the total energy requirement (Table 6.8). There is great potential for exploiting solar energy in South Africa to cultivate microalgae commercially (Figure 2.6). If solar energy is harnessed to supply light to the photobioreactors, the energy efficiency of the different photobioreactors could be greatly improved. However, it should be noted that day-night cycles and daily fluctuations in light intensity due to weather conditions such as cloud cover and rain would adversely affect biomass productivity. Furthermore, daily fluctuations in temperature, evaporative losses and contamination by predatory species would also affect the biomass productivity achieved (Ugwu *et al.,* 2008; Sanchez *et al.*, 2008). Thus, in order to maintain high levels of biomass productivity, it would be better to supply a closed photobioreactor with a combination of solar and artificial illumination. For example, Ogbonna *et al.* (1999) designed a light supply system whereby an internally illuminated stirred tank photobioreactor was supplied with solar illumination via optic fibres during the day, until a sensor detected that the light intensity dropped to values below 50 $\mu mol.m^{-2}.s^{-1}$. When this occurred, the sensor triggered a response that turned on a metal halide lamp.

However, it should be noted that apart from the environmental conditions, the amount of solar energy that a photobioreactor is able to utilize depends on other factors such as the light exposure that the photobioreactor design receives as well as the method of light supply. For example, one of the current key disadvantages of using fibre optics is the significant loss of light that occurs at the coupling points between different light guide fibres and during transport of light through the fibres (Gordon, 2002; Ogbonna *et al.*, 1999; Usui and Ikenouchi, 1997). For the purposes of this analysis, two scenarios were considered. In the first scenario, it was assumed that only 30% of the total light energy input could be supplied from solar irradiation and the remainder would be provided by fluorescent light, LEDs or a combination of the two. In the second scenario, it was assumed that the total light energy input was supplied from solar irradiation and that half the biomass productivity would be obtained in the photobioreactors due to day/night cycling and fluctuations in other environmental conditions. It can be observed from Table 6.8, that if 30% of the total light energy input was supplied from solar irradiation, the biomass productivity per unit power input in the flat plate, tubular and vertical airlift photobioreactors would increase to 0.125-0.198 $g.W^{-1}.day^{-1}$, 0.058-0.135 $g.W^{-1}.day^{-1}$ and 0.083-0.091 $g.W^{-1}.day^{-1}$ respectively. Further, if the total light energy input was supplied

from solar irradiation, the biomass productivities obtained per unit mechanical power input in the tubular, flat plate and airlift photobioreactors would increase to 459.1-708.0 $g.W^{-1}.day^{-1}$, 3.172-9.609 $g.W^{-1}.day^{-1}$ and 0.482-2.462 $g.W^{-1}.day^{-1}$ under the mixing conditions specified for each of the reactors respectively. It is evident that the biomass productivity per unit mechanical power input could be further improved by decreasing the aeration rate. However, the impact of reduced aeration rate on the overall mass transfer coefficient and the efficiency of light/dark cycling are yet to be assessed in the airlift photobioreactors by Sarah Jones (PhD student at UCT).

Alternatively, if *Scenedesmus sp.* was cultivated as an energy product, the energetic value of the biomass produced must be greater than the process energy requirement for the cultivation system to be considered feasible (Richardson, 2011). Thus, the net energy ratio (NER) should be at least above 1 (Equation 2.12). Figures 6.15 and 6.16 present the NERs obtained in the different photobioreactors as a function of light intensity, when the light energy input was supplied by artificial illumination and when 30% of the total light energy input was supplied by solar energy respectively. Figure 6.17 presents the NERs that would be obtained in the different photobioreactors if the total light energy requirement was supplied by solar energy. As mentioned earlier, for this case, it was assumed that the biomass productivity was halved due to fluctuations in environmental conditions (day/night cycling). The energetic value of the biomass was calculated based on an average calorific value of 23 $MJ.kg^{-1}$ for *Scenedesmus sp.* (Illman *et al.*, 2000; McGinn *et al.,* 2012).

From Figure 6.15, it can be seen that at the current operating conditions, none of the reactors are feasible for producing energy products, as the energy requirement for the cultivation systems were greater than the amount of energy accumulated in the biomass. It can also be observed from Figure 6.16, that if the 30% of the light energy input for the reactors was supplied from solar irradiation, the NERs in all of the reactors would increase. However, it is evident that the NERs are still well below 1. If the total light energy requirement was supplied by solar energy, the tubular reactors would achieve NERs of between 254 to 390. The large NERs are attributed to the high degree of light exposure and the small working volume of the tubular reactors. However, as mentioned previously in Section 6.2.1, the tubular photobioreactors would not be feasible for scale-up. Figure 6.17 shows that if the total light energy requirement was supplied by solar energy, the flat plate reactors would be feasible. Further, if the light supply and

penetration as well as the gas supply for mixing were improved in the airlifts, these reactors could also become feasible. Thus, it is evident that in order to improve the net energy ratios obtained in each of the reactors, it is important to increase the amount of solar irradiation that is captured and the distribution of light in the reactors.

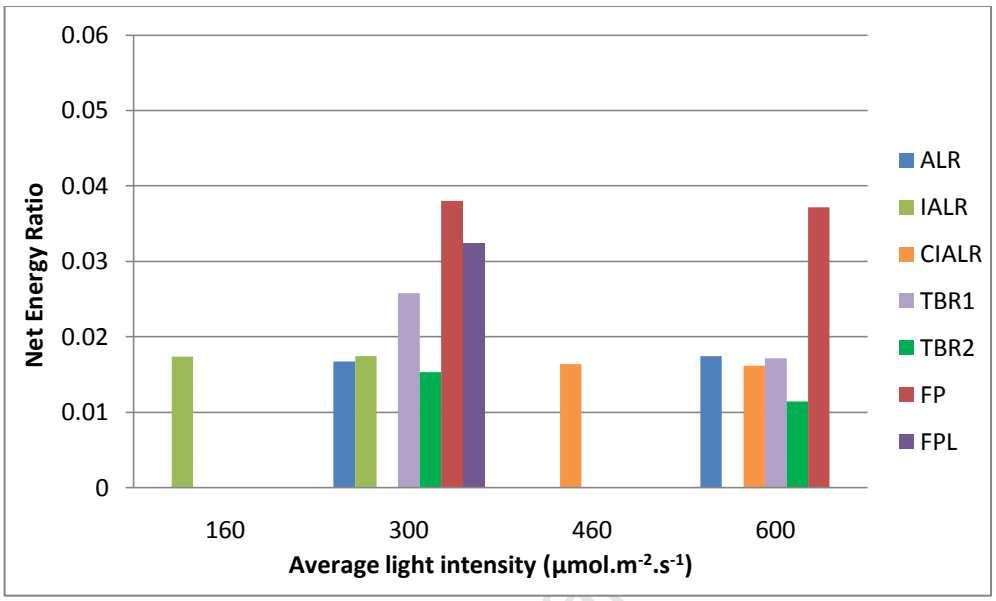

Figure 6. 15: Comparison of the performance of the different photobioreactors in terms of NER, where the light energy input is supplied from LEDs, fluorescent light or a combination thereof (ALR-airlift photobioreactor, IALR-internally illuminated airlift photobioreactor, CIALR-combination of internally illuminated photobioreactor with external fluorescent lighting, TBR1-209 mL tubular photobioreactor, TBR2-330 mL tubular photobioreactor , FP-flat plate photobioreactor with external fluorescent lighting and FPL-flat plate photobioreactor illuminated with LEDs)

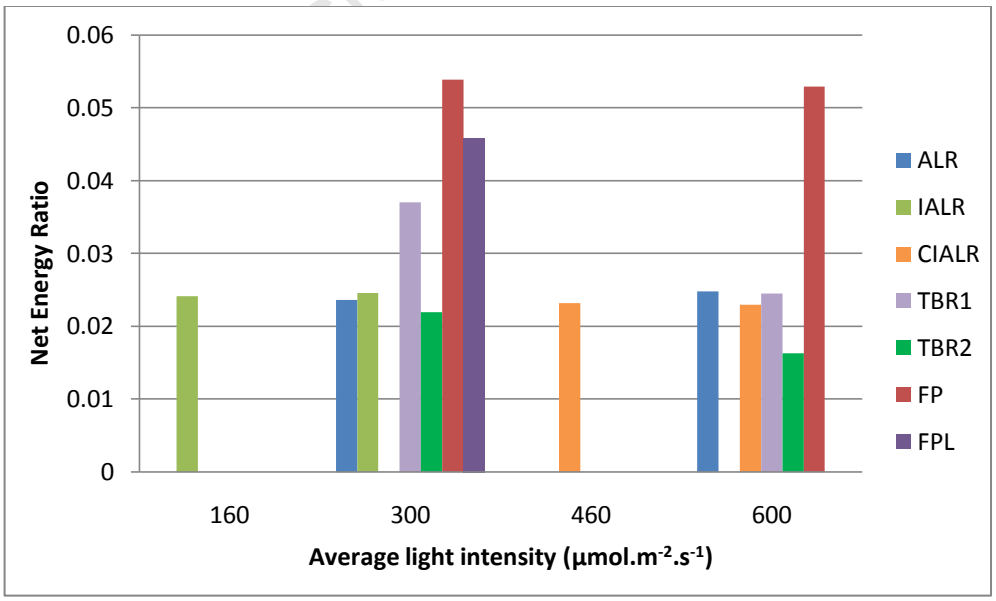

Figure 6. 16: Comparison of the performance of the different photobioreactors in terms of NER, when 30% of the light energy input is supplied from solar irradiation (ALR-airlift photobioreactor, IALR-internally illuminated airlift photobioreactor, CIALR-combination of internally illuminated photobioreactor with external fluorescent lighting, TBR1-209 mL tubular photobioreactor , TBR2-330 mL tubular photobioreactor , FP-flat plate photobioreactor with external fluorescent lighting and FPL-flat plate photobioreactor illuminated with LEDs)

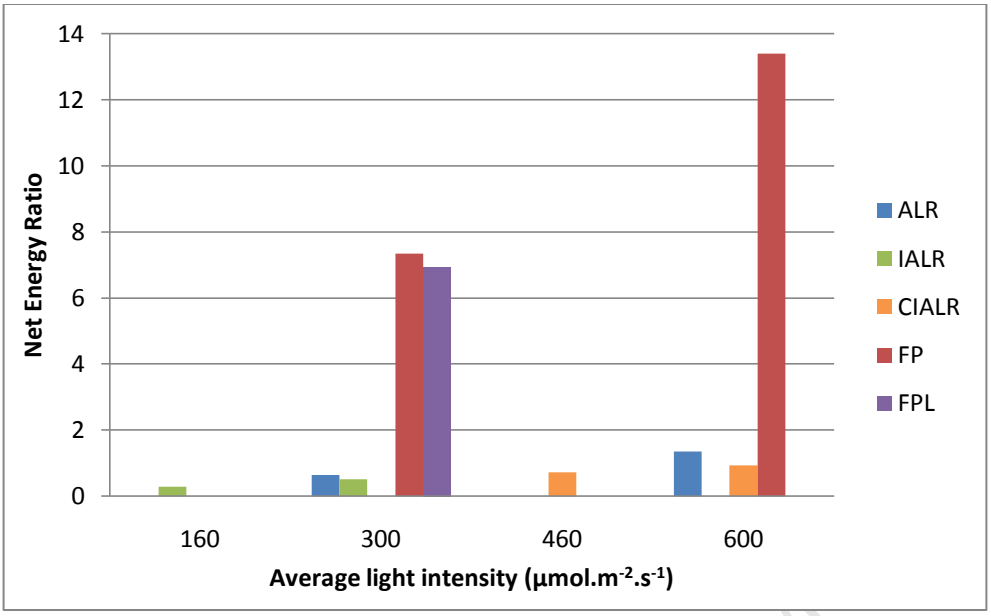

Figure 6. 17: Comparison of the performance of the different photobioreactors in terms of NER, when 100% of the light energy input is supplied from solar irradiation
(ALR-airlift photobioreactor, IALR-internally illuminated airlift photobioreactor, CIALR-combination of internally illuminated photobioreactor with external fluorescent lighting, FP-flat plate photobioreactor with external fluorescent lighting and FPL-flat plate photobioreactor illuminated with LEDs)

6.5 Conclusions

From the results obtained for investigating the effects of light intensity, light fraction and cycle time on the growth of *Scenedesmus sp.* in the tubular photobioreactors, it was found that increasing the light fraction (volume fraction of photobioreactor exposed to light) from 0.4 to 1 (full light exposure) at 300 µmol.m^{-2}.s^{-1} increased the incident surface area to culture volume ratio from 95.6 to 239 m^{-1} and from 86.4 to 216 m^{-1} in the 330 mL and 209 mL reactors respectively, consequently resulting in an increase in the maximum specific growth rate from 0.0323 h^{-1} to 0.0725 h^{-1} and from 0.0429 h^{-1} to 0.0834 h^{-1} at cycle times of 33 s and 21 s respectively. Furthermore, increasing the light intensity from 300 to 600 µmol.m^{-2}.s^{-1} at a constant light fraction also improved the amount of light exposure and penetration that was achieved. At a light fraction of 1, increasing the light intensity from 300 to 600 µmol.m^{-2}.s^{-1} resulted in an increase in the maximum specific growth rate from 0.0725 h^{-1} to 0.097 h^{-1} and from 0.0834 h^{-1} to 0.1035 h^{-1} at cycle times of 33 s and 21 s respectively.

Decreasing the cycle time from 33 s (330 mL tubular reactor operated at 376 mL.min^{-1}) to 21 s (209 mL tubular photobioreactor operated at 432 mL.min^{-1}) also resulted in a 15% and 6.7% increase in the maximum specific growth rate at 300 and 600 µmol.m^{-2}.s^{-1}

respectively. This result is attributed to the shorter fraction of time (0.54) that algal cells spend under high light exposure in the downcomer (7 mm ID glass tubes) before returning to the light-limited riser (18 mm ID glass tube) to recover from the effects of photoinhibition. At a cycle time of 33 s, cells spent a longer fraction of time (0.6) in the downcomer before returning to the riser and hence had less time for cellular recovery. These results highlight the importance of improving the frequency of light/dark cycling to optimize light utilization and hence the maximum specific growth rate of *Scenedesmus sp*.

Based on these results, the efficiency of light/dark cycling in the airlift photobioreactors was assessed. In order to perform this analysis, it was assumed that the riser and the downcomer were the light and dark zones in the airlift photobioreactor. Based on previous experimental circulation time data, it was established that both photobioreactors experienced a light fraction of approximately 0.75. It was found that the different lighting regimes and the different hydrodynamics associated with each of the photobioreactors affected the maximum specific growth rates obtained. The tubular and airlift photobioreactors had downcomer light path lengths of 0.007 m and 0.025 m respectively. The higher degree of light exposure and penetration in the tubular photobioreactors resulted in maximum specific growth rates that were approximately 0.59 to 1.5 times and 0.75 to 1.1 times greater than those achieved in the airlift photobioreactors at external fluorescent light intensities of 300 and 600 $\mu mol.m^{-2}.s^{-1}$ respectively. However, the provision of internal illumination in the airlift reactor (light path length of 0.0175 m), coupled with an external fluorescent light bank at an overall light intensity of 600 $\mu mol.m^{-2}.s^{-1}$, improved light penetration and consequently resulted in a maximum specific growth rate that was 18% greater than that achieved in the externally illuminated airlift photobioreactor at 600 $\mu mol.m^{-2}.s^{-1}$. It was observed that both the airlift and tubular photobioreactors transitioned from exponential to linear growth at biomass concentrations where the light intensity available in the downcomer regions was approximately 30-75 $\mu mol.m^{-2}.s^{-1}$, suggesting that light availability is one of the major factors affecting the growth of *Scenedesmus sp.*

In terms of hydrodynamics, the tubular and airlift photobioreactors had aeration rates of 376-432 $mL.min^{-1}$ and 2 $L.min^{-1}$, and mean circulation times of 21-33 and 7 s respectively. The greater degree of turbulence improved mixing in the airlift reactor and resulted in an overall mass transfer coefficient of 0.0094 ± 0.00026 s^{-1}. However, no

experimental data for the overall mass transfer coefficient in the tubular photobioreactor was recorded. Thus, the airlift and tubular photobioreactors could not be compared in terms of mixing and mass transfer. Fraser (2011) used a simplistic model to demonstrate that the tubular photobioreactors were not mass transfer limited when provided with 1% CO_2.

In the flat plate photobioreactor, it was found that increasing the external fluorescent light intensity and the aeration rate both had significant impacts on the growth of *Scenedesmus sp.* Increasing the aeration rate from 2.5 $L.min^{-1}$ to 5 $L.min^{-1}$ at a constant light intensity of 300 $\mu mol.m^{-2}.s^{-1}$ had a minimal effect on the growth rate up to approximately 125 hours. However, increasing the light intensity from 300 to 600 $\mu mol.m^{-2}.s^{-1}$ resulted in a 22 to 42% increase in the linear growth rates, over the range of aeration rates investigated. The increase in light intensity and the provision of illumination on both sides of the flat plate photobioreactor increased the amount of light exposure and penetration that was achieved. At 2.5 $L.min^{-1}$ and 600 $\mu mol.m^{-2}.s^{-1}$, the system appeared both mass-transfer and light limited, whereas at 3.5 and 5 $L.min^{-1}$, it appeared light limited. It was found that the flat plate photobioreactor transitioned from exponential to linear growth at biomass concentrations where the light intensity available was approximately 25-50 $\mu mol.m^{-2}.s^{-1}$.

Later in the growth cycle (after 100-125 hours), a change in the linear slope was observed, suggesting that another factor became limiting. It was observed that at biomass concentrations of between 1.26 and 2.43 $g.L^{-1}$, increasing the aeration rate allowed the linear slope to be maintained for longer so that the maximum biomass concentration was obtained more rapidly. These results suggest that at higher biomass concentrations, mass transfer may have become limiting, since increasing the aeration rate from 2.5 to 5 $L.min^{-1}$ improved the overall mass transfer coefficient of carbon dioxide from 0.0063 ± 0.00020^{-1} to $0.0101 \pm 0.00029\ s^{-1}$ in the flat plate photobioreactor. It is well recognised that the mass transfer rate required increases as a function of the biomass concentration and the specific growth rate where the yield coefficient of biomass on CO_2 is constant.

Furthermore, from the investigation of the effects of external fluorescent and LED illumination on the growth of *Scenedesmus sp.* in the flat plate photobioreactor, it was found that the maximum specific and linear growth rates achieved using LEDS were approximately 14-18% and 12-21% lower compared to when fluorescent light was used

to provide illumination. Since the LEDs and fluorescent light sources had similar emission spectra, the poor performance of the LEDs could be attributed to differences in light penetration or distribution patterns. It was found that LEDs achieved better light penetration than fluorescent light. However, LEDs emitted light in a _point-specific manner‘ where the light intensity decreased from approximately 370 to 170 $\mu mol.m^{-2}.s^{-1}$ as the algal culture moved past the surface of a LED to the space between two LEDs respectively. Hence, in the spaces between diodes the algal cells at the surface of the reactor were exposed to a far lower light intensity. The fluorescent light bulbs diffused light more evenly at average light intensities of between 280 to 300 $\mu mol.m^{-2}.s^{-1}$.Thus, it can be concluded that the growth of *Scenedesmus sp.* was more limited by light availability when the LED light bank was used to provide constant illumination, compared to the fluorescent light bank.

From the performance evaluation of the different photobioreactors, it was evident that the different light and mixing regimes in each of the photobioreactors affected the maximum specific, linear growth rates and biomass concentrations of *Scenedesmus sp*. It was found that the tubular photobioreactors achieved the highest maximum specific growth rates and biomass concentrations, followed by the flat plate and airlift photobioreactors respectively. The tubular photobioreactors achieved the highest maximum specific growth rates for *Scenedesmus sp.* because they experienced the highest degree of light exposure due to their short light path length and high incident surface area to volume ratios. Similarly, the flat plate photobioreactor achieved both higher maximum specific and linear growth rates than the vertical airlift photobioreactors because of the shorter light path length and greater illumination surface area to volume ratio which improved light penetration. At similar overall mass transfer coefficients of 0.094-0.0101 s^{-} in the flat plate and airlift photobioreactors, the volumes of gas sparged per unit culture volume per minute were 3.1 and 0.625 $m^3.min^{-1}.m^3$ respectively (approximately five times greater in the flat plate photobioreactor). The greater degree of mixing in the flat plate photobioreactor resulted in a shorter mean circulation time, which may have improved the frequency of light/dark cycling which would have also resulted in an increase in the maximum specific and linear growth rates of *Scenedesmus sp.*

In terms of energy efficiency, the flat plate photobioreactor achieved the highest biomass productivities per unit power input (including light and mixing energy inputs) of 0.088-0.140 $g.W^{-1}.day^{-1}$, followed by the tubular and airlift photobioreactors that

achieved 0.041-0.095 $g.W^{-1}.day^{-1}$ and 0.060-0.064 $g.W^{-1}.day^{-1}$ respectively. For all of the photobioreactors, the light energy input accounted for over 93.4% of the total energy requirement. The tubular photobioreactors had the highest light energy inputs that were approximately five to eight times greater than the light energy inputs of the flat plate and airlift photobioreactors respectively. Consequently, the tubular photobioreactors achieved relatively low biomass productivities per unit power input, despite the high biomass productivities achieved. In terms of mixing energy inputs, the tubular photobioreactors had the lowest mixing energy inputs due to the low aeration rates and small working volumes. The flat plate photobioreactor achieved higher biomass productivities at lower mixing energy inputs compared to the airlift photobioreactors because of the difference between the ratios of the areas of the riser and downcomers which were 1 and 0.3-0.5 in the flat plate and airlift (externally and internally illuminated) photobioreactors respectively.

Furthermore, it was calculated that if 30% (assumption based on loss of light encountered from daily fluctuations in light intensity, weather conditions such as cloud cover and rain as well as the losses encountered during transportation through optic fibre cables) of the total light energy input was supplied from solar energy, the biomass productivity per unit power input in the flat plate, tubular and vertical airlift photobioreactors would increase to 0.125-0.198 $g.W^{-1}.day^{-1}$, 0.058-0.135 $g.W^{-1}.day^{-1}$ and 0.083-0.091 $g.W^{-1}.day^{-1}$ respectively. In terms of the feasibility of cultivating *Scenedesmus sp*. as an energy product, it was found that none of the photobioreactors at their respective operating conditions, were suitable as the net energy ratios (NERs) were below 1. In order to assess whether or not these photobioreactors would be feasible in the future, the NERs were calculated, assuming that 100% of the light energy requirement would be provided by solar energy. For this scenario, it was assumed that the biomass productivity would be halved due to daily fluctuations in light intensity and environmental conditions. At these conditions, it was found that the tubular, flat plate and airlift photobioreactors would achieve NERs of between 254 to 390, 7.3 to 13.4 and 0.64 to 1.35 respectively. The large NERs attained in the tubular reactors are attributed to the high degree of light exposure and the small working volumes. However, these tubular reactors would not be feasible for scale-up. The flat plate and airlift photobioreactors would be feasible, if solar light supply and penetration was improved in these photobioreactors.

7. Conclusions

Commercial microalgae production has been limited due to the lack of efficient photobioreactors and low biomass productivities. According to literature, one of the main factors limiting growth is the inefficiency of light delivery and its distribution in photobioreactors (Carvalho *et al.*, 2006; Posten, 2009; Chisti, 2008). In order to improve the overall biomass productivity that can be achieved, a thorough understanding of the algal response to light needs to be acquired. This study has investigated the effect of light supply, light intensity and photobioreactor design (column, tubular and flat plate) on the biomass productivity and energy efficiency of *Scenedesmus sp.* cultures. In particular, the effect of light source, light intensity and configuration (internal and external) as well as the related variation in light/dark cycling were investigated. The key objectives of this study were:

- To demonstrate that inefficient light supply is a major factor limiting algal growth
- To determine how *Chlorella vulgaris* and *Scenedesmus sp*. respond to similar changes in lighting conditions
- To design and evaluate the performance of an internally lit LED airlift reactor, in order to investigate the effect of variation of the incident surface area to culture volume ratio on biomass productivity.
- To determine the effect of different light sources (fluorescent and LEDs) on biomass productivity
- To assess the effect of light/dark cycling on *Scenedesmus sp*.
- To analyse the effect of reactor configuration (flat plate, airlift and tubular) on algal cultivation in terms of biomass productivity and energy utilization.

The hypotheses formulated for this study were:

- The internally illuminated airlift photobioreactors achieve a higher biomass productivity than a similarly externally illuminated airlift photobioreactor because of the higher degree of light provision by the larger incident surface area to volume ratio coupled with the reduced light path length.
- Higher biomass productivities are obtained when using LEDs as compared to fluorescent lighting, since LEDs are able to emit light at higher light intensities.

- Higher maximum specific growth rates and biomass productivities are obtained in the tubular photobioreactors at shorter light/dark cycling times coupled with higher incident surface area to volume ratios.
- The flat plate photobioreactor achieves a higher biomass productivity than the airlift photobioreactors because of the higher degree of light provision by the larger incident surface area to volume ratio coupled with the reduced light path length.

To meet the 1st and 2nd objectives, *Chlorella vulgaris* and *Scenedesmus sp.* were cultivated in 3.2 L externally fluorescent lit airlift photobioreactors at 24±1°C. When the light intensity was increased from 300 to 600 μmol.m^{-2}.s^{-1} after 2 days, *Scenedesmus sp.* was able to achieve and sustain a 22% higher linear growth rate of 0.0118 g.L^{-1}.h^{-1} than *Chlorella vulgaris,* which achieved 0.0097 g.L^{-1}.h^{-1}. Maximum biomass concentrations of 1.88 g.L^{-1} and 3.62 g.L^{-1} were obtained for *Chlorella vulgaris* and *Scenedesmus sp.* after 13 and 15 days of growth respectively. Furthermore, it was found that *Scenedesmus sp.* could withstand high light intensities at low cell densities without becoming photo inhibited. Based on these findings, *Scenedesmus sp.* was selected as algal species of choice for the remainder of the study.

In order to investigate the effect of internal illumination in the airlift reactor as well as to compare fluorescent and LED lighting (objectives 3 and 4), a standard vertical airlift photobioreactor (Langley, 2010) was modified to include an internal glass compartment for internal LED illumination. From the results obtained for investigating the effects of light intensity and configuration (internal, external or a combination thereof) on the growth of *Scenedesmus sp.* at 26±1°C, it was found at 300 μmol.m^{-2}.s^{-1}, the internally illuminated LED airlift photobioreactor achieved both a slightly lower maximum specific growth rate of 0.0248 h^{-1} and a biomass productivity of 0.0064 g.L^{-1}.h^{-1} than the externally lit fluorescent airlift reactor that achieved 0.0275 h^{-1} and 0.0070 g.L^{-1}.h^{-1} respectively. This is contradictory to the 1st hypothesis, as one would expect the reduced light path length and higher light intensities provided by LEDs to lead to better light penetration. An explanation for these results is that LEDs provide light in a ‗point-specific' manner i.e. the light intensity at the LED is high (1059 μmol.m^{-2}.s^{-1}), but drops off (35 μmol.m^{-2}.s^{-1}) between successive LEDs.

The combination of the internally lit LED photobioreactor with an external fluorescent bank at overall average light intensities of 460 and 600 μmol.m^{-2}.s^{-1} allowed maximum

specific growth rates and linear productivities to be achieved that were approximately 21-36% and 53-56% greater than the maximum and linear growth rates achieved in the standard externally lit fluorescent photobioreactor at 300 μmol.m^{-2}.s^{-1} respectively. Further, the combination of the internally LED illuminated airlift reactor with an external fluorescent light bank at an overall light intensity of 600 μmol.m^{-2}.s^{-1}, resulted in a maximum specific growth rate that was 18% greater than that achieved in the externally illuminated airlift photobioreactor at 600 μmol.m^{-2}.s^{-1}. The increase in the maximum specific and linear growth rates may be attributed to the reduced light path length provided by internal illumination coupled with an increase in light intensity. Both of these factors contributed to increasing the volume fraction of the photobioreactor that was exposed to light as well as the amount of light penetration that was achieved in the downcomer region. It was found that across the range of light intensities of 160-600 μmol.m^{-2}.s^{-1}, the linear productivity of *Scenedesmus sp.* was light limited. At a depth of 2 cm less than 100 μmol.m^{-2}.s^{-1} was available at biomass concentrations of 0.5 g.L^{-1} or greater.

The presence of internal lighting and higher external fluorescent lighting resulted in an increase in culture temperature and a fan was required to maintain the temperature at 26±1°C. The dependence of the maximum specific growth rate on temperature could be modelled by the Arrhenius equation. Similar activation energies of 39.7 and 38.7 kJ.mol^{-1} were required at external fluorescent average light intensities of 300 and 600 μmol.m^{-2}.s^{-1} respectively.

To meet the 5th objective centred on light/dark cycling, the effect of varying light intensity, light fraction (volume fraction of photobioreactor exposed to light) and cycle time on the maximum specific growth rate in 209 mL and 330 mL tubular photobioreactors was investigated. On increasing the light fraction from 0.4 to 1 (full light exposure) at 300 μmol.m^{-2}.s^{-1}, the incident surface area to culture volume ratio increased from 95.6 to 239 m^{-1} and from 86.4 to 216 m^{-1} in the 330 mL and 209 mL reactors respectively, consequently resulting in an increase in the maximum specific growth rate from 0.0323 h^{-1} to 0.0725 h^{-1} and from 0.0429 h^{-1} to 0.0834 h^{-1} at cycle times of 33 s (330 mL tubular reactor operated at 376 mL.min^{-1}) and 21 s (209 mL tubular reactor operated at 432 mL.min^{-1}) respectively. Furthermore, increasing the light intensity from 300 to 600 μmol.m^{-2}.s^{-1} at a constant light fraction also improved the amount of light exposure and penetration that was achieved. At a light fraction of 1, increasing the light

intensity from 300 to 600 μmol.m^{-2}.s^{-1} resulted in an increase in the maximum specific growth rate from 0.0725 h^{-1} to 0.097 h^{-1} and from 0.0834 h^{-1} to 0.1035 h^{-1} at cycle times of 33 s and 21 s respectively. Decreasing the cycle time from 33 s to 21 s also resulted in a 15% and 6.7% increase in the specific growth rate at 300 and 600 μmol.m^{-2}.s^{-1} respectively. These results are in agreement with the 3rd hypothesis and can be attributed to the shorter fraction of time (0.54) that algal cells spend under high light exposure in the downcomer (7 mm ID glass tubes) before returning to the light-limited riser (18 mm ID glass tube) to recover from the effects of photoinhibition. At a cycle time of 33 s, cells spent a longer fraction of time (0.6) in the downcomer before returning to the riser and hence had less time for cellular recovery. These results highlight the importance of improving the frequency of light/dark cycling to optimize light utilization and hence the maximum specific growth rate of *Scenedesmus sp*.

Based on these results, the efficiency of light/dark cycling in the airlift photobioreactors was assessed. In order to perform this analysis, it was assumed that the riser and the downcomer were the light and dark zones in the airlift photobioreactor. Based on previous experimental circulation time data, it was established that both photobioreactors experienced a light fraction of approximately 0.75. It was found that the different lighting regimes and the different hydrodynamics associated with each of the photobioreactors affected the maximum specific growth rates obtained. The tubular and airlift photobioreactors had downcomer light path lengths of 0.007 m and 0.025 m respectively. The higher degree of light exposure and penetration in the 330 mL and 209 mL tubular photobioreactors resulted in maximum specific growth rates that were approximately 0.59 to 1.5 times and 0.75 to 1.1 times greater than those achieved in the airlift photobioreactors at external fluorescent light intensities of 300 and 600 μmol.m^{-2}.s^{-1} respectively. It was observed that both the airlift and tubular photobioreactors transitioned from exponential to linear growth at biomass concentrations where the light intensity available in the downcomer regions was approximately 30-75 μmol.m^{-2}.s^{-1}, suggesting that light availability is one of the major factors affecting the growth of *Scenedesmus sp.*

In terms of hydrodynamics, the airlift and tubular photobioreactors had cycle times of 7 s and 21-33 s respectively. The greater degree of turbulence in the airlift photobioreactor improved the amount of mixing in the airlift reactor, resulting in an overall mass transfer coefficient of 0.0094 ± 0.00026 s^{-1}. Although it was determined by Fraser (2011) that the tubular photobioreactors were not mass transfer limited, no experimental data for the

overall mass transfer coefficient was recorded. Thus, the airlift and tubular photobioreactors could not be compared in terms of mixing and mass transfer.

In order to investigate the effects of reactor configuration on biomass productivity and energy efficiency (objective 6), the effects of light intensity and aeration rate on the growth of *Scenedesmus sp.* in the 1.6 L perspex flat plate photobioreactor was firstly investigated. It was found that increasing the external fluorescent light intensity (300 to 600 $\mu mol.m^{-2}.s^{-1}$) and the aeration rate (2.5, 3.5 and 5 $L.min^{-1}$) both had significant impacts on the growth of *Scenedesmus sp.* Increasing the aeration rate at a constant light intensity of 300 $\mu mol.m^{-2}.s^{-1}$ had a minimal effect on the growth rate up to approximately 125 hours. However, increasing the light intensity from 300 to 600 $\mu mol.m^{-2}.s^{-1}$ resulted in a 22 to 42% increase in the linear growth rates. At 2.5 $L.min^{-1}$ and 600 $\mu mol.m^{-2}.s^{-1}$, the system appeared both mass-transfer and light limited, whereas at 3.5 and 5 $L.min^{-1}$, it appeared light limited. The increase in light intensity and the provision of illumination on both sides of the flat plate photobioreactor increased the amount of light exposure and penetration that was achieved. It was found that the flat plate photobioreactor transitioned from exponential to linear growth at biomass concentrations where the light intensity available was approximately 25-50 $\mu mol.m^{-2}.s^{-1}$.

Later in the growth cycle (after 100-125 hours), a change in the linear slope was observed, suggesting that another factor became limiting. It was observed that at high biomass concentrations (1.26 and 2.43 $g.L^{-1}$), increasing the aeration rate allowed the linear slope to be maintained for longer so that the maximum biomass concentration was obtained more rapidly. These results suggest that at higher biomass concentrations, mass transfer may have become limiting, since increasing the aeration rate from 2.5 to 5 $L.min^{-1}$ improved the overall mass transfer coefficient of carbon dioxide from 0.0063 ± 0.00020^{-1} to $0.0101 \pm 0.00029\ s^{-1}$ in the flat plate photobioreactor. It is well recognised that the mass transfer rate required increases as a function of the biomass concentration and the specific growth rate where the yield coefficient of biomass on CO_2 is constant.

Furthermore, lower maximum specific (14-18%) and linear growth rates (12-21%) were obtained when an LED light bank was used as compared to a fluorescent light bank to provide illumination for the flat plate photobioreactor at 300 $\mu mol.m^{-2}.s^{-1}$. This result was attributed to the fact that LEDs provide light in a _point-specific' manner i.e. the light intensity is high at the site of diode but drops off between successive diodes (similar to

results observed in the internally LED illuminated airlift photobioreactor). Thus, it can be concluded that the growth of *Scenedesmus sp.* was more limited by light availability when the LED light bank was used to provide constant illumination, compared to the fluorescent light bank, which provided more even light distribution.

From the comparative performance evaluation of the different photobioreactors, it was found that the different light and mixing regimes in each of the photobioreactors affected the maximum specific, linear growth rates and biomass concentrations of *Scenedesmus sp*. The tubular photobioreactors achieved the highest maximum specific growth rates of 0.0725-0.1035 h^{-1}. The flat plate photobioreactor achieved maximum specific growth rates and biomass productivities of 0.0459-0.0642 h^{-1} and 0.0174-0.0276 $g.L^{-1}.h^{-1}$ respectively. The airlift reactors achieved maximum specific growth rates and biomass productivities of 0.0248-0.0443 h^{-1} and 0.0064-0.0114 $g.L^{-1}.h^{-1}$ respectively. These results were attributed to the highest degree of light exposure per unit culture volume experienced in the tubular photobioreactor (65-143 $mmol.m^{-3}.s^{-1}$), followed by the flat plate (14.2-28.4 $mmol.m^{-3}.s^{-1}$) and airlift photobioreactors (8.9-17.7 $mmol.m^{-3}.s^{-1}$) respectively. These results validate the 4th hypothesis. At similar overall mass transfer coefficients of 0.094-0.0101 s^{-1} in the flat plate and airlift photobioreactors, the volumes of gas sparged per unit culture volume per minute was approximately five times greater in the flat plate photobioreactor compared to the airlift photobioreactor. The greater degree of mixing in the flat plate photobioreactor resulted in a shorter mean circulation time, which may have improved the frequency of light/dark cycling consequently resulting in an increase in the maximum specific and linear growth rates of *Scenedesmus sp.*

In terms of energy efficiency, it was found that the flat plate photobioreactor achieved the highest biomass productivities per unit power input (including light and mixing energy inputs) of 0.088-0.140 $g.W^{-1}.day^{-1}$, followed by the tubular and airlift photobioreactors that achieved 0.041-0.095 $g.W^{-1}.day^{-1}$ and 0.060-0.064 $g.W^{-1}.day^{-1}$ respectively. For all of the photobioreactors, the light energy input accounted for over 93.4% of the total energy requirement. In terms of mixing energy inputs, the tubular photobioreactors had the lowest mixing energy inputs (0.86-1.38 $W.m^{-3}$) due to the low aeration rates and small working volumes. The flat plate reactor achieved higher biomass productivities at lower mixing energy inputs (29.36-58.73 $W.m^{-3}$) compared to the airlift reactors (51.40-70.57 $W.m^{-3}$) because of the difference between the ratios of the areas of the riser and

downcomers which were 1 and 0.3-0.5 in the flat plate and airlift (externally and internally illuminated) reactors respectively.

It was calculated that if 30% (assumption based on light losses that would occur from daily weather fluctuations and losses that would occur during transportation through optic fibres) of the light energy requirement was supplied by solar energy, the biomass productivity per unit power input in the flat plate, tubular and vertical airlift photobioreactors would increase to 0.125-0.198 $g.W^{-1}.day^{-1}$, 0.058-0.135 $g.W^{-1}.day^{-1}$ and 0.083-0.091 $g.W^{-1}.day^{-1}$ respectively. In terms of the feasibility of cultivating *Scenedesmus sp*. as an energy product, it was found each of the photobioreactors at their respective operating conditions, achieved net energy ratios well below 1.

In order to assess whether or not these photobioreactors would be feasible in the future, a scenario was considered where the full light energy requirement would be supplied by solar energy. As a basis of calculation, it was assumed that only half the biomass productivity would be achieved in each of the photobioreactors due to diurnal cycling and fluctuations in environmental conditions. It was calculated that at these conditions, the tubular, flat plate and airlift photobioreactors would achieve NERs of between 254 to 390, 7.3 to 13.4 and 0.64 to 1.35 respectively. The large NERs attained in the tubular reactors are attributed to the high degree of light exposure and the small working volumes. However, these tubular reactors would not be feasible for scale-up. The flat plate and airlift photobioreactors would be feasible options to consider, if solar light supply and penetration was improved in these photobioreactors.

Thus, it is evident that in order to improve the energy efficiency of *Scenedesmus sp.* cultures, the amount of solar energy that can be captured (in South Africa the average irradiation received per day is 1130-1341 $\mu mol.m^{-2}.s^{-1}$) as well as the efficiency of the light supply and distribution in photobioreactors need to be improved, whilst ensuring that sufficient mixing is provided to ensure adequate mixing and mass transfer. The provision of internal illumination has been shown to be a viable option for improving light distribution photobioreactors.

Recommendations to be made for this study include carrying out outdoor runs in order to assess the combined effects of fluctuations in light intensity, diurnal cycling and temperature on the growth and biomass productivity of *Scenedesmus sp.* In particular, it is important to consider the arrangement of the reactors to prevent shading. Characterisation

of the effect of temperature on linear growth rate should be further investigated. For the flat plate photobioreactor, understanding the temperature control and its effect out of doors is also important to consider as the thin layer of liquid makes it much more difficult to control. In the airlift photobioreactors, the effects of aeration rate on the biomass productivity and energy efficiency of *Scenedesmus sp.* needs to be further investigated. Additionally, the effects of photobioreactor design and light intensity on the lipid productivity of *Scenedesmus sp.* should be investigated. Lastly, more detailed studies of the fluid dynamics and flow patterns present in the different photobioreactors need to be carried out in order better understand and assess the efficiency of light/dark cycling in different photobioreactor configurations.

References

Akita, K. and Yoshida, F. (1973). Gas holdup and volumetric mass transfer coefficient in bubble columns. Effects of liquid properties. *Industrial and Engineering Chemistry Process Design and Dev*elopment, **12** (1), 76-80.

Amin, S. (2009). Review on biofuel oil and gas production processes from microalgae. *Energy Conversion and Management,* **50** (7), 1834-1840.

Andersen, R.A. (ed.). (2005). *Algal Culturing Techniques.* Elsevier Academic Press, San Diego, CA.

Bailey, J.E. and Ollis, D.F. (1986). *Biochemical engineering fundamentals*. McGraw-Hill Education, Chicago.

Barsanti, L. and Gualtieri, P. (2006). *Algae: Anatomy, Biochemisty and Biotechnology*, Florida: CRC Press, Taylor and Francis Group.

Bass, M., DeCusatis, C., Enoch, J., Lakshminarayanan, V., Li, G., Macdonald, C., Mahajan, V. and Van Stryland, E. (2009). *Handbook of Optics, Third Edition Volume IV: Optical Properties of Materials, Nonlinear Optics, Quantum Optics (set)*. McGraw Hill Professional , New York.

Benemann, J.R. (2009). Microalgae biofuels: a brief introduction. Available at: www.adelaide.edu.au/biogas/renewable/biofuels_introduction.pdf [Accessed on 4 February 2013].

Bouaifi, M., Hebrard, G., Bastoul, D. and Roustan, M. (2001). A comparative study of gas hold-up, bubble size, interfacial area and mass transfer coefficients in stirred gas-liquid reactors and bubble columns. *Chemical Engineering and Processing*, **40** (2), 97-111.

Borowitzka, M.A. (1999). Commercial production of microalgae: ponds, tanks, tubes and fermenters. *Journal of Biotechnology*, **70**, 313-321.

Bruhn, A., Dahl, J., Nielsen, H.B., Nikolaisen, L., Rasmussen, M.B., Markager, S., Olesen, B., Arias, C. and Jensen, P.D. (2011). Bioenergy potential of Ulva lactuca: Biomass yield, methane production and combustion. *Bioresource Technology*, **102**, 164-172.

Burgess, G. and Fernandez-Velasco, J.G. (2007). Materials, operational energy inputs, and net energy ratio for photobiological hydrogen production. *International Journal of Hydrogen Energy*, **32** (9), 1225-1234.

Calderbank, P.H. and Moo-Young, M.B. (1961). The continuous phase heat and mass transfer properties of dispersions. *Chemical Engineering Science*, **16** (1),39-54.

Carvalho, A.P., Meireles, L.A. and Malcata, F.X. (2006). Microalgal reactors: a review of enclosed system designs and performances. *Biotechnology Progress*, **22**, 1490-1506.

Chisti, Y. (2002). *Mass Transfer. In: Kirk-Othmer Encyclopaedia of Chemical Technology, 5th Edition Volume 15*. (pp. 670-740): John Wiley & Sons, New York.

Chisti, Y. (2007). Biodiesel from microalgae. *Biotechnology Advances*, **25** (3), 294-306.

Chisti, Y. (1989). *Airlift photobioreactors*. Elsevier Applied Science, London.

Chisti, Y. (1998). Pneumatically agitated bioreactors in industrial and environmental bioprocessing: hydrodynamics, hydraulics and transport phenomena. Special issue: fluid mechanics problems in biotechnology. *Applied Mechanics Review*, **51**, 33-112.

Chisti, M.Y. and Moo-Young, M. (1988). Gas holdup in pneumatic reactors. *The Chemical Engineering Journal*, **38**, 149-152.

Contreras, A., Garcia, F., Molina, E. and Merchuk, J. C. (1998). Interaction between CO_2-mass transfer, light availability, and hydrodynamic stress in the growth of *Phaeodactylum tricornutum* in a concentric tube airlift photobioreactor. *Biotechnology and Bioengineering*, **60**, 317-325.

Converti, A., Lodi, A., Del Borghi, A and Solisi, C. (2006). Cultivation of *Spirulina platensis* in a combined airlift-tubular system, *Biochemical Engineering Journal,* **32**, 13-18.

Converti, A., Casazza, A.A., Ortiz, E.Y., Perego, P. and Del Borghi, M. (2009). Effect of temperature and nitrogen concentration on the growth and lipid content of *Nannochloropsis oculata* and *Chlorella vulgaris* for biodiesel production. *Chemical Engineering and Processing*, **48**, 1146-1151.

Chiu, S., Tsai, M., Kao, C., Ong, S. and Lin, C. (2009). The air-lift photobioreactors with flow patterning for high-density cultures of microalgae and carbon dioxide removal. *Engineering in Life Sciences Journal*, **3** (9), 254-260.

Daya, T. (2011). *The utilization of carbon dioxide by the microalgal species Scenedesmus.* Master's dissertation. University of Cape Town

Degen, J., Uebele, A., Retze, A., Schmid-Staiger, U., Trosch, W. (2001). A novel airlift photobioreactor with baffles for improved light utilization through the flashing light effect. *Journal of Biotechnology,* **92**, pp. 89-94.

de Morais, M.G. and Costa, J.A.V. (2007). Isolation and selection of microalgae from coal fired thermoelectric power plant for biofixation of carbon dioxide. *Energy Conversion and Management*, **48**(7),2169-2173.

Eriksen, N.T. (2008). The technology of microalgal culturing. *Biotechnology Letters*, **30**, 1525-1536.

Fraser, M. (2011). *Modelling airlift photobioreactors for algal bioenergy, using Scenedesmus sp. as the model species*. Master's dissertation. University of Cape Town

Franco, M.C. (2011). *Cultivation of microalgae in a high irradiance area*. Doctoral thesis. Wageningen University

Geider, R.J. and Osbourne, B.A. 1992. *Algal photosynthesis: The measurement of algal gas exchange*. Chapman and Hall, New York.

Gordon, J. M. (2002). Tailoring optical systems to optimized photobioreactors. *International Journal of Hydrogen Energy,* **27**,1175-1184.

Griffiths, M.J. (2011). *Optimising Microalgal Lipid Productivity For Biodiesel Production.* Doctoral thesis. University of Cape Town

Griffiths, M. J., Garcin, C., van Hille, R. P., and Harrison, S. T.L. (2011a). Interference by pigment in the estimation of microalgal biomass concentration by optical density. *Journal of microbiological methods*, **85(**2), 119-123.

Griffiths, M.J., van Hille R.P. and Harrison S.T.L. (2011). Lipid productivity, settling potential and fatty acid profile of 11 microalgal species grown under nitrogen replete and limited conditions. *Journal of Applied Phycology,* **24** (5), 989-1001.

Griffiths, M.J. and Harrison, S.T.L. (2009). Lipid productivity as a key characteristic for choosing algal species for biodiesel production. *Journal of Applied Phycology*, **21**, 493-507.

Grobbelaar, J. U. (2000). Physiological and technological considerations for optimising mass algal cultures. *Journal of Applied Phycology,* **12**, 201-206.

Hall, D.O., Scurlock, J.M.O., Bolhar-Nordenkampf, H.R., Leegood, R.C. and Long, S.P. (ed.). (1993). *Photosynthesis and Production in a Changing Environment*. Chapman and Hall, London, pp. 425-444.

Harrison, S. T. L.; Griffiths, M. J.; Langley, N.; Vengadajellum, C.; Hille, R. P. Van. (2010). Microalgal culture as a feedstock for bioenergy, chemicals, and nutrition, *Manual of Industrial Microbiology and Biotechnology,* **1**, 577-590.

Higbie, R. (1935).The rate of absortion of a pure gas into a still liquid during short periods of exposure. *Transactions of the American Institute of Chemical Engineers*, **31**, 365-389.

Hills, J.H. (1976). The operation of a bubble column at high throughputs: I. Gas holdup measurements. *Chemical Engineering Journal*, **12**, 89-99.

Hu, Q., Kurano, N., Kawachi, M., Iwasaki, I. and Miyachi, A. (1998). Ultrahigh-cell density culture of a marine alga *Chlorococcum littorale* in a flat-plate photobioreactor. *Applied Microbiology and Biotechnology,* **49** (6), 655-662.

Hulatt, C.J. and Thomas, D.N. (2011). Productivity, carbon dioxide uptake and net energy return of microalgal bubble column photobioreactors. *Bioresource Technology*, **102**, 5775-5787.

Illman, A., Scragg, A.H. and Shales, S.W. (2000). Increase in *Chlorella* strains calorific values when grown in low nitrogen medium. *Enzyme and Microbial Technology*, **27**(8): 631-635.

Javanmardian, M. and Palsson, B.O. (1991). High-density photoautotrophic algal cultures: design, construction and operation of a novel photobioreactor system, *Biotechnology and Bioengineering*, **38** (1), 1182-1189.

Janssen, M., de Bresser, L., Baijens, T., Tramper, J., Mur, L.R., Snel, J.F.H. and Wijffels, R.H. (2000). Scale-up aspects of photobioreactors: effects of mixing-induced light/dark cycles, *Journal of Applied Phycology*, **12** (1), 225-237.

Janssen, M., Tramper, J., Mur, L. and Wijffels, R. (2003). Enclosed outdoor photobioreactors: light regime, photosynthetic efficiency, scale-up, and future prospects. *Biotechnology and Bioengineering*, **81** (2), 193-210.

Kaewpintong, K., Shotipruk, A., Powtongsook, S. and Pavasant, P. (2007). Photoautotrophic high-density cultivation of vegetative cells of Haematococcus pluvialis in airlift photobioreactor. *Bioresource Technology,* **98**, 288-295.

Kasarova, S.N., Sultanova, N.G., Ivanov, C.D and Nikolov, I.D. (2007). Analysis of the dispersion of optical plastic materials. *Optical Materials*, **29** (11),1481-1490.

Kelkar, B.G., Phulgaonkar, S.R and Shah, Y.T. (1983). The effect of electrolyte solutions on hydrodynamics and backmixing characteristics in bubble columns. *Chemical Engineering Journal*, **27** (3), 125-133.

Kirk, J.T.O. (1994). *Light and photosynthesis in aquatic ecosystems. 2nd edition*, Cambridge University Press.

Kunjapur, A.M. and Eldridge, R.B. (2010). Photobioreactor design for commercial biofuel production from microalgae. *Industrial and Engineering Chemistry Research,* **49**, 3516-3526.

Langley, N.M., Harrison, S.T.L. and van Hille, R.P. (2012). A critical evaluation of CO_2 supplementation to algal systems by direct injection. *Biochemical Engineering Journal*, **68**(1), 70-75.

Langley, N. (2010). *Strategies for carbon dioxide delivery to microalgal cultures and their potential for the reduction of emissions*. Master's dissertation. University of Cape Town.

Lee, C. G. and Palsson, B. O. (1994). High-density algal photobioreactors using light-emitting-diodes, *Biotechnology and Bioengineering*, **44**, 1161–1167.

Lehr, F. and Posten, C. (2009). Closed photo-bioreactors as tools for biofuel production. *Current Opinion in Biotechnology,* **20** (3), 280-285.

Malitson, I.H. (1965). Interspecimen comparison of the refractive index of fused silica. *Journal of the Optical Society of America*, **55** (10), 1205-1208.

Mata, T.M., Martins, A.A. and Caetano, N.S. (2010). Microalgae for biodiesel production and other applications: A review. *Renewable and Sustainable Energy Reviews,* **14**, 217-212.

McGinn P.J., Dickinson, K.E., Park, K.C., Whitney, C.G., MacQuarrie, S.P., Black, F.J., Frigon, J., Guiot, S.R. and O'Leary, S.J.B. (2012). Assessment of the bioenergy and bioremediation potentials of the microalga *Scenedesmus* sp. AMDD cultivated in municipal wastewater effluent in batch and continous mode. *Algal Research,* **1**(2), 155-165.

McNaught, A.D. and Wilkinson, A. (1997). *IUPAC. Compendium of Chemical Terminology. 2nd edition* . Blackwell Scientific Publications, Oxford.

Merchuk, J.C., Gluz, M. and Mukmenev, I. (2000). Comparison of photobioreactors for cultivation of the red microalga *Porphyridium sp. Journal of Chemical Technology and Biotechnology*, **75**, 1119-1126.

Miron, A.S., Garcia, M.C., Camacho, F.G., Grima, E. M. and Chisti, Y. (2002). Growth and biochemical characterization of microalgal biomass produced in bubble column and airlift photobioreactors: studies in fed-batch culture. *Enzyme and Microbial Technology*, **31**, 1015-1023.

Molina, E.G., Fernandez, A.F.G., Garcia, F.C. and Chisti, Y. (1999). Photobioreactors: light regime, mass transfer, and scaleup, *Journal of Biotechnology*, **70** (1), 231-247.

Molina, E.G., Fernandez, J., Acien, F.G., and Chisti Y. (2001). Tubular photobioreactor design for algal cultures, *Journal of Biotechnology*, **92**, 113-131.

Molina, E.G., Sanchez Perez, J.A., Garcia Camacho, F., Fernandez, S. and Acien, F.G. (1997). Productivity analysis of outdoor chemostat culture in tubular air-lift photobioreactors. *Journal of Applied Phycology*, **8**, 369-380.

Ogbonna, J.C., Yada, H. And Tanaka, H. (1995). Light supply coefficient: a new engineering parameter for photobioreactor design. *Journal of Fermentation and Bioengineering,* **80** (4), 369-376.

Ogbonna, J. C., Soejima, T., Tanaka, H. (1999). An integrated solar and artificial light system for internal illumination of photobioreactors. *Journal of Biotechnology,* **70**, 289-297.

Ogbonna, J. C., Tanaka, H. (2000). Light requirement and photosynthetic cell cultivation-development of processes for efficient light utilization in photobioreactors*, Journal of Applied Phycology*, **12**, 207–218.

Perry, R.H. and Green, D.W. (2007) *Perry's Chemical Engineer's Handbook*. 7th ed., New York: McGraw Hill.

Pegallapati, A.K. and Nimalakhandan N. (2011). Energetic evaluation of an internally illuminated photobioreactor for algal cultivation, *Biotechnology Letters*, **33**, 2161-2167.

Photosynthesis (2010) *Photosynthesis* [Online] Available at: http://www.uic.edu/classes/bios/bios100/lecturesf04am/lect10.htm [accessed: 13th April 2011]

Posten, C. (2009). Design principles of photo-bioreactors for cultivation of microalgae, *Engineering Life Science*, **9**, 165–177.

Pulz, O. and Scheibenbogen, K. (1998). Photobioreactors: design and performance with respect to light energy input. *Advances in Biochemical Engineering/Biotechnology,* **59**, 123-152.

Pulz, O. (2001). Photobioreactors: production systems for phototrophic microorganisms, *Applied Microbiology and Biotechnology,* **57**, 287-293.

Ratchford, I.A.J. and Fallowfield, H.J. (1992). Performance of a flat plate, air-lift reactor for the growth of high biomass algal cultures, *Journal of Applied Phycology,* **4**, 1-9.

Reyna-Velarde, R., Christiani-Urbina, E., Hernandez-Melchor, D.J., Thalassoa, F and Canizares-Villanuevaa, R.O. (2010). Hydrodynamic and mass transfer characterization of a flat-panel airlift photobioreactor with high light path, *Chemical Engineering and Processing,* **49**, 97-103.

Richardson, C. (2011). *Investigating the role of reactor design to maximize the environmental benefit of algal oil for biodiesel*. Master's dissertation. University of Cape Town.

Richmond, A. (2004). Principles for attaining maximal microalgal productivity in photobioreactors: an overview, *Hydrobiologia,* **512**, 33-37.

Ryu, H.J., Oh, K.K. and Kim, Y.S. (2009). Optimization of the influential factors for the improvement of CO_2 utilization efficiency and CO_2 mass transfer rate, *Journal of Industrial and Engineering Chemistry,* **15**, 471-475.

Sanchez, J.F., Fernandez-Sevilla, J.M., Acien, F.G., Ceron, M.C., Perez-Parra, J and Molina-Grima, E. (2008). Biomass and lutein productivity of *Scenedesmus almeriensis*: influence of irradiance, dilution rate and temperature, *Applied Microbiology and Biotechnology*, **79**, 719-729.

Schamphelaire, L. De. And Verstraete, W. (2009). Revival of the Biological Sunlight-to-Biogas Energy Conversion System. *Biotechnology and Bioengineering*, **103** (2), 296-304.

Shah, Y.T., Kelkar, B.G., Godbole, S.P. and Deckwer, W.D. (1982). Design parameters estimations for bubble column reactors. *AIChE Journal*, **28** (3),353-379.

Sheehan, J., Dunahay, T., Benemann, J.R. & Roessler, P. (1998). *A look back at the US Department of Energy's Aquatic Species Program: Biodiesel from algae*, Close-Out report. National Renewable Energy Lab, Department of Energy, Golden, Colorado, U.S.A. Report number NREL/TP-580-24190, dated July 1998.

Sierra, E., Acien, F.G., Fernandez, J.M., Garcia, J.L., Gonzalez, C. and Molina, E. (2008). Characterization of a flat plate photobioreactor for the production of microalgae. *Chemical Engineering Journal*, **138**(1), 136-147.

Torzillo, G., Carlozzi, P., Pushparaj, B., Montaini, E. and Materass, R. (1993). A two-plane tubular photobioreactor for outdoor culture of Spirulina. *Biotechnology and bioengineering,* **42**(7),891-898.

Tamburic, B., Fessehaye, W., Zemichael, Crudge, P and Maitland, G.C. (2011). Design of a novel flat-plate photobioreactor system for green algal hydrogen production. *International Journal of Hydrogen Energy*, **36**(11), 6578-6591.

Tribe, L.A., Briens, C.L. and Margaritis, A. (1995). Determination of the Volumetric Mass Transfer Coefficient (k_La) Using the Dynamic –Gas Out-Gas In" Method: Analysis of Errors Caused by Dissolved Oxygen Probes. *Biotechnology and Bioengineering*, **46** (4), 388-392.

Ugwu, C. U., Aoyagi, H., Uchiyama, H. (2008). Photobioreactors for mass cultivation of algae. *Bioresource Technology*, **99** (10), 4021-4028.

Usui, N. and Ikenouchi, M. (1997). The biological CO2 fixation and utilization project by RITE(1) — Highly-effective photobioreactor system, *Energy Conversion and Management,* **38**, 487- 492.

Wang, C., Yingying, S., Xing, R. and Liqin, S. (2005). Effect of liquid circulation velocity and cell density on the growth of *Parietochloris incise* in flat plate photobioreactors. *Biotechnology and Bioprocess Engineering*, **10**, 103-108.

Watanabe, Y. and Saiki, H. (1997). Development of a photobioreactor incorporating *Chlorella sp.* for the removal of CO_2 in stack gas. *Energy Conversion and Management,* **38**, 499-503.

Wilkinson, P.M., Spek, A.P and van Dierendonck, L.L. (1992). Design parameters estimation for scale-up of high-pressure bubble columns. *AIChE Journal*, **38** (4), 544-554.

Williams, P.J., Thomas, D.N., Reynolds, C.S. (Editors).(2002). *Phytoplankton Productivity*. Blackwell Science.

Wu, X. and Merchuk, J.C.(2004). Simulation of algae growth in a bench scale internal loop airlift reactor, *Chemical Engineering Science*, **59**, 2899-2912.

Xin, L., Hong-ying, H. and Yu-ping, Z. (2011). Growth and lipid accumulation properties of a freshwater microalga *Scenedesmus sp.* under different cultivation temperature. *Bioresource Technology*, **102**, 3098-3102.

Zhang, X., Zhou, B., Zhang, Y., Cai, Z., Cong, W. and Ouyang, F. (2002). A simple and low-cost airlift photobioreactor for microalgal mass culture. *Biotechnology Letters,* **24**, 1767-1771.

Appendices

Appendix A: Sample Calculations

Appendix A-1:Sample calculation for estimating the hydrodynamic regime of the flat plate photobioreactor

The following set of sample calculations show the estimation of the hydrodynamic regime in the flat plate photobioreactor at an aeration rate of 2 L.min^{-1} (3.33 x 10^{-5} m^3.s^{-1}). A detailed explanation for all of the equations used are provided in Sections 4.2.2.1. Table A.1 provides a summary of the reactor dimension specifications.

Table A. 1: Selection of flat plate photobioreactor dimensions

Length (m)	0.240
Height (m)	0.250
Width (m)	0.029
ID of sparger (m)	0.0064
ID of sparger holes (m)	0.001
Spacing between holes (m)	0.01
Length of sparger (m)	0.240

The following set of sample calculations show the estimation of the mean circulation time, overall gas hold up and sparged liquid height in the flat plate photobioreactor.

1. Working volume

In order to estimate a working volume, it was assumed that the algal culture would occupy 80% of the reactor.

$$V_L = 0.80 * (0.240 \times 0.250 \times 0.029) = 0.0016\, m^3$$

2. Superficial gas velocity

$$U_G = \frac{V_G}{A}$$

$$U_G = \frac{3.33 \times 10^{-5}}{(0.240 \times 0.029)} = 0.0048\, m/s$$

3. Superficial liquid velocity

$$U_L = \frac{-0.42vvm^4 + 1.49vvm^3 - 1.20vvm^2 + 0.90vvm + 0.14}{8}$$

$$U_L = \frac{-0.42(1.277)^4 + 1.49(1.277)^3 - 1.20(1.277)^2 + 0.90(1.277) + 0.14}{8} = 0.1648\, m/s$$

4. Estimation of mean circulation time

Assuming that the liquid follows a circular path due to the physics of the system (Tamburic *et al.*, 2011):

$$t_c = \frac{x}{U_L}$$

$$t_c = \frac{2\pi(0.1175)}{0.1648} = 4.48s$$

5. Estimation of overall gas hold up

$$\varepsilon = \frac{U_G}{0.24 + 1.35(U_G + U_L)^{0.93}}$$

$$\varepsilon = \frac{0.0048}{0.24 + 1.35(0.0048 + 0.1648)^{0.93}} = 0.0096$$

6. Estimation of sparged liquid height

$$h_D = \frac{h_L}{(1-\varepsilon)}$$

$$h_D = \frac{0.225}{(1-0.0096)} = 0.227m$$

Appendix A-2: Sample calculation for estimating the overall mass transfer coefficient of the flat plate photobioreactor

The following set of sample calculations illustrate the steps taken to calculate the overall mass transfer coefficient for the flat plate photobioreactor (Section 4.2.2.2). Based on preliminary testing and photographic evidence, it was found that the sparger produced bubbles with a mean diameter (d_b) of 3 mm (Figure 4.8). As a basis of calculation, it was assumed that the bubbles produced were spherical.

1. Estimation of the total gas volume

$$\varepsilon = \frac{V_G}{V_G + V_L}$$

$$\therefore V_G = \frac{\varepsilon \times V_L}{(1-\varepsilon)} = \frac{0.0096 \times 0.0016}{(1-0.0096)} = 1.517 \times 10^{-5} m^3$$

2. Estimation of bubble volume (V_b), area of a bubble (A_b) and the total gas-liquid interfacial area ($A_{i,\,total}$)

$$V_b = \left(\frac{4\pi}{3}\right) \times \frac{d_b^{\,3}}{8} = \left(\frac{4\pi}{3}\right) \times \frac{0.003^3}{8} = 1.414 \times 10^{-8} m^3$$

$$A_b = 4\pi \times \frac{d_b^{\,2}}{4} = 2.827 \times 10^{-5} m^2$$

$$N_b = \frac{V_G}{V_b} = \frac{1.517 \times 10^{-5}}{1.414 \times 10^{-8}} = 1073$$

$$A_{itotal} = N_b A_b$$

$$A_{itotal} = 1073 \times (2.827 \times 10^{-5}) = 0.0303 m^2$$

3. Estimation of the overall mass transfer coefficient

$$Gr = \frac{d_b^{\,3} \rho_{H_2O} g \Delta\rho}{\mu_{H_2O}^{\,2}} = \frac{(0.003^3 \times 1000 \times 9.81 \times 998.8)}{0.001^2} = 264552$$

$$Sc = \frac{\mu_{H_2O}}{\rho_{H_20} D_{CO_2.H_2O}} = \frac{0.001}{(1000 \times (1.77 \times 10^{-9}))} = 565$$

$$\frac{k_L a d_b}{D_{CO_2.H_2O}} = 0.31 Gr^{\frac{1}{3}} Sc^{\frac{1}{3}} \frac{A_{i,total}}{V_L}$$

$$\therefore k_L a = 0.31(264552^{\frac{1}{3}})(565^{\frac{1}{3}})\left(\frac{0.0303}{0.0016}\right)\left(\frac{1.77 \times 10^{-9}}{0.003}\right) = 0.00188 s^{-1}$$

Appendix A-3: Sample calculation for estimating the energetic performance of a standard airlift photobioreactor

The following set of sample calculations present the steps taken to evaluate the energetic performance of a standard airlift photobioreactor at 300 μmol.m^{-2}.s^{-1} using the equations provided in Section 2.3.

1. Calculation of energy input for illumination

$$E_L = \frac{0.22 I_O A}{V}$$

$$E_L = \frac{0.22 \times 300 \times 0.094}{0.0032}$$

$$E_L = 1944 W.m^{-3}$$

2. Calculation of mixing energy input for airlift photobioreactor

$$E_{M,A} = \left| \frac{\gamma U_g}{1 + \frac{A_d}{A_r}} \right|$$

$$E_{M,A} = \left\lfloor \frac{(9810 \times 0.0209)}{1 + \left(\frac{0.00477}{0.00159} \right)} \right\rfloor$$

$$E_{M,A} = 51.40 W.m^{-3}$$

3. Calculation of biomass productivity per unit power input

For the case where the total power input includes both the light and mixing energy inputs, the biomass productivity per unit power input is calculated as follows:

$$P / E = \frac{P}{E_L + E_M}$$

$$P / E = \frac{0.12 \times 1000}{1944 + 51.40}$$

$$P / E = 0.060 \text{ g.W}^{-1}.\text{day}^{-1}$$

For the case where the light energy requirement would be provided from solar irradiation, it was assumed that biomass productivity would be halved. Thus, the biomass productivity per unit mechanical power input would be calculated as follows:

$$P / E_M = \frac{P}{E_M}$$

$$P / E_M = \frac{0.12 \times 1000}{51.40 \times 2}$$

$$P / E_M = 1.169 \text{ g.W}^{-1}.\text{day}^{-1}$$

4. Calculation of Net energy ratio

For the case where the total power input includes both the light and mixing energy inputs, the net energy is calculated as follows:

$$NER = \frac{\textit{Energy out}}{\textit{Energy in}} = \frac{\textit{Energy accumulated in biomass}}{\textit{Energy input}}$$

$$NER = \frac{\left[\left(\frac{1.74}{1000}\right) \times 23 \times 0.0032 \times 1000\right]}{\left[\frac{(1995 \times 0.0032 \times 13.9 \times 24 \times 60 \times 60)}{1 \times 10^6}\right]}$$

$$NER = 0.0167$$

For the case where the light energy requirement would be provided from solar irradiation, the net energy ratio would be calculated as follows:

$$NER = \frac{\left[\left(\frac{1.74}{1000}\right) \times 23 \times 0.0032 \times 1000\right]}{\left[\frac{(51.40 \times 0.0032 \times 13.9 \times 24 \times 60 \times 60)}{1 \times 10^6}\right]}$$

$$NER = 0.648$$

Appendix B: Light intensity data for calculating average light intensities of fluorescent and LED light sources

Appendix B-1: Light intensity data for the flat plate and tubular photobioreactors

The experimental data presented in Table B.1 was used to calculate the average light intensity of the fluorescent light bank which was used to provide illumination for the tubular and flat plate photobioreactors described in Sections 3.1.3.3 and 4.2.3 respectively. The light intensity data for the fluorescent light bank was recorded at each of the grid points illustrated by Figure 3.3.

Table B. 1: Light intensity data measured for a single fluorescent light bank

Grid point	I_o (µmol.m^{-2}.s^{-1})	Grid point	I_o (µmol.m^{-2}.s^{-1})	Grid point	I_o (µmol.m^{-2}.s^{-1})
1	263.8	24	307.9	47	328.2
2	311.4	25	301.8	48	332.5
3	318.4	26	298.6	49	337.2
4	333.5	27	299.8	50	318.3
5	285.4	28	324.6	51	295.7
6	287.5	29	314.5	52	310.3
7	295.6	30	326.8	53	317.6
8	306.8	31	324.3	54	322.4
9	313.7	32	318.1	55	329.7
10	285.7	33	293.4	56	323.8
11	316.4	34	289.5	57	333.2
12	325.4	35	315.6	58	317.5
13	322.7	36	323.8	59	323.5
14	316.3	37	318.4	60	258.5
15	282.5	38	329.8	61	278.4
16	298.6	39	324.3	62	298.5
17	283.6	40	325.1	63	287.6
18	294.8	41	323.2	64	305.8
19	316.8	42	298.5	65	313.2
20	318.4	43	310.5	66	311.9
21	335.8	44	313.8	67	304.6
22	326.4	45	318.9	68	301.7
23	306.4	46	325.6		
Average light intensity (µmol.m^{-2}.s^{-1})				**307.74**	

The light intensity data used to calculate the average light intensity of the LED light bank which was used to illuminate the flat plate photobioreactor is provided in Table B.2. The light intensity data was recorded at each of the grid points illustrated by Figure B.1.

Table B. 2: Light intensity data measured for the LED light bank

Grid point	I_o ($\mu mol.m^{-2}.s^{-1}$)	Grid point	I_o ($\mu mol.m^{-2}.s^{-1}$)	Grid point	I_o ($\mu mol.m^{-2}.s^{-1}$)
1	394	18	165.6	35	385.5
2	394.9	19	169.8	36	185.4
3	385	20	183.4	37	174.7
4	382.6	21	167.5	38	168.3
5	394.4	22	385.5	39	179.1
6	383.3	23	375.6	40	181.8
7	386.4	24	388.6	41	188.7
8	163.8	25	384.9	42	176.9
9	185.4	26	378.3	43	383.9
10	175.6	27	387.3	44	397.7
11	176.6	28	373.3	45	385.3
12	169.3	29	379.8	46	390.5
13	163.7	30	386.7	47	389.8
14	164.2	31	374.1	48	388.3
15	164.8	32	384.3	49	377.4
16	181.4	33	383.7		
17	169.7	34	388.1		
Average light intensity ($\mu mol.m^{-2}.s^{-1}$)					**295**

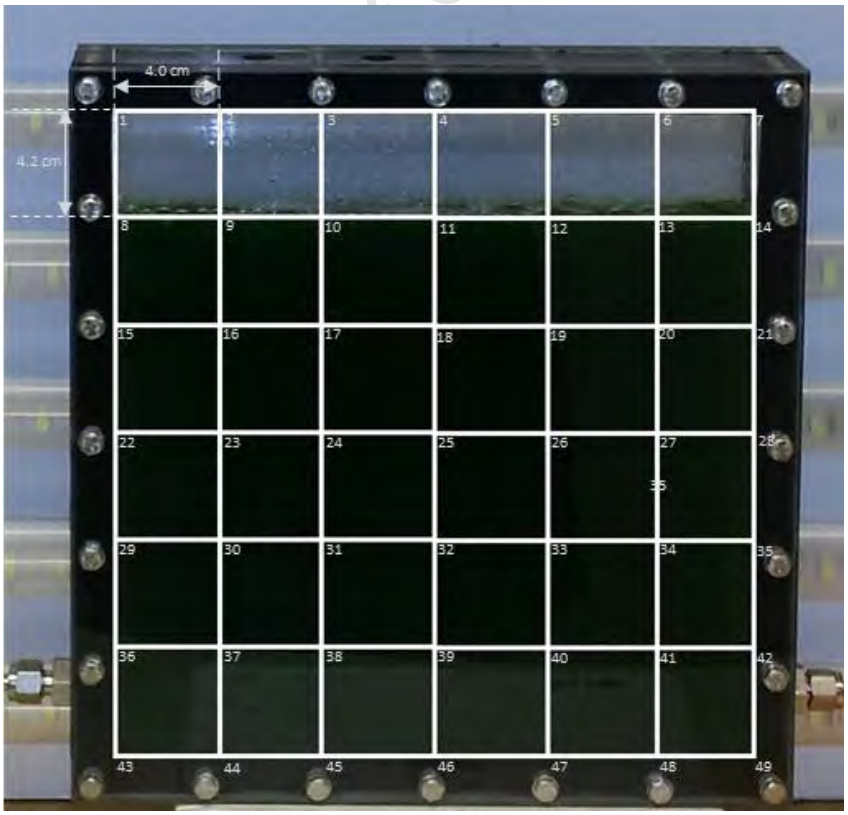

Figure B. 1: Diagram of grid points used to measure the average light intensity of the LED light bank for the flat plate photobioreactor

Appendix B-2: Light intensity data for the internally illuminated LED vertical airlift photobioreactor

Light intensity data were recorded at the front, back, left and right sides of the LED airlift photobioreactor according to the grid points illustrated in Figure B.2. The experimental data used to calculate the average light intensity when 1 and 1.8 m of cool white LED light tape were used in the modified vertical airlift photobioreactor are presented in Table B.3 and Table B.4 respectively.

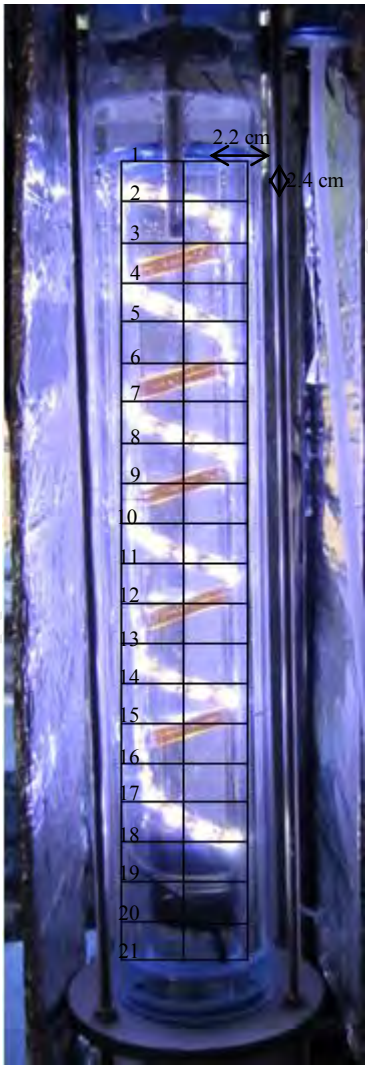

Figure B. 2: Diagram of grid points used to measure the average light intensity of the LED light tape in the internally illuminated vertical airlift photobioreactor

Table B. 3: Light intensity data measured for the modified internally lit airlift photobioreactor containing 1 m of LED light tape

I_o (µmol.m^{-2}.s^{-1})	Front Centre	Back Centre	Left side	Right side
1	19.97	16.64	20.87	18.78
2	1068.5	19.87	36.74	20.12
3	22.81	38.35	20.22	33.45
4	15.36	23.89	38.55	20.22
5	1067.8	21.27	20.24	22.31
6	21.78	39.46	21.26	1056.74
7	28.75	21.35	1063.8	21.4
8	48.69	22.74	24.31	38.85
9	23.78	1063.5	22.78	38.75
10	21.26	33.97	1058.7	21.56
11	1066.8	22.84	21.87	33.71
12	23.23	1036.8	22.75	24.61
13	21.54	21.97	30.25	21.12
14	38.97	22.74	22.98	32.46
15	21.38	1064.6	1058.7	38.14
16	13.56	20.84	30.35	22.22
17	33.14	25.83	21.34	19.87
18	35.76	18.75	20.41	1059.5
19	16.34	18.31	10.45	20.19
20	13.31	12.21	10.33	18.74
21	11.83	12.87	9.87	16.63
Average light intensity (µmol.m^{-2}.s^{-1})			**159.5**	

Table B. 4: Light intensity data measured for the modified internally lit airlift photobioreactor containing 1.8 m of LED light tape

I_o (µmol.m^{-2}.s^{-1})	Front Centre	Back Centre	Left side	Right side
1	1058.5	21.64	31.29	22.24
2	38.97	19.87	1068.2	1058.7
3	32.81	1068.5	30.22	38.45
4	1057.8	28.31	38.56	33.34
5	37.78	24.25	1058.3	38.71
6	38.46	1059.46	33.61	1058.6
7	1058.4	31.35	38.45	31.32
8	38.58	21.31	1055.3	33.74
9	24.74	1059.8	37.33	1058.4
10	1057.5	31.35	30.31	35.16
11	38.75	30.34	35.78	37.45
12	33.23	1055.8	1058.5	39.13
13	1061.1	35.51	30.25	34.11
14	21.97	29.74	34.41	30.36
15	37.88	1053.8	1068.5	1068.7
16	33.56	34.31	34.12	38.33
17	35.55	28.41	30.2	39.61
18	21.76	22.84	1058.8	1065.5
19	1053.8	21.31	20.11	34.31
20	23.61	19.37	15.45	20.74
21	15.45	10.87	13.37	18.36
Average light intensity (µmol.m^{-2}.s^{-1})			**299.8**	

Appendix C: Experimental data

Appendix C-1: Data for the vertical airlift photobioreactors

Appendix C-1-1: Evaluating the effect of light intensity on the growth of *Chlorella vulgaris* and *Scenedesmus sp.*

Figure C.1 and Figure C.2 present the linear plots used to calculate the exponential and linear growth rates of *Chlorella vulgaris* at the different light conditions described in Section 5.2.1. respectively.

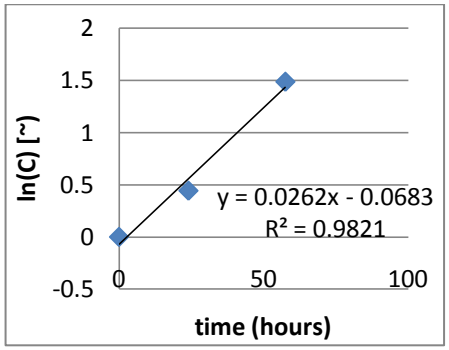

a) *Chlorella vulgaris* at 300 µmol.m^{-2}.s^{-1}

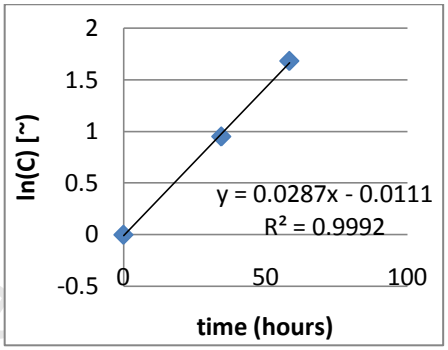

b) *Chlorella vulgaris* at 600 µmol.m^{-2}.s^{-1}after 2 days

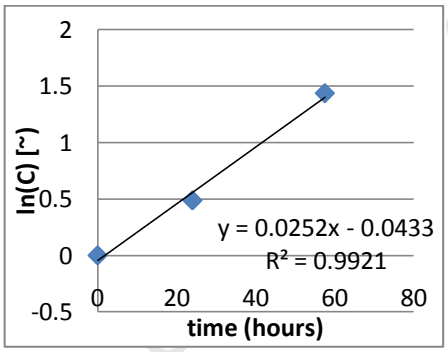

c) *Chlorella vulgaris* at 600 µmol.m^{-2}.s^{-1} after 7 days

Figure C. 1: Linear plot of ln (C_x) as a function of time for calculation of the exponential growth rates of *Chlorella vulgaris* in the vertical airlift photobioreactors at different light intensities (a)-(c)

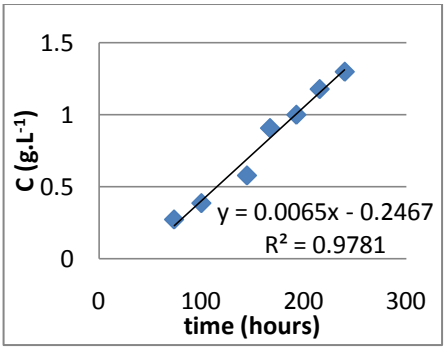

a) *Chlorella vulgaris* at 300 µmol.m^{-2}.s^{-1}

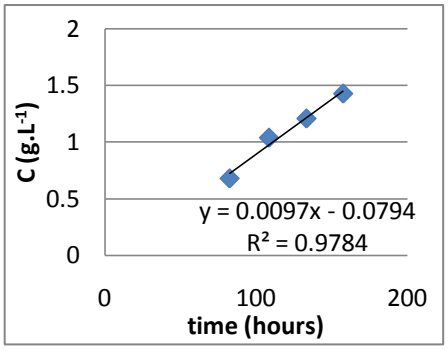

b) *Chlorella vulgaris* at 600 µmol.m^{-2}.s^{-1} after 2 days

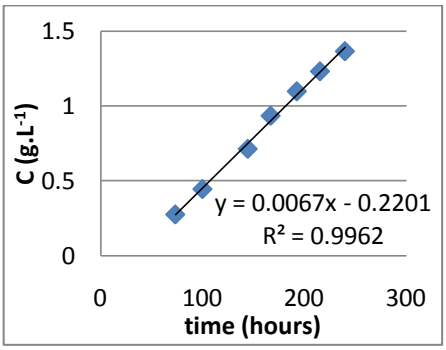

c) *Chlorella vulgaris* at 600 µmol.m^{-2}.s^{-1} after 7 days

Figure C. 2: Linear plot of C_x as a function of time for calculation of the linear growth rates of *Chlorella vulgaris* in the vertical airlift photobioreactors at different light intensities (a)-(c)

Figure C.3 presents the dry weight data that was obtained for the experiment which was carried out to compare the growth of *Scenedesmus sp.* and *Chlorella vulgaris* at different light intensities in the vertical airlift photobioreactors.

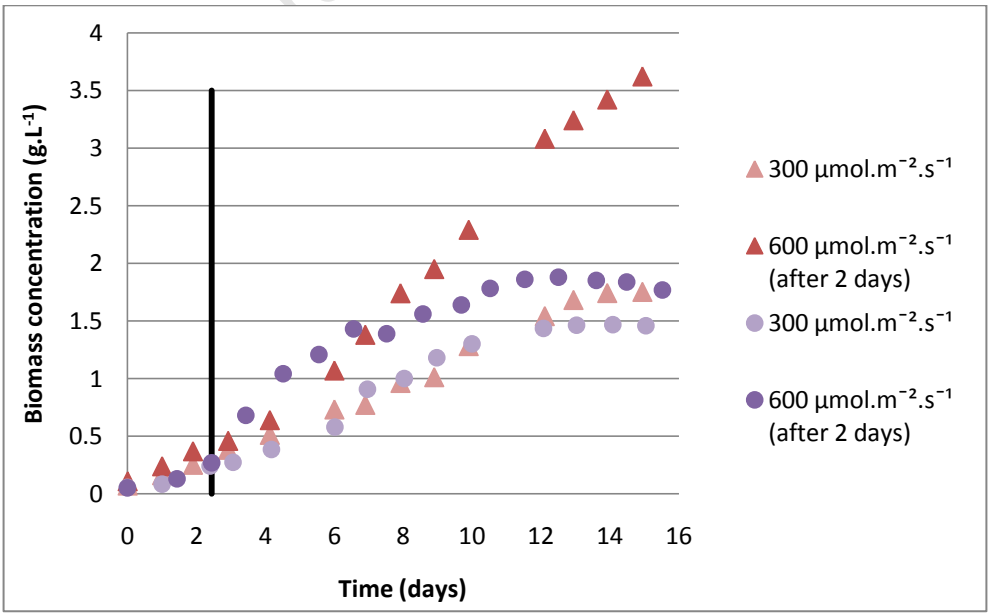

Figure C. 3: Comparison between the growth curves of *Scenedesmus sp.* and *Chlorella vulgaris* at different light intensities and 25±1°C in the vertical airlift photobioreactors (triangles and circles represent *Scenedesmus sp.* and *Chlorella vulgaris* respectively)

Figure C.4 and Figure C.5 present the linear plots used to calculate the exponential and linear growth rates of *Scenedesmus sp.* in the vertical airlift photobioreactors at the different light conditions described in Section 5.2.1.

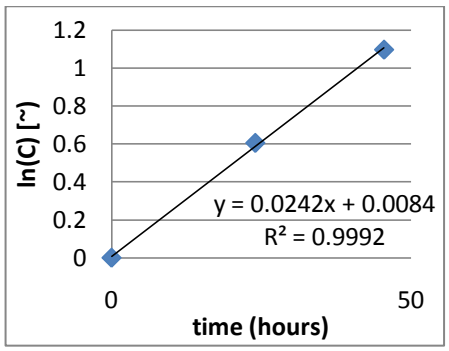

a) *Scenedesmus sp.* at 300 µmol.m^{-2}.s^{-1}

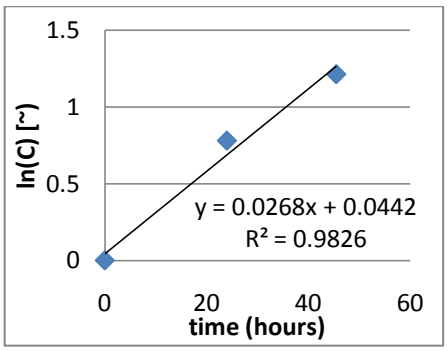

b) *Scenedesmus sp.* at 600 µmol.m^{-2}.s^{-1}after 2 days

Figure C. 4: Linear plot of ln (C_x) as a function of time for calculation of the exponential growth rates of *Scenedesmus sp.* in the vertical airlift photobioreactors at different light intensities (a)-(b)

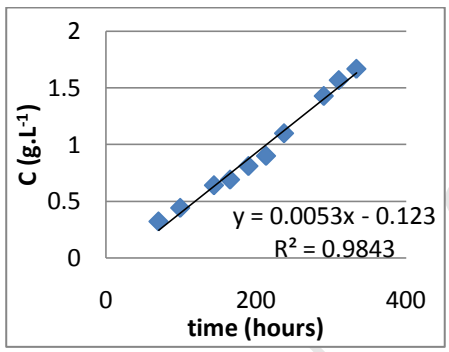

a) *Scenedesmus sp.* at 300 µmol.m^{-2}.s^{-1}

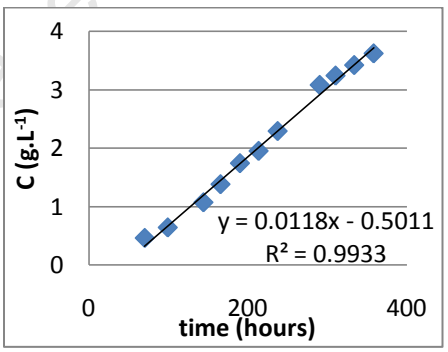

b) *Scenedesmus sp.* at 600 µmol.m^{-2}.s^{-1} after 2 days

Figure C. 5: Linear plot of C_x as a function of time for calculation of the linear growth rates of *Scenedesmus sp.* in the vertical airlift photobioreactors at different light intensities (a)-(b)

Appendix C-1-2: Evaluating the effect of light intensity and configuration on the growth of *Scenedesmus sp.* in the vertical airlift photobioreactors

Figures C.6 and C.7 illustrate the linear plots used to calculate the exponential and linear growth rates of *Scenedesmus sp.* at 26±1°C and the different lighting conditions described in Section 5.2.2 respectively.

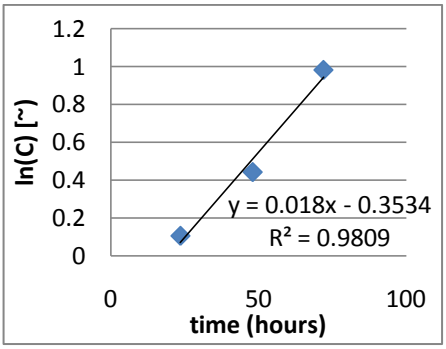

a) LED light only at 160 µmol.m^{-2}.s^{-1}

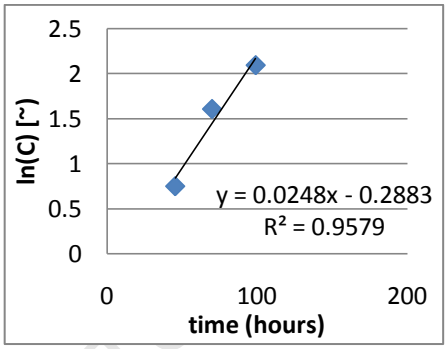

b) LED light only at 300 µmol.m^{-2}.s^{-1}

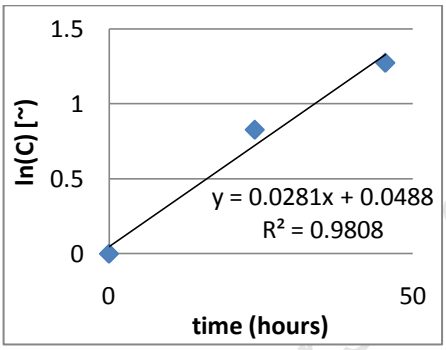

c) Fluorescent light at 300 µmol.m^{-2}.s^{-1}

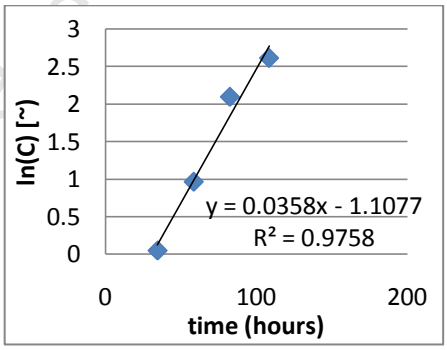

d) LED and fluorescent light at 460 µmol.m^{-2}.s^{-1}

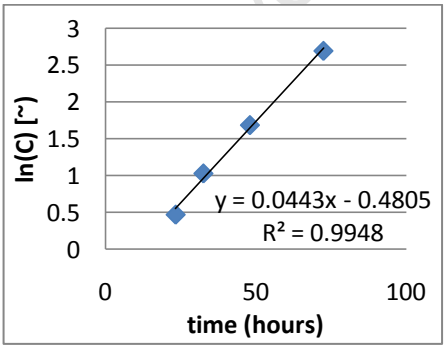

e) LED and fluorescent light at 600 µmol.m^{-2}.s^{-1}

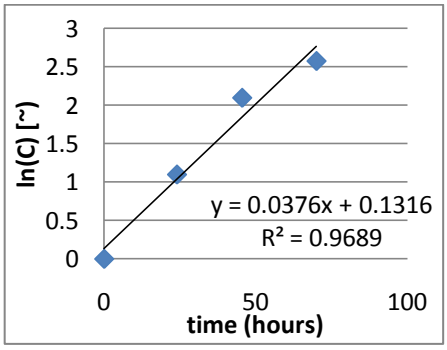

f) Fluorescent light at 600 µmol.m^{-2}.s^{-1}

Figure C. 6: Linear plots to calculate the exponential growth rate of *Scenedesmus sp.* as a function of light intensity and configuration in the vertical airlift photobioreactors

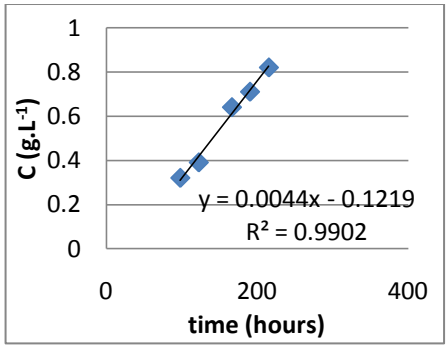

a) LED light only at 160 µmol.m^{-2}.s^{-1}

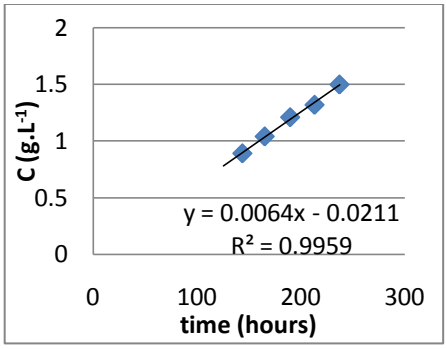

b) LED light only at 300 µmol.m^{-2}.s^{-1}

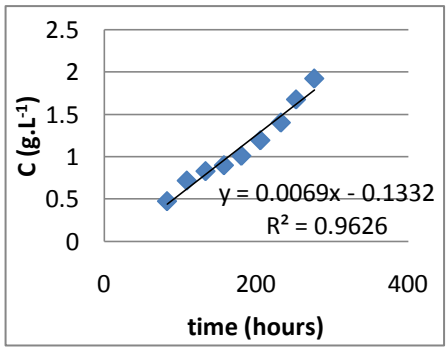

c) Fluorescent light at 300 µmol.m^{-2}.s^{-1}

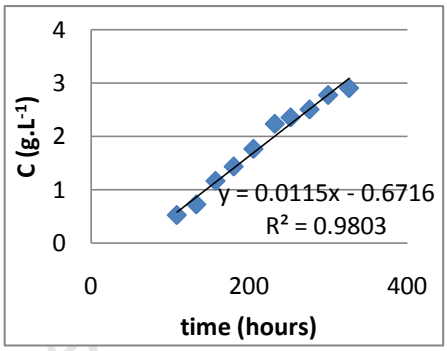

d) LED and fluorescent light at 460 µmol.m^{-2}.s^{-1}

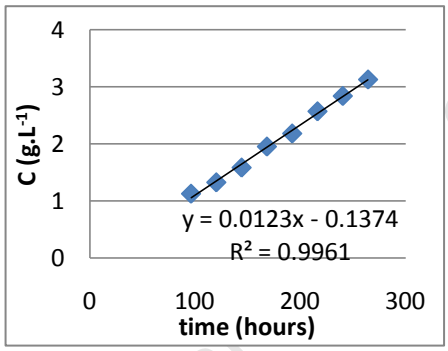

e) LED and fluorescent light at 600 µmol.m^{-2}.s^{-1}

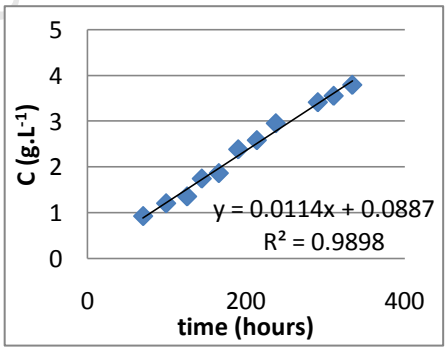

f) Fluorescent light at 600 µmol.m^{-2}.s^{-1}

Figure C. 7: Linear plots to calculate the linear growth rate of *Scenedesmus sp.* as a function of light intensity and configuration in the vertical airlift photobioreactors

Appendix C-1-3: Evaluating the effect of light intensity and temperature on the growth of *Scenedesmus sp.* in the vertical airlift photobioreactors

Figures C.8 and C.9 present the linear plots used to calculate the exponential and linear growth rates of *Scenedesmus sp.* at the different lighting and temperature conditions described in Section 5.2.3 respectively. In order to establish whether or not the maximum specific and linear growth rates of *Scenedesmus sp.* were modified by the culture temperature according to the Arrhenius equation, these exponential and linear growth rates were fitted to the Arrhenius equation at light intensities of 300 and 600 µmol.m^{-2}.s^{-1}.

Figures C.10-C.13 illustrate the Arrhenius plots for the maximum specific and linear growth rates at 300 and 600 µmol.m^{-2}.s^{-1} respectively.

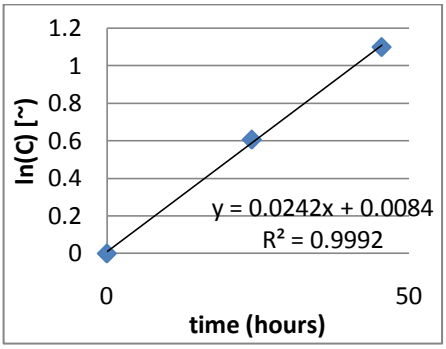

a) 300 µmol.m^{-2}.s^{-1}at 24°C

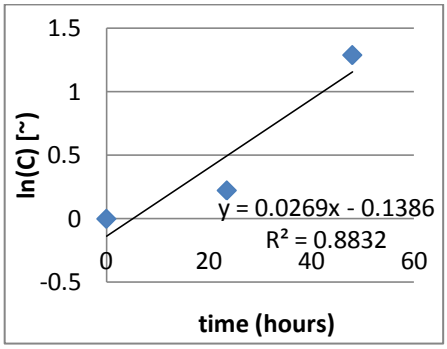

b) 300 µmol.m^{-2}.s^{-1} at 26°C

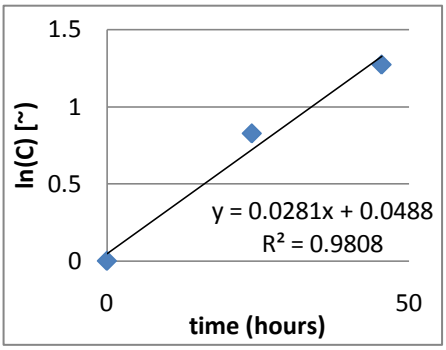

c) 300 µmol.m^{-2}.s^{-1} at 26°C (Repeat run)

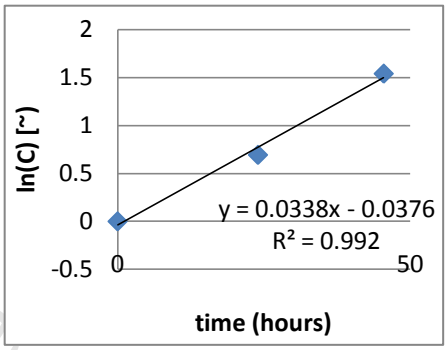

d) 300 µmol.m^{-2}.s^{-1} at 30°C

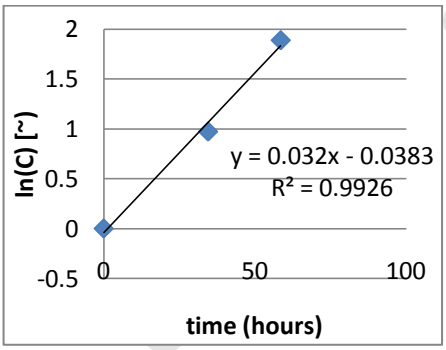

e) 600 µmol.m^{-2}.s^{-1} at 24°C

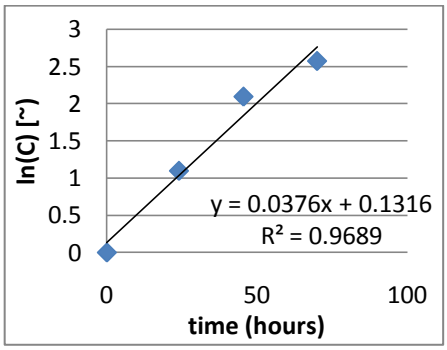

f) 600 µmol.m^{-2}.s^{-1} at 26°C

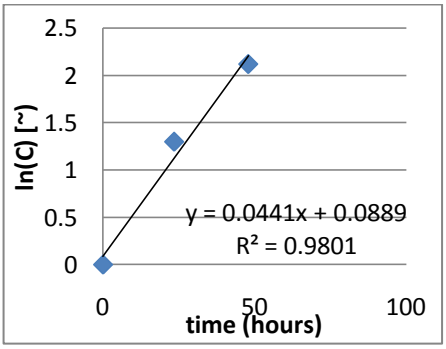

g) 600 µmol.m^{-2}.s^{-1} at 30°C

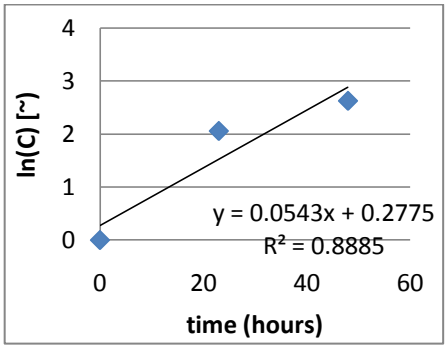

h) 600 µmol.m^{-2}.s^{-1} at 30°C (Repeat run)

Figure C. 8: Linear plots to estimate the effect of light intensity and temperature on the exponential growth rate of *Scenedesmus sp.* in the airlift photobioreactors

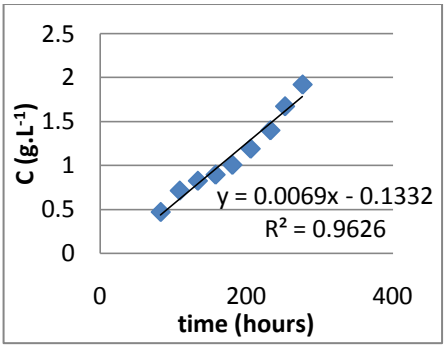

a) 300 µmol.m^{-2}.s^{-1} at 24°C

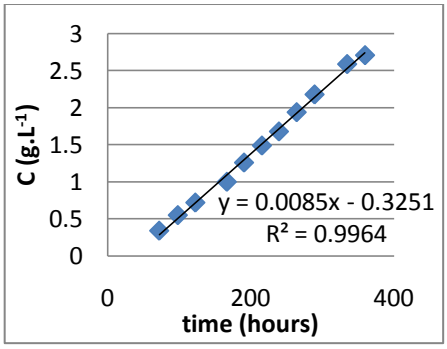

b) 300 µmol.m^{-2}.s^{-1} at 26°C

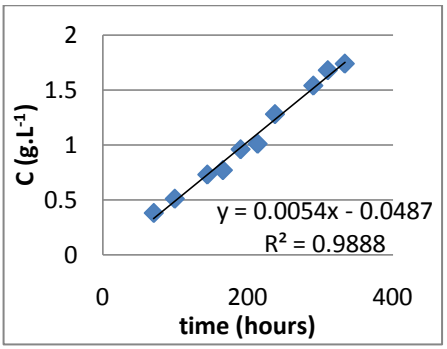

c) 300 µmol.m^{-2}.s^{-1} at 26°C (Repeat run)

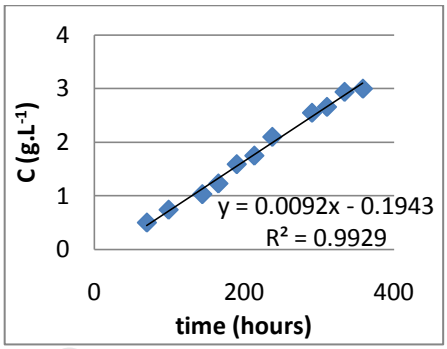

d) 300 µmol.m^{-2}.s^{-1} at 30°C

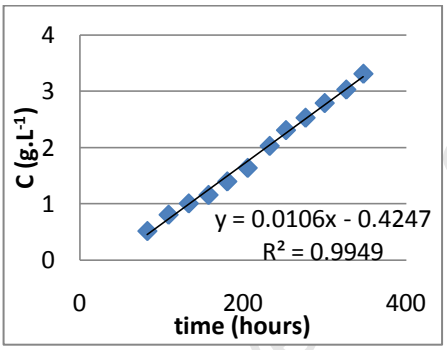

e) 600 µmol.m^{-2}.s^{-1} at 24°C

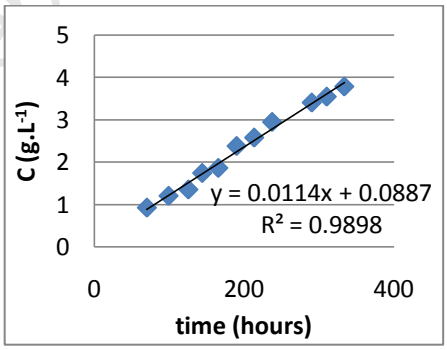

f) 600 µmol.m^{-2}.s^{-1} at 26°C

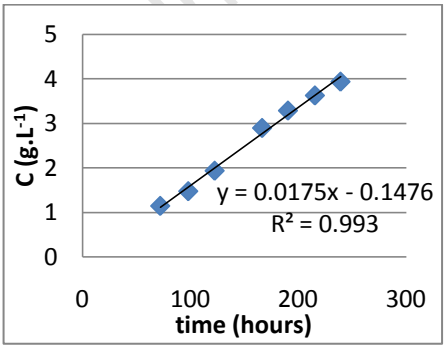

g) 600 µmol.m^{-2}.s^{-1} at 30°C

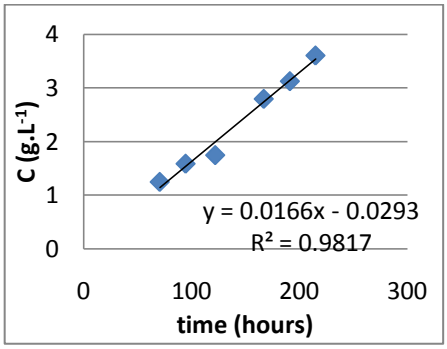

h) 600 µmol.m^{-2}.s^{-1} at 30°C (Repeat run)

Figure C. 9: Linear plots to estimate the effect of light intensity and temperature on the linear growth rate of *Scenedesmus sp.* in the airlift photobioreactors

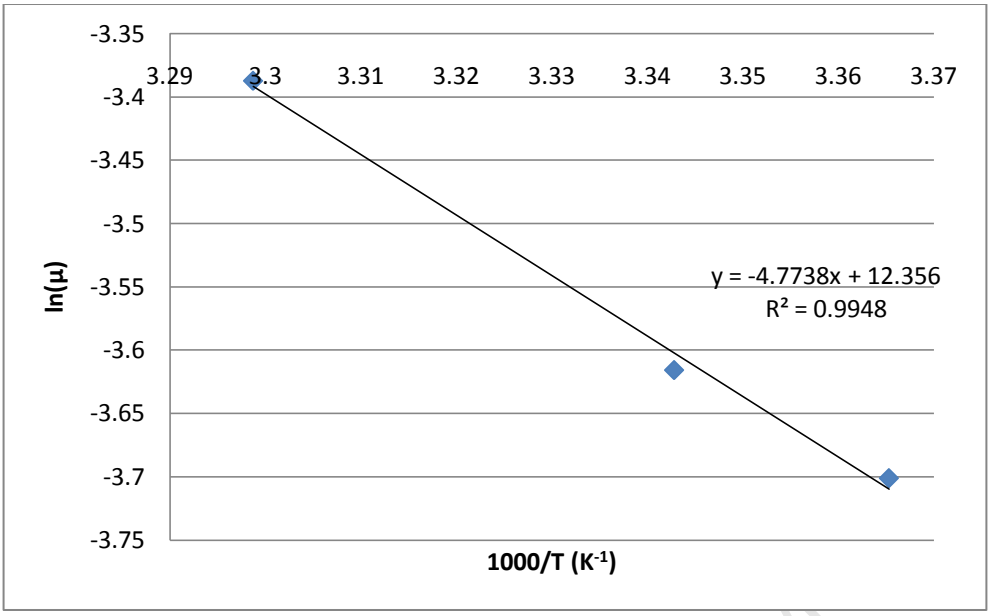

Figure C. 10: Arrhenius plot for maximum specific growth rate data of *Scenedesmus sp.* at 300 µmol.m^{-2}.s^{-1} in the range of 24-30°C

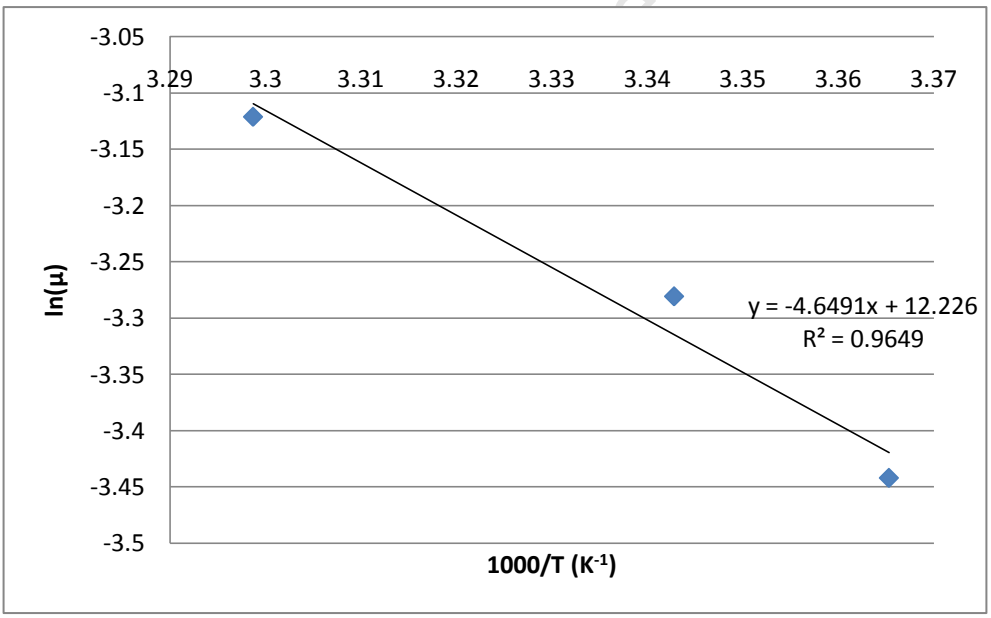

Figure C. 11: Arrhenius plot for maximum specific growth rate data of *Scenedesmus sp.* at 600 µmol.m^{-2}.s^{-1} in the range of 24-30°C

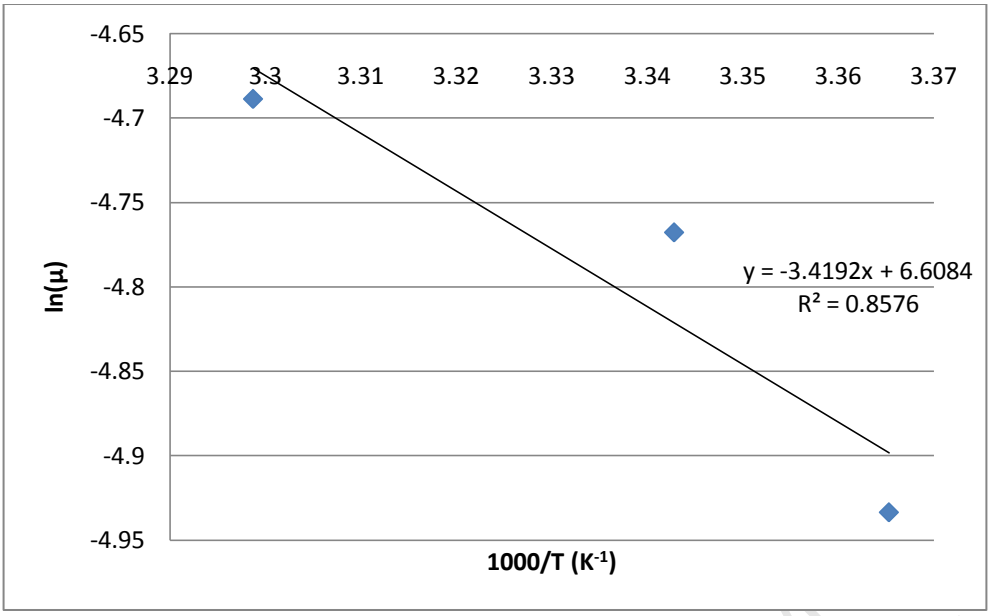

Figure C. 12: Arrhenius plot for linear growth rate data of *Scenedesmus sp.* at 300 µmol.m^{-2}.s^{-1} in the range of 24-30°C

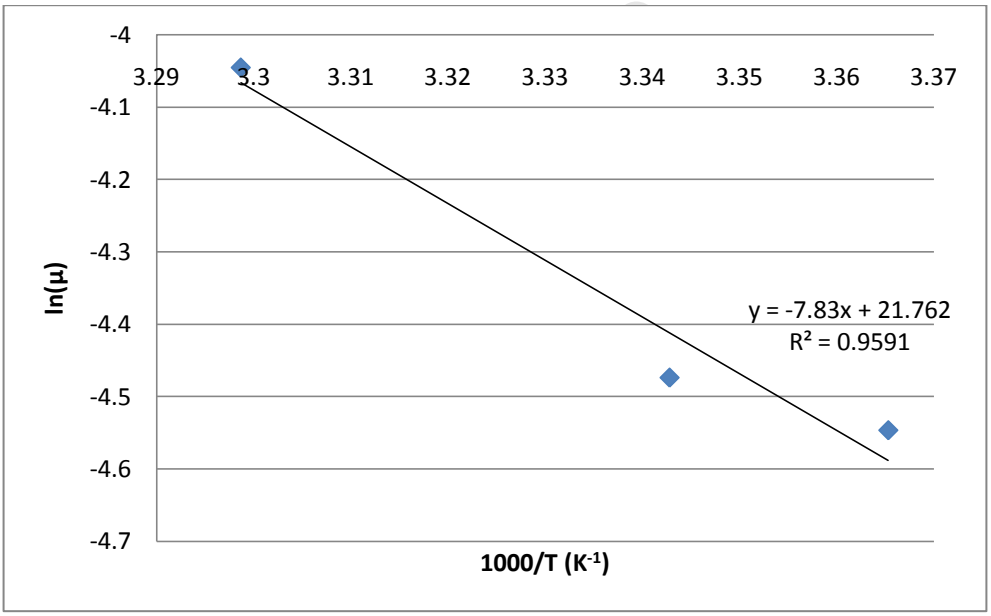

Figure C. 13: Arrhenius plot for linear growth rate data of *Scenedesmus sp.* at 600 µmol.m^{-2}.s^{-1} in the range of 24-30°C

Appendix C-2: Data for the tubular photobioreactors

Figures C.14 and C.15 present the linear plots used to calculate the exponential growth rates of *Scenedesmus sp.* at the different lighting conditions illustrated in Table 3.5, at cycle times of 21 s and 33 s respectively.

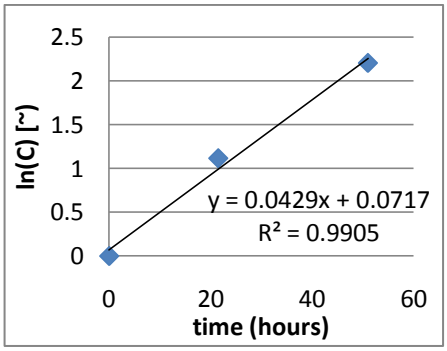

a) I_{ave} = 300 µmol.m^{-2}.s^{-1} and f = 0.4

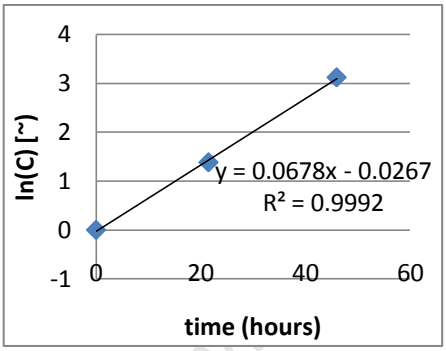

b) I_{ave} = 300 µmol.m^{-2}.s^{-1} and f = 0.75

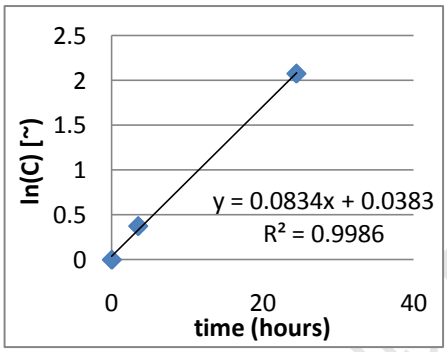

c) I_{ave} = 300 µmol.m^{-2}.s^{-1} and f = 1

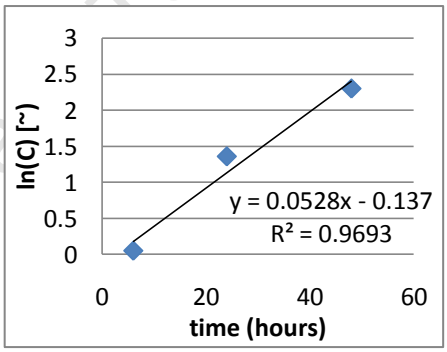

d) I_{ave} = 600 µmol.m^{-2}.s^{-1} and f = 0.4

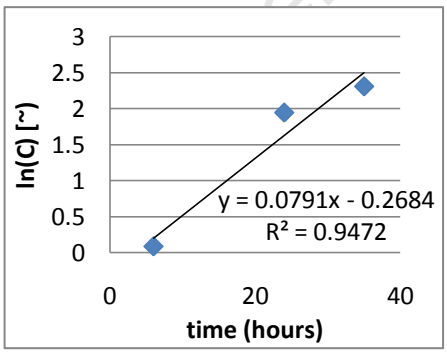

e) I_{ave} = 600 µmol.m^{-2}.s^{-1} and f = 0.75

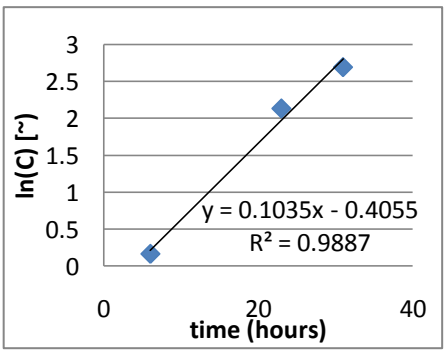

f) I_{ave} = 600 µmol.m^{-2}.s^{-1} and f = 1

Figure C. 14: Linear plots to estimate the effect of altering light intensity and light fraction on the exponential growth rate of *Scenedesmus sp.* at a cycle time of 21 s in the tubular photobioreactor

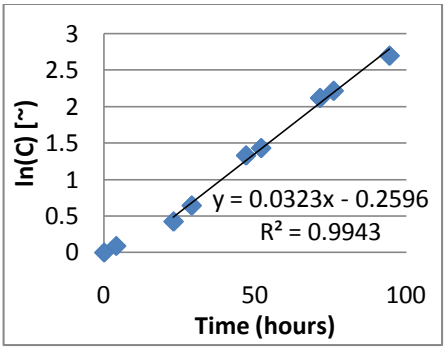

a) I_{ave} = 300 µmol.m^{-2}.s^{-1} and f = 0.4

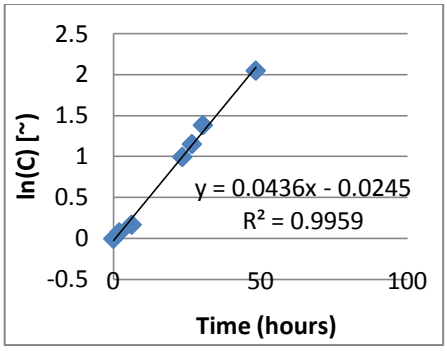

b) I_{ave} = 300 µmol.m^{-2}.s^{-1} and f = 0.75

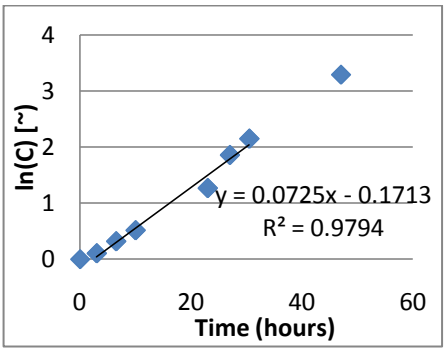

c) I_{ave} = 300 µmol.m^{-2}.s^{-1} and f = 1

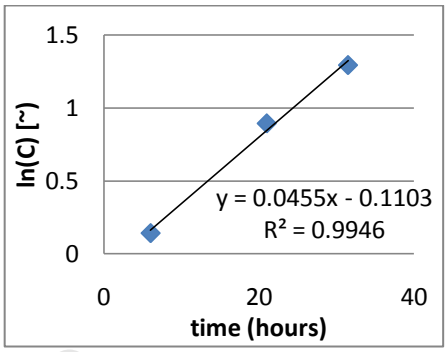

d) I_{ave} = 600 µmol.m^{-2}.s^{-1} and f = 0.4

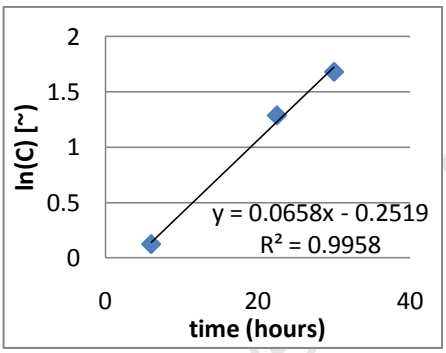

e) I_{ave} = 600 µmol.m^{-2}.s^{-1} and f = 0.75

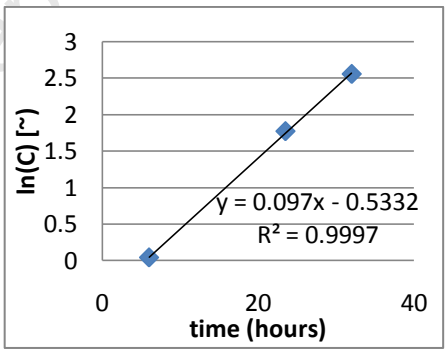

f) I_{ave} = 600 µmol.m^{-2}.s^{-1} and f = 1

Figure C. 15: Linear plots to estimate the effect of altering light intensity and light fraction on the exponential growth rate of *Scenedesmus sp.* at a cycle time of 33 s in the tubular photobioreactor

Appendix C-3: Data for the flat plate photobioreactor

Appendix C-3-1: Estimation of the overall mass transfer coefficient

As mentioned previously in Section 3.2.5, for practical reasons, it was easier to measure $k_La(O_2)$ rather than $k_La(CO_2)$. Figure C.16 presents the $k_La(O_2)$ data obtained in the flat plate photobioreactor across a range of different aeration rates. The overall mass transfer data in Figure C.16 was converted to $k_La(CO_2)$ using Equation 2.5, where $D_{C02} = 1.77 \times 10^{-9}$ m^2s^{-1} and $D_{02} = 1.97 \times 10^{-9}$ m^2s^{-1}. Figure 4.11 illustrates the estimated $k_La(CO_2)$ obtained in the flat plate photobioreactor over a range of aeration rates.

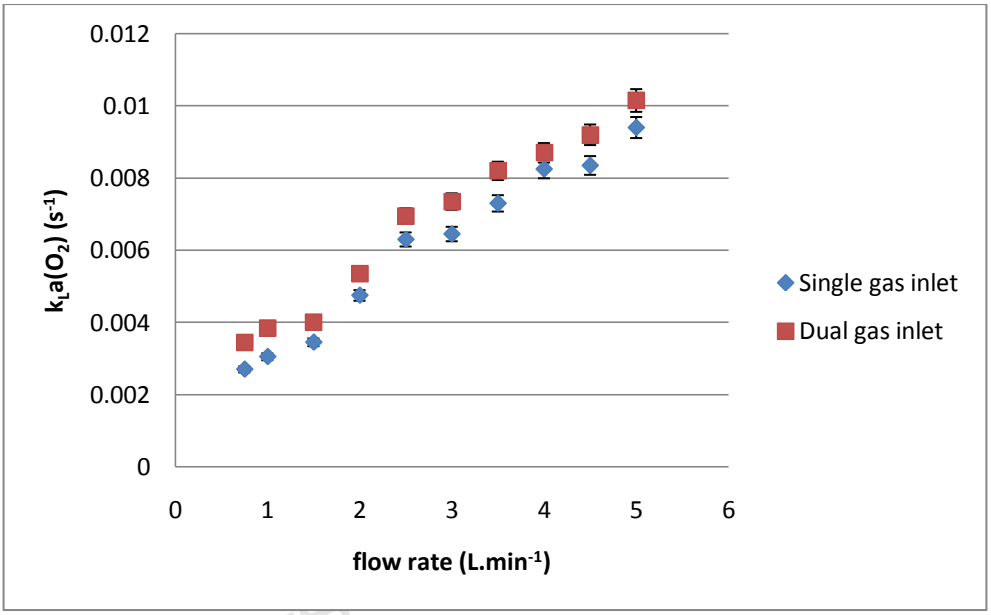

Figure C. 16:Overall mass transfer coefficient of O_2 at different gas flow rates in the flat plate photobioreactor filled with media at 23±1°C
(An average experimental error of 3.1% was assumed based on repeat runs)

In order to estimate the effect of aeration rate on the experimental gas hold up in the flat plate photobioreactor, the change in liquid height was recorded at different aeration rates. Equation 4.3 was used to calculate the experimental gas hold up data which is presented in Table C.1. The initial unsparged liquid height was 0.206 m.

Table C. 1: Experimental gas hold up in the flat plate photobioreactor as a function of aeration rate

Aeration rate ($L.min^{-1}$)	h_d (m)	Ɛ
1	0.2079	0.009579
1.5	0.2089	0.01369
2	0.2097	0.01760
2.5	0.2105	0.02116
3	0.2112	0.02463
3.5	0.2120	0.02849
4	0.2132	0.03373

Appendix C-3-2: Effect of light intensity and aeration rate on the growth of *Scenedesmus sp.* in the flat plate photobioreactor

Figures C.17 and C.18 present the linear plots used to calculate the exponential and linear growth rates of *Scenedesmus sp.* cultivated using fluorescent light at the conditions provided in Table 3.7 respectively.

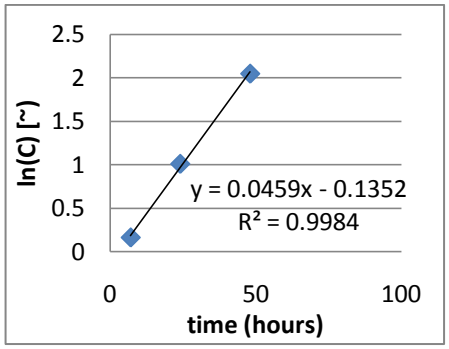

a) I_{ave} = 300 µmol.m^{-2}.s^{-1} and f = 2.5 L.min^{-1}

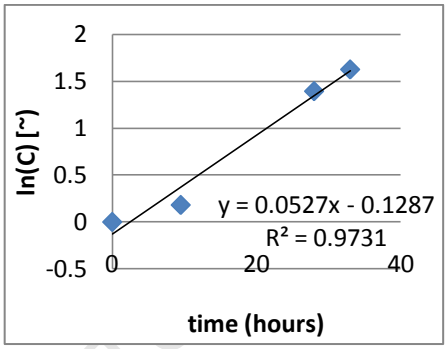

b) I_{ave} = 300 µmol.m^{-2}.s^{-1} and f = 3.5 L.min^{-1}

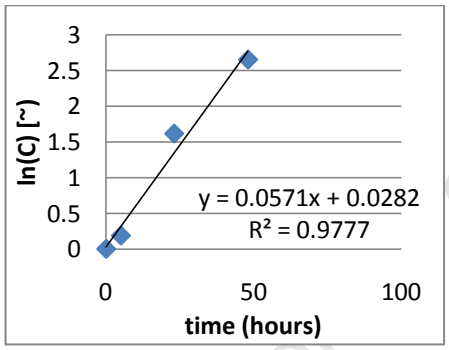

c) I_{ave} = 300 µmol.m^{-2}.s^{-1} and f = 5 L.min^{-1}

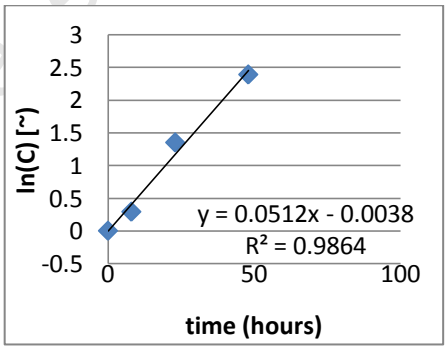

d) I_{ave} = 600 µmol.m^{-2}.s^{-1} and f = 2.5 L.min^{-1}

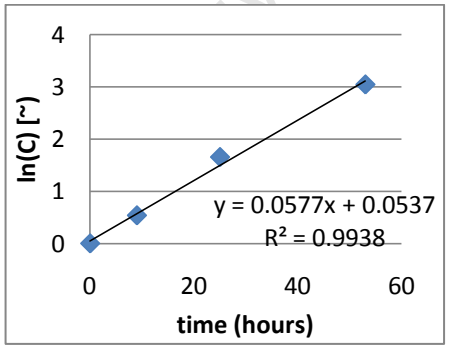

e) I_{ave} = 600 µmol.m^{-2}.s^{-1} and f = 3.5 L.min^{-1}

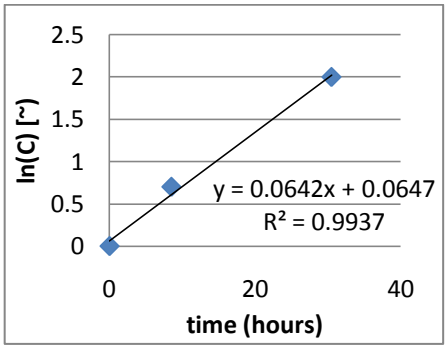

f) I_{ave} = 600 µmol.m^{-2}.s^{-1} and f = 5 L.min^{-1}

Figure C. 17: Linear plots to estimate the effect of light intensity and aeration rate on the exponential growth rate of *Scenedesmus sp.* in the flat plate photobioreactor

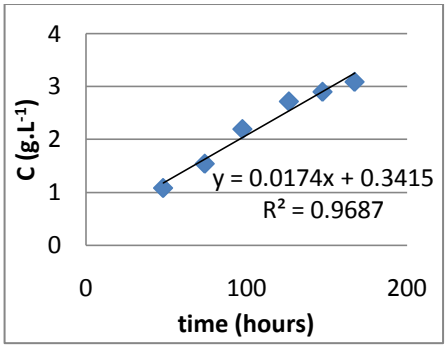

a) I_{ave} = 300 µmol.m^{-2}.s^{-1} and f = 2.5 L.min^{-1}

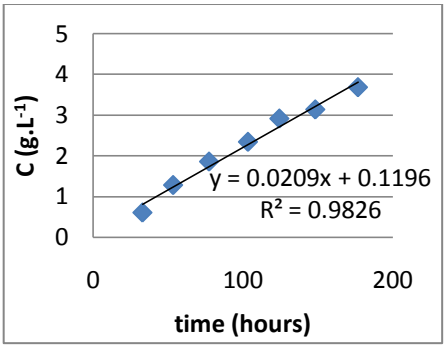

b) I_{ave} = 300 µmol.m^{-2}.s^{-1} and f = 3.5 L.min^{-1}

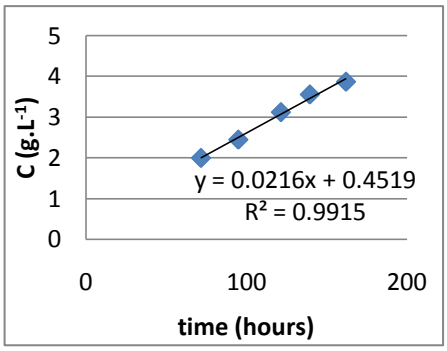

c) I_{ave} = 300 µmol.m^{-2}.s^{-1} and f = 5 L.min^{-1}

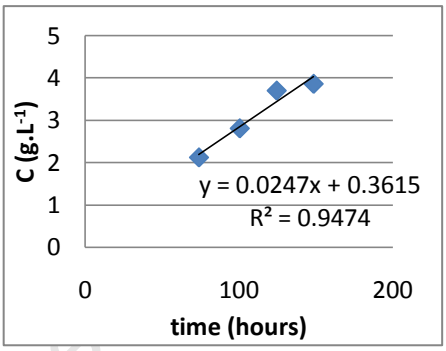

d) I_{ave} = 600 µmol.m^{-2}.s^{-1} and f = 2.5 L.min^{-1}

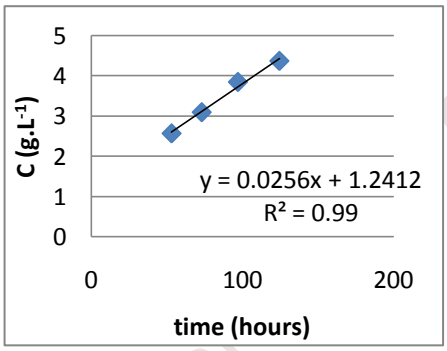

e) I_{ave} = 600 µmol.m^{-2}.s^{-1} and f = 3.5 L.min^{-1}

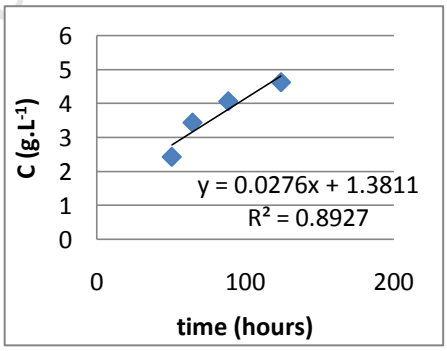

f) I_{ave} = 600 µmol.m^{-2}.s^{-1} and f = 5 L.min^{-1}

Figure C. 18: Linear plots to estimate the effect of light intensity and aeration rate on the linear growth rate of *Scenedesmus sp.* in the flat plate photobioreactor

Appendix C-3-3: Effect of using LEDs as a light source on the growth of *Scenedesmus sp.* in the flat plate photobioreactor

Figures C.19 and C.20 present the linear plots used to calculate the exponential and linear growth rates of *Scenedesmus sp.* cultivated using LED light at the conditions provided in Table 3.8 respectively.

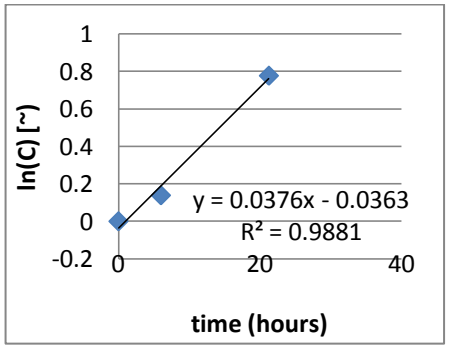

a) I_{ave} = 300 µmol.m^{-2}.s^{-1} and f = 2.5 L.min^{-1}

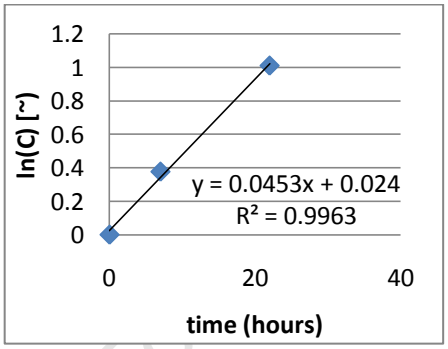

b) I_{ave} = 300 µmol.m^{-2}.s^{-1} and f = 3.5 L.min^{-1}

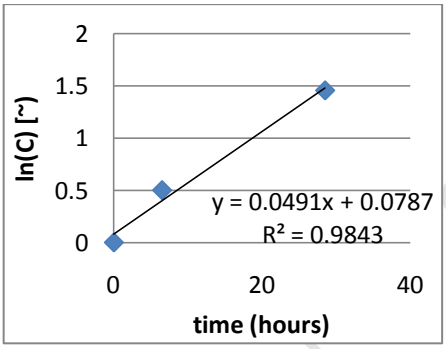

c) I_{ave} = 300 µmol.m^{-2}.s^{-1} and f = 5 L.min^{-1}

Figure C. 19: Linear plots to estimate the effect of using LEDs on the exponential growth rate of *Scenedesmus sp.* in the flat plate photobioreactor

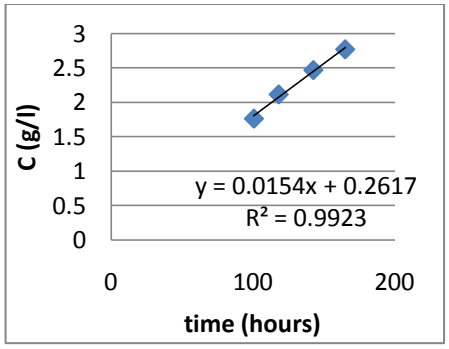

a) I_{ave} = 300 µmol.m^{-2}.s^{-1} and f = 2.5 L.min^{-1}

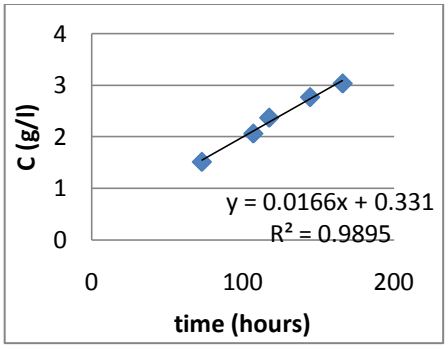

b) I_{ave} = 300 µmol.m^{-2}.s^{-1} and f = 3.5 L.min^{-1}

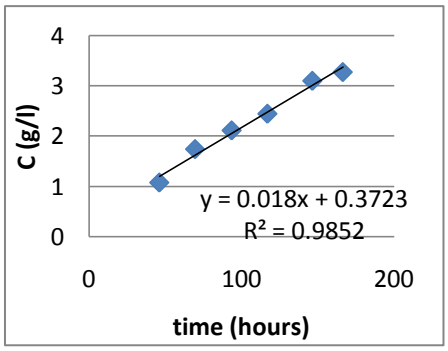

c) I_{ave} = 300 µmol.m^{-2}.s^{-1} and f = 5 L.min^{-1}

Figure C. 20: Linear plots to estimate the effect of using LEDs on the linear growth rate of *Scenedesmus sp.* in the flat plate photobioreactor

Appendix C-4: Calibration curves

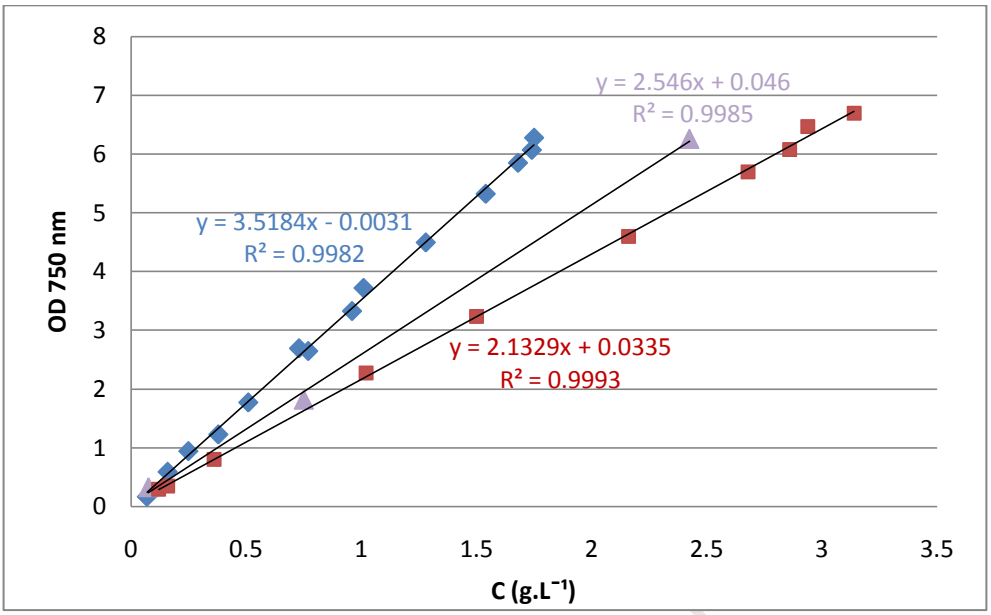

Figure C. 21: *Scenedesmus sp.* absorbance as a function of dry weight concentration, measured at 750 nm in a Helios spectrophotometer at 300 µmol.m^{-2}.s^{-1} and 25±1°C (diamond, triangle and square symbols represent airlift, tubular and flat plate photobioreactors respectively)

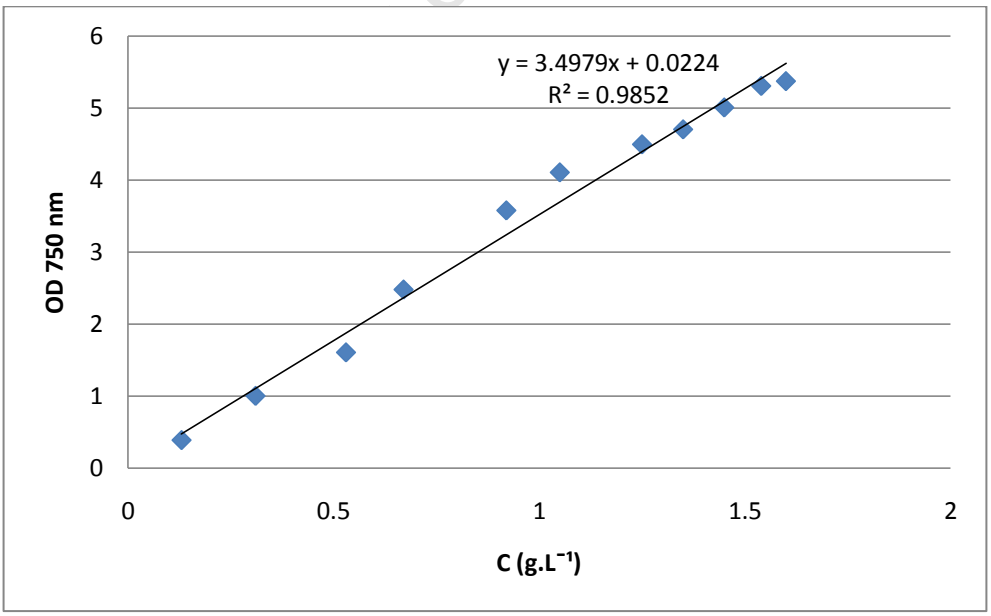

Figure C. 22: *Chlorella vulgaris* absorbance as a function of dry weight concentration, measured at 750 nm in a Helios spectrophotometer at 300 µmol.m^{-2}.s^{-1} and 25±1°C in an airlift photobioreactor